The synthesis and characterisation of some novel compounds containing Pt-Se bonds.

Webster, Christopher Alan

The Synthesis and Characterisation of Some Novel Compounds Containing Pt-Se Bonds

Christopher Alan Webster

Department of Chemistry
University of Wales Swansea
November 2006

Acknowledgements

Firstly I would like to thank Dr. Chris Morley, my supervisor for his invaluable support, guidance and encouragement.

My thanks also go to Prof. Massimo Di Vaira for all his support during my stay at the University of Florence and for the crystal structure determinations he carried out.

Thanks to Su Jing, the other half of Swansea's Inorganic/Organometallic Research Group, for doing such a phenomenal amount of work that I had to work hard just to keep up!

Thanks to the players of chemistry rugby past and present - Lee, Paul, Des, Dave, Hans, Big Chris, Bleddyn, Fergus, Matt B, Dave (undergrad), Geraint, Will, John T and Brendan – for making Friday lunchtimes something to look forward to.

Thanks to Ian Matthews and Dr. Suzy Kean for running NMR spectra, John Tregembo for glass blowing and Stan Szajda for finding equipment and chemicals whenever I needed them.

Thanks to the EPSRC Mass Spectrometry Service Centre for all of the mass spectral data.

Thanks to Johnson Matthey plc for the loan of platinum and palladium salts.

Contents

Abstract

The main aim of the work described in this thesis was to investigate the potential of reactions of Pt(0) phosphine complexes with selected organoselenium reagents to provide routes to diselenolenes and related compounds with Pt-Se bonds.

Chapter 1 reviews the background to this work, and introduces some relevant classes of compound. Surveys of the coordination chemistry of organoselenium ligands such as selenoethers, 1,2,3-selenadiazoles, 1,4-diselenins and selenophenes are included. The properties of dithiolenes and diselenolenes are also discussed.

Each of Chapters 2-5 deals with a specific type of reaction, and the characterisation of the products, in particular by multinuclear NMR spectroscopy, X-ray diffraction and mass spectrometry, supplemented by other techniques as appropriate.

Chapter 2 describes the synthesis of the new platinum diselenolenes $[Pt\{Se_2C_{n+4}H_{2n+4}\}(PR_3)_2]$ (n = 2, 3 or 4; R = Ph, Et or Bu) and $[Pt\{Se_2C_8H_{12}\}\{Ph_2P(CH_2)_mPPh_2\}]$ (m = 1, 2 or 3), *via* the reactions of $[Pt(PPh_3)_4]$ with cycloalkeno-1,2,3-selenadiazoles, of $[Pt(C_2H_4)(PR_3)_2]$ (R = Et, Bu) with *bis*-cycloalkeno-1,4-diselenins, or phosphine exchange.

In Chapter 3 the reactions of cycloalkeno-1,2,3-thiadiazoles and cycloalkeno-1,2,3-selenadiazoles with $[Pt(C_2H_4)(PR_3)_2]$, or a mixture of $[Pt(C_2H_4)(PR_3)_2]$ and $[PtCl_2(PR_3)_2]$ (R = Et or Bu), are discussed. Five new classes of compound were prepared and characterised: the azo-compounds $[PtL(PR_3)]$ (L = $EC(R^1)=C(R^2)N=NC(R^1)=C(R^2)E$; R^1-R^2 = $(CH_2)_5$ or $(CH_2)_6$; E = S or Se); the selenaplatinacyclobutenes $[Pt\{SeC_{n+4}H_{2n+4}\}(PR_3)_2]$ and their derivatives $[PtI\{Se(Me)C_{n+4}H_{2n+4}\}(PR_3)_2]$, $[Pt\{Se(Me)C_{n+4}H_{2n+4}\}(PR_3)_2]PF_6$ (n = 2, 3 or 4).

Chapter 4 describes the first observation of direct insertion of Pt(0) into the Se-C bond of selenophene, leading to the formation of $[Pt(SeC_4H_4)(PR_3)_2]$ (R = Et or Bu), and related reactions.

Oxidative addition of a Se-Se bond to Pt(0) or Pd(0) is considered in Chapter 5. The reactions of $[Pt(C_2H_4)(PR_3)_2]$ or $[Pd_2(dba)_3]/PR_3$ (R = Et or Bu; dba = dibenzylideneacetone) with R'_2Se_2 (R' = Ph or Fc, ferrocenyl) or *bis*-benzo-1,2-diselenin lead to the new complexes *trans*-$[M(SeR')_2(PR_3)_2]$, $[M(Se_2C_{12}H_8)(PR_3)_2]$ (M = Pd or Pt) and $[Pd_2(Se_2C_{12}H_8)_2(PR_3)_2]$

Chapter 6 summarises the results of X-ray diffraction studies undertaken by the author. As well as compounds described elsewhere in this thesis, several examples of ferrocenyl chalcogenides and their complexes were investigated.

The experimental details for the work are provided in Chapter 7.

Abbreviations

COD	1,5-cyclooctadiene
Cp	cyclopentadienyl (C_5H_5)
Cp*	pentamethylcyclopentadienyl (C_5Me_5)
Cy	cyclohexyl (c-C_6H_{11})
dba	dibenzylideneacetone
DEPT	Distortionless Enhancement by Polarisation Transfer
dppm	*bis*(diphenylphosphino)methane
dppe	1,2-*bis*(diphenylphosphino)ethane
dppp	1,3- *bis*(diphenylphosphino)propane
DCM	dichloromethane
DMSO	dimethylsulphoxide
E	chalcogen
EI/CI	electronic/chemical ionisation
ESI	electrospray ionisation
Et	ethyl (C_2H_5)
EtOAc	ethyl acetate
EtOH	ethanol
FAB	fast atom bombardment
Fc	ferrocenyl ([Fe(η^5-C_5H_5) (η^5-C_5H_4)])
hr	hour
IR	infrared
L	ligand
M	metal
Me	methyl (CH_3)
MeCN	acetonitrile
MeOH	methanol
MS	mass spectrometry
NMR	nuclear magnetic resonance
Ph	phenyl (C_6H_5)
R/R'	alkyl or aryl
RT	room temperature
THF	tetrahydrofuran
UV-vis	ultraviolet-visible
X	halogen

Chapter 1

Introduction

1.1 Introduction

Before considering the 'novel' chemistry presented in this thesis, it is useful to review some of the work that has preceded it. This brief introduction begins with a summary of the discovery and early uses of the key elements (Pt, S, Se), and continues with a consideration of some of the compounds formed by these elements in combination. The final parts of the introduction will consider the syntheses and reactions of 1,2,3-selena- and 1,2,3-thiadiazoles, diselenins and diselenolenes, these compounds being specifically related to the chemistry discussed in following chapters.

In addition there are also short sections on the use of phosphines as ligands in transition metal complexes, and the properties of transition metal dithiolenes. The majority of the complexes presented in this thesis contain phosphine ligands, and many were synthesised in the hope that they would share the desirable electrochemical and photochemical properties exhibited by dithiolenes.

By no means is this a comprehensive review; for more detail, it is suggested that the reader follow up the references provided.

1.2 Platinum, Sulphur and Selenium

The use of platinum can be traced back to Egyptian times: a piece detached from a metallic casket from Thebes was found to be an alloy of platinum. The hieroglyphics on the casket showed it had been dedicated to Queen Shapenapit, and thus dates back to the seventh century B.C. Silver and gold alloys of platinum were also used by the pre-Columbian Indians of Ecuador in jewellery and ornaments.[1,2] In both of these cases it is doubtful that platinum was recognised as a separate body, and it wasn't until 1736 that the metal was introduced to Europe by the Spanish astronomer and naval officer, A. de Ulloa. After publication of his report in 1748, a full investigation into platinum and its properties began.[3] Since this time platinum has found many uses including applications in catalytic converters, jewellery, and electronics. Platinum is rare having a crustal abundance of 0.01ppm, with large deposits found in Canada, South Africa and Russia.

Platinum has a spin-active isotope, ^{195}Pt, which is present in 33.7% natural abundance and has a spin ½. Indeed, ^{195}Pt NMR has been known since 1951,[4] although due to its low relative sensitivity of 9.94×10^{-3} (cf. ^{13}C 1.59×10^{-2}) it wasn't until the advent of Fourier transform spectroscopy that ^{195}Pt NMR spectroscopy became easily accessible.[5] The presence of this spin-active isotope in relatively high natural abundance provides a useful analytical probe in NMR studies of platinum-containing species.

Only two non-metallic elements were known to the ancient peoples, sulphur and carbon, as both these elements occur uncombined in many parts of the world. References to sulphur (as brimstone) are found frequently in the bible, where its flammability was used to symbolise torment and destruction.[6] Sulphur has found many uses through the course of history including: as a fumigant, bleaching agent, or medicine; in gunpowder; and most recently in the production of sulphuric acid, which has become the world's most important industrial chemical.[1,3] Sulphur also held particular significance for the early alchemists (tenth century onwards) who believed that metals were compounds of sulphur and mercury.[1] Sulphur has a crustal abundance of 340 ppm; this makes it the sixteenth most abundant element. Sulphur is obtained by mining of the caprock salt domes in the USA and Mexico and the sedimentary evaporate deposits of Poland. Compounds of sulphur can be extracted

from natural gas, crude oil, tar sands, shale, coal and from sulphide minerals such as pyrites (FeS_2).[3]

Sulphur has only one naturally occurring spin-active isotope in ^{33}S. Unfortunately it has a low natural abundance (0.76%), a low receptivity (0.097 relative to ^{13}C) and is quadrupolar (I = 3/2). An early paper predicted a gloomy future for ^{33}S NMR;[7] however, to date hundreds of compounds have now been examined successfully. Unfortunately examination is limited to compounds with a high degree of symmetry, where the electric field gradient (and thus the quadrupolar broadening) is reduced at the sulphur nucleus.[8,9] These limitations prevent the use of ^{33}S NMR spectroscopy as a routine analytical tool.

Selenium was first isolated in 1817 (35 years after the isolation of tellurium) by J.J. Berzelius and J.G. Gahn. They observed a reddish brown deposit formed during the burning of copper pyrites from the Fahlun copper mine in Sweden, reduction of which gave selenium.[1, 3] Selenium is a comparatively rare element comprising some 0.05 ppm of the earths crust (66th in order of crustal abundance).[3] Its name was derived from the Greek, selene, meaning moon, following tellurium's derivation from the Latin, tellus, earth.

Selenium and its compounds are used for a number of applications, including: as a decolouriser of glass and in xerography;[3] and more recently as semiconductors,[10] in ion-sensitive electrodes,[11] and in catalysis.[12]

Selenium possesses a spin-active isotope ^{77}Se, present in 7.6% natural abundance, with a spin of ½ and a receptivity 2.98 times that of ^{13}C. These properties allow investigation of the nuclear interactions of selenium-containing compounds, and since the advent of Fourier transform, ^{77}Se NMR spectroscopy has been used as a routine analytical tool.[8, 9]

1.3 Organoselenium Coordination Chemistry

Despite the discovery of selenium almost two centuries ago, it is only in the past 30 years that the ligand properties of organoselenium reagents have been systematically investigated. Organoselenium compounds were prepared as early as 1847,[13] and there were several reasons for the neglect of this aspect of selenium chemistry. It was believed for several years that they were weak donors and would only coordinate to class b metals; even then they were assumed to be little different from their thio-analogues.[14] This is exemplified in Livingstone's review of metal complexes with heavy group 16 donor ligands in 1965, by a clear dominance of sulphur compounds.[15] In addition the belief that selenium compounds had a high toxicity probably dissuaded people from their use; to quote from Sax's [16] assessment of selenium and its compounds in 1960: 'Its (selenium's) pathology has not as yet been adequately studied...In human beings, gastrointestinal disturbances have been noted and it causes respiratory irritation, cough, oedema of the lungs, vomiting diarrhoea, abdominal pain or cramps, loss of reflexes, cerebral irritation as manifested by convulsions, and ultimately death.' This conception of the toxicity of selenium may have contributed to the lack of investigation into organoselenium chemistry. A recent assessment of selenium and its compounds by Luxon[17] is a little more forgiving: 'The chlorides and solutions of the acids and salts (of selenium) may burn the skin...Selenium dioxide dust...irritates the respiratory system, eyes and skin...Inhalation of selenium dust over a prolonged period may cause fatigue, loss of appetite, digestive disturbance and bronchitis...Some salts have shown signs of carcinogenicity and mutagenicity.'

In contrast to the coordination chemistry of organoselenium reagents, the coordination chemistry of organosulphur compounds has been known for some time; indeed the coordination of thioether (R_2S, R = alkyl, aryl) ligands has been reported as early as 1883, with Tschugajeff studying d^8 metal complexes with thioether ligands in the early 1900's.[18] Due to the variation of R, several thioether complexes are known and the reader is referred to reviews by Murray and Hartley,[19] and Kuehn and Isiad[20] for a comprehensive listing.

1.4 Complexes with Selenoether Ligands

One of the most explored areas of organoselenium chemistry is that of coordination compounds containing selenoether ligands (R_2Se); these complexes have been subject to several reviews.[19,21]

1.4.1 Complexes Containing Monodentate Selenoether Ligands

In the 1950's Chatt and Venanzi reported halogen-bridged platinum and palladium complexes containing simple selenoether ligands (figure 1.1).[22, 23, 24]

Figure 1.1:

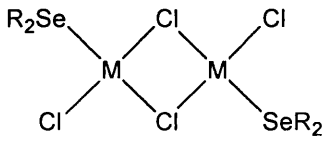

M = Pd, Pt
R = Et, ^{i}Pr

To date, dimethyl selenide (Me_2Se) has been the most studied selenoether; dimethyl selenide bonds readily to platinum and palladium to give complexes with an M(II) centre, which can be oxidised to an M(IV) centre by treatment with a halogen (figure 1.2).[25,26]

Figure 1.2:

$$[PtCl_2(Me_2Se)_2] \xrightarrow[CCl_4]{Cl_2} [PtCl_4(Me_2Se)_2]$$

$$[NBu_4][PdCl_3(SeMe_2)] \xrightarrow[CCl_4]{Cl_2} [NBu_4][PdCl_5(SeMe_2)]$$

These simple dialkyl selenide complexes of platinum and palladium have been the subject of extensive spectroscopic studies,[27,28] with much focus on the pyramidal inversion of the chalcogen.[29]

More recently complexes containing ligands of the type $MeSe(C_4H_3E)$ (E = O, S), have been investigated. [30] These ligands bond only via the Se donor in $[MCl_2\{MeSe(C_4H_3E)\}_2]$ (M = Pd, Pt); the bonding of 1,4-oxaselenan in $[MCl_2L_2]$ (M = Pd, Pt, L = 1,4-oxaselenan) is similar.[31] These complexes only exist as the *trans*-isomers, whereas the tellurium analogues exist as *cis/trans*- mixtures in solution and *cis*- isomers in the solid state. In acetone $[PdCl_2\{MeSe(C_4H_3O)\}_2]$ gives small amounts of a rearrangement product (figure 1.3), as a result of dimerisation with incorporation of acetone and loss of two 2-chlorofuran units.[32]

Figure 1.3:

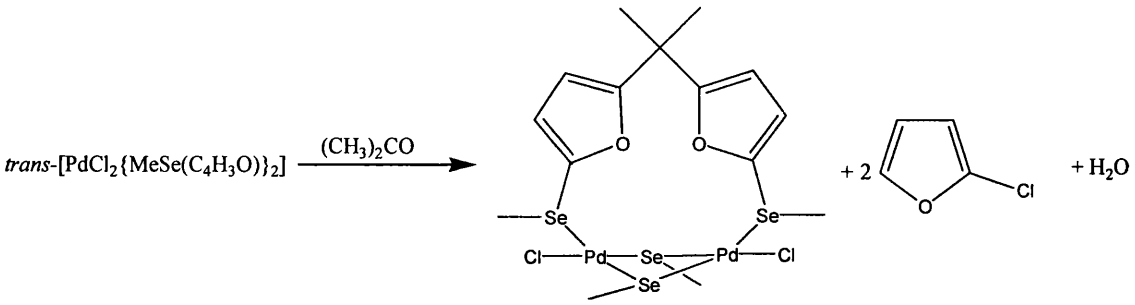

Monodentate ferrocenyl selenoethers are easily prepared by mono-lithiation of ferrocene and subsequent reaction with a diorganodiselenide and have been well studied.[33,34] Ferrocenyl selenoethers with a dimethylamino group *ortho* to the Se group will coordinate to Pt or Pd via Se and N (figure 1.4); these types of complexes can be used as catalysts in Grignard cross-coupling and hydrogenation reactions.

Figure 1.4:

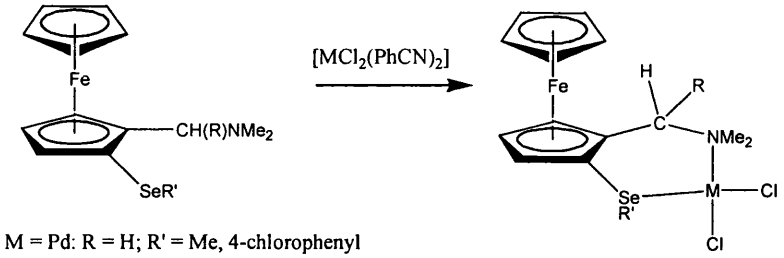

M = Pd: R = H; R' = Me, 4-chlorophenyl
R = Me; R' = Ph
M = Pt: R = H; R' = Me

1.4.2 Complexes Containing Bidentate Selenoether Ligands

Perhaps the most studied bidentate selenoether ligands are the compounds of the general formula $RSe(CH_2)_nSeR$ (R = alkyl, aryl; n = 1, 2, 3, 6, 12), which have been extensively reviewed in the literature.[14,21] The preparation of these complexes is straightforward; addition of the appropriate dihaloalkane to R_2Se_2 in $Na/NH_3(l)$/THF gives the diselenoether in mostly high yield.[35]

The methylene backboned diselenoethers $RSeCH_2SeR$ have been shown to exhibit both monodentate and bridging coordination to M(II) (M = Pt, Pd) centres (Figure 1.5); chelate coordination is not observed, presumably due to the high ring strain which would result from coordination to a single metal centre.[36] These species degrade to what is thought to be a polymeric species $[MCl_2(MeSeCH_2SeMe)_2]_n$.

Figure 1.5:

$$M'_2[MCl_4] + 2\ MeSeCH_2SeMe \xrightarrow[CH_2Cl_2]{EtOH} [MCl_2(MeSeCH_2SeMe)_2]$$

M' = Na; M = Pd
M' = K; M = Pt

In a similar reaction with the trimethylplatinum(IV) cation $MeSeCH_2SeMe$ is observed to form dinuclear complexes with the diselenoether bridging the metal atoms; in contrast $MeSe(CH_2)_2SeMe$ and $MeSe(CH_2)_3SeMe$ gave mononuclear complexes with both selenium atoms coordinated to one metal centre (figure 1.6). The same effect was also observed for the analogous dithioether complexes.[37]

Figure 1.6:

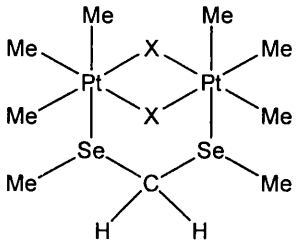

X = Cl, Br, I

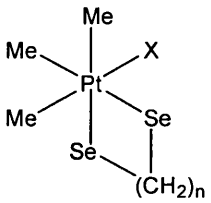

n = 2, 3

Longer chain diselenoethers are more likely to form bidentate chelate complexes with Pt(II) and Pd(II), and complexes of the type $[MCl_2L]$ (M = Pt, Pd; L = $RSe(CH_2)_nSeR$, $n \geq 2$) have been well investigated.[38,39,40,41] In particular the fluxional behaviour of these species due to the pyramidal inversion of the coordinated selenium atoms has been studied. [40,41,42,43,44,45] At room temperature there are two distinct geometric isomers which readily interconvert at elevated temperatures (figure 1.7); it has been found that the barrier to this inversion is lowest in diselenoethers (30-40 kJ mol^{-1}) and highest in dithioethers, with the mixed dichalcogenoethers having intermediate values.

Figure 1.7:

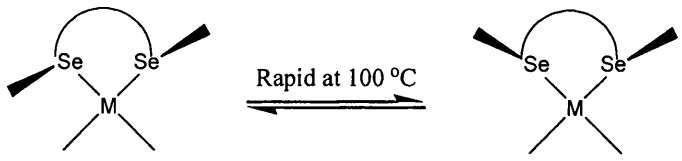

DL-isomer meso-isomer

Not all diselenoethers with a longer chain backbone exhibit bidentate chelating coordination; the diselenoether $^{i}PrSe(CH_2)_2Se^{i}Pr$ has been observed to form monomeric species with Pt(II) and Pd(II) in chloroform and dimeric species in acetone (figure 1.8).[46,47] As would be expected species with a still longer backbone do

not exhibit bidentate chelation due to the distance between the selenium atoms. The diselenoethers $MeSe(CH_2)_6SeMe$ and $MeSe(CH_2)_{12}SeMe$ react with $[PdCl_4]^{2-}$, giving what are believed to be polymeric species with the diselenoether ligands adopting a bridging role.[41]

Figure 1.8:

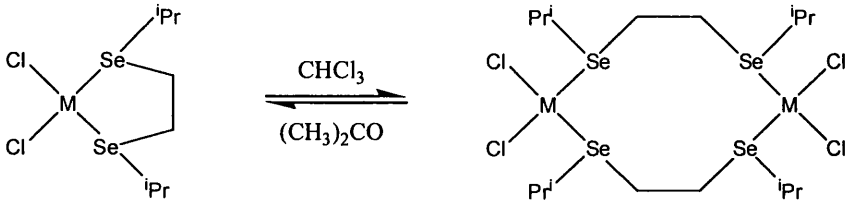

M = Pd, Pt

In addition diselenoethers with a ferrocene backbone can be prepared; reaction of dilithiated ferrocene with RSeSeR gives ferrocenyl selenoethers capable of bidentate coordination (figure 1.9).[33]

Figure 1.9:

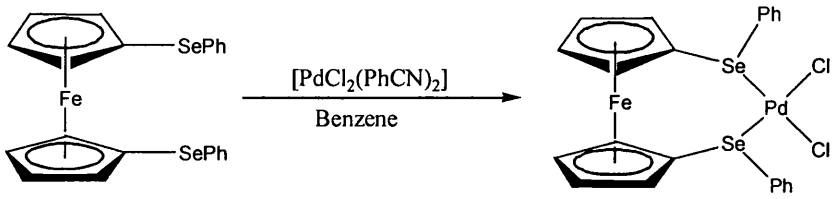

It is worthy of note that, if there is an amine group also connected to one of the Cp rings, then palladium will preferentially bind to the nitrogen and selenium of the same ring. A complex is formed similar to that in figure 4, with a redundant SeR group on the upper Cp ring.[48]

Ligands which exhibit bidentate coordination through selenium and a non-chalcogen group are common, for example unsaturated organoselenides. Here coordination through selenium and the unsaturated moiety is observed. Monosubstituted selenides readily coordinate to M(II) (M = Pd, Pt) to give complexes of the type $[MX_2L]$ (figure 1.10).[49]

Figure 1.10:

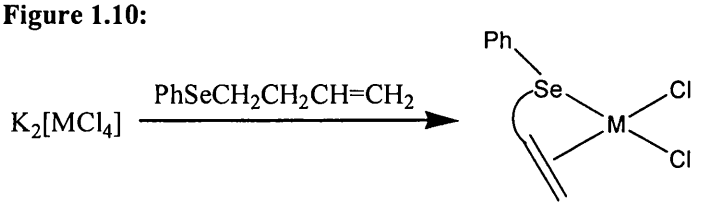

However, organoselenides disubstituted with unsaturated groups do not exhibit the expected tridentate coordination; instead bidentate coordination through selenium and one of the unsaturated moieties is observed, with the coordinated and uncoordinated alkene moieties undergoing facile exchange.[50] Further work has shown that these ligands can bridge to form dimeric species (figure 1.11).[51]

Figure 1.11:

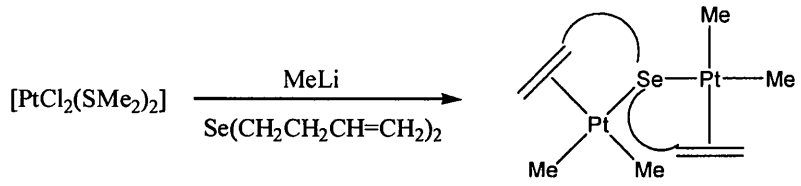

1.4.3 Complexes Containing Polydentate Selenoether Ligands

Reports on the chemistry of selenoethers containing three or more selenium atoms are sparser in the literature. Triselenoethers can act as tridentate ligands and chelate to one metal centre. The ligand 2,5,8-triselenanonane ($MeSe(CH_2)_2Se(CH_2)_2SeMe$) reacts with trimethylplatinum(IV) iodide to give a cation in which one ligand occupies all *trans*- sites of *fac*-Pt(IV)Me_3 (figure 1.12).[52,53] Fluxional NMR studies have shown that only the terminal selenium atoms can undergo pyramidal inversion in these triselenoether complexes.

Figure 1.12:

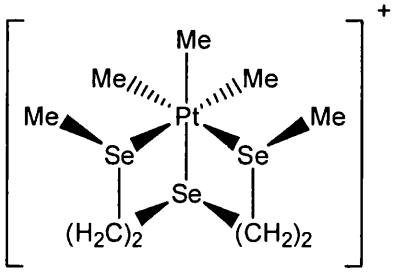

Triselenoethers may not always use all three selenium atoms to coordinate to a metal centre. For example 1,1,1-tris(methylselenomethyl)ethane (tmse) can only coordinate in a *cis*- bidentate fashion to planar metal centres (figure 1.13) due to steric constraints. However, its isomer, bis(3-methylselenopropyl)selenide (bmsp) can coordinate to a metal centre through all three selenium atoms.[54]

Figure 1.13:

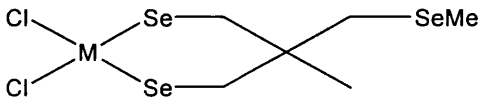

M = Pd, Pt

The first quadridentate selenoether 1,3-bis(methylselenoethylseleno)propane (bsep) was prepared in 1976.[55] Quadridentate coordination to one d^8 metal centre wasn't observed; instead the dimeric species $[Pd_2X_4L]$ (X = Cl, Br, I; L = bsep) (figure 1.14) was formed when $Na_2[PdX_4]$ was reacted with the ligand.

Figure 1.14:

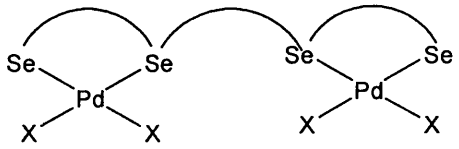

When the analogous nickel chemistry was attempted, octahedral $[Ni_2I_4L]$ was formed; the species is believed to be polymeric with the proposed structure shown in figure 1.15. The analogous thioether forms a complex of the type '$[NiX_2(S_4)]$'. It is unknown whether the difference in behaviour is due to a steric or electronic effect.

Figure 1.15:

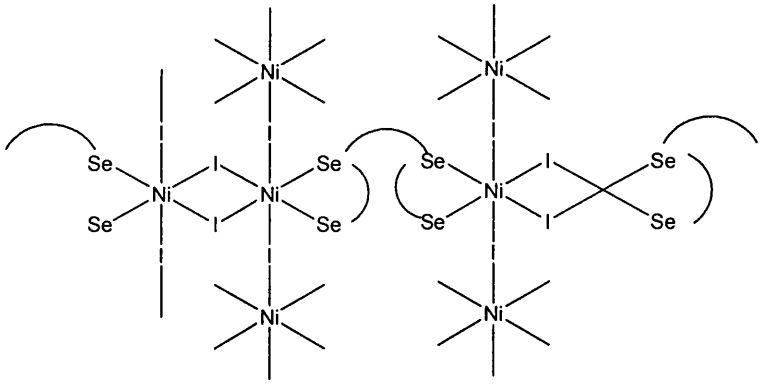

Recently the coordination chemistry of macrocyclic selenoethers has been investigated. Heavier chalcogen analogues of crown ethers are of particular interest due to their redox activity, thus finding use as metalloenzyme and metalloprotein models.[56,57] The syntheses of these macrocyclic selenium ligands is straightforward, typical preparations involving the reaction of the desired *bis*(selenocyanato)alkane with sodium, followed by the addition of the appropriate dihalogenated alkane (figure 1.16).[58]

Figure 1.16:

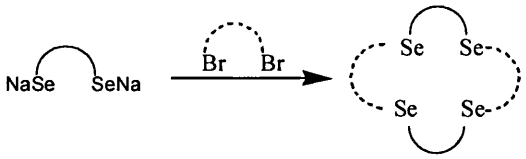

Typically chain lengths of 1-3 carbon atoms are used

In a study examining the ability of these macrocycles to extract heavy metals from solution it was found that they coordinate in a bidentate manner, forming $[MCl_2L]$ or $[\{MCl_2\}_2L]$ (M = Pd, Pt).[59] It was later shown that the selenium coronands [14]aneSe_4, [16]aneSe_4, [24]aneSe_6 *etc.* could act as quadridentate ligands with Pd(II) and Pt(II) (figure 1.17).[60] The metal has square planar geometry and sits in the middle of the ligand.

Figure 1.17:

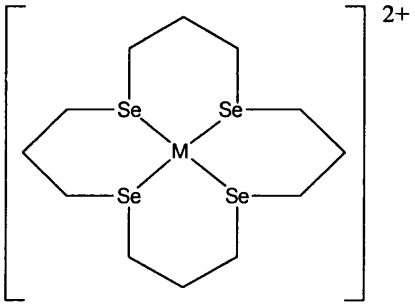

$[M([16]aneSe_4)]^{2+}$
M = Pd, Pt

Upon increasing the size of the macrocycle it is possible to coordinate two metal centres. With a controlled reaction stoichiometry [24]aneSe_6 will react with $PdCl_2$ to give $[(PdCl)_2[24]aneSe_6]^{2+}$.[61] This complex can be electrochemically reduced to give a Pd(I)-Pd(I) bonded dimer (figure 1.18).

Figure 1.18:

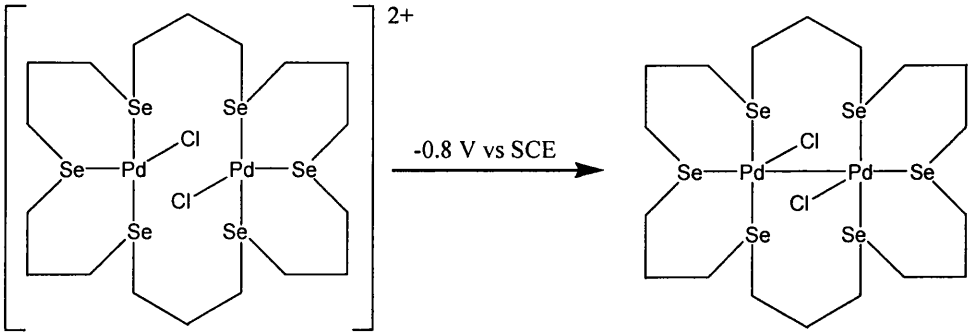

1.4.4 Complexes of Unsaturated Diselenoethers

Unsaturated diselenoethers are synthesised by the stereospecific reaction of a terminally dihalogenated alkene with RSe^- in the presence of NaOEt.[35] The unsaturated diselenoether is produced in moderate yield only; this has resulted in less investigation being carried out on these species. The main difference between unsaturated and saturated diselenoethers is the 'bite' angle of the ligand; unsaturated diselenoethers are typically restricted to forming monomeric *cis*-planar structures (figure 1.19).[26,41]

Figure 1.19:

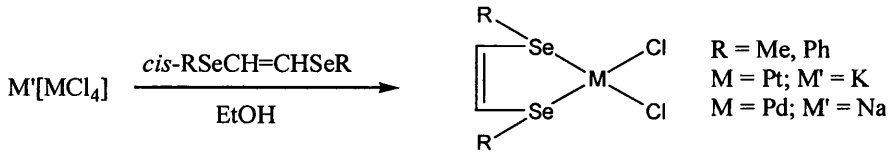

Other ligands of this type are the *o*-phenylene diselenoethers. These were first synthesised in low yield (5%) by the direct reaction of RSeSeR with benzyne.[35] Later an alternative synthesis from dibromobenzene (figure 1.20) was found to give a much better yield (53%).[62]

Figure 1.20:

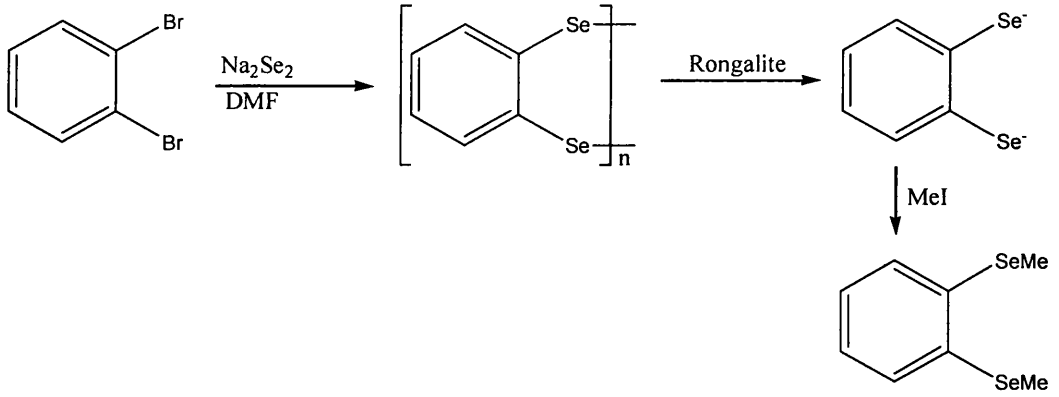

These unsaturated diselenoethers will complex with trimethylplatinum(IV) halides, giving $[PtXMe_3(MeSeBSeMe)]$ (X = Cl, Br, I; B = *cis*-HC=CH, *o*-C_6H_4).[63] These complexes can also be generated by halogen oxidation of $[PtCl_2(MeSeBSeMe)]$, as has been seen for simple monodentate selenoethers. The analogous Pd(IV) species cannot be prepared in this case.[26] This is presumably due to the moderate σ-donor properties of the ligands, resulting in them not being able to stabilise this higher oxidation state for Pd.

1.5 Phosphines as Ligands in Transition Metal Complexes

Tertiary phosphines (PR_3, R = alkyl or aryl group) are used as ligands in a wide variety of transition metal complexes. The reasons for this are the relatively easy synthesis of tertiary phosphines and their properties; these properties depend on the nature of the phosphine substituents.

1.5.1 Synthesis

The syntheses of phosphines trisubstituted with alkyl/aryl groups are relatively straightforward: reacting PCl_3 with organolithium[64] or Grignard (RMgX, X = Cl, Br, I)[3] reagents gives the trialkyl/aryl phosphines. The product will depend on the stioichiometry of the reactants and by careful control it is possible to synthesise phosphines with mixed substituents (figure 1.21).

Figure 1.21:

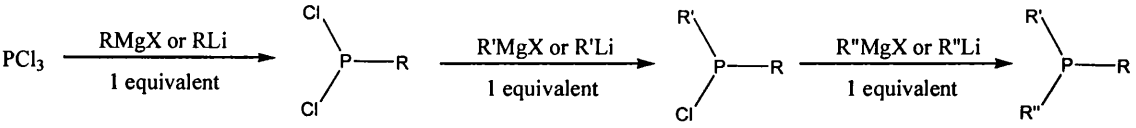

X = Cl, Br, I
R, R', R" = alkyl/aryl group

1.5.2 The Metal-Phosphine Bond

Phosphines, like CO, are classed as π-ligands and they form a synergic bonding system with transition metals. The lone pair of the phosphine acts as a weak donor and forms a σ-bond with the metal; in turn there is electron donation from the d-orbitals of the metal to the phosphine (π-backbonding). In the classical model phosphorus utilises a pair of its 3d orbitals to accept metal electrons,[65] but, recently a model has been proposed (using quantum mechanical calculations) in which the phosphine utilises the P-R σ* antibonding orbital formed from the phosphorus 3p orbitals;[66,67,68,69,70] both of these models are shown in figure 1.22. This π-backbonding increases the strength of the metal-phosphine bond; it is however, dependent on the substituents of the phosphine. In general the π-backbonding is greatest for phosphines with highly electron-withdrawing substituents (e.g. PF_3), but strongly electron-withdrawing substituents will also cause some weakening of the M-P σ-bond.

Figure 1.22:

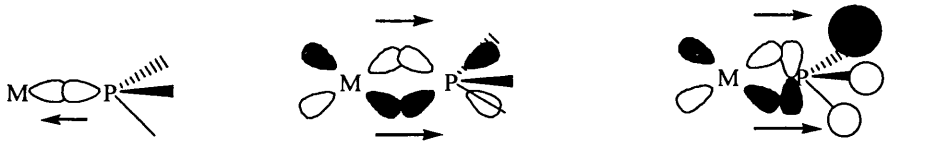

P-M sigma bond Classical M-P pi backbonding Alternative M-P pi backbonding

1.5.3 Steric Factors

A wide variety of PR_3 compounds can be synthesised, and it is known that their steric influence is directly dependent on the bulk of the R group. In 1970 Tolman studied the ligand exchange equilibria of a wide range of $[Ni(PR_3)_4]$ (R = alkyl/aryl group) complexes,[71] and he found that the steric effects of the ligand were much more important than electronic factors. It was found that in general smaller ligands gave the most stable complexes, as it is easier to fit four small ligands around the relatively small Ni(0) than four larger ligands. It was on the basis of these findings that Tolman proposed the 'cone angle' (figure 1.23) as a quantitative measure of a phosphine's size, and thus steric influence. The spheres shown are the van der Waals radii of the substituents.

Figure 1.23:

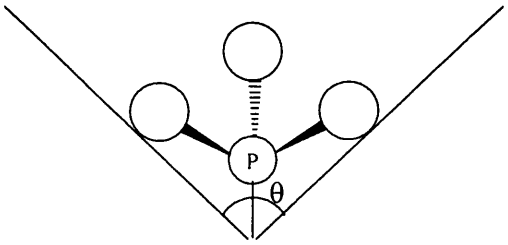

Tolman's cone angle

Tolman further proved the importance of steric effects by investigating the substitution reactions of $[Ni(CO)_4]$ with various phosphines: he found that the degree of substitution was completely dependent on the cone angle of the phosphine. The degree of substitution ranged from 3.7 for $P(OCH_2)_3CCH_3$ (cone angle = 101°), to 0.3 for $P(C_6F_5)_3$ (cone angle = 184°). Tolman later extended this work by proposing a method by which the cone angle of unsymmetrical ligands could be calculated (figure 1.24).[72] The effective cone is defined by the relation $\theta = 2/3 \sum\theta_i/2$ (i = 1-3).

Figure 1.24:

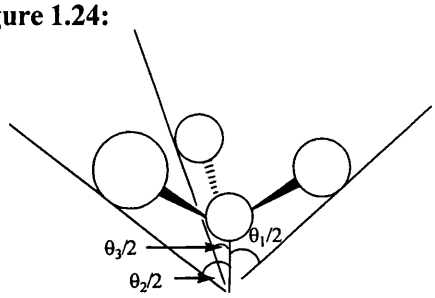

Tolman's cone angle for unsymmetrical phosphines

Investigation into the steric influence of phosphines has been extended to the other group 10 metals,[73] and it has been found that M(0) (M = Ni, Pd, Pt) phosphine complexes can exhibit coordination numbers of 2, 3 or 4 depending on the size of the phosphine ligand(s). A study carried out on the synthesis and reactions of palladium phosphine complexes has shown that an equilibrium exists between $[PdL_n]$ (L = phosphine; n = 3, 4) and free L.[74]

$$1.\ PdL_4 \rightleftharpoons PdL_3 + L$$
$$2.\ PdL_3 \rightleftharpoons PdL_2 + L$$

For smaller phosphines such as PEt_3 and PBu_3 (θ = 130°) equilibrium 1 applies in solution and can be driven to the right under vacuum. For the phosphine $PMePh_2$ (θ = 136°) the equilibrium lies to the left. For medium sized phosphines such as PPh_3 (θ = 145°) both equilibria apply in solution, and for large phosphines such as PCy_3 (θ = 179°) the dominant species is PdL_2. PdL_2 is a 14 electron species and from an electronic point of view is not stable, but if a large enough phosphine is used then the steric effect gives the compound stability. This is exemplified by the compounds $[Pd(PPh^tBu_2)_2]$ and $[Pd(P^tBu_3)_2]$:[75] $[Pd(PPh^tBu_2)_2]$ reacts readily with O_2 to give the complex $[PdO_2(PPh^tBu_2)_2]$; $[Pd(P^tBu_3)_2]$ however, is stable in air but will react with hydrogen. It is believed that this stability towards air is due to the ligands (P^tBu_3, θ = 182°) shielding the palladium from O_2; the reaction with hydrogen is possible though, as H_2 is much smaller than O_2 and can thus find its way to the palladium.

1.5.4 NMR

Modern NMR techniques have permitted the study of many nuclei other than ^1H; among these is ^{31}P which, with a spin of ½, a natural abundance of 100% and a receptivity 7% that of ^1H, is ideally suited for NMR studies.[76] These properties have resulted in ^{31}P NMR spectroscopy becoming a routinely used tool in both organic and

inorganic chemistry. In metal complexes containing phosphine ligands, if the metal has a spin active isotope then the M-P coupling contants can be used to give information about the substituents and geometry of a complex. For example, $^{1}J(^{31}P\text{-}^{195}Pt)$ in square planar Pt(II) complexes is sensitive to the substituent *trans-* to the phosphine group, the value increasing as the electron-withdrawing ability of the substituent increases. This can be used to determine the geometry of a complex: it is observed that *cis*-$[PtCl_2(PEt_3)_2]$ has a $^{1}J(^{31}P\text{-}^{195}Pt)$ coupling of approximately 3500 Hz, whereas for *trans*-$[PtCl_2(PEt_3)_2]$ the coupling is approximately 2400 Hz; these values allow an easy differentiation of *cis-* and *trans-* isomers.[66]

1.5.5 Metal Phosphine Complexes in Catalysis

Metal complexes containing phosphine ligands have found a wide variety of uses, but perhaps the area where they have made the most impact is in catalysis. Successful catalysis by an organometallic complex is dependent on that complex's ability to switch between 18 electron species and 16 electron species by the removal/addition of, or reaction with a ligand.[77] It is also now accepted that 17 and 19 electron species may take part in catalysis under some conditions.[78] The electronic and steric properties of phosphines (as discussed above) make them useful ligands for stabilising the intermediate states during a catalytic cycle. Here a few of the catalytic applications of metal phosphine complexes are discussed.

One of the first complexes containing phosphine ligands to be used in catalysis was Wilkinson's catalyst $[RhCl(PPh_3)_3]$.[79,80] This complex was found to catalyse the hydrogenation of alkenes and alkynes at room temperature with a H_2 pressure of 1 bar (figure 1.25); later the catalyst $[RhH(CO)(PPh_3)_3]$ was synthesised which specifically hydrogenates terminal alkenes (figure 25).[81] $[RhH(CO)(PPh_3)_3]$ is also the catalyst used in the Union Carbide hydroformylation process.[64]

Figure 1.25:

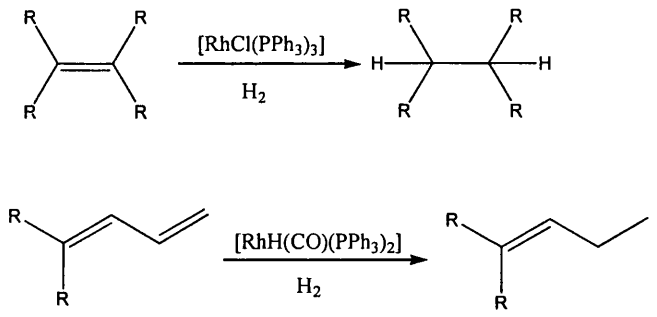

R = H or alkyl group

The specificity of these catalytic hydrogenation reactions has been increased further by the use of the species $[RhL_2(solvent)_2]^+$ (solvent = THF/CH_3CN),[82] where L_2 is an optically active diphosphine such as DIOP or CHIRAPHOS (figure 1.26).[83,84] These species asymmetrically catalyse the hydrogenation of prochiral, unsaturated species to chiral products, often with high optical purity.

Figure 1.26:

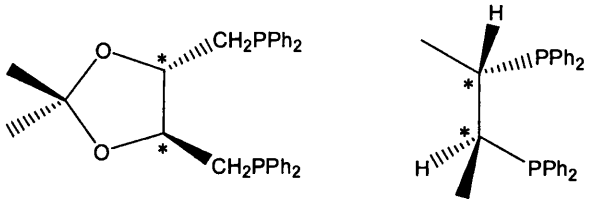

DIOP CHIRAPHOS

Investigation into the use of metal complexes with phosphine ligands as catalytic C-H bond activators has been carried out.[85] It has been found that polyhydride complexes such as $[IrH_5\{P(CH_3)_3\}_2]$ and $[ReH_5\{P(CH_3)_3\}_2]$ catalyse the H/D exchange between benzene and D_2. In the complex *trans*-$[Pt_2Cl_2(\mu_2\text{-}Cl)_2(P^iPr_3)_2]$ the platinum can insert into the C-H bonds of the methyl groups of ^{i}Pr, and in the presence of D_2O deuterium incorporation into the phosphine ligand is observed.

Another area where these complexes find use is in the catalysed formation of C-C bonds; examples of this include the Heck reaction[86] and the use of Grubbs' catalyst.[87,88] In the Heck reaction $[Pd(PR_3)_4]$ (R = aryl) reacts with an aryl bromide R'Br to give $[Pd(Br)R'(PR_3)_2]$; this then reacts with an α-olefin to give $[PdHBr(PR_3)_2]$ and a trans-arylated product (figure 1.27).

Figure 1.27:

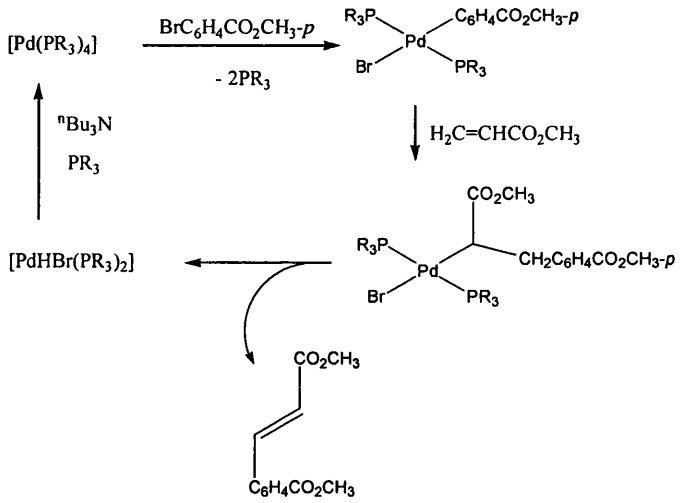

Grubbs' catalyst is a carbene complex of the type $[RuCl_2(=C\text{-}CH=CPh_2)(PR_3)_2]$ (R = Ph, Cy) which has found use as a ring opening metathesis polymerisation catalyst (figure 1.28); it has also recently found use as a ring closing metathesis catalyst, and many variations of the catalyst using different carbenes have been synthesised.

Figure 1.28:

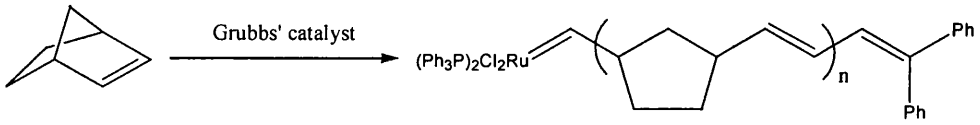

1.6 Complexes of 1,2,3-Selenadiazoles and 1,2,3-Thiadiazoles

Before the reactions of 1,2,3-selenadiazoles and 1,2,3-thiadiazoles are considered, a brief overview of the syntheses of these compounds is given.

1.6.1 The Syntheses of 1,2,3-Selena- and 1,2,3-Thiadiazoles

The first reported general synthesis of 1,2,3-selenadiazoles was by Lalezari and Shafiee in 1969 when an attempted synthesis of phenyl glyoxal keto-semicarbazone took an unexpected path. [89] They found that the reaction of acetophenone semicarbazone with SeO_2 in acetic acid gave 4-phenyl-1,2,3-selenadiazole in good yield (66%). This method has subsequently been used to synthesise a variety of 4,5-disubstituted 1,2,3-selenadiazoles (figure 1.29, E = Se).[90,91]

Figure 1.29:

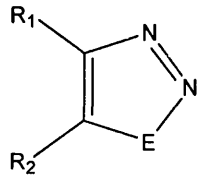

R_1, R_2 = alkyl, aryl
E = S, Se

In 1972 Meier and Voigt extended this synthesis to cycloalkeno-1,2,3-selenadiazoles (R_1-R_2 = $(CH_2)_n$) by reacting cyclic semicarbazones with SeO_2 in dioxane.[92] They used this method to synthesise cyclopenteno-, cyclohexeno-, cycloheptено- and cycloocteno-1,2,3-selenadiazoles.

1,2,3-Thiadiazoles (figure 1.29, E = S) can be synthesised by the reaction of acetylhydrazones, ethoxycarbonylhydrazones, *p*-tolylsulphonylhydrazones, or semicarbazones with thionyl chloride ($SOCl_2$). This method can be used for both 4,5-disubstituted 1,2,3-thiadiazoles and cycloalkeno-1,2,3-thiadiazoles.[93,94,95]

1.6.2 Complexes Containing 1,2,3-Selena- and 1,2,3-Thiadiazole Ligands

The only complexes reported containing intact 1,2,3-selenadiazole ligands are those of the group 6 carbonyls and Mn. Reaction of cycloalkeno-1,2,3-selenadiazoles with the group 6 carbonyl complexes $[M(CO)_5(THF)]$ (M = Cr, Mo, W), gave $[M(CO)_5$(selenadiazole)] (figure 1.30). [96] In addition the reaction of $[Mo(CO)_4(nbd)]$ (nbd = norbornadiene) and $[Mo(CO)_3(MeCN)_3]$ with cyclohexeno-1,2,3-selenadiazole

gave the complexes $[Mo(CO)_4(selenadiazole)_2]$ and $[\{Mo(CO)_3\}_2(selenadiazole)_3]$ respectively (figure 1.30). The dimeric species comprises three selenadiazole ligands bridging through both nitrogen atoms.

Figure 30:

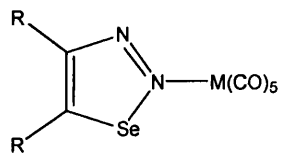

M = Cr,Mo,W
$R_2 = (CH_2)_n$
n = 4-6

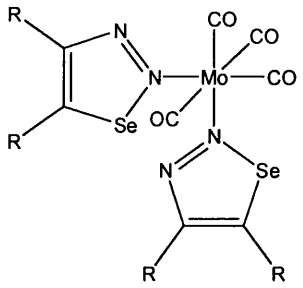

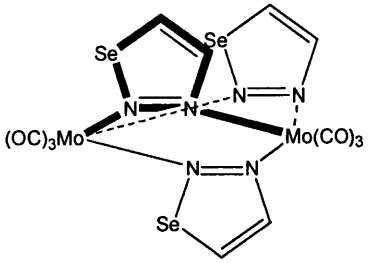

Selenadiazole substituents omitted for clarity

The reaction of $[Mn(\eta^5C_5H_4Me)(CO)_2(THF)]$ with 4-*tert*-butyl-, cyclohexeno- or cyclooctено-1,2,3-selenadiazole gives the complexes $[Mn(\eta^5\text{-}C_5H_4Me)(CO)_2(selenadiazole)]$ (figure 1.31).[97] The selenadiazole ligand is bound to the metal through the N(2) atom as was seen for the group 6 complexes.

Figure 1.31:

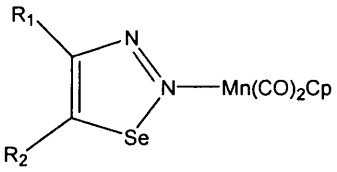

$R_1 = {}^tBu$; $R_2 = H$
$R_1 - R_2 = (CH_2)_4$
$R_1 - R_2 = (CH_2)_6$

Complexes containing 1,2,3-thiadiazole ligands analogous to the above species have also been synthesised. Of the group 6 carbonyl derivatives only $[W(CO)_5$(cyclooctено-1,2,3-thiadiazole)] has been synthesised.[96] However, all the manganese complexes analogous to those in figure 1.31 have been synthesised with 1,2,3-thiadiazoles as have the complexes $[MnCp'(CO)_2$(benzo-1,2,3-thiadiazole)] (Cp' = $\eta^5\text{-}C_5H_5$, $\eta^5\text{-}C_5H_4Me$).[97] In addition the complex $[PtCl_2(NH_3)$(benzo-1,2,3-thiadiazole)] (figure 1.32) has been synthesised by the reaction of $K[PtCl_3(NH_3)]$ with benzo-1,2,3-thiadiazole.[98] Here the 1,2,3-thiadiazole ligand is coordinated to platinum through the sulphur atom and not through the N(2) atom as seen with the group 6 and 7 species investigated.

Figure 1.32:

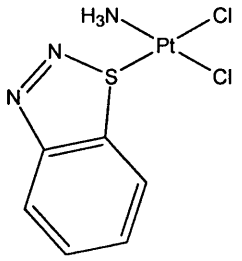

1.6.3 Reactions of 1,2,3-Selenadiazoles and 1,2,3-Thiadiazoles

Although reports of complexes containing intact 1,2,3-selena- and 1,2,3-thiadiazole ligands are rare, their reactions with the later transition metals are well known. The reaction of 1,2,3-selena- and 1,2,3-thiadiazoles with $[Fe_2(CO)_9]$ was investigated in the early 1970's by Rees and Schrauzer[99,100] in attempts to trap the 1,3-dipolar thiaketocarbenes and selenaketocarbenes. It was found that reaction of various 4,5-disubstituted 1,2,3-thia- and 1,2,3-selenadiazoles with $[Fe_2(CO)_9]$ at elevated temperatures gave a hexacarbonyldiiron-thia/selenaketocarbene complex (figure 1.33).

Figure 1.33:

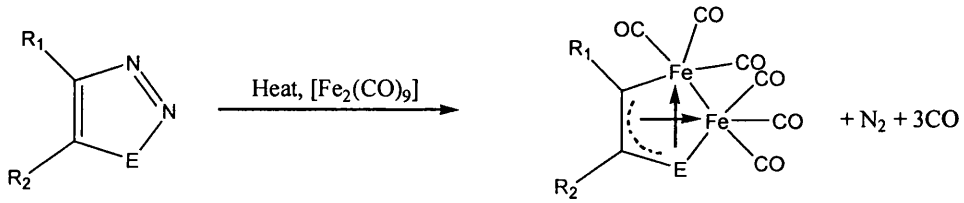

This reaction was further investigated by Mayr, Pannell and co-workers,[101] who found that the selenaketoketene complex shown in figure 1.34 is an intermediate,[102] and readily decarbonylates to give the product observed by Rees and Schrauzer.

Figure 1.34:

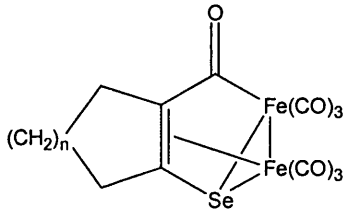

n = 2, 3, 4

Further work showed that 1,2,3-thiadiazoles would react with $[Fe_2(CO)_9]$ to give ring-opened products with partial or no loss of N_2. Several imine hexacarbonyldiiron complexes were synthesised,[103] and benzo-1,2,3-thiadiazole gave a linear triiron cluster containing two ring-opened diazole molecules (figure 1.35).[104] It is believed that these species are formed with 1,2,3-thiadiazoles and not 1,2,3-selenadiazoles due

to the stability of the α-diazothioketone which forms upon ring opening. If an α-diazoselenoketone is formed it immediately loses nitrogen to give a selenaketocarbene.

Figure 1.35:

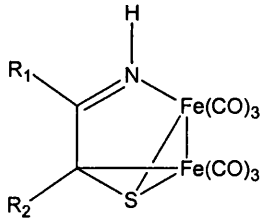

R_1-R_2 = $(CH_2)_4$, $(CH_2)_6$
R_1 = *p*-^{t}BuC_6H_5; R_2 = C_6H_5
R_1 = CH_3; R_2 = H
R_1 = ^{t}Bu; R_2 = H

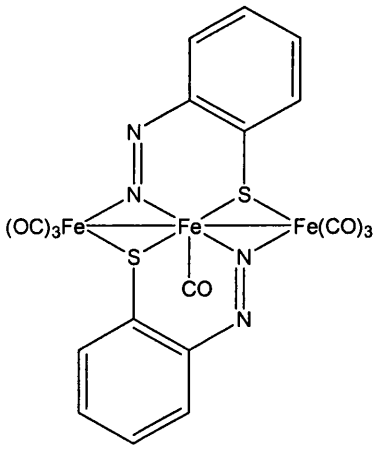

It has also been found that [$W(CO)_5$(cyclohexeno-1,2,3-thiadiazole)] will react with [$Fe_2(CO)_9$] to give the hexacarbonyldiiron thiaketocarbene complex and the imine hexacarbonyldiiron complex.[96] [$W(CO)_5$(cyclohexeno-1,2,3-selenadiazole)] will react with [$Fe_2(CO)_9$] to give the hexacarbonyldiiron selenaketocarbene complex, and [$W(CO)_5$(THF)] has been shown to decarbonylate the cyclohexeno-selenaketoketene complex giving the hexacarbonyldiiron selenaketocarbene complex.

The same research group later showed how 1,2,3-selenadiazoles could be used as precursors to metal-stabilised alkynes.[105,106] Reaction of [$Mo_2(\eta^5$-$C_5H_5)_2(CO)_4$] with 4-phenyl-1,2,3-selenadiazole gave [$Mo_2(\eta^5$-$C_5H_5)_2(\mu$-η^2,η^2-PhCCH)$(CO)_4$] in good yield. When cycloalkeno-1,2,3-selenadiazoles were used in the reaction, intermediates could be isolated and are shown in figure 1.36.

Figure 1.36:

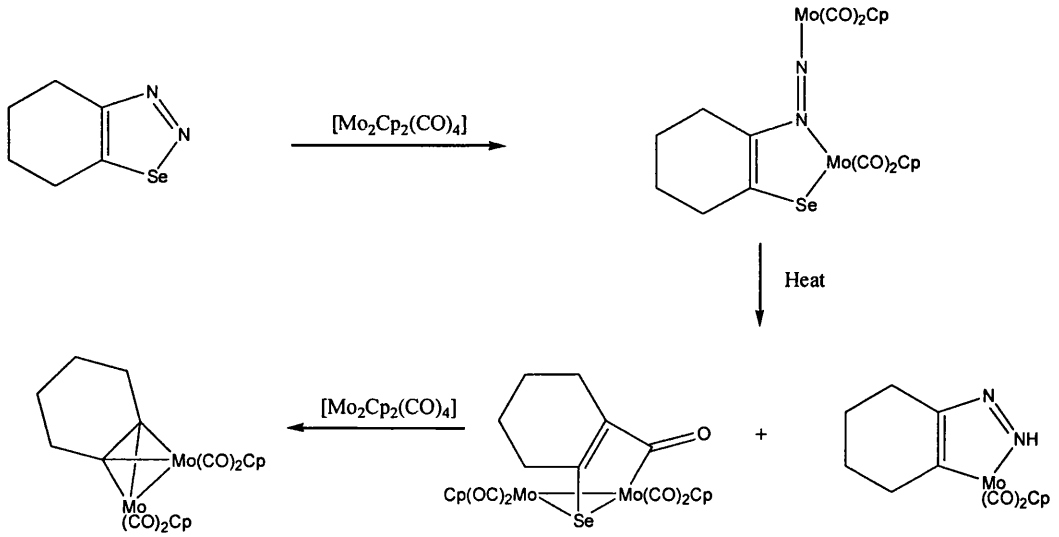

The hydrazonato complex is a dead end in the transformation; it decomposes without formation of isolable products.

In 1987 Morley and co-workers began investigating the reactions of cobalt complexes with 1,2,3-selenadiazoles.[107] They found that the reaction of cycloocta-1,2,3-selenadiazole with $[Co(\eta^5\text{-}C_5H_5)(PPh_3)_2]$ in refluxing toluene gave a selenaketocarbene complex (figure 1.37) analogous to the hexacarbonyldiiron selenaketocarbene complex shown in figure 1.33. This is not surprising as CoCp is isolobal with $Fe(CO)_3$.[108] The reaction was also found to proceed at room temperature using $[Co(\eta^5\text{-}C_5H_5)(C_2H_4)_2]$ in ether, and was later extended to 6,7-dihydrocycloocta-, 6,7,8,9-tetrahydro- and 4,5,6,7,8,9-hexahydrocycloocta-1,2,3-selenadiazoles.[109]

Figure 1.33:

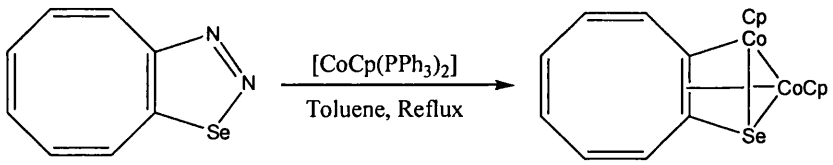

The reaction of $[Co(\eta^5\text{-}C_5Me_5)(C_2H_4)_2]$ with these 1,2,3-selenadiazoles gave quite different products.[109] In this case the products were mononuclear with a structure dependent on the degree of unsaturation of the 1,2,3-selenadiazole. For cycloocta- and 6,7-dihydrocycloocta-1,2,3-selenadiazoles, incorporation of a C_2H_4 unit leads to a product with a 5-membered heterocyclic ring system; whereas 6,7,8,9-tetrahydocycloocta and 4,5,6,7,8,9-hexahydrocycloocta-1,2,3-selenadiazole give a product with a 4-membered heterocyclic ring system and an intact 1,2,3-selenadiazole

ligand (figure 1.38). The formation of mononuclear products is believed to be due to the steric effect of the Cp* substituent and the reaction is believed to proceed via the Co-C_2H_4 intermediate shown.

Figure 1.38:

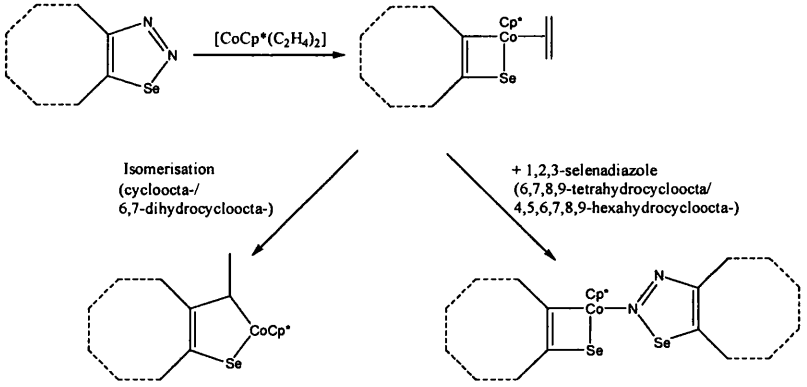

It was also found that the reaction of $[Co(\eta^5\text{-}C_5H_5)(PPh_3)_2]$ or $[Co(\eta^5\text{-}C_5R_5)(CO)_2]$ (R = H or Me) with 1,2,3-selenadiazoles, in the presence of excess elemental selenium, leads to the formation of cyclopentadienyl/pentamethylcyclopentadienylcobalt diselenolenes.[110,111] The reaction is believed to proceed via a cobalt selenaketocarbene intermediate (figure 1.39) which then undergoes a C-Se bond formation to give the diselenolene in moderate yield.

Figure 1.39:

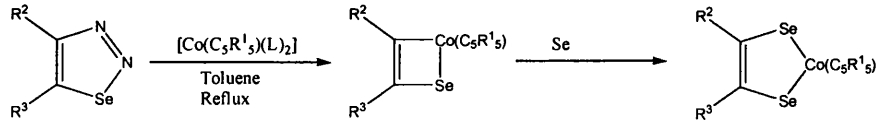

L = CO, PPh_3
R^1 = H: R^2 = Ph; R^3 = H
R^2 = Ph; R^3 = Ph
R^2-R^3 = $(CH_2)_6$,
CH=CH-$(CH_2)_4$,
CH= CH-$(CH_2)_2$-CH=CH

R^1 = Me: R^2 = Ph,; R^3 = H
R^2-R^3 = $(CH_2)_6$,
CH=CH-$(CH_2)_4$,
CH= CH-$(CH_2)_2$-CH=CH

For cyclocteno-1,2,3-selenadiazole, if excess elemental sulphur is used instead of selenium then a cyclopentadienylcobalt dithiolene can be formed.[112] When this reaction was performed with one equivalent of sulphur the thiaselenolene was also produced, but it was found that the dithiolene was still the favoured product by a molar ratio of 1.5:1 (figure 1.40).

Figure 1.40:

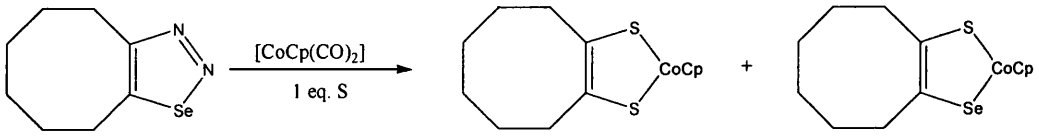

1.5:1

Evidence was found that a Se_3-chelate species (figure 1.41)[113] could be formed by direct reaction of cycloocteno-1,2,3-selenadiazole with $[Co(\eta^5\text{-}C_5H_5)(CO)_2]$ and elemental selenium or by the reaction of the cyclopentadienylcobalt diselenolene with cycloocteno-1,2,3-selenadiazole and elemental selenium.

Figure 1.41:

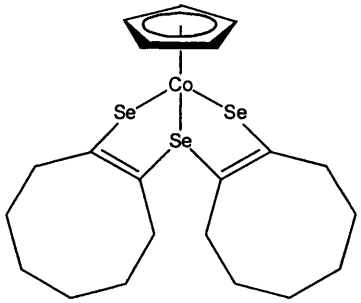

Morley's group then went on to look at some reactions of platinum and palladium complexes with cycloalkeno-1,2,3-selenadiazoles. They found that the reaction of cycloocteno-1,2,3-selenadiazole with $[Pt(PPh_3)_4]$ gave two products, a selenaketocarbene complex and a species believed to be polymeric (figure 1.42).[114]

Figure 1.42:

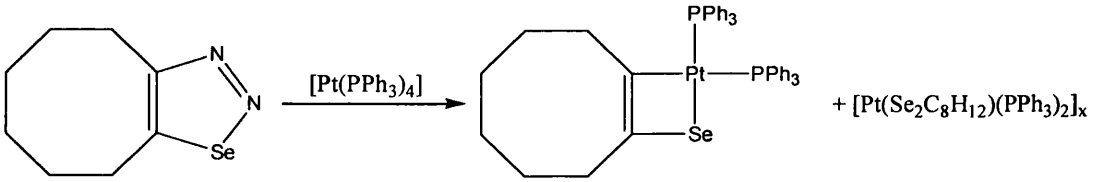

Investigation of the reaction of Pd(0) phosphine complexes with cycloalkeno-1,2,3-selenadiazoles found that two types of product could be formed, dependent on the phosphine used. When trialkylphosphinepalladium(0) complexes were used compounds with the general formula $[PdL(PR_3)]$ (R = Et, Bu) were isolated, where L is a Se,N,Se tridentate ligand (figure 1.43).[115,116]

Figure 1.43:

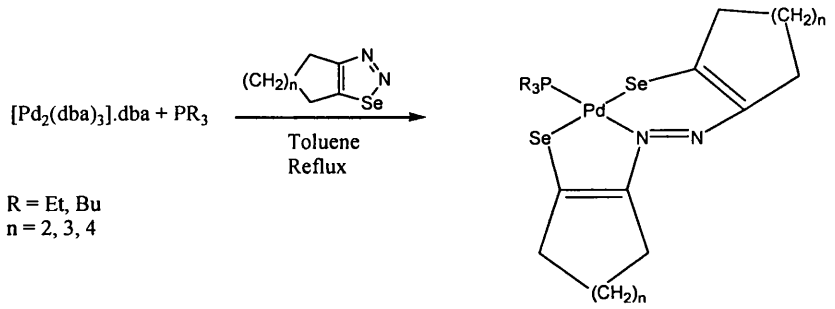

When $[Pd(PPh_3)_4]$ was used then a dinuclear diselenolene was isolated (figure 1.44).[117] It was found that at slightly lower temperatures, trace amounts of $[PdL(PPh_3)]$ (L as above) were also formed. The formation of the dinuclear

diselenolene is believed to proceed via the formation of a 1,4-diselenin from the 1,2,3-selenadiazole.[92]

Figure 1.44:

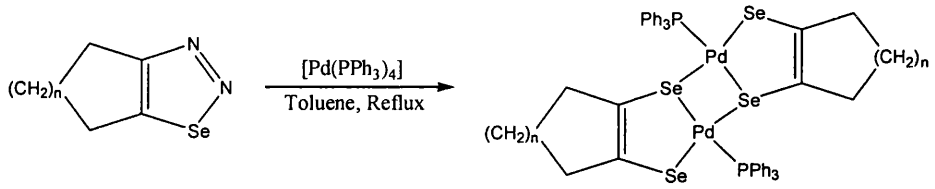

Recently the reaction of $[Pt(PPh_3)_4]$ with 4-methyl-5-ethoxycarbonyl-1,2,3-selenadiazole in toluene, in a sealed vessel, has been shown to give a complex of the type $[PtL(PPh_3)]$ (figure 1.45),[118] where L is a Se,N,Se tridentate ligand analogous to that in figure 1.43. The complex was found to act as a selective catalyst in the hydrosilylation of terminal acetylenes.

Figure 1.45:

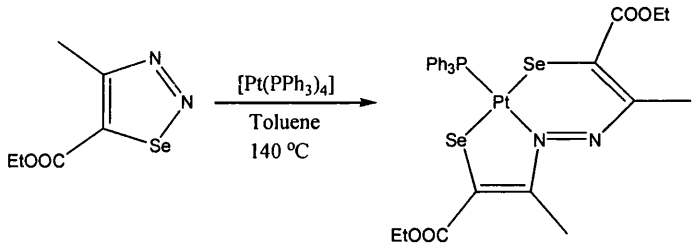

1.7 Synthesis and Reactions of 1,4-Diselenins

1,4-Diselenins can be synthesised from cyclic 1,2,3-selenadiazoles by vacuum pyrolysis,[92,119] or by refluxing in xylene in the presence of elemental selenium (figure 1.46).[120]

Figure 1.46:

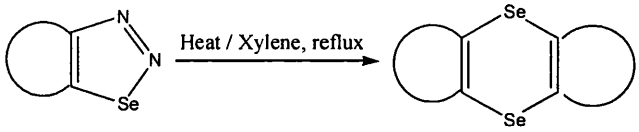

Despite this ready preparation there has been little investigation of the chemistry of 1.4-diselenins. In 1985 Mayr, Pannell and co-workers investigated the reactions of $[Fe_2(CO)_9]$ with some *bis*-cycloalkeno-1,4-diselenins.[121] They found that a variety of products were given, some of which were dependent on the size of the cycloalkene ring (figure 1.47).

Figure 1.47:

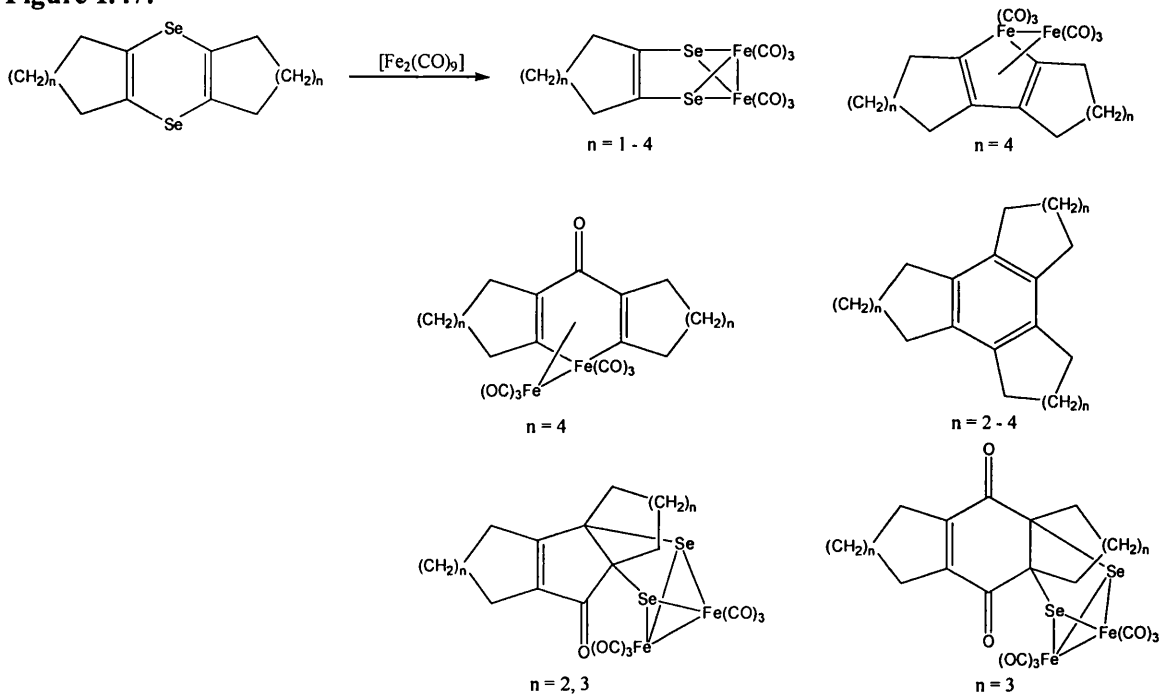

It had been previously reported that the reaction of tetraphenyl-1,4-dithiin with $[Fe_2(CO)_9]$ gave analogues of the first three products in figure 1.47.[122] Mayr and Pannell repeated the reaction and found a diironhexacarbonyl-diphenylacetylene complex and hexaphenylbenzene to be present. The presence of the acetylene may explain the formation of the hexa-substituted benzene species in figure 1.47.

At around the same time the coordination of intact selanthrene (*bis*-benzo-1,4-diselenins) ligands to some group 10, 11 and 12 metals was reported.[123,124] It was

found that 2,3,7,8-tetramethoxyselanthrene and 2,3,7,8-*bis*(methylenedioxy)selanthrene would coordinate to these metals forming $[PdCl_2L_2]$, $[PtCl_2L]$, $[AgL]NO_3$ and $[HgCl_2L]$ (L = selanthrene ligand). Note the difference in behaviour of Pd which coordinates two selanthrene ligands.

Recently Morley's group has investigated the reactions of *bis*-cycloalkeno-1,4-diselenins with platinum and palladium. They found that the reactions of *bis*-cycloheptено-1,4-diselenin and $[MCl_2(PhCN)_2]$ (M = Pd, Pt) gave different products (figure 1.48).[125] In the reaction of the palladium compound the expected $[MCl_2L_2]$ complex was formed; for platinum however, an oxidative addition of a C-Se bond to Pt(II) occurs and a dinuclear Pt(IV) complex is formed.

Figure 1.48:

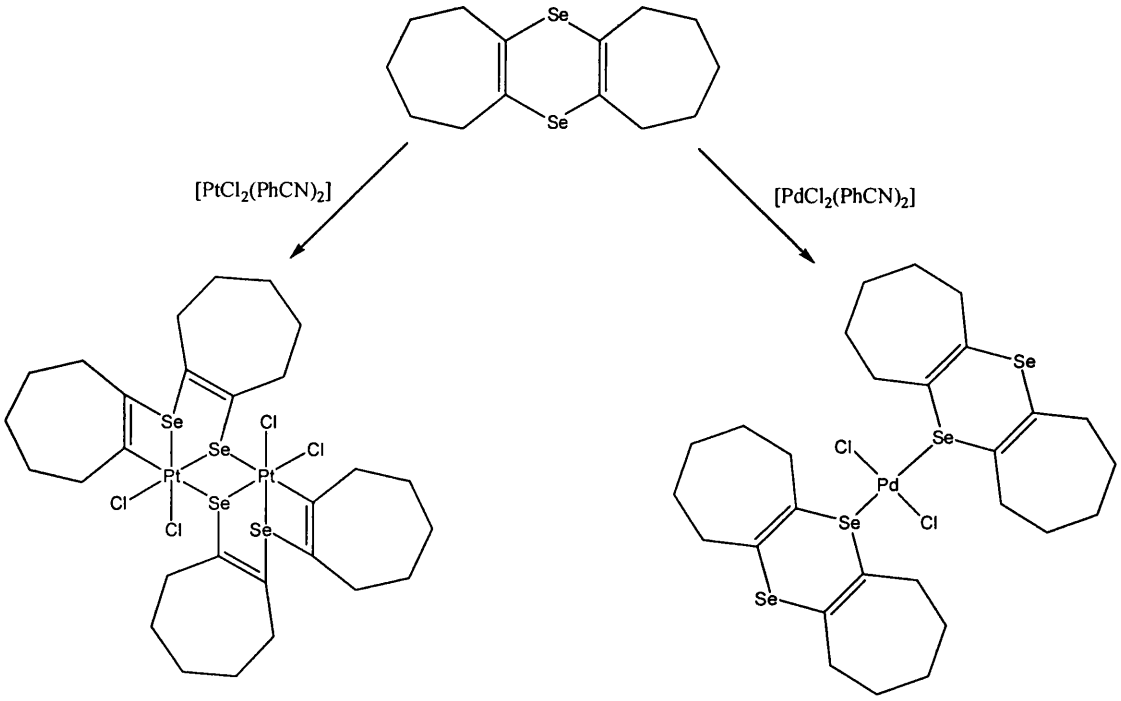

They have also investigated the reactions of some Pd(0) complexes with *bis*-cycloalkeno-1,4-diselenins. They found that the reactions of $[Pd(PPh_3)_4]$ with a *bis*-cycloalkeno-1,4-diselenin gave a dinuclear diselenolene of the type in figure 1.44.[117] Similarly the reaction of $[Pd_2(dba)_3].dba$ with PBu_3 and a *bis*-cycloalkeno-1,4-diselenin gives a dinuclear diselenolene if two equivalents of phosphine are used, or a mononuclear diselenolene if four equivalents of phosphine are used (figure 1.49).[126,127]

Figure 1.49:

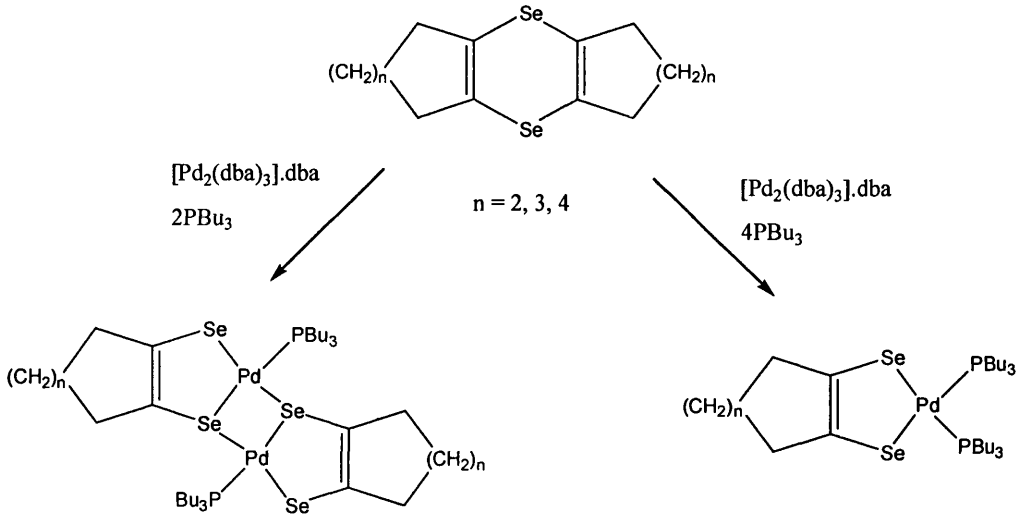

It was found that the tributylphosphine dinuclear diselenolenes reacted with dppe (1,2-*bis*(diphenylphosphino)ethane) to give the mononuclear diselenolenes $[Pd(Se_2C_{n+4}H_{2n+4})(dppe)]$ in good yield.

1.8 Synthesis and Reactions of 1,2-Diselenins and Other Compounds with an Se-Se Bond.

The chemistry of 1,2-diselenins, like that of 1,4-diselenins, has not been well explored. 1,2-Diselenins with an aromatic backbone (figure 1.50) are most common due to their relatively easy synthesis from brominated aromatic systems via lithiation and subsequent treatment with elemental selenium.[128,129,130] Recently the synthesis of 1,2-diselenins 3,6-disubstituted with ^{i}Pr or ^{t}Bu has been documented.[131] The synthesis involves the treatment of butadienes with $Ti(O^{i}Pr)_4$; subsequent treatment with elemental selenium and reduction gives the 3,6-disubstituted-1,2-diselenins.

Figure 1.50:

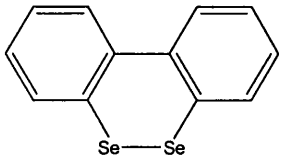

bis-benzo-1,2-diselenin

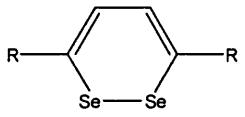

3,6-disubstituted-1,2-diselenin
R = ^{i}Pr, ^{t}Bu

There are no reported reactions of 1,2-diselenins with transition metal complexes; there is a report, however, on the reaction of a 1,2-dithiin with $[Pt(COD)_2]$.[132] The report documents the oxidative insertion of $[Pt(COD)_2]$ into the S-S bond of diacenaphtho[1,2-c:1',2'-e]-1,2-dithiin, giving $[Pt(S_2C_{24}H_{12})(COD)]$ (figure 1.51).

Figure 1.51:

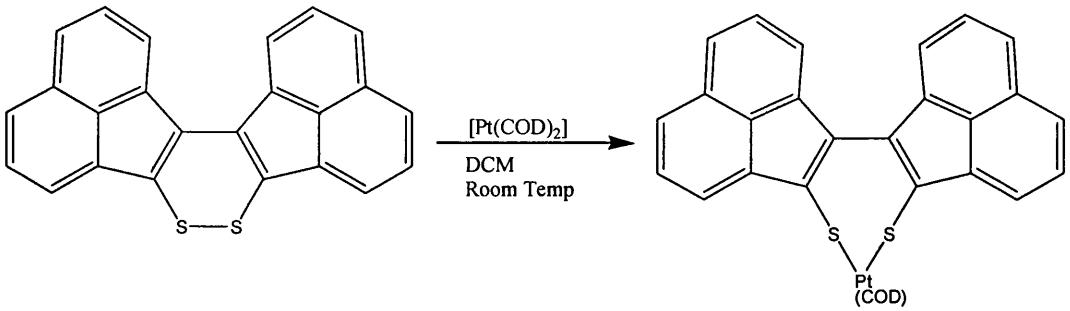

There have been some reports of cyclic compounds containing an Se-Se bond reacting with transition metal complexes. The group of Abel and Orrell has reported on the reactions of 4,4-dimethyl-1,2-diselenacyclopentane with Pt(IV)[133,134] and Re(I)[135] complexes. They found that the reactions of $[Pt_4Me_{12}I_4]$ and $[Re_2Cl_2(CO)_6(THF)_2]$ with 4,4-dimethyl-1,2-diselenacyclopentane gave $[Pt_2Me_6I_2(SeCH_2CMe_2CH_2Se)]$ and $[Re_2Cl_2(CO)_6(SeCH_2CMe_2CH_2Se)]$ respectively; both complexes are dinuclear and

contain an intact molecule of 4,4-dimethyl-1,2-diselenacyclopentane which bonds via Se to the metal centres (figure 1.52).

Figure 1.52:

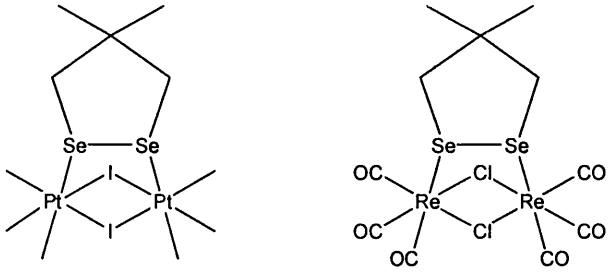

The reactions of 4,4-dimethyl-1,2-diselenacyclopentane with $[MX(CO)_5]^-$ (M = Cr, Mo, W; X = Cl, Br, I) in the presence of a Lewis acid were also investigated.[136] It was found that the ligand would coordinate to the metal through one selenium atom to give complexes of the type $[M(CO)_5(SeCH_2CMe_2CH_2Se)]$. It was found that a 1,2-metal shift process occurs, with the metal able to bond to either selenium; a variable temperature NMR study showed this process to be rapid at >80 °C. The complexes $[M(CO)_5(EE'C_{10}H_6)]$ (E = S; E' = S, Se) were also prepared from naphtho[1,8-c,d]-dithiole and diselenole, and were observed to show no 1,2-metal shift. Complexes of a similar ligand - tetrathionaphthalene (TTN, $C_{10}H_4S_4$) - have been investigated for their potential electronic uses.[137,138]

As part of their investigation of the syntheses and reactions of heterocyclic rings containing nitrogen and a chalcogen,[139,140] the group of Chivers investigated the reaction of a $P_2N_4Se_2$ ring with $[Pt(C_2H_4)(PPh_3)_2]$. They found that oxidative addition of the Se-Se bond to $[Pt(C_2H_4)(PPh_3)_2]$ occurred giving $[Pt(Se_2N_4P_2)(PPh_3)_2]$ (figure 1.53). They also found that $P_2N_4Se_2$ η^1-*N*-coordinated to $[PtCl(PEt_3)_2]$, would undergo the same reaction to give the bimetallic species $[Pt\{\eta^2\text{-}Se,Se'\text{-}PtCl(\eta^1\text{-}N\text{-}P_2N_4Se_2)(PEt_3)_2\}(PPh_3)_2]$.

Figure 1.53:

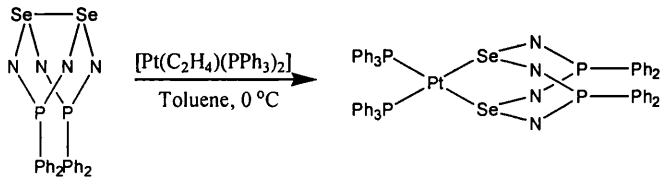

The reactions of low-valent platinum and palladium complexes with simple diselenides have been fairly well studied. In 1982 Day, Lesch and Rauchfuss reported the reaction of $[Pt(C_2H_4)(PPh_3)_2]$ with diphenyl diselenide (PhSeSePh), which gave *trans*-$[Pt(SePh)_2(PPh_3)_2]$, as a result of oxidative addition of the Se-Se bond to

platinum.[141] In 2003 Ananikov *et al.* showed that the same product was given when $[Pt(PPh_3)_4]$ was reacted with PhSeSePh.[142] In addition, they found that the reaction of $[Pd(PPh_3)_4]$ with PhSeSePh gave the dinuclear species $[Pd_2(SePh)_4(PPh_3)_2]$. Laitinen's group found the same behaviour when investigating the reactions of $[M(PPh_3)_4]$ (M = Pd, Pt) with *bis*-(2-thienyl) diselenide (ThSeSeTh);[143] the complexes $[Pd_2(ThPh)_4(PPh_3)_2]$ and $[Pt(ThPh)_2(PPh_3)_2]$ were the major products formed in each reaction (figure 1.54).

Figure 1.54:

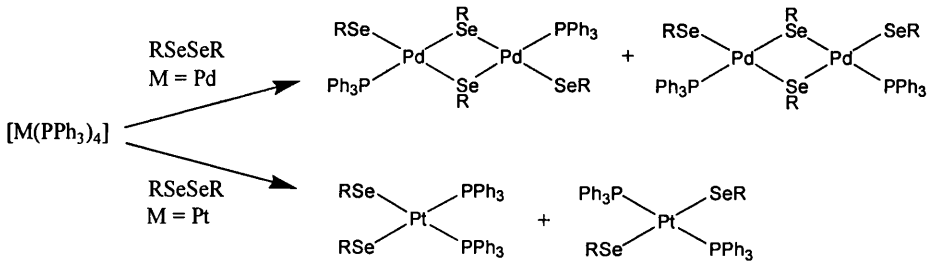

Several reports have been published on the reactions of Pd(II) and Pt(II) complexes containing a chelating N-donor ligand with diselenides. Puddephat showed in 1993 that $[PtMe_2(phen)]$ (phen = 1,10-phenanthroline) reacts with PhSeSePh through an oxidative addition of the Se-Se bond, to give $[PtMe_2(SePh)_2(phen)]$.[144] In 1998 Canty synthesised $[PtMe_2(SePh)_2(bipy)]$ (bipy = 2,2'-bipyridine) by an analogous method, and also extended the study to palladium species.[145] They found that the reaction of $[PdMe_2(L)]$ and $[Pd(CH_2CH_2CH_2CH_2)(L)]$ (L = bipy, phen) with PhSeSePh gave the Pd(IV) complexes $[PdMe_2(SePh)_2(L)]$ and $[Pd(CH_2CH_2CH_2CH_2)(SePh)_2(bipy)]$ respectively (figure 1.55). As expected these Pd(IV) complexes were found to be less stable than their platinum analogues.

Figure 1.55:

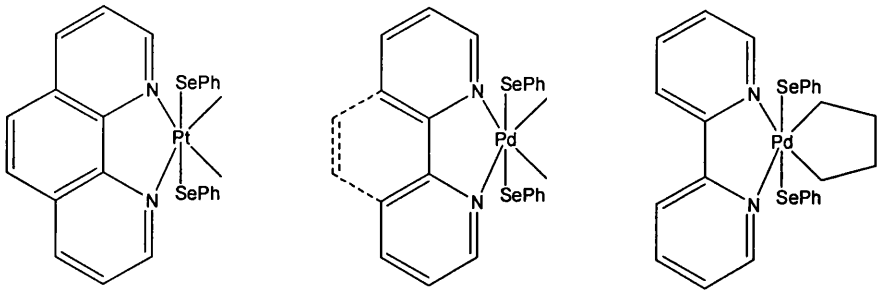

The reactions of [Pt(dmphen)(olefin)] (dmphen = 2,9-dimethyl-1,10-phenanthroline) with MeSeSeMe and PhSeSePh also follow a similar path.[146,147] It has been found that under certain conditions the reaction is reversible.[148] This has been found for the

platinum complexes [Pt(4-$MeOC_6H_4$)($CH\{CO_2R\}_2$)(*N,N'*-chelate)] (R = Me, Et, ^{i}Pr) reacting with MeSeSeMe and PhSeSePh.

1.9 Diselenolenes

Although there has been a large amount of investigation into the syntheses and properties of dithiolenes (see next section),[149] their selenium analogues, diselenolenes, are less well known. One of the first reported syntheses of diselenolenes was by Davison and Shawl in 1970;[150] they found that the reaction of *bis*-(trifluoromethyl)-1,2-diselenetene with $[Ni(CO)_4]$ gave $[Ni\{Se_2C_2(CF_3)_2\}_2]$ (figure 1.56). The 1,2-diselenetene is prepared by the reaction of hexafluorobut-2-yne with refluxing selenium and so the procedure is limited to the preparation of 1,2-diselenetenes containing electron-withdrawing groups that can withstand the harsh conditions involved. This synthesis of diselenolenes was later extended to Pt, Cu and Au diselenolenes.[151,152]

Figure 1.56:

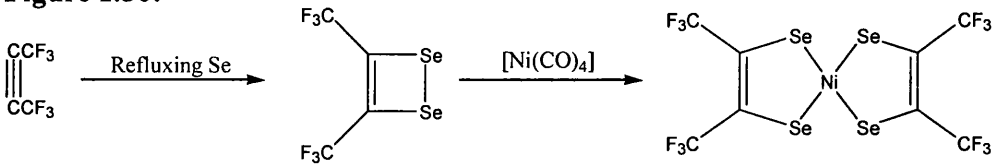

In 1982 Bolinger and Rauchfuss reported a synthesis of diselenolenes from dicyclopentadienyltitanium pentaselenide and activated alkynes.[153] They found that refluxing $[Ti(\eta^5\text{-}C_5H_4R)_2Se_5]$ (R = H, Me) with ZCCZ (Z = CO_2CH_3 or CF_3) gave titanium diselenolenes of the type $[Ti(\eta^5\text{-}C_5H_4R)_2(Se_2C_2Z_2)]$. These species were found to act as chelate transfer reagents and would react with $[MCl_2L_2]$ (M = Ni, L_2 = dppp; M = Pt, L = PPh_3) and $[Pt_2Cl_4(Ph_2PCCCPPh_2)_2]$ to give Ni and Pt diselenolenes (figure 1.57). Note how $[Ti(\eta^5\text{-}C_5H_4R)_2Cl_2]$ is essentially catalytic in this process.

Figure 1.57:

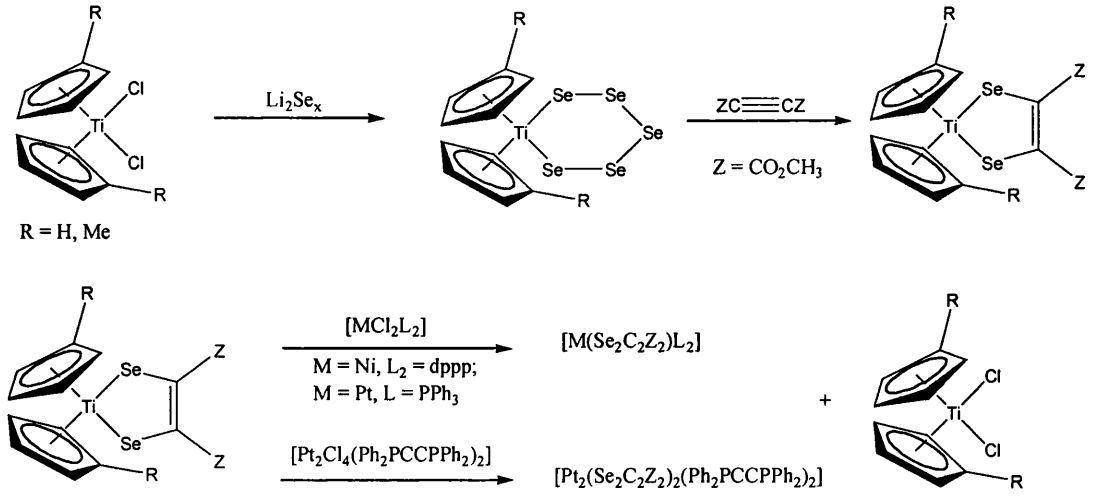

In 1984 Gautheron's group reported the syntheses of more group 4 diselenolenes.[154] They found that the reaction of metallocene aryne complexes with elemental selenium gave diselenolenes of the type $[M(\eta^5\text{-}C_4H_4R)_2(Se_2C_6H_4)]$ (M = Zr, R = ^{t}Bu; M = Ti, R = H).

In 1985 Wudl's group reported a synthesis of $[Ni\{Se_2C_2(CF_3)_2\}_2]^{2-}$ using *bis*-(trifluoromethyl)-1,3-diselenole-2-selone as a precursor instead of a diselenetene.[155] This method was a lot less harsh than the diselenetene method; in addition the synthesis was extended by the use of a nitrogen-containing derivative (figure 1.58).

Figure 1.58:

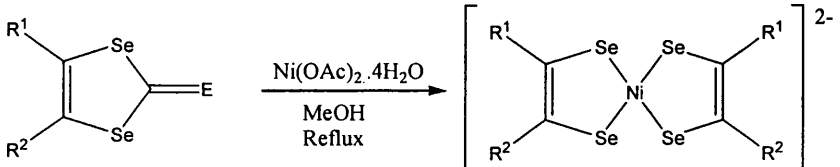

E = Se; $R^1 = R^2 = CF_3$

E = $N(CH_3)_2^+$; $R^1 = CH_3$; R^2 = H, CH_3

The use of 1,3-diselenole-2-selones as precursors to diselenolenes was extended to gold, nickel and palladium by Matsubayashi in the early 1990's.[156,157] Treatment of C_3Se_5 with sodium metal gives $Na_2[C_3Se_5]$; this is then reacted with the appropriate metal chloride to give $[M(C_3Se_5)L]^{n-}$ (M = Au, L = C_3Se_5, n = 0 - 1; M = Ni, Pd, L = C_3S_5, n = 2). Cassoux *et al.* used this type of reaction to prepare nickel and palladium diselenolenes with mixed S/Se ligands.[158,159] These complexes $[M(C_3S_3Se_2)_2]^{2-}$ (M = Ni, Pd) have been found to have temperature and pressure dependent conductivities, with superconductivity observed under pressure. In their oxidised form these species crystallise as the dimers $[M(C_3S_3Se_2)_2]_2$ with the nickel species linked by Ni-Se bonds and the palladium species linked by a Pd-Pd bond (figure 1.59).

Figure 1.59:

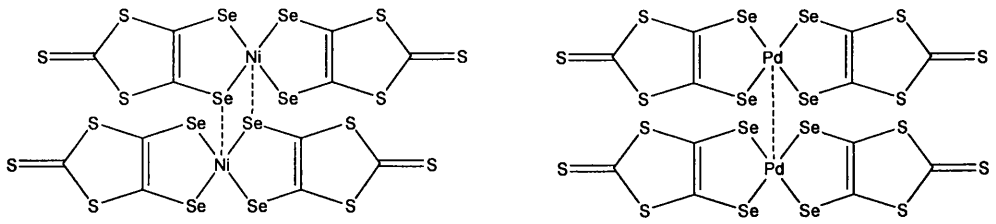

It was found that similar systems could be synthesised containing the 1,2,5-thiadiazole-3,4-dithiolate ligand (tdas – $C_2N_2S_3^{2-}$),[160,161,162,163] and recently a nickel complex of this type with a mixed S/Se occupancy ($[Ni(C_2N_2S_{2.2}Se_{0.8})_2]^{2-}$) has been

reported.[164] The ratio of S:Se at the thiolic sites is 3:2, and the presence of selenium makes the dianion easier to oxidise than $[Ni(tdas)_2]^{2-}$.

In 1986 Kajitani's group reported a synthesis of a cobalt diselenolene from a cyclopentadienylcobalt(I) precursor, elemental Se and di-2-pyridylethyne.[165] They found that when this diselenolene was refluxed in toluene with elemental S, the dithiolene and thiolatoselenolato species were formed (figure 1.60).

Figure 1.60:

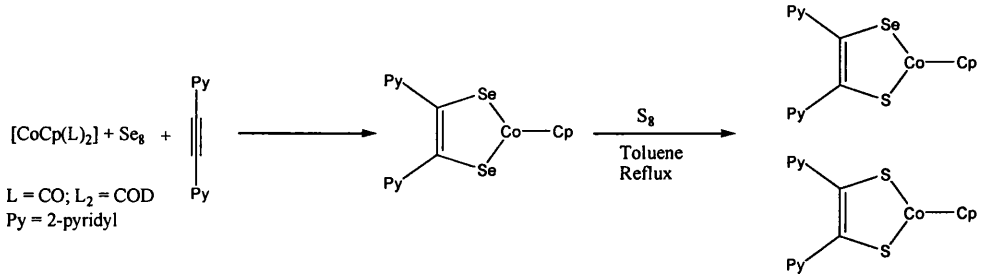

The reaction was extended to diphenylethyne;[166] in part of the investigation the group found a cubane-type species formed in the absence of the alkyne (figure 1.61). This could be reacted with an alkyne to give dithio/diselenolenes and so is believed to be an intermediate in the reaction.

Figure 1.61:

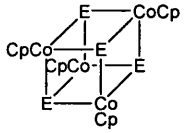

E = S/Se

In 1987 a selenolatotellurolato platinum complex – $[Pt(SeTeC_6H_4)(PPh_3)_2]$ – was reported, along with the analogous ditellurolene and thiolatotellurolato complexes (figure 1.62).[167] The complexes were synthesised by the reaction of the appropriate *o*-dichalcogenolatobenzene with $[PtCl_2(PPh_3)_2]$.

Figure 1.62:

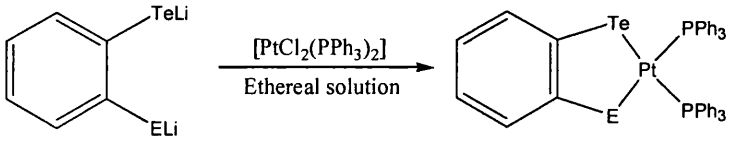

E = S, Se, Te

In 1989 a tungsten *tris*-diselenolene and dinuclear tungsten *bis*-diselenolene were reported by Ibers *et al.*[168] They found that the reaction of $[WSe_9]^{2-}$ and $[W_2Se_{10}]^-$ with DMAD (dimethyl acetylenedicarboxylate) in toluene at room temperature gave

$[W\{Se_2C_2(COOCH_3)_2\}_3]^{2-}$ and $[W_2Se_2\{Se_2C_2(COOCH_3)_2\}_4]^-$ respectively (figure 1.63).

Figure 1.63:

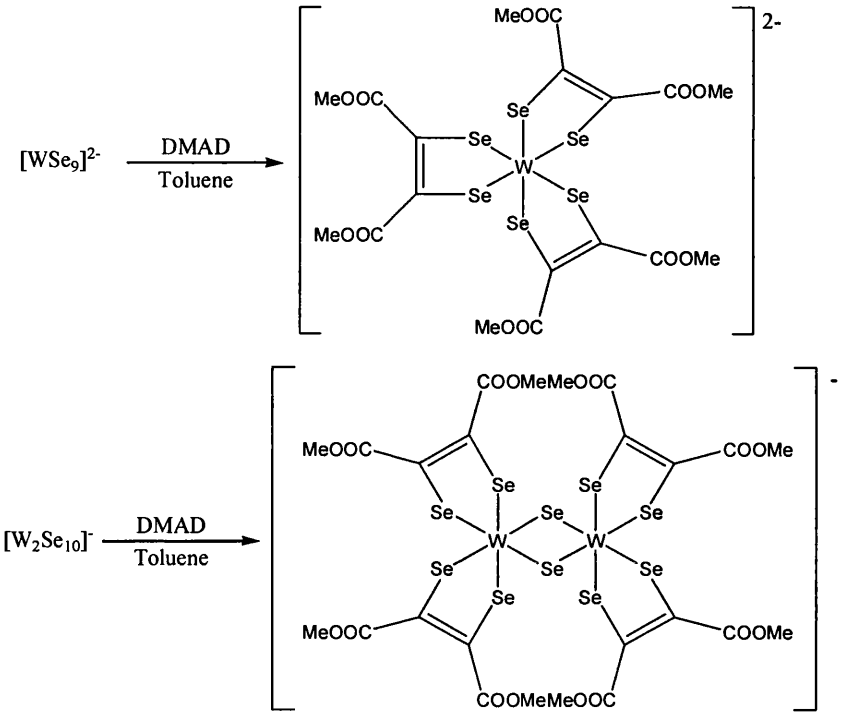

The syntheses of cobalt, palladium and platinum diselenolenes from 1,2,3-selenadiazoles and 1,4-diselenins by Morley *et al.* has been discussed in previous sections; the group have also reported syntheses of diselenolenes from the tetrachalcogenides $[ME_4(dppe)]$ (M = Pd: E = S; M = Pt: E = S, Se).[169,170] They found that $[ME_4(dppe)]$ would react with DMAD and DEAD (diethyl acetylenedicarboxylate) to give the diselenolenes $[M\{E_2C_2(COOR)_2\}(dppe)]$ (R = Me, Et). They found that less activated alkynes (R = H, Ph) gave no isolatable products after reaction. They also found that $[PdS_4(dppe)]$ would react with the carbene complex $[W(CO)_5\{C(OEt)C{\equiv}CPh\}]$ giving an unsymmetrical dithiolene (figure 1.64); no reaction occurs with $[PtE_4(dppe)]$.

Figure 1.64:

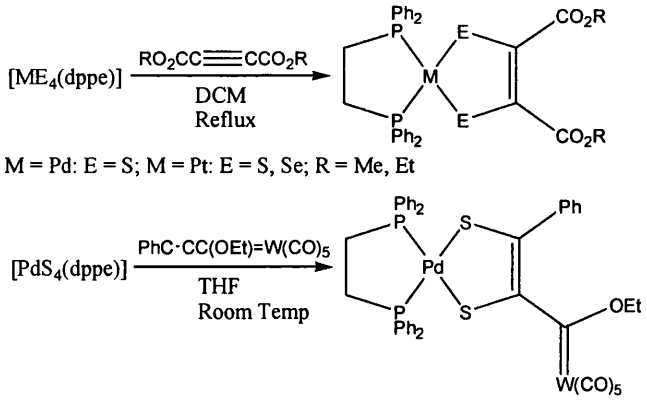

Mizobe and Hidea reported a similar reaction of the dinuclear iridium polyselenide $[Ir_2Cp^*_2(\mu\text{-}Se_4)_2]$ with DMAD and MAMC ($HC{\equiv}CCO_2Me$).[171] They found that the reaction of $[Ir_2Cp^*_2(\mu\text{-}Se_4)_2]$ with one equivalent of DMAD gave a mixture of the dinuclear diselenolene $[Ir_2Cp^*_2(\mu\text{-}Se_4)\{\mu\text{-}Se_2C_2(CO_2Me)_2\}]$ and the mononuclear diselenolene $[IrCp^*\{Se_2C_2(CO_2Me)_2\}]$. The reaction with two equivalents of DMAD gave rise to a third product $[IrCp^*\{Se,Se,C\text{-}Se_2C_4(CO_2Me)_4\}]$ which results from the addition of DMAD to $[IrCp^*\{Se_2C_2(CO_2Me)_2\}]$ (Figure 1.65). Upon treatment of $[Ir_2Cp^*_2(\mu\text{-}Se_4)_2]$ with one equivalent of MAMC, two dinuclear complexes were produced $[Ir_2Cp^*_2(\mu\text{-}Se_4)\{\mu\text{-}Se_2C_2H(CO_2Me)\}]$ and $[Ir_2Cp^*_2\{\mu\text{-}Se_2C_2H(CO_2Me)\}_2]$, corresponding to the addition of one and two molecules of MAMC respectively (figure 1.65). In the presence of excess MAMC only $[Ir_2Cp^*_2\{\mu\text{-}Se_2C_2H(CO_2Me)\}_2]$ was formed.

Figure 1.65:

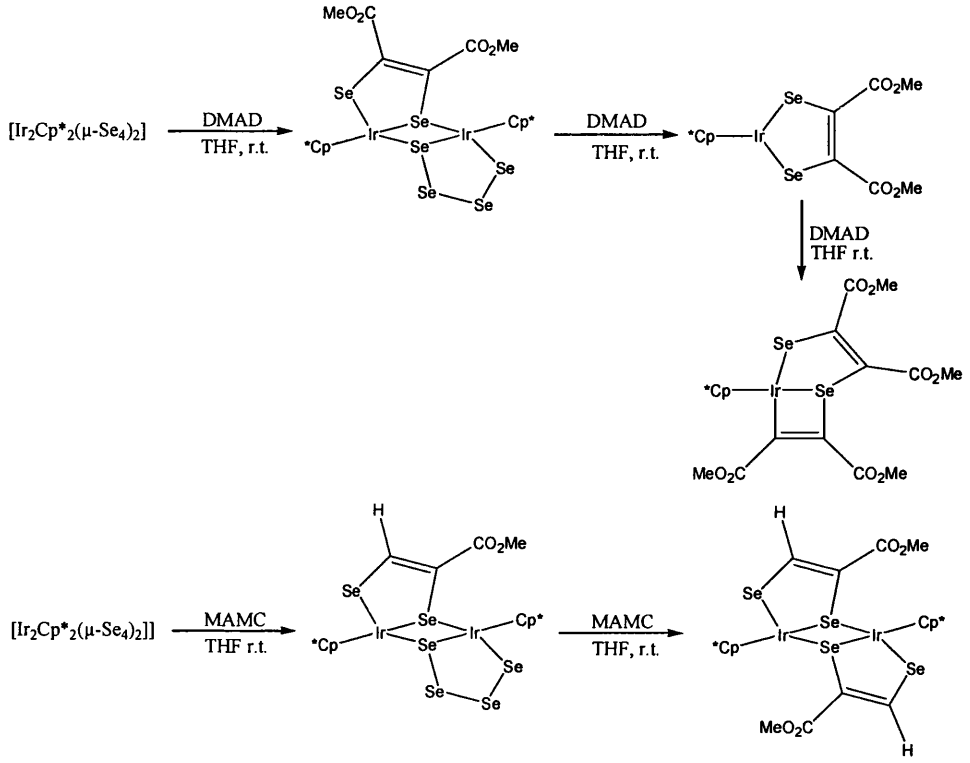

Recently Morley's group have reported the reactions of the dinuclear diselenolenes $[Pd_2(Se_2C_{n+4}H_{2n+4})_2(PR_3)_2]$ (n = 2, 3, 4; R = Bu, Ph) with some alkyl halides.[172] The work concentrated on $[Pd_2(Se_2C_8H_{12})_2(PR_3)_2]$ and they found that bridge cleavage reactions occurred to give species of the type $[PdX(Se\{R'\}C_8H_{12}Se)(PR_3)]$ (X = Br, I; R' = Me, Et, etc.). Although not fully characterised they also proposed the formation of $[Pd_2I_2\{\mu\text{-}SeC_8H_{12}Se(CH_2)_3SeC_8H_{12}Se\}(PBu_3)_2]$ (figure 1.66) from $[PdI(Se\{(CH_2CH_2CH_2I\}C_8H_{12}Se)(PR_3)]$ and $[Pd_2(Se_2C_8H_{12})_2(PR_3)_2]$. This species consists of two square planar palladium units linked by a hydrocarbon bridge.

Figure 1.66:

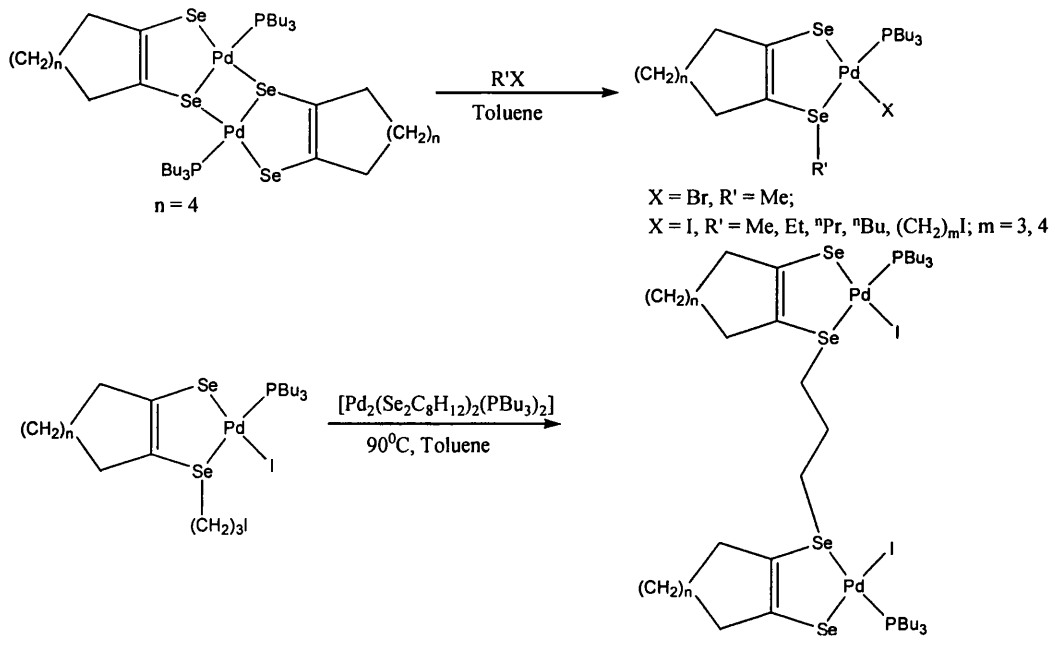

Although platinum(diimine)(dithiolene) complexes are well known for their desirable electronic and photochemical properties, [173] there are only two reports of platinum(diimine)(diselenolene) complexes (figure 1.67).[174,175] The first report by Matsubayashi documents the syntheses of $[Pt(C_3Se_5)(L)]$ (L = *N*-ethyl/i-propyl-2-methylpyridine-2-carbaldimine, 2,2'-bipyridine (bipy)), and the second report documents the syntheses of $[M(Se_2C_6H_4)(bipy)]$ (M = Ni, Pt). In both cases the properties of the complexes proved less desirable than those of the sulphur analogues.

Figure 1.67:

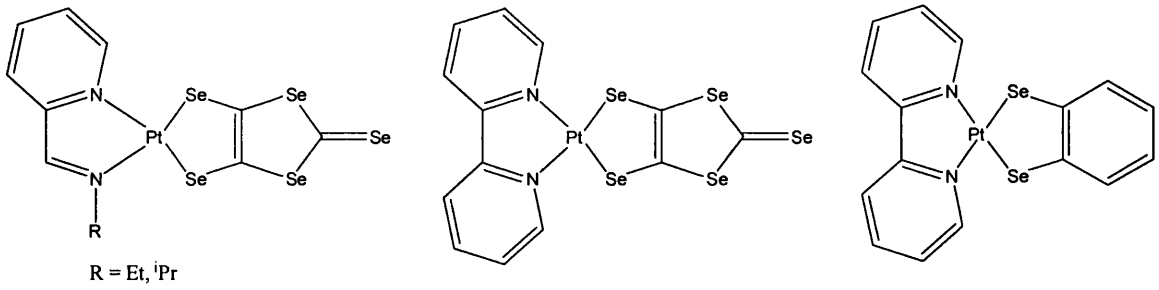

Recently Corrigan and Brown have reported the syntheses of ferrocenylselenolate bridged Pd(II) and Pt(II) complexes.[176] Although these are not diselenolenes they have similar structures with a ferrocenyl backbone replacing the -C=C- backbone. They found that the reaction of 1,1'-*bis*(trimethylsilylseleno)ferrocene with *trans*-$[MCl_2(PBu_3)_2]$ (M = Pd, Pt) gave the dimeric species $[M_2\{\mu\text{-}Fe(\eta^5\text{-}C_5H_4Se)_2\}_2(PBu_3)_2]$; the reaction of *cis*-$[PtCl_2(PBu_3)_2]$ with 1,1'-

bis(trimethylsilylseleno)ferrocene gave the monomer $[Pt\{Fe(\eta^5\text{-}C_5H_4Se)_2\}(PBu_3)_2]$ (figure 1.68). An electrochemical study showed that there was electronic communication between the Fe centres in the dinuclear complexes.

Figure 1.68:

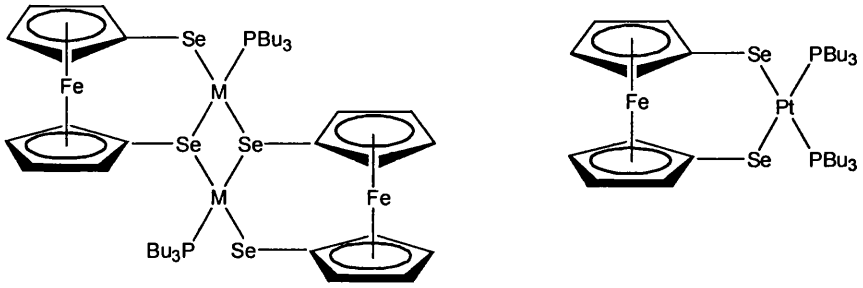

M = Pd, Pt

1.10 Transition Metal Dithiolenes

Since there has been relatively little research into diselenolenes and those considerations have been mostly synthetic, here is presented a short summary of the properties of the sulphur-containing analogues dithiolenes. It is hoped that some of these properties will be present in the diselenolenes discussed in the later chapters. The chemistry of dithiolenes has been covered in several recent reviews,[177,178,179,180,181] and it is important to note that this is only a brief overview of some dithiolene complexes and their properties. The structure of metal 1,2-dithiolene complexes (figure 1.69) comprises of a metal atom, two sulphurs and a C=C unit over which there is electronic delocalisation; in the case of *bis*- and *tris*-1,2-dithiolene complexes the delocalisation is more extensive, covering the metal, sulphurs and C=C units. Note that this delocalisation can be extended by appropriate choice of R groups.

Figure 1.69:

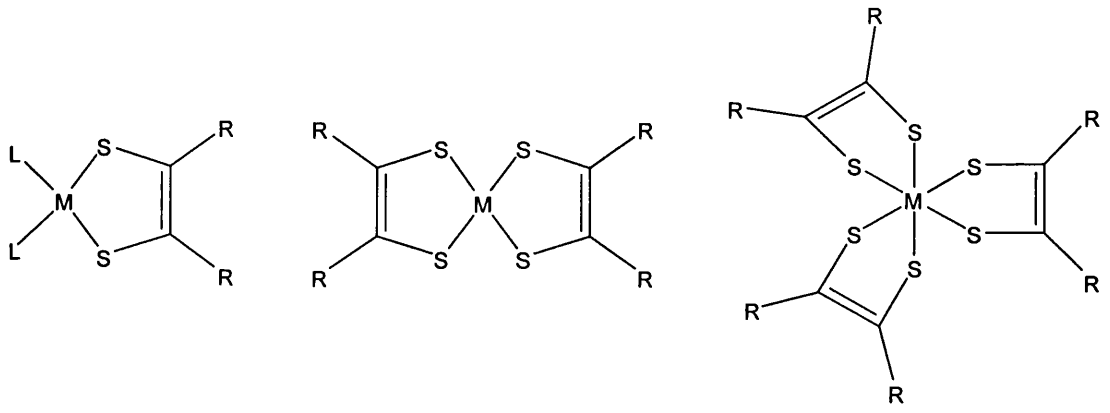

1,2-Dithiolene *bis*-1,2-Dithiolene *tris*-1,2-Dithiolene

It is this delocalisation which can lead to a number of important properties including:[1]

(i) The ability to undergo one or more reversible redox processes;

(ii) A low energy absorption into the visible/NIR region;

(iii) A frontier orbital distribution over much or all of the molecule;

(iv) Often a planar arrangement of the complex which allows for good stacking and close inter-molecular contacts in the crystal phase;

(v) Sulphur-mediated intermolecular interactions.

1.10.1 Dithiolenes Containing the dmit Ligand

Perhaps the most studied of the metal dithiolenes are salts of $[M(dmit)_2]^{n-}$ (n = 0, 1, 2),[3,182] where dmit is 4,5-dimercapto-1,3-dithiol-2-thione. In 1986 Cassoux *et al.*

studied the properties of some of these complexes where M is a group 10 metal.[183] They found that a needle of the complex $[TTF][Ni(dmit)_2]_2$ (TTF = tetrathiafulvalene) exibited metal-like conductivity down to 4 K along the needle axis (parallel to the 010 direction). Later investigation showed that under pressure (7 kbar) the complex exibited superconductivity at 1.6 K;[3] this was the first dmit-based superconducting molecular metal. The superconductivity is associated with both S-S and S-M interactions between lattice planes due to the efficient stacking of these types of compound, and with S-S interactions between stacks. Since this time eight superconducting compounds containing $[M(dmit)_2]$ have been synthesised (figure 1.70), some of which can also exhibit semiconductivity under certain conditions.[3]

Figure 1.70:

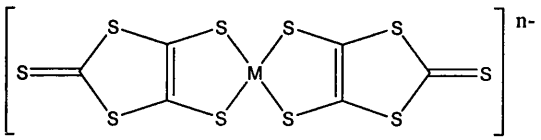

$[M(dmit)_2]^{n-}$

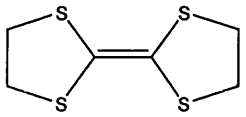

TTF

Superconducting compounds: $[D]_x[M(dmit)_2]_y$
D = TTF; M = Ni, Pd (2 forms); x = 1, y = 2;
D = Me_4N; M = Ni, Pd; x = 0.5, y = 1;
D = Me_2Et_2N; M = Pd; x = 0.5, y = 1;
D = Me_2Et_2P; M = Pd; x = 0.5, y = 1;
D = EDT-TTF; M = Ni; x = 1, y = 1.

Recently it has been found that salts of $[Ni(dmit)_2]$ incorporating crown ether macrocycles which contain alkali metals can be synthesised; these give supramolecular cation structures.[2] One compound of interest, $[Li_{0.6}(15\text{-crown-}5)H_2O][Ni(dmit)_2]_2$ formed a structure in which stacks of macrocyclic molecules formed an ion channel between stacks of $[Ni(dmit)_2]$.[184] Since in this compound, the number of Li^+ ions corresponds to the number of conduction electrons in the LUMO band of $[Ni(dmit)_2]$, there is the possibility of band-filling control by altering the ratio of Li^+ to $[Ni(dmit)_2]$.

There have been some examples of *tris*-dithiolenes containing the dmit ligand; of particular note are the complexes $[BEDT\text{-}TTF]_3[V(dmit)_3]$ [185, 186] (BEDT-TTF = *bis*(ethylenedithio)tetrathiafulvalene) and $[Fe(C_5Me_5)_2][M(dmit)_3]$ (M = Mo, W),[187] which both exhibit semiconducting properties.

1.10.2 Ferromagnetic and Antiferromagnetic Dithiolenes

Ferromagnetism and antiferromagnetism have been observed in some transition metal dithiolene complexes.[66] In ferromagnetic substances the spins on different metal centres are coupled into parallel alignment across thousands of atoms (or in the case of crystals the spins of unit cells align). Below the Curie temperature the spins are locked and the magnetism persists. The magnetization is not linearly proportional to the applied field and a hysterisis loop is observed. This loop is broad for hard ferromagnets (permanent magnets) and narrow for soft ferromagnets (magnets which respond to changes in the applied field). In antiferromagnets neigbouring spins are locked in an antiparallel alignment (leading to a low magnetic moment) through a mechanism called superexchange: the spin on one metal atom induces a small polarisation of an occupied ligand orbital which results in the opposite spin on an adjacent metal. Ferromagnetic and antiferromagnetic materials are used in data recording and storage devices such as computer hard drives.[188]

There are few examples of transition metal dithiolenes which exibit ferromagnetism; one example is the complex $[NH_4][Ni(mnt)_2].H_2O$ (figure 1.71, mnt = maleonitriledithiolate).[189,190] Above 100 K the complex displays antiferromagnetic coupling; ferromagnetic coupling is observed at 4 K at normal pressure, which increases to 7 K at 7 kbar. It has been observed that at 98 K the repeat distance of the anionic stack in the crystal doubles; this suggests dimerisation of the anions, and may be the reason for the switch from antiferromagnetism to ferromagnetism.

Figure 1.71:

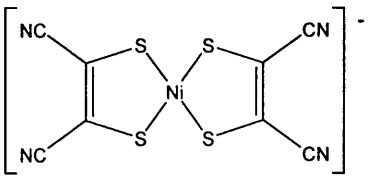

Many more examples of antiferromagnetic dithiolene complexes are known, including the dinuclear complexes $[AsPh_4]_2[(C_3OS_4)CuC_2S_4Cu(C_3OS_4)]$,[191] $[NEt_4]_2[Fe_2(bdt)_4]$[192] and $[Hpy][\{Fe(mnt)_2\}_2]$[193] (figure 1.72, bdt = 1,2-benzenedithiolate; Hpy = pyridinium). Note that $[AsPh_4]_2[(C_3OS_4)CuC_2S_4Cu(C_3OS_4)]$ contains a bridging C_2S_4 unit, through which the two Cu(II) centres are antiferromagnetically coupled, and shows a deviation from planar geometry. This, however, only has a small effect on the magnetic properties as the CuC_2S_4Cu unit is planar and allows a good interaction between the magnetic orbitals through the bridge.

In the iron complexes the Fe(III) centres are antiferromagnetically coupled through the bridging sulphur atoms.

Figure 1.72:

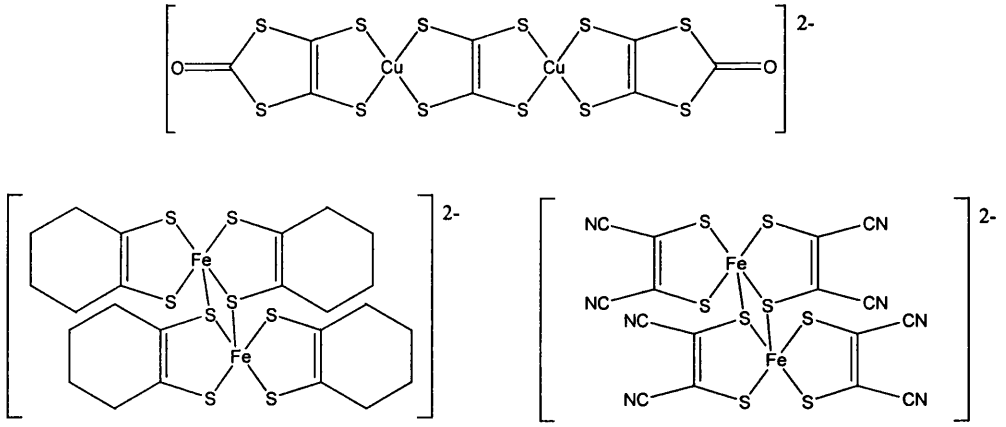

1.10.3 Dithiolenes as Q-Switch Dyes in Near-IR Lasers

It has been observed that some bis-1,2-dithiolenes (in particular nickel dithiolenes) have a broad absorption with no vibrational fine structure, at the visible edge of the near-IR spectrum.[194] Altering the substituents of these dithiolenes can bring this absorption into the near-IR region and these dithiolenes can be used as dyes in Q-switching lasers. Q-switching is the compression of the full output energy of a laser into ultra-short pulses of extremely high peak power. If a 'dye' which absorbs radiation of similar wavelength to the laser is placed in the laser cavity it acts initially as a closed shutter absorbing the radiation. As pumping continues and the population inversion increases, the photon flux in the laser cavity reaches a level where the excited state lifetime of the dye molecules is too long to allow enough molecules to return to a ground state at a rate sufficient to sustain absorption of the laser light. At this point the dye temporarily 'bleaches out' effectively opening the 'shutter' and a pulse of laser light in excess of 100 MW is released. Both the laser and dye molecules return to the ground state and the process restarts. Since a mechanical shutter is not used, this system is referred to as passive Q-switching. The properties required for a good Q-switch dye include an absorption maximum close to the wavelength of the laser, a reasonable lifetime of the excited state (if the lifetime is too long, it bleaches out too soon; if too short bleaching may not occur), and a good photochemical and thermal stablity.

One of the first dithiolenes prepared for use as a Q-switching dye was JUL2 – tetrajulolidynylnickel dithiolene (figure 1.73);[194] note the planar structure and delocalisation which contribute to the shift in absorption to the near-IR region. The absorption maximum is at 1270 nm; in 1977 it was used successfully in an iodine laser (λ = 1300 nm). The analogous palladium and platinum compounds were synthesised and these complexes also have absorption maxima at 1270 nm.

Figure 1.73:

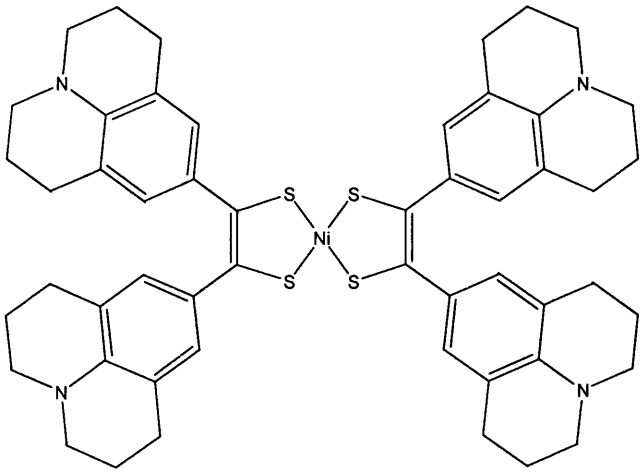

JUL2

There has also been work on ferrocenyl substituted dithiolene complexes; the complex $[Ni(S_2C_2(Fc)_2)_2]$[195] (figure 1.74; Fc = ferrocenyl) was found to have an absorption maximum of 1310 nm and is very stable. These properties make it a potential Q-switch dye.

Figure 1.74:

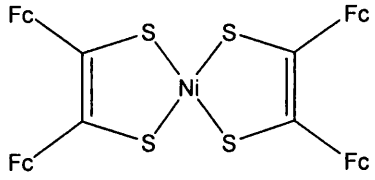

1.11 The Reactions of Selenophenes with Transition Metal Complexes

The reactions of selenophenes and thiophenes with transition metal complexes have been well studied, with particular attention paid to hydrodesulphurisation (HDS) processes.[196] Sulphur contamination of petroleum feedstocks is a problem: sulphur oxides produced upon combustion are pollutants and sulphur poisons precious metal catalysts used in the production of high octane gasoline. HDS is used to remove the sulphur from petroleum; the process used currently involves treatment with H_2 at up to 200 atm and 350-400 °C in the presence of a Mo/Co catalyst supported on Al_2O_3. In this process thiols, sulphides and disulphides are easily removed, but aromatic species, especially 4,6-disubstituted dibenzothiophenes, are more difficult to remove. In the search for a catalyst which will be more efficient at removing these aromatic species the reactions of many transition metal complexes with both thiophenes and selenophenes have been investigated.

Complexes of the group 6 metals will undergo contrasting reactions with selenophenes (and thiophenes). Angelici found that when $[Cr(CO)_6]$ was reacted with selenophene, thiophene and 2-, 3-, 2,5- and 2,3,4,5- alkyl-substituted derivatives, complexes of the type $[Cr(\eta^5\text{-selenophene})(CO)_3]$ were formed.[197] They later found that the use of $[Cr(CO)_3(MeCN)_3]$ gave a more efficient reaction, requiring the use of less ligand.[198] The group of W. D. Jones then showed that the photolysis of $[MoCp_2H_2]$ in the presence of thiophene results in the Mo fragment inserting into the C-H bond at the 2-position to give $[MoCp_2(H)(SC_4H_3)]$.[199] They also showed that the photolysis of $[WCp_2H_2]$ in the presence of thiophene gave $[WCp_2(H)(SC_4H_3)]$, but the intermediate thiatungstacycle $[WCp_2(SC_4H_4)]$ could be isolated if shorter irradiation times were employed. Figure 1.75 shows the different products of the group 6 metals with thio/selenophenes.

Figure 1.75:

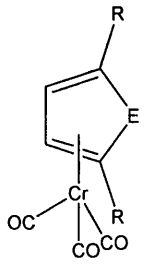

E = S, Se; R = H, Me

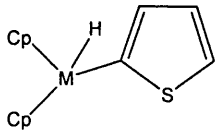

M = Mo, W

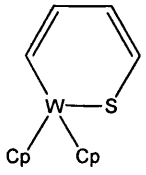

Manganese forms similar complexes with selenophene as chromium: $[Mn(OTf)(CO)_5]$ (Tf = SO_2CF_3) reacts with selenophene, 2-methylselenophene and 2,5-dimethylselenophene to give complexes of the type $[Mn(\eta^5\text{-selenophene})(CO)_3](OTf)$.[198] The species derived from selenophene and 2-methylselenophene would undergo nucleophilic addition to the 5-position of the selenophene giving $[Mn\{\eta^4\text{-SeCH(nuc)CHCHCR}\}(CO)_3]$ (nuc = H, CN, PBu_3; R = H, Me). The behaviour of rhenium when reacted with selenophene is quite different. The reactions of $[Re(\eta^5\text{-}C_5R_5)(CO)_2(THF)]$ (R = H or Me) with selenophenes gave products, the structures of which are dependent on whether R = H or Me, and the amount of substitution of the selenophenes used (figure 1.76).[200,201] Reaction of $[ReCp^*(CO)_2(THF)]$ with selenophene gave the complex $[ReCp^*(\eta^2\text{-selenophene})(CO)_2]$ where Re is η^2-bound to a C=C bond of selenophene; reaction with 2-methylselenophene gave an isomeric mix of $[ReCp^*(\eta^2\text{-2-methylselenophene})(CO)_2]$ and the Se-coordinated $[ReCp^*(2\text{-methylselenophene})(CO)_2]$; and reaction with 2,5-dimethylselenophene gave only the Se-coordinated $[ReCp^*(2,5\text{-dimethylselenophene})(CO)_2]$. For $[ReCp(CO)_2(THF)]$ reaction with selenophene gave an isomeric mix of $[ReCp(\eta^2\text{-selenophene})(CO)_2]$ and Se-coordinated $[ReCp(selenophene)(CO)_2]$; and reaction with 2-methylselenophene gave only $[ReCp(2\text{-methylselenophene})(CO)_2]$.

Figure 1.76:

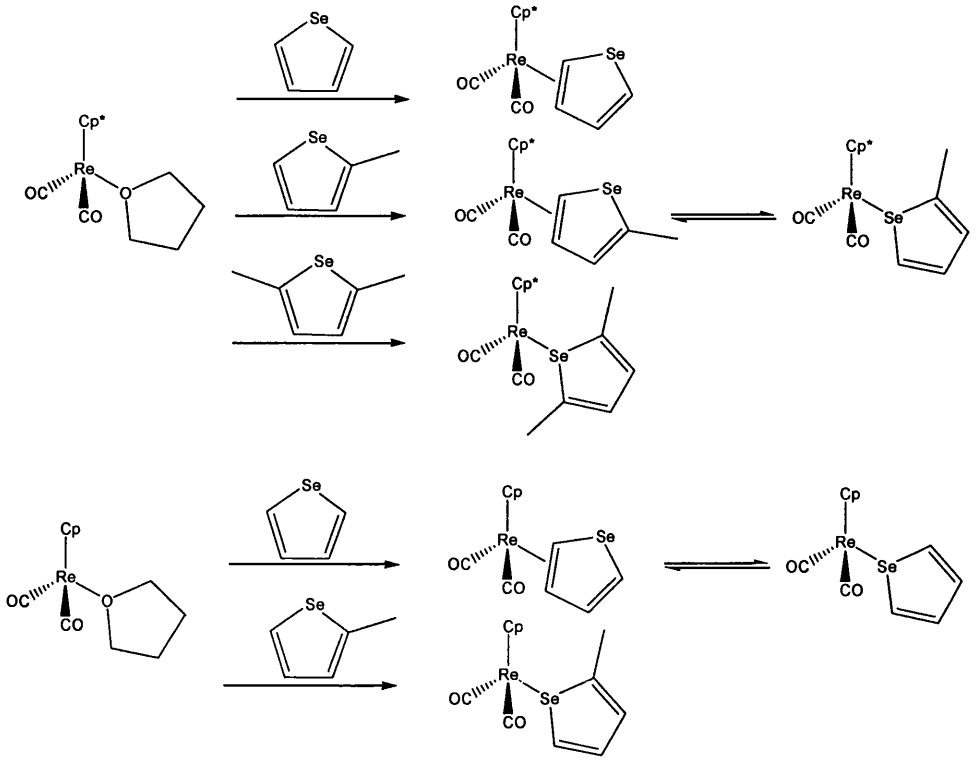

The differing behaviours observed are attributed to the enhanced donor ability of the selenium on substitution of selenophene with electron-donating methyl groups, therefore favouring Se-bonded isomers. The differences observed in the behaviour of Cp and Cp* complexes are attributed to the Cp* ligand's increased electron density, increasing π-backbonding in the olefinic system, favouring the η^2-bonded isomer. The chemistry of [ReCp*(η^2-selenophene)$(CO)_2$] was further investigated and it was found that reaction with $[M(CO)_4(L)(THF)]$ (M = Cr, Mo: L = CO; M = W: L = CO, PPh_3) gave complexes with M bound to Se (figure 1.77). Reaction with $[Fe_2(CO)_9]$ gave a complex with $Fe(CO)_4$ bound to Se, a complex with $Fe(CO)_3$ η^4-bound to the selenophene ligand, and a complex where $Fe(CO)_3$ had inserted into the selenophene ring and another $Fe(CO)_3$ is coordinated to it (figure 1.77).

Figure 1.77:

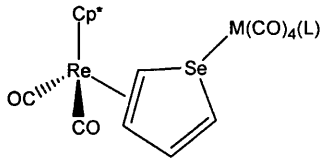

M=Cr, Mo; L=CO
M=W; L=CO, PPh_3

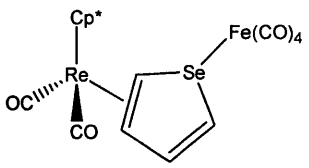

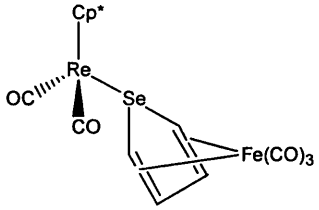

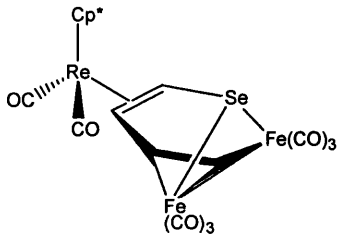

A complex with rhenium bound to the 2-position of selenophene has also been synthesised.[202] Deprotonation of $[ReCp(NO)(PPh_3)(L)]^+$ (L = selenophene, 2-methylselenophene) gives complexes with Re bound at the 2-position of the selenophene ring. When L = selenophene, further reaction with $HBF_4.Et_2O$ or CF_3SO_3H gives a carbene complex (figure 1.78).

Figure 1.78:

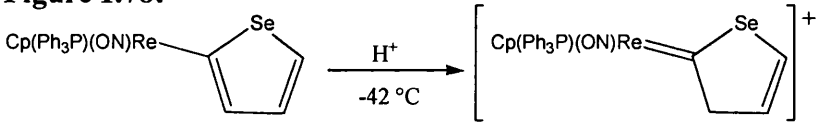

The reactions of the group 8 metals with selenophene were investigated by Arce *et al.* in 1990/1.[203,204] They initially investigated the reaction of $[Os_3(CO)_{10}(MeCN)_2]$ with selenophene and found that two products were given, the 1:1 product $[Os_3(CO)_{10}(SeC_4H_4)]$ which includes a selenaosmacycle unit, and the 2:1 product $[\{Os_3(CO)_{10}\}_2(SeC_4H_4)]$ in which the selenophene has been opened and acts as a bridge between the $Os_3(CO)_{10}$ units. Heating $[Os_3(CO)_{10}(SeC_4H_4)]$ to 125 °C in octane resulted in the loss of an $Os(CO)_4$ unit to give $[Os_2(CO)_6(SeC_4H_4)]$. Figure 1.79 shows the structures of $[Os_3(CO)_{10}(SeC_4H_4)]$, $[\{Os_3(CO)_{10}\}_2(SeC_4H_4)]$ and $[Os_2(CO)_6(SeC_4H_4)]$.

Figure 1.79:

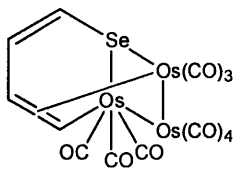

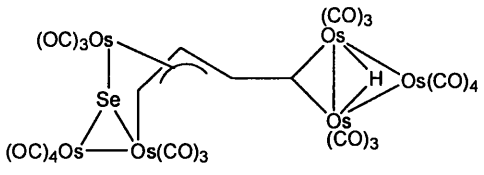

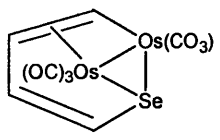

The reaction of $[Ru_3(CO)_{12}]$ with selenophene in refluxing THF gave two products, the first of which, $[Ru_2(CO)_6(\mu\text{-}C_4H_4)]$, is presumed to result from the exchange of Se

for a $Ru(CO)_3$ unit, followed by π-complexation to another $Ru(CO)_3$ unit. The second product is the tetranuclear $[Ru_4(\mu_3\text{-}Se)(\mu\text{-}C_4H_4)(CO)_{11}]$. The reaction of $[Fe_3(CO)_{12}]$ with selenophene in refluxing cyclohexane gave $[Fe_2(CO)_6(\mu\text{-}C_4H_4)]$, directly analogous to $[Ru_2(CO)_6(\mu\text{-}C_4H_4)]$, and $[Fe_2(CO)_6(SeC_4H_4)]$ which is analogous to $[Os_2(CO)_6(SeC_4H_4)]$. Figure 1.80 shows the products of these reactions.

Figure 1.80:

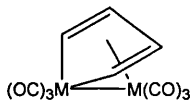

M = Fe, Ru

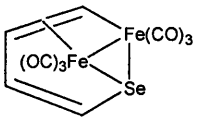

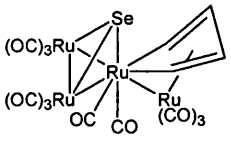

Some ruthenium complexes containing ring-opened selenophene without loss of selenium have also been reported. Angelici has reported that the reaction of $[RuCp^*(MeCN)_3](OTf)$ with selenophene gave the complex $[RuCp^*(\eta^5\text{-selenophene})](OTf)$.[198] Upon treatment with Red-Al ($Na[Al(OC_2H_4OCH_3)_2H_2]$) the selenophene ring opened to give $[RuCp^*(SeCHCHCHCH_2)]$. The group of Chung has also demonstrated this type of ring opening for the complex $[Ru(\eta^6\text{-}C_6H_6)(\eta^5\text{-selenophene})]^{2+}$.[205] Treatment of this complex with $[CoCp_2]$ and $[Mn(CO)_3(\eta^6\text{-1-methylnaphthalene})]$, in DCM at -78 °C, gave a C-Se cleaved $RuMn_2$ complex (figure 1.81).

Figure 1.81:

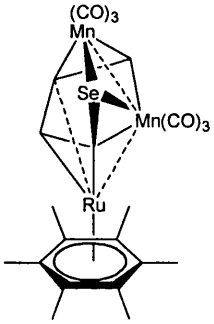

A ring opening reaction of the complex $[Os(NH_3)_5(\eta^2\text{-selenophene})](OTf)_2$ has also been reported.[206] The reaction of $[Os(NH_3)_5(\eta^2\text{-selenophene})]^{2+}$ with MeOTf results in methylation of the selenium atom; subsequent treatment with TBAB (tetra-butylammonium borohydride) results in the ring-opened product shown in figure 1.82.

Figure 1.82:

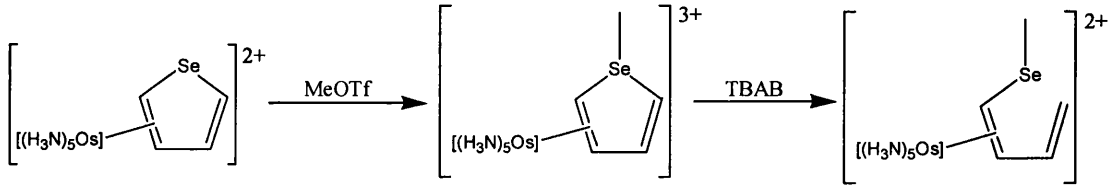

There have been few reports concerning the group 9 metals and selenophene, and only of reactions involving rhodium and iridium. The group of W. D. Jones has reported the reactions of $[CoCp^*(C_2H_4)_2]$ with thiophene[207] and dibenzothiophene.[208] The reactions gave complexes of the type $[Co_2Cp^*_2(SC_4H_4)]$, with a structure analogous to that of $[Fe_2(CO)_6(SeC_4H_4)]$, with one $CoCp^*$ unit inserted into the thiophene ring and the other coordinated to the thiacobaltacycle via bonds to S, Co and C=C. They have also reported on the reaction of the rhodium complex $[RhCp^*(Ph)(H)(PMe_3)]$ with selenophene.[209] The complex thermally eliminates benzene at elevated temperatures to give the 16-electron fragment $[RhCp^*(PMe_3)]$; this will insert into the C-Se bond of selenophene to give the selenarhodacycle $[RhCp^*(SeC_4H_4)(PMe_3)]$ (Figure 1.83). The reduction of $[IrCp^*(\eta^5\text{-}2,5\text{-dimethylselenophene})]$ with Red-Al gives the selenairidacycle $[IrCp^*\{SeC(CH_3)CHCHC(CH_3)\}]$ (figure 1.83).[198]

Figure 1.83:

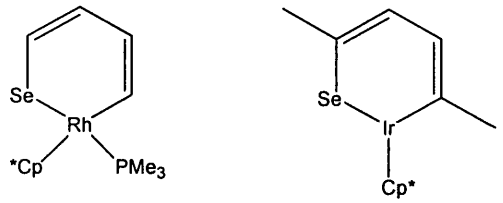

The chemistry of the group 10 metals with selenophenes has not been thoroughly investigated. There are no reports of the reactions of nickel complexes with selenophene, although there is a report of the reactions of $[Ni(PEt_3)_3]$ with substituted thiophenes.[210] It was found that $[Ni(PEt_3)_3]$ inserted into the C-S bond of 3-chlorothiophene giving the thianickelacycle $[Ni(SCHCClCHCH)(PEt_3)_2]$. However $[Ni(PEt_3)_3]$ inserted into the C-Cl bond of 2-chlorothiophene giving the complex $[NiCl(\eta^1\text{-}SC_4H_3)(PEt_3)_2]$, and inserted into the C-H bond at the 4-position of 2-nitrothiophene giving the complex $[NiH(\eta^1\text{-}SC_4H_2NO_2)(PEt_3)_2]$; these complexes are shown in figure 1.84. It was found that the analogous reactions with $[M(PEt_3)_3]$ (M = Pd, Pt) gave C-S insertion products in all cases.

Figure 1.84:

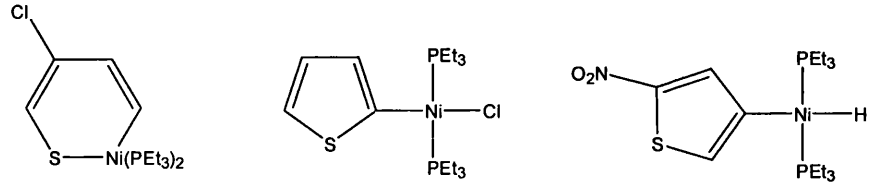

Although the reactions of platinum complexes with thiophenes have been thoroughly investigated, in particular the reactions of $[Pt(PEt_3)_3]$,[211,212,213,214,215,216] there is only one report of a reaction with selenophenes.[217] It was found that the reaction of $[Pt(C_2H_4)(PPh_3)_2]$ with $Mn(CO)_3^+$ activated selenophene and benzoselenophene gave the C-Se insertion products $[\{Pt(SeC_4H_4)(PPh_3)_2\}Mn(CO)_3]^+$ and $[\{Pt(Se(C_6H_4)CHCH)(PPh_3)_2\}Mn(CO)_3]^+$ (figure 1.85). The palladium species $[\{Pd(SeC_4H_4)(PPh_3)_2\}Mn(CO)_3]^+$ was synthesised by an analogous method using $[Pd(C_2H_4)(PPh_3)_2]$.

Figure 1.85:

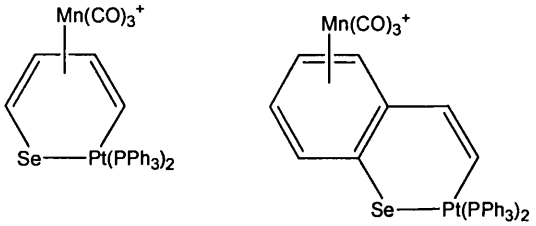

This concludes the summary of the chemistry relevant to this thesis; general uses of the elements concerned have been covered, as have specific examples of compounds and reactions highly relevant to the following work. This introduction was necessarily brief, but has hopefully provided a platform from which the following work can be understood. More detailed discussion (where relevant) will appear with the work presented in the next chapters.

Chapter 2

The Syntheses, Reactions and Characterisation of Some Platinum Diselenolenes

2.1 The Synthesis and Reactions of $[Pt(Se_2C_8H_{12})(PPh_3)_2]$

2.1.1 The Synthesis of $[Pt(Se_2C_8H_{12})(PPh_3)_2]$

In 1995 Khanna and Morley reported the reaction of $[Pt(PPh_3)_4]$ with cyclooctено-1,2,3-selenadiazole (4,5,6,7,8,9-hexahydrocycloocta-1,2,3-selenadiazole) in refluxing toluene.[114] They found that the reaction gave two products, the compound $[Pt(SeC_8H_{12})(PPh_3)_2]$ containing the selenaketocarbene ligand and a poorly soluble yellow powder with empirical formula $[Pt(Se_2C_8H_{12})(PPh_3)_2]_x$. In addition to a poor solubility the latter product had a high melting point (> 300 °C) and so was believed, at the time, to be polymeric. The poor solubility prohibited a full spectral analysis, but it was possible to obtain a MALDI mass spectrum of this species (figure 2.1). The peak at m/z = 986 (100% relative abundance) is attributed to $[^{195}Pt(^{80}Se^{79}SeC_8H_{12})(PPh_3)_2]$; as can be seen the isotope match is very good. The peaks at m/z = 907 and 1445 are attributed to $[Pt(SeC_8H_{12})(PPh_3)_2]$ and $[Pt_2(Se_2C_8H_{12})_2(PPh_3)_2]$ respectively; it is believed that $[Pt_2(Se_2C_8H_{12})_2(PPh_3)_2]$ was probably generated in the mass spectrometer.

Figure 2.1: MALDI mass spectrum and isotope profile match of $[Pt(Se_2C_8H_{12})_2(PPh_3)_2]$

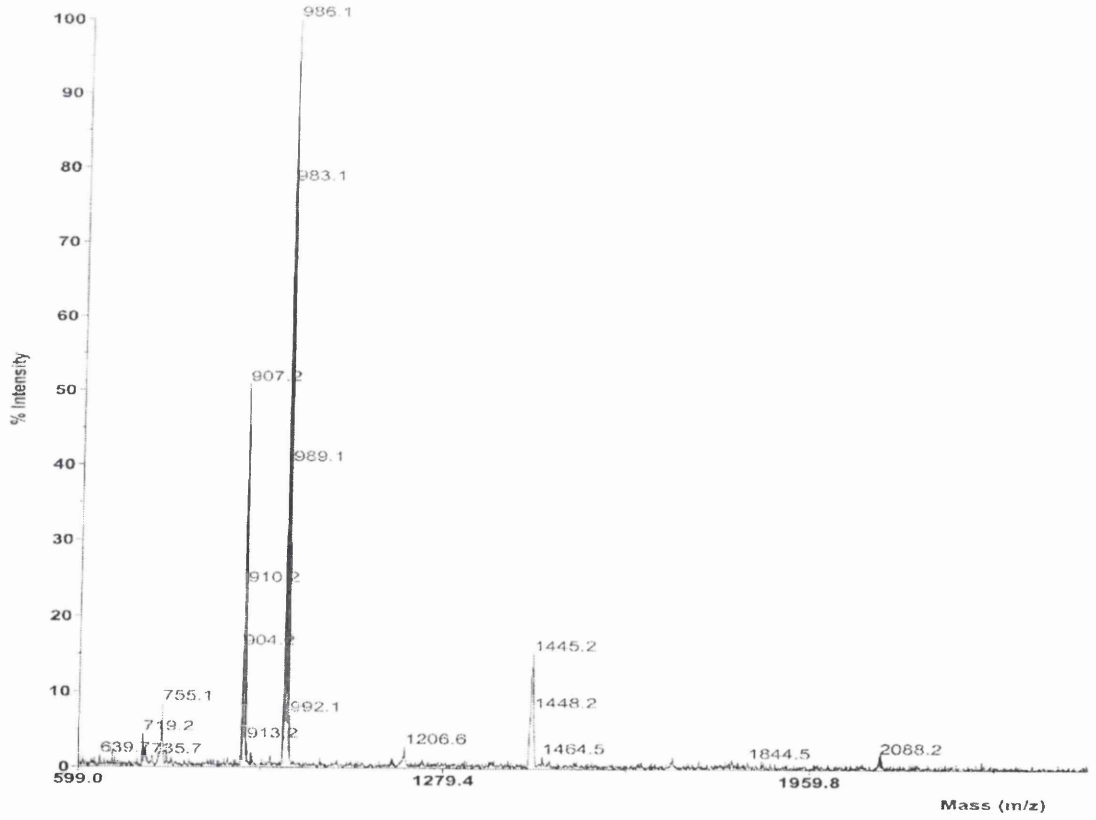

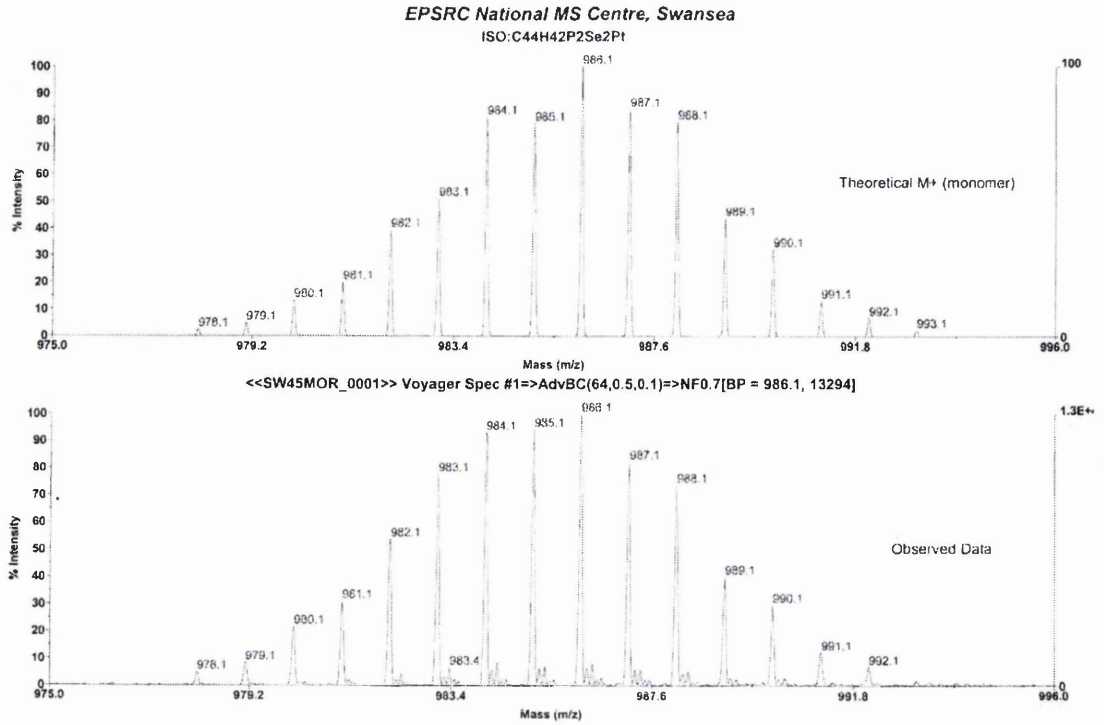

On the basis of this result it was concluded that the poorly soluble yellow powder was, in fact, the diselenolene $[Pt(Se_2C_8H_{12})(PPh_3)_2]$ (figure 2.2). Unfortunately, it was still not possible conclusively to characterize this species as ^{31}P was the only NMR nucleus that could be investigated and it was not possible to obtain a crystal of this compound.

Figure 2.2:

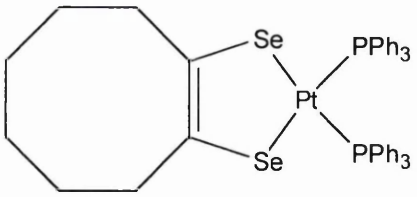

Due to the moderate yield (26%) reported for $[Pt(Se_2C_8H_{12})(PPh_3)_2]$ (experimentally this was not exceeded) some alternative routes to this compound were investigated. The reaction of $[Pt(PPh_3)_4]$ with *bis*-cycloocteno-1,4-diselenin in refluxing toluene was found to give $[Pt(Se_2C_8H_{12})(PPh_3)_2]$ in 33% yield; there was no evidence of the formation of $[Pt(SeC_8H_{12})(PPh_3)_2]$. Reaction of $[Pt(\eta^2\text{-}C_2H_4)(PPh_3)_2]$ with cycloocteno-1,2,3-selenadiazole in refluxing toluene also gives $[Pt(Se_2C_8H_{12})(PPh_3)_2]$. There was no evidence for the formation of $[Pt(SeC_8H_{12})(PPh_3)_2]$, although due to the small scales on which the reactions were carried out (< 0.1 mmol), it cannot be presumed that it wasn't formed at all. In fact $[Pt(\eta^2\text{-}C_2H_4)(PPh_3)_2]$ reacts with

cycloocteno-1,2,3-selenadiazole at room temperature in Et_2O to give small amounts of $[Pt(SeC_8H_{12})(PPh_3)_2]$ (see chapter 3).

Reaction of $[Pt(SeC_8H_{12})(PPh_3)_2]$ with elemental selenium or with cycloocteno-1,2,3-selenadiazole in refluxing toluene has not yielded $[Pt(Se_2C_8H_{12})(PPh_3)_2]$.[114] This indicates that $[Pt(SeC_8H_{12})(PPh_3)_2]$ is not an intermediate in the formation of $[Pt(Se_2C_8H_{12})(PPh_3)_2]$. It is not known whether $[Pt(Se_2C_8H_{12})(PPh_3)_2]$ is formed by direct reaction of '$Pt(PPh_3)_2$' with cycloocteno-1,2,3-selenadiazole and selenium, or whether it is formed by reaction of '$Pt(PPh_3)_2$' with *bis*-cycloocteno-1,4-diselenin formed in solution from cycloocteno-1,2,3-selenadiazole.[92,120] Figure 2.3 shows the proposed reaction routes, all of which are dependent on the loss of dinitrogen from the selenadiazole to give the selenaketocarbene.

Figure 2.3:

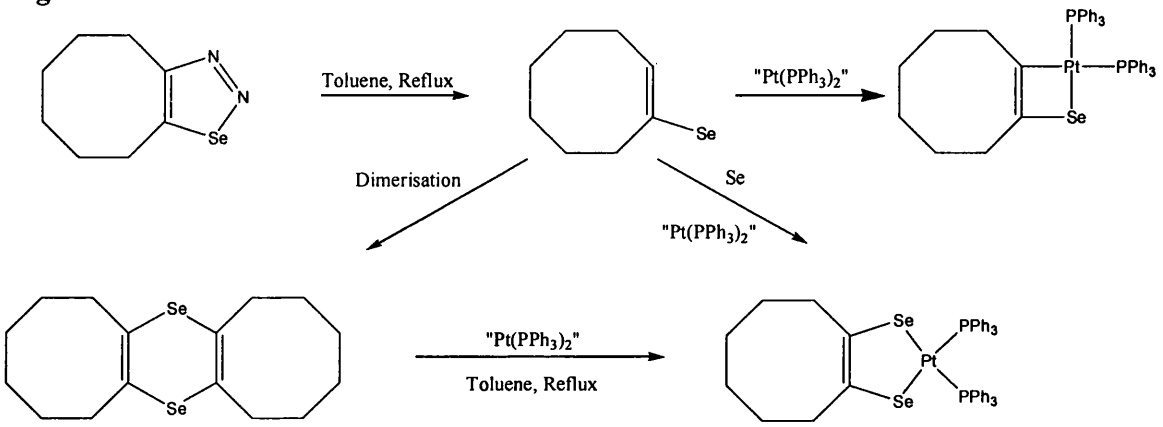

Due to the limited studies that could be carried out on $[Pt(Se_2C_8H_{12})(PPh_3)_2]$ directly, some derivatives were synthesised which could be characterised more easily.

2.1.2 Reactions of $[Pt(Se_2C_8H_{12})(PPh_3)_2]$ with trialkylphosphines and phosphites

Prolonged stirring of $[Pt(Se_2C_8H_{12})(PPh_3)_2]$ with an excess of PR_3 (R = Et, Bu, *i*-C_5H_{11}, OMe) in toluene at elevated temperatures yields diselenolenes of the type $[Pt(Se_2C_8H_{12})(PR_3)_2]$ (figure 2.4). Since $[Pt(Se_2C_8H_{12})(PPh_3)_2]$ is immobile on alumina purification of **1c, 2c, 3c** and **4c** is straightforward. The diselenolenes **1c** and **2c** have been fully characterised and these data are presented later on in this chapter. Compounds **3c** and **4c** were characterised by ^{31}P NMR spectroscopy and FAB mass spectrometry only; they were synthesised to test the range of applicability of the phosphine exchange reaction, so a complete spectral characterisation was not

undertaken. Table 2.1 shows the ^{31}P NMR and mass spectral data for **1c, 2c, 3c** and **4c** (for comparative purposes the data for $[Pt(Se_2C_8H_{12})(PPh_3)_2]$ are also shown).

Figure 2.4:

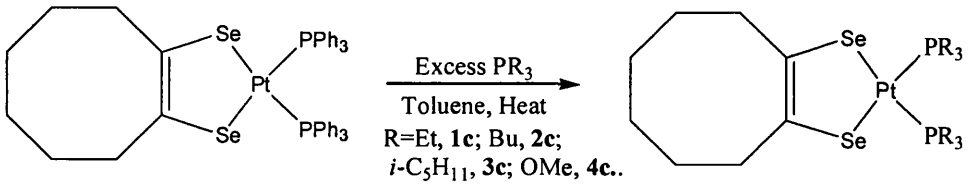

Table 2.1: ^{31}P NMR ($CDCl_3$ solution) and mass spectral data for **1c, 2c, 3c** and **4c**

	1c	**2c**	**3c**	**4c**
^{31}P: δ/ppm	2.4	-5.1	-4.1	107.0
$^1J(^{31}P\text{-}^{195}Pt)$/Hz	2781	2780	2788	4512
MS:[a] *m/z* (%)				
$[M]^+$	699 (20)	867 (30)	951 (10)	711 (15)
$[Pt(PR_3)_2]^+$	431 (100)	599 (100)		

[a] Recorded using FAB; figures are for isotopomers containing ^{195}Pt, ^{80}Se

Compounds **1c, 2c, 3c** and **4c** decompose in air-exposed solution, eventually to a blue coloured species; the decomposition is particularly rapid in $CHCl_3$. The rate of decomposition is dependent upon the phosphine/phosphite substituent in the order **1c** > **2c** > **3c** > **4c**; compound **1c** completely decomposes in hours, whereas **4c** takes several weeks. It is believed that the first stage of this decomposition is actually an oxidation of one of the phosphine substituents. Following the decomposition by ^{31}P NMR spectroscopy shows loss of the diselenolene resonance accompanied by the emergence of two resonances of equal intensity, one of which is at a much lower field (> 100 ppm) than the diselenolene resonance (figure 2.5). Table 2.2 shows the ^{31}P NMR and FAB mass spectral data following decomposition of **1c** and **2c** (this process was not thoroughly investigated for **3c** and **4c** due to the long reaction times).

Table 2.2: ^{31}P NMR ($CDCl_3$ solution) and mass spectral data for **1c** and **2c** decomposition products

	1c	**2c**
^{31}P: $\delta(P_A)$/ppm	6.0	-1.9
$^1J(^{31}P\text{-}^{195}Pt)$/Hz	2777	2808
$\delta(P_B)$/ppm	119.3	114.7
$^1J(^{31}P\text{-}^{195}Pt)$/Hz	3317	3339
MS:[a] *m/z* (%)		
$[M]^+$	714 (30)	883 (90)

[a] Recorded using FAB; figures are for isotopomers containing ^{195}Pt, ^{80}Se

Figure 2.5: ^{31}P NMR spectrum of decomposition product of **1c**

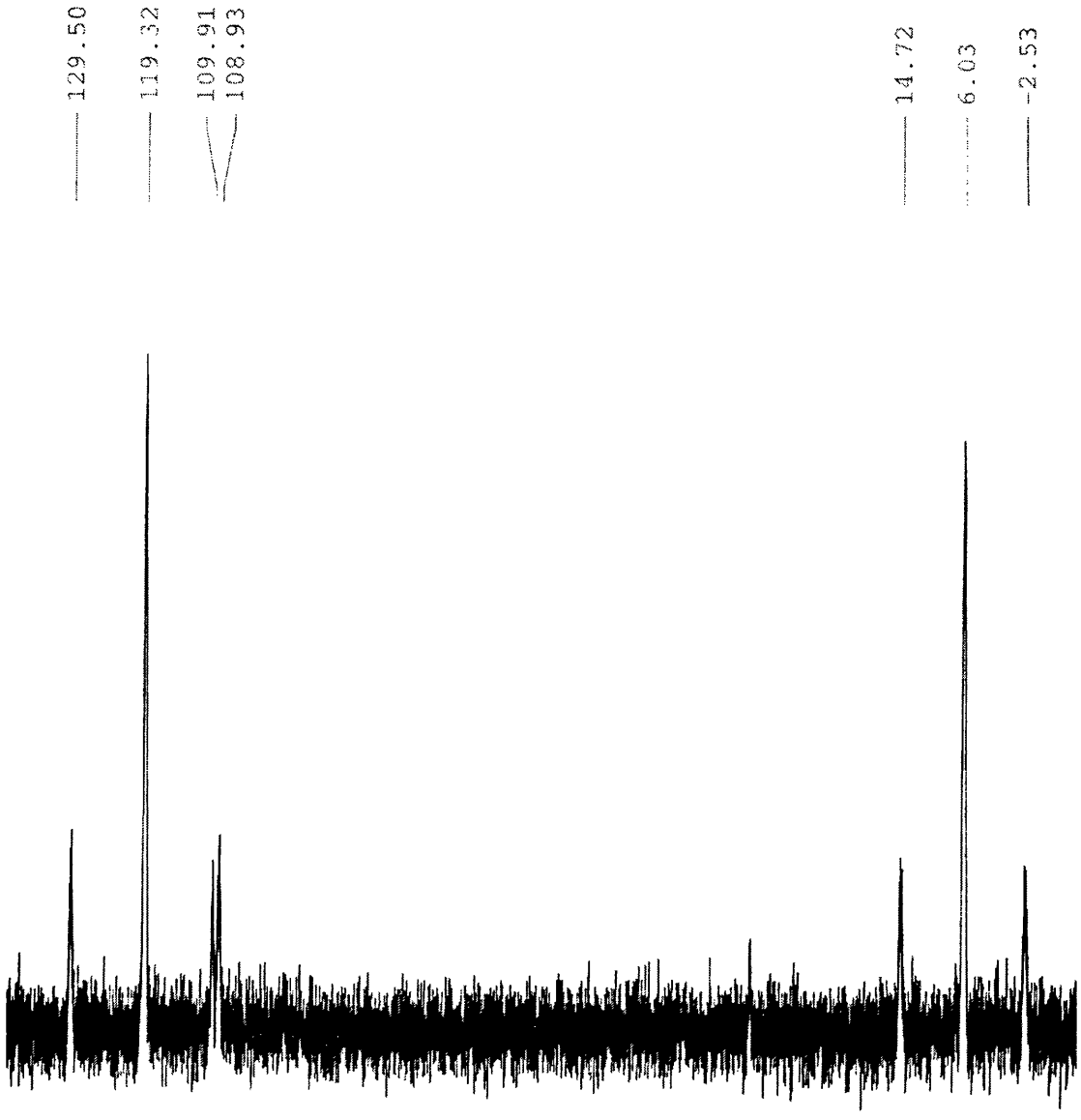

The mass increase of 16 mass units (compared to the diselenolenes) suggests that an oxygen atom is incorporated into the diselenolene. The emergence of two phosphorus resonances in the ^{31}P NMR spectra suggests that it adds asymmetrically to the molecule, with the low field phosphorus resonance suggesting it adds to one of the phosphine ligands (in general phosphorus(V) compounds resonate at much lower field than phosphorus(III) compounds[8]). An infra-red spectrum of a sample of **1c** which had been left to decompose showed a strong absorption band at 1270 cm^{-1}, indicative of a P=O stretch.[218] The rate of decomposition is sensitive to the phosphine substituent: decomposition is slower where bulky phosphines are used (steric hindrance), and slowest for the phosphite-substituted diselenolene (where there is a lower electron density at the phosphorus atom). Based on this information figure 2.6 shows the structure proposed for these species. This is, however, a tentative assignment, as there are two problems associated with it: although there are reports of chelating phosphine oxides bonding to platinum,[219, 220, 221] and one report of $[Pt(C_6F_5)_2(OPPh_3)_2]$,[222] there appears to be no precedent for a platinum trialkylphosphine oxide complex; secondly the large ^{31}P-^{195}Pt coupling constant for the low-field ^{31}P resonance suggests that this phosphorus is bound directly to the platinum.

Figure 2.6:

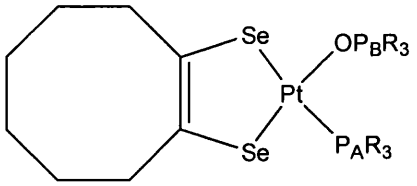

These species undergo further decomposition to dark blue solids that are insoluble in organic solvents. This has prevented in-depth analysis of these compounds.

2.1.3 Reactions of $[Pt(Se_2C_8H_{12})(PPh_3)_2]$ with chelating phosphines

Due to the instability of compounds **1c, 2c, 3c** and **4c** the reactions of $[Pt(Se_2C_8H_{12})(PPh_3)_2]$ with the chelating phosphines dppm, dppe and dppp were carried out. Prolonged stirring of $[Pt(Se_2C_8H_{12})(PPh_3)_2]$ with an excess of L (L = dppm, dppe, dppp) in toluene at 90 °C, followed by column chromatography, led to the isolation of the diselenolenes $[Pt(Se_2C_8H_{12})(L)]$ (L = dppm, **5c**; dppe, **6c**; dppp, **7c**) as green-yellow solids in good yield (figure 2.7).

Figure 2.7:

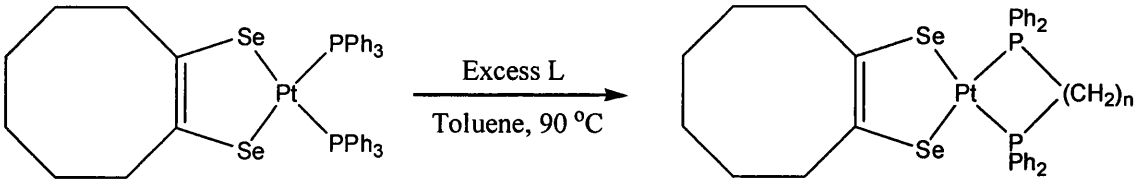

L = dppm, dppe, dppp n = 1, **5c**; 2, **6c**; 3, **7c**.

These compounds have a much greater stability than **1c, 2c, 3c** and **4c**, although prolonged standing in $CHCl_3$ does lead to some decomposition, evidenced by the formation of a blue solid. The greater stability of these compounds is attributed to the lower electron density that results upon changing from a trialkyl- to diarylalkylphosphine.

Crystals of **5c** suitable for x-ray diffraction were grown from a hexane/DCM mixture. The molecular structure is shown in figure 2.8; thermal ellipsoids are drawn at 30% probability and hydrogens are omitted for clarity. The crystal data are summarised in table 2.3, with selected bond lengths and angles listed in table 2.4. Diffraction data were collected on an Oxford Diffraction Excalibur 3 CCD diffractometer with Mo-K_α radiation (λ = 0.71069 Å); structure solution was by heavy atom methods (Patterson methods) with refinement by SHELXL 97.[223]

Figure 2.8: Crystal structure of **5c**

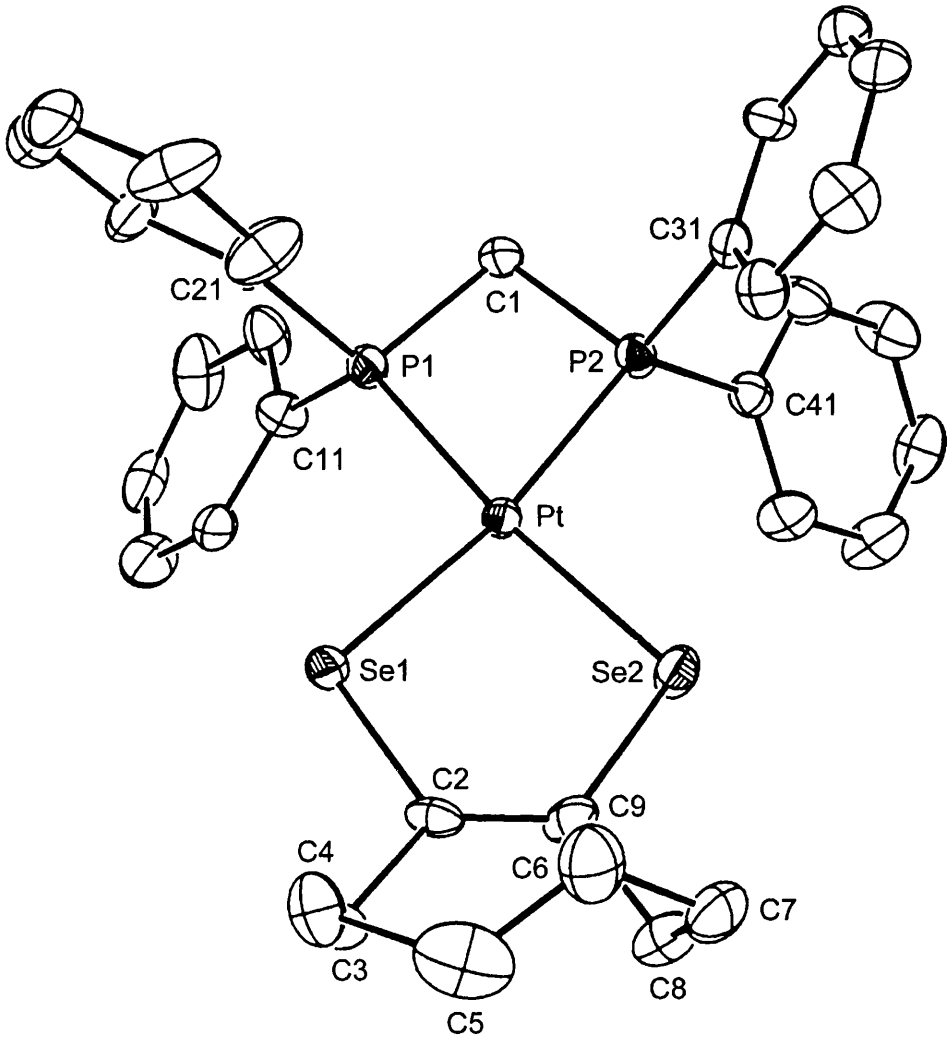

Table 2.3: Crystallographic data for **2a**

Empirical formula	$C_{33}H_{34}P_2Se_2Pt$
Formula weight	845.55
Crystal system	orthorhombic
Space group	P c 2_1 n
Crystal dimensions (mm)	0.40 x 0.40 x 0.25
a/Å	13.504(1)
b/Å	14.049(2)
c/Å	16.183(2)
α/°	90.00
β/°	90.00
γ/°	90.00
V/Å	3070.2(6)
Z	4
F(000)	1632
D_{calc} (g cm^{-3})	1.829
μ (Mo-K_α/mm^{-1})	7.067
Temperature (K)	293
Reflections collected	26820
Independent reflections	6358
θ Range (°)	4.19-27.33
Reflect. with $I > 2\sigma(I)$	4882
No. of parameters	343
R_1; wR_2 [$I > 2\sigma(I)$]	0.0495; 0.1159
R_1; wR_2 (all data)	0.0602; 0.1230
GoF	1.053

Table 2.4: Selected bond lengths and angles of **2a**

Bond lengths (Å)	
Pt-P(1)	2.256(3)
Pt-P(2)	2.254(3)
Pt-Se(1)	2.395(1)
Pt-Se(2)	2.404(1)
Se(1)-C(2)	1.936(12)
Se(2)- C(9)	1.904(12)
C(2)-C(9)	1.282(19)
Bond angles (°)	
P(1)-Pt-P(2)	73.92(9)
P(1)-Pt-Se(1)	98.33(7)
Se(1)-Pt-Se(2)	88.79(4)
Se(2)-Pt-P(2)	99.15(7)
Pt-Se(1)-C(2)	102.50(37)
Pt-Se(2)-C(9)	103.24(38)
Pt-P(1)-C(1)	96.14(34)
Pt-P(2)-C(1)	96.17(36)

As expected the molecule has a square-planar PtP_2Se_2 core; the square plane is quite distorted as a result of the acute P-Pt-P angle (73.92(9)°) imposed by the dppm ligand. The phenyl groups and hydrocarbon ring deviate significantly from the plane of the PtP_2Se_2 core. The square plane is essentially symmetrical with the individual Pt-P (2.25 Å avg.), Pt-Se (2.40 Å avg.) bond lengths and P-Pt-Se (98.8° avg.) bond angles having very similar values; the asymmetry that has been reported for some platinum dithiolenes is not observed.[169] The average Pt-Se bond lengths (2.40 Å) are slightly longer than in the related complexes $[Pt\{Se_2C_2(CF_3)_2\}_2]$[151] and $[Pt(Se_2C_6H_4)(bipy)]$[175] (average 2.37 Å, bipy = 2,2'-bipyridyl). The Se-Pt-Se angle (88.79(4)°) is smaller than in $[Pt\{Se_2C_2(CF_3)_2\}_2]$ (90.24° and 90.32°) and approximately the same as in $[Pt(Se_2C_6H_4)(bipy)]$ (89.72°); The P-Pt-P angle of 73.92(9)° imposed by the dppm ligand is far from the ideal 90° angle of a square planar complex; this will probably result in a poorer Pt-P orbital overlap, which may be reflected in the lower ^{31}P-^{195}Pt and avg. ^{31}P-^{77}Se coupling constants observed for **5c**.

The NMR spectroscopic data for compounds **5c, 6c** and **7c** are shown in tables 2.5 and 2.6 and are in accord with the proposed structures. What is notable here is that there are significant differences in the ^{31}P chemical shifts of the complexes, but the ^{77}Se chemical shifts are very similar. This suggests that the selenium atoms of the diselenolene are not greatly influenced by the ligands present. The ^{77}Se NMR spectra show the expected AA'X pattern (^{77}Se is the X part, with the ^{31}P nuclei magnetically inequivalent), but unfortunately only in **6c** were all five lines visible. In this complex we can see large differences in the *cis-* and *trans-* coupling constants (6 and 86 Hz respectively); the small ^{77}Se-$^{31}P_{cis}$ coupling in these complexes is in part the reason the AA'X pattern was not fully resolved in **5c** and **7c**. The ^{77}Se NMR spectra of diselenolenes will be discussed in more depth later in the chapter.

Compounds **5c, 6c** and **7c** have also been characterized by mass spectrometry and infrared and UV-visible spectroscopies; these data are shown in table 2.7. The crystallographic and spectroscopic data detailed here provide conclusive proof that diselenolenes of the type $[Pt(Se_2C_8H_{12})(L)]$ have been synthesized; therefore the compound of molecular formula $[Pt(Se_2C_8H_{12})(PPh_3)_2]$ can be confidently assigned the structure in figure 2.2.

Interestingly $[Pt(Se_2C_8H_{12})(PPh_3)_2]$ will not undergo substitution reactions with bipy (2,2'-bipyridyl) or mnt (maleonitriledithiolate – $[S_2C_2(CN)_2]^{2-}$). This 'selectivity' of

substitution suggests the electronic influence of the phosphine ligands is important in these complexes.

Table 2.5: ^{1}H and ^{13}C NMR spectroscopic data for **5c, 6c** and **7c** in $CDCl_3$ solution.

		5c	**6c**	**7c**
$\delta\ ^{1}H$	α -*CH*$_2$	2.73-2.90 (4H, m)	2.55-2.70 (4H, m)	2.45-2.70 (4H, m)
	β-*CH*$_2$	1.56-1.69 (4H, m)	1.29-1.59 (4H, m)	1.20-1.60 (4H, m)
	γ -*CH*$_2$	1.32-1.46 (4H, m)	1.29-1.59 (4H, m)	1.20-1.60 (4H, m)
	CH$_2$P	4.61 (2H, t)[a]	2.20-2.45 (4H, m)	1.20-1.60 (4H, m)
	CH$_2$*CH*$_2$CH$_2$	-	-	0.76-0.90 (2H, m)
	PhP	7.25-7.42 (12H, m)	7.25-7.45 (12H, m)	7.15-7.45 (12H, m)
		7.72-7.78 (8H, m)	7.70-7.80 (8H, m)	7.50-7.65 (8H, m)
$\delta\ ^{13}C$	α-*CH*$_2$	37.3[b]	36.7[b]	37.6[b]
	β-*CH*$_2$	31.4	30.3	31.2
	γ-*CH*$_2$	27.1	26.1	27.1
	CH$_2$P	48.0[c]	28.5[c]	26.5[c]
	CH$_2$*CH*$_2$CH$_2$	-	-	24.5
	C=C	not observed	139.2	not observed
	C$_6$H$_5$ - *ortho*	133.6[d]	133.1[d]	134.1[d]
	ipso	132.6	130.9	not observed
	para	131.9	130.7	131.2
	meta	129.5[e]	128.2[e]	128.4[e]

[a] ^{2}J (^{1}H-^{31}P) = 10 Hz, ^{3}J (^{1}H-^{195}Pt) = 42 Hz; [b] ^{3}J (^{13}C-^{195}Pt) = 49 Hz (**5c**), 47 Hz (**6c**), 47 Hz (**7c**); [c] ^{1}J (^{13}C-^{31}P) = 31 Hz (**5c**), for **6c** complex multiplet with avg. J (^{13}C-^{31}P) = 21 Hz, for **7c** coupling unresolved; [d] AA'X system, avg. J (^{13}C-^{31}P) = 6 Hz (**5c, 6c**), 5 Hz (**7c**); [e] AA'X system, avg. J (^{13}C-^{31}P) = 6 Hz (**5c**), 5 Hz (**6c, 7c**).

Table 2.6 ^{31}P and ^{77}Se NMR spectroscopic data for **5c, 6c** and **7c** in $CDCl_3$ solution

	5c	**6c**	**7c**
^{31}P: δ/ppm	-47.4	44.2	-6.6
$^{1}J(^{31}P\text{-}^{195}Pt)$/Hz	2377	2784	2676
^{77}Se: δ/ppm	457	452[a]	466
$^{1}J(^{77}Se\text{-}^{195}Pt)$/Hz	294	268	260
avg. $^{2}J(^{77}Se\text{-}^{31}P)$/Hz	35	46	47
$^{2}J(^{77}Se\text{-}^{31}P_{cis})$/Hz	-[b]	6	-[b]
$^{2}J(^{77}Se\text{-}^{31}P_{trans})$/Hz	-[b]	86	-[b]

[a] AA'X system, $^{2}J(^{31}P\text{-}^{31}P)$ by calculation = 7 Hz; [b] AA'X system but only 3 lines observed.

Table 2.7 Mass spectral, infrared and UV-Vis data for compounds **5c, 6c** and **7c**

		5c	**6c**	**7c**
Mass Spectrum[a]	$[M]^+$	847 (100)	861 (100)	875 (100)
Infrared[b]		2927(m)	2914(m)	2921(m)
		2834(w)	2842(w)	2837(w)
		1584(m)	1586(m)	1585(m)
		1572(w)	1483(w)	1572(w)
		1481(w)	1434(s)	1482(w)
		1459(w)	1260(m)	1433(s)
		1434(s)	1186(w)	1350(w)
		1349(w)	1099(s)	1305(w)
		1308(w)	1025(m)	1259(w)
		1276(w)	998(m)	1186(w)
		1262(w)	906(s)	1156(m)
		1159(m)	878(m)	1124(m)
		1125(m)	817(s)	1099(s)
		1096(s)	715(s)	998(w)
		1026(w)	702(s)	967(m)
		997(m)	688(vs)	906(s)
		878(w)	527(vs)	881(w)
		739(s)		829(m)
		729(vs)		786(m)
		700(s)		715(vs)
		688(vs)		689(vs)
		616(w)		662(s)
		542(s)		615(m)
				550(w)
UV-Vis[c]		365 (3,700)	350 (3,050)	325 (4,000)

[a] *m/z* (%); recorded using FAB; figures are for isotopomers containing ^{195}Pt, ^{80}Se. [b] Selected bands (cm^{-1}) only. [c] λ_{max} (nm); ε (cm^{-1} M^{-1}) in parentheses; recorded in MeCN solution (10^{-4} M) between 300 and 800 nm.

2.1.4 Attempted Syntheses of $[Pt(Se_2C_7H_{10})(PPh_3)_2]$ and $[Pt(Se_2C_6H_8)(PPh_3)_2]$

$[Pt(Se_2C_7H_{10})(PPh_3)_2]$ (figure 2.9) can be synthesised by methods analogous to the syntheses of $[Pt(Se_2C_8H_{12})(PPh_3)_2]$. Refluxing $[Pt(PPh_3)_4]$ with cyclohepteno-1,2,3-selenadiazole or *bis*-cyclohepteno-1,4-diselenin in toluene gave $[Pt(Se_2C_7H_{10})(PPh_3)_2]$ as a poorly soluble yellow solid, in a 14% yield. This yield is lower than that of $[Pt(Se_2C_8H_{12})(PPh_3)_2]$ (~33%), and upon prolonged standing in $CDCl_3$ decomposition occurs ($[Pt(Se_2C_8H_{12})(PPh_3)_2]$ appears to be indefinitely stable in $CHCl_3$).

Figure 2.9:

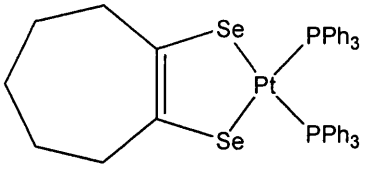

The reaction of $[Pt(\eta^2\text{-}C_2H_4)(PPh_3)_2]$ and cyclohepteno-1,2,3-selenadiazole at room temperature in Et_2O gave $[Pt(SeC_7H_{10})(PPh_3)_2]$ in a 23% crude yield (compounds of this type are discussed in chapter 3). Due to the poor yield of these reactions and apparent instability of the compounds produced only a ^{31}P NMR and mass spectral analysis were carried out; table 2.8 shows the data collected.

Table 2.8: ^{31}P NMR ($CDCl_3$ solution) and mass spectral data for $[Pt(Se_2C_7H_{10})(PPh_3)_2]$ and $[Pt(SeC_7H_{10})(PPh_3)_2]$

	$[Pt(Se_2C_7H_{10})(PPh_3)_2]$	$[Pt(SeC_7H_{10})(PPh_3)_2]$
^{31}P: $\delta(P_A)$/ppm	18.4	22.7
$^1J(^{31}P\text{-}^{195}Pt)$	2914	1905
$\delta(P_B)$/ppm	-	23.0
$^1J(^{31}P\text{-}^{195}Pt)$	-	3598
MS:[a] *m/z* (%)		
$[M]^+$	973 (100)	893 (100)

[a] Recorded using FAB; figures are for isotopomers containing ^{195}Pt, ^{80}Se

Attempts to prepare and isolate $[Pt(Se_2C_6H_8)(PPh_3)_2]$ (figure 2.10) in reasonable yield were unsuccessful. Treatment of $[Pt(PPh_3)_4]$ with cyclohexeno-1,2,3-selenadiazole or *bis*-cyclohexeno-1,4-diselenin in refluxing toluene yielded very small amounts of crude $[Pt(Se_2C_6H_8)(PPh_3)_2]$, evidenced by a resonance in the ^{31}P NMR spectra at δ = 17.8 ppm ($^1J(^{31}P\text{-}^{195}Pt)$ ~ 2900 Hz). The spectra also showed peaks indicative of decomposition of $[Pt(PPh_3)_4]$, or possibly the product. The mass spectra showed weak peaks around *m/z* = 959 ($[M]^+$) and 982 ($[M + Na]^+$).

Figure 2.10:

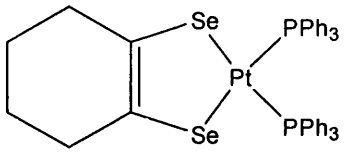

Interestingly in the reaction of $[Pt(PPh_3)_4]$ (or $[Pt(\eta^2\text{-}C_2H_4)(PPh_3)_2]$) with cyclohexeno-1,2,3-selenadiazole, the reaction mixture becomes a purple colour at both room temperature and at reflux probably due to the formation of $[Pt\{SeC(R^1)=C(R^2)N=NC(R^1)=C(R^2)Se\}(PPh_3)]$ (R^1-R^2 = $(CH_2)_4$). This was also observed at room temperature when $[Pt(PPh_3)_4]$ was reacted with cycloheptenо-1,2,3-selenadiazole (although this reaction took several days). The formation of these types of compounds will be discussed in full later. No evidence for the formation of $[Pt(SeC_6H_8)(PPh_3)_2]$ was found in the reaction carried out at room temperature; it should also be noted, in a prolonged reaction of $[Pt(PPh_3)_4]$ with cycloocteno-1,2,3-selenadiazole at room temperature there was no evidence of the above type of complex being formed.

2.2 The Synthesis of Platinum Diselenolenes $[Pt(Se_2C_{n+4}H_{2n+4})(PR_3)_2]$ (n = 2, 3, 4; R = Et, Bu)

The platinum diselenolenes $[Pt(Se_2C_{n+4}H_{2n+4})(PR_3)_2]$ (n = 2, 3, 4; R = Et, Bu) were obtained by refluxing $[Pt(C_2H_4)(PR_3)_2]$ with *bis*-cycloalkeno-1,4-diselenins in a dioxane/toluene/THF mixture. Subsequent column chromatography led to the isolation of $[Pt(Se_2C_{n+4}H_{2n+4})(PR_3)_2]$ as pale green solids (figure 2.11).

Figure 2.11:

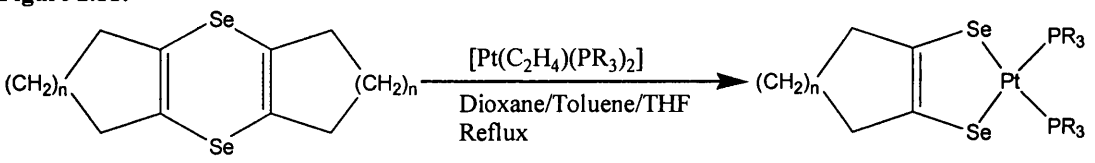

	n = 2	3	4
R = Et	**1a**	**1b**	**1c**
Bu	**2a**	**2b**	**2c**

Since *bis*-cycloalkeno-1,4-diselenins can be synthesised by heating the corresponding cycloalkeno-1,2,3-selenadiazoles, the synthesis of **1a-c** and **2a-c** in this way provides further evidence that in the reaction of $[Pt(PPh_3)_4]$ with cycloocteno-1,2,3-selenadiazole, $[Pt(Se_2C_8H_{12})(PPh_3)_2]$ is produced via *bis*-cycloocteno-1,4-diselenin.

The yields of compounds **1a** and **2a** are poor (the crude yields appear high but the material is very impure). It is believed that a cycloalkyne is generated in the reaction pathway (figure 2.12); cyclohexyne is a very strained alkyne (due to sp hybridisation at carbon, alkynes are ideally linear[224]) and would not be easily formed. It is proposed that this is responsible for the poor yield of **1a** and **2a**; even with a prolonged reflux the reaction yield is not improved. A similar situation was encountered in the synthesis of $[Pd(Se_2C_6H_8)(PBu_3)_2]$ from $[Pd_2(dba)_3]$.dba, PBu_3 and *bis*-cyclohexeno-1,4-diselenin, where a prolonged reflux in xylene was necessary to give the product;[127] unfortunately the ethereal solvents used in the *in situ* synthesis of $[Pt(C_2H_4)(PR_3)_2]$ reduce the temperature at which the reaction can be carried out. Cycloheptyne and cyclooctyne are less strained and so **1b,c** and **2b,c** are more easily accessed.

The synthesis of diselenolenes of the type $[Pt(Se_2C_{n+4}H_{2n+4})(L)]$ (L = dppm, dppe), was attempted by reaction of $[Pt(C_2H_4)(L)]$ with *bis*-cycloalkeno-1,4-diselenins. These reactions were unsuccessful; there was no trace of the desired products. This result reinforces the proposed reaction pathway (figure 2.12); it appears a phosphine dissociation step is necessary, which for chelating phosphines (dppm, dppe) is not

favoured, and this would explain why the reaction is unsuccessful. The synthesis of **2a** was attempted in the presence of excess tributylphosphine, in an attempt to increase the yield by favouring the final step of the mechanism; this however failed to give any of the product, which suggests, *if* the mechanism in figure 2.12 is correct, that alkyne formation is the key step. The synthesis of **2c** was carried out in the presence of tetraphenylcyclopentadienone to trap any cyclooctyne generated via a Diels-Alder reaction;[92] unfortunately the presence of the tetraphenylcyclopentadienone appears to have interfered in the reaction and no diselenolene was produced.

Figure 2.12:

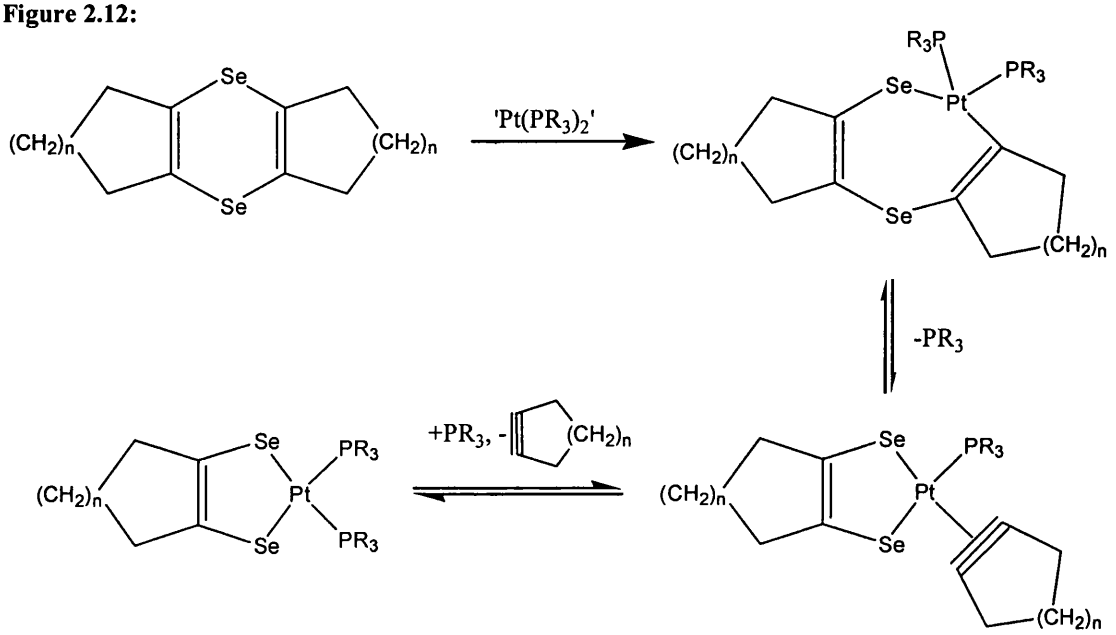

Although it is possible to synthesise mononuclear or dinuclear palladium diselenolenes (figure 2.13),[117,126,127] there is no evidence for the formation of dinuclear platinum diselenolenes in these reactions. This is probably due to the platinum-phosphine stoichiometry of 1:2 imposed by the starting material; with the palladium compounds the palladium-phosphine stoichiometry could be altered to give either the mononuclear or dinuclear product.

Figure 2.13:

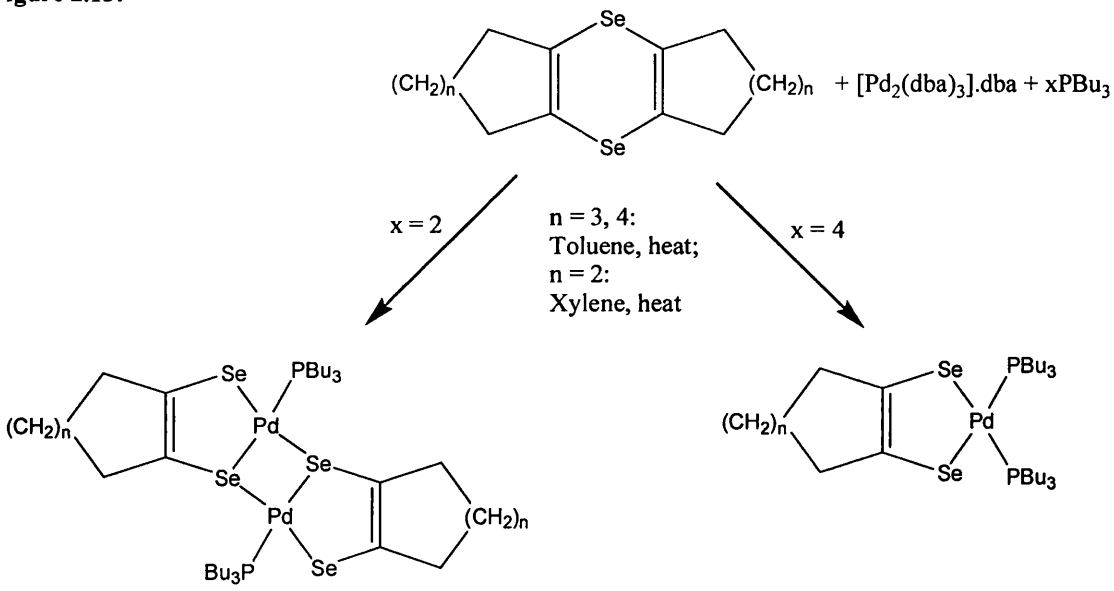

Compounds **1a-c** and **2a-c** appear to be stable in hexane, toluene, EtOAc, acetone and DCM; it seems that the decomposition documented earlier only occurs at an appreciable rate in $CHCl_3$. It was possible to obtain crystals of **1b,c** and **2b** by recrystallisation from hexane/DCM. Full crystallographic characterisations of **1b** and **1c** were obtained, along with a partial crystallographic characterisation of **2b**. Diffraction data were collected on an Oxford Diffraction Excalibur 3 CCD diffractometer with Mo-K_α radiation (λ = 0.71069 Å); structure solution was by SIR 97[225] with refinement by SHELXL 97.[223]

Figures 2.14 and 2.15 show the crystal structures of **1b** and **1c**; thermal ellipsoids are drawn at 30% probability and hydrogen atoms are omitted for clarity. The structures are presented using the Mercury program (version 1.4.1).

Figure 2.14: Crystal structure of **1b**

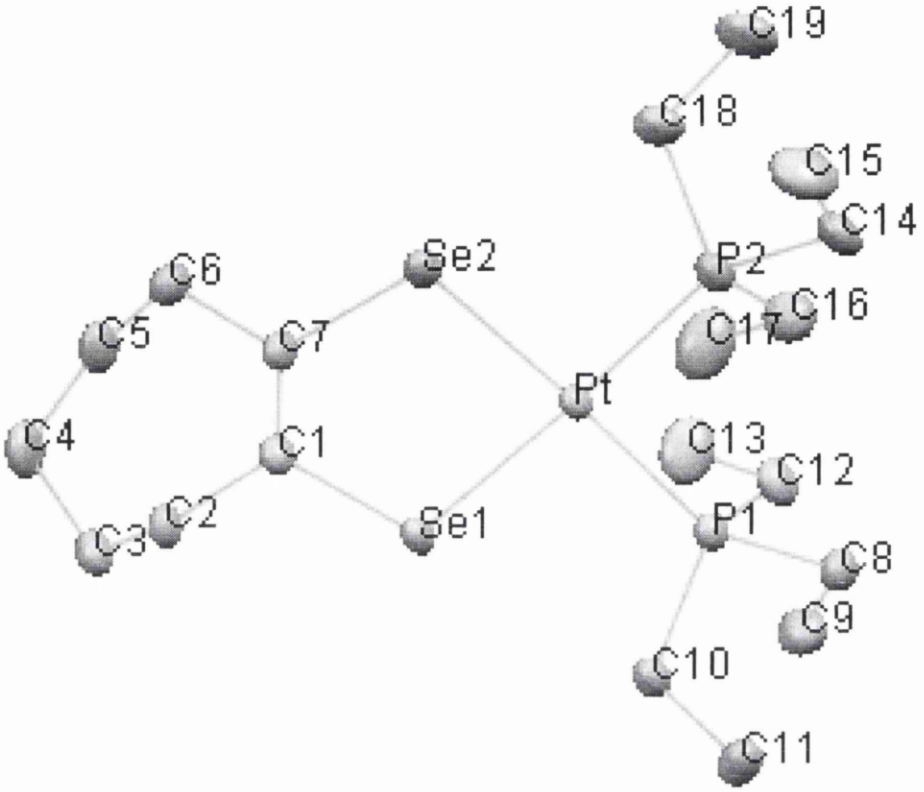

Figure 2.15: Crystal structure of **1c**

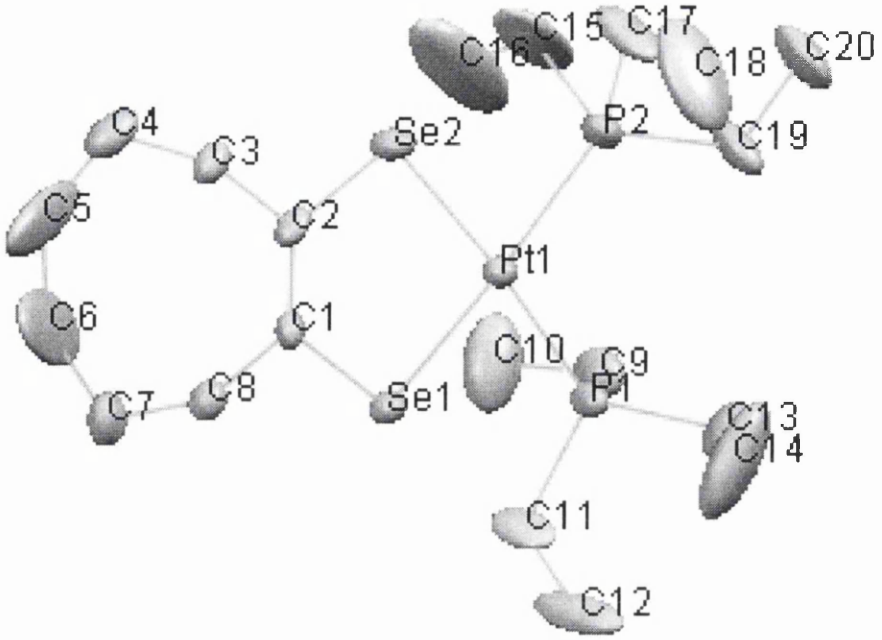

Table 2.9 shows the crystallographic data for **1b,c** and **2b**; table 2.10 shows some selected bond lengths and angles of **1b,c** and **2b**. As can be seen from the data, it was not possible to determine the bond lengths and angles of **2b** to a reasonable degree of accuracy. For this reason these data are not considered in the discussion. The crystal structure is still chemically meaningful, however, and is shown in figure 2.16. Thermal ellipsoids are shown at 30% probability and hydrogen atoms are omitted for clarity.

Table 2.9: Crystallographic data for **1b,c** and **2b**

	1b	**1c**	**2b**
Empirical formula	$C_{19}H_{40}P_2Se_2Pt$	$C_{20}H_{42}P_2Se_2Pt$	$C_{31}H_{64}P_2Se_2Pt$
Formula weight	683.46	697.49	851.80
Crystal system	orthorhombic	triclinic	monoclinic
Space group	P bca	P –1	P 2_1/c
Crystal dimensions (mm)	0.45 x 0.40 x 0.36	0.70 x 0.60 x 0.40	Not recorded
a/Å	11.584(1)	12.75(2)	10.40(2)
b/Å	15.516(2)	14.07(2)	22.06(3)
c/Å	27.248(2)	16.77(3)	16.71(4)
α/°	90.00	110.40(10)	90.00
β/°	90.00	108.6(2)	95.9(2)
γ/°	90.00	99.40(10)	90.00
V/Å	4897.5(8)	2542(7)	3813.4(1)
Z	8	2	4
F(000)	2640	1352	1634
D_{calc} (g cm^{-3})	1.854	1.823	1.130
μ (Mo-K_α/mm^{-1})	8.834	8.514	5.69
Temperature (K)	293	293	293
Reflections collected	49970	28249	31125
Independent reflections	9495	16443	12817
θ Range (°)	4.04-34.51	4.32-33.92	Not recorded
Reflect. with $I > 2\sigma(I)$	5117	6914	3056
No. of parameters	229	467	331
R_1; wR_2 [$I > 2\sigma(I)$]	0.0570; 0.01322	0.0465; 0.0909	0.1073; -
R_1; wR_2 (all data)	0.1135; 0.1520	0.0984; 0.1023	0.3768; 0.3511
GoF	0.935	0.770	0.908

Table 2.10: Selected bond lengths and angles for **1b, 1c** and **2b**

	1b	**1c**	**2b**
Bond lengths (Å)			
Pt-P(1)	2.290(2)	2.277(5)	2.308(7)
Pt-P(2)	2.296(2)	2.272(4)	2.283(5)
Pt-Se(1)	2.4169(7)	2.400(4)	2.404(3)
Pt-Se(2)	2.4137(7)	2.408(5)	2.425(6)
Se(1)-C(1)	1.898(7)	1.894(8)	1.913(25)
Se(2)-C(7)	1.893(7)		1.904(19)
Se(2)-C(2)		1.870(8)	
C(1)-C(7)	1.316(9)		1.256(31)
C(1)-C(2)		1.298(9)	
Bond angles (°)			
P(1)-Pt-P(2)	95.69(6)	96.68(13)	99.37(20)
P(1)-Pt-Se(1)	89.22(5)	90.09(12)	89.01(17)
Se(1)-Pt-Se(2)	86.76(2)	86.72(11)	87.20(14)
Se(2)-Pt-P(2)	88.60(5)	86.67(13)	84.41(17)
Pt-Se(1)-C(1)	104.78(21)	104.25(24)	103.42(65)
Se(1)-C(1)-C(7)	121.47(5)		123.33(1.42)
Se(1)-C(1)-C(2)		122.12(56)	
C(1)-C(7)-Se(2)	122.26(48)		122.38(1.81)
C(1)-C(2)-Se(2)		122.20(53)	
Pt-Se(2)-C(7)	104.68(20)		103.42(88)
C(2)-Se(2)-Pt		104.71(23)	

*Note that the C(2) atom of **1c** is equivalent to the C(7) atoms of **1b** and **2b**

Each complex consists of a (slightly distorted) square planar $PtSe_2P_2$ core, with only the hydrocarbon ring and ethyl groups protruding significantly from the plane. The size of the hydrocarbon ring appears to have a slight effect on the bond lengths, with the Pt-P, Pt-Se and C=C bond lengths in **1b** approximately 0.2 Å longer than those in **1c**. Within the square plane of **1b** the pairs of Pt-P, Pt-Se lengths and P-Pt-Se angles are close in value, but the square plane of **1c** is slightly asymmetric with one Pt-Se bond slightly longer (*ca.* 0.01 Å) than the other, and the P-Pt-Se angles significantly different (90.1° *vs.* 86.7°). A similar distortion has been observed in the structures of palladium diselenolenes[127] and platinum dithiolenes.[169] The average Pt-Se bond lengths in **1b** and **1c** (2.41 Å) are slightly longer than in the related complexes $[Pt\{Se_2C_2(CF_3)_2\}_2]$[152,155] and $[Pt(Se_2C_6H_4)(bipy)]$[175] (average 2.37 Å, bipy = 2,2'-bipyridyl). This can be attributed to the hydrocarbon backbone being less electron-withdrawing than CF_3 and benzene substituents. Also the Se-Pt-Se angles in **1b** and **1c** (average 86.7°) are smaller than those in $[Pt(Se_2C_2(CF_3)_2)_2]$ (90.24° and 90.32°) and

[$Pt(Se_2C_6H_4)(bipy)$] (89.72°); this is probably a result of the large P-Pt-P angles of 95.7° (**1b**) and 96.7° (**1c**), which can be attributed to the steric repulsion of the ethyl groups.

Figure 2.16: Crystal structure of **2b**

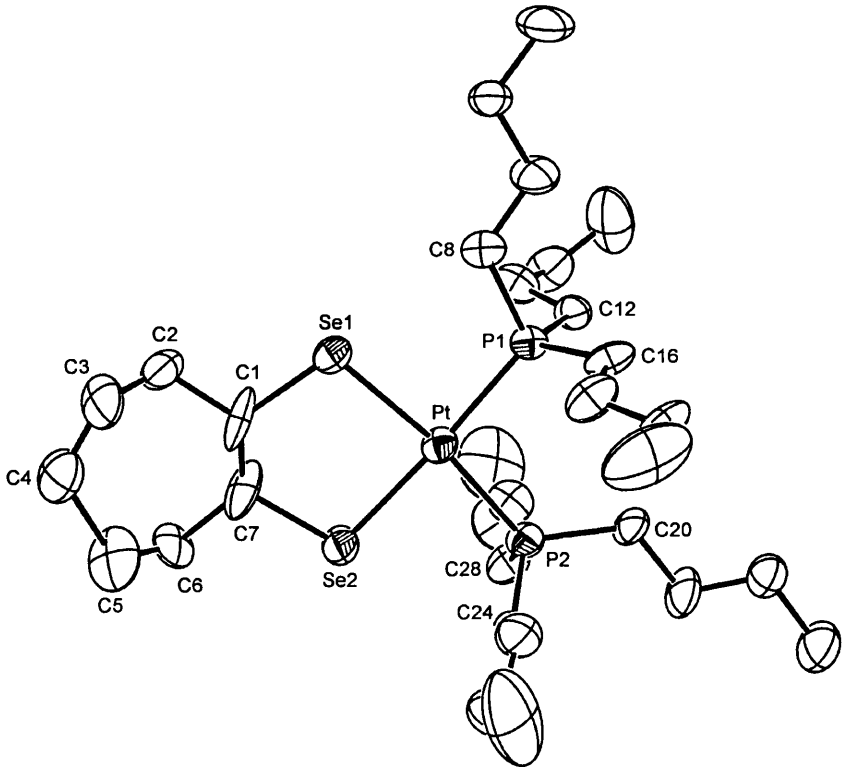

The NMR spectroscopic data for **1a-c** and **2a-c** are shown in tables 2.11 and 2.12. Due to the difficulties in synthesizing and purifying **1a** and **2a**, the spectroscopic characterisations of these complexes are incomplete, although the spectroscopic data it was possible to obtain fit well with the data obtained for **1b,c** and **2b,c**. The spectra are in accord with the proposed structures with the ^{77}Se NMR resonances showing the patterns expected for the X part of an AA'X spin system (a result of the ^{31}P nuclei being chemically but not magnetically equivalent). These consist of five lines (ignoring the satellites due to ^{77}Se-^{195}Pt coupling) from which the coupling constants $^1J(^{77}Se\text{-}^{195}Pt)$, $^2J(^{77}Se\text{-}^{31}P_{cis})$, $^2J(^{77}Se\text{-}^{31}P_{trans})$ and $^2J(^{31}P\text{-}^{31}P)$ can be established by calculation based on the relative intensities of the lines. These parameters are more precisely accessible by analysis of the ^{77}Se satellite structure of the single ^{31}P resonance, but difficulties were encountered in obtaining ^{31}P NMR spectra with

sufficiently good signal-to-noise ratios. All five lines of the AA'X pattern were observed in **1b,c** and **2b,c**; as an example figure 2.17 shows the ^{77}Se resonance of **2c.**

Figure 2.17: ^{77}Se NMR spectrum of **2c**

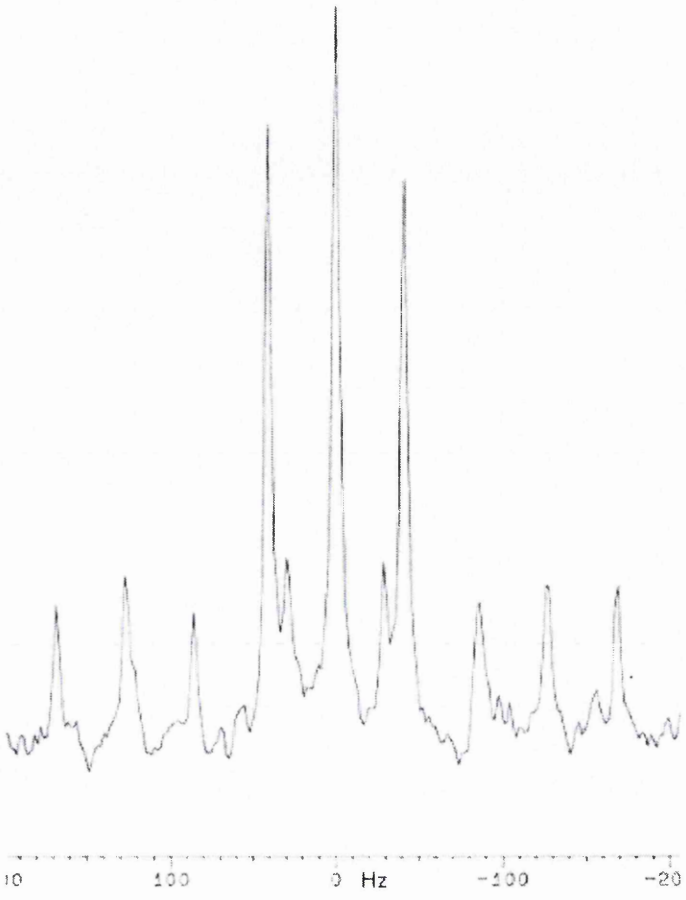

Table 2.11: ^{1}H and ^{13}C NMR spectroscopic data for **1a-c** and **2b,c** in d_6-acetone solution

		1a	**1b**	**1c**	**2b**	**2c**
^{1}H	*CH*$_3$	Not recorded	0.89 (18H, dt)[a]	0.99 (18H,dt)[a]	0.81 (18H, t)[a]	0.80 (18H, t)[a]
	CH$_2$P		1.78-1.90 (12H, m)	1.90-2.10 (12H, m)	1.85-2.10 (12H, m)	1.90-2.01 (12H, m)
	CH$_3$*CH*$_2$CH$_2$		-	-		
	CH$_2$CH$_2$P		-	-	1.25-1.60 (24H, m)	1.24-1.50 (24H, m)
	γ -CH$_2$		1.75-1.83 (2H, m)	1.41-1.57 (4H, m)	1.85-2.10 (2H, m)	1.90-2.01 (4H, m)
	β-CH$_2$		1.27-1.35 (4H, m)	1.24-1.34 (4H, m)	1.25-1.60 (4H, m)	1.24-1.50 (4H, m)
	α -CH$_2$		2.29-2.50 (4H, m)	2.42-2.56 (4H, m)	2.40-2.50 (4H, m)	2.41-2.46 (4H, m)
^{13}C	*CH*$_3$	8.6[b]	8.2[b]	8.2[b]	13.9	14.0
	CH$_2$P	18.3	17.9[c]	18.0[c]	25.9[c]	26.0[c]
	CH$_2$CH$_2$P	-	-	-	24.5[d]	24.5[d]
	CH$_3$*CH*$_2$CH$_2$	-	-	-	26.7[e]	26.7[e]
	C=C	-	131.1	130.2	130.8	130.0
	α-CH$_2$	35.7[f]	39.3[f]	37.0[f]	39.3[f]	37.0[f]
	β-CH$_2$	31.4	33.8	31.2	33.8	31.2
	γ-CH$_2$	-	27.7	26.7	27.7	26.7

[a] $^{3}J(^{1}H\text{-}^{1}H)$ = 7.6 Hz (**1b,c, 2c**), 7.2 Hz (**2b**) $^{3}J(^{1}H\text{-}^{31}P)$ = 16 Hz (**1b,c**); [b] $^{3}J(^{13}C\text{-}^{195}Pt)$ = 21 Hz (**1a**), 20 Hz (**1b**), 24 Hz (**1c**); [c] AA'X system, avg. $J(^{13}C\text{-}^{31}P)$ = 16 Hz (**1b**), 18 Hz (**1c, 2b,c**), $^{2}J(^{13}C\text{-}^{195}Pt)$ = 26 Hz (**1b,c**), 25 Hz (**2b,c**); [d] AA'X system, avg. $J(^{13}C\text{-}^{31}P)$ = 7 Hz; [e] $^{4}J(^{13}C\text{-}^{195}Pt)$ = 19 Hz; [f] $^{2}J(^{13}C\text{-}^{195}Pt)$ = 45 Hz (**1b**), 44 Hz (**1c**), 47 Hz (**2b**), 46 Hz (**1a, 2c**).

Table 2.12: ^{31}P and ^{77}Se NMR spectroscopic data for **1a-c** and **2a-c** in d_6-acetone solution

		1a	**1b**	**1c**	**2a**	**2b**	**2c**
^{31}P:	δ/ppm	2.8	2.5	2.4	-4.8	-5.3	-5.1
	$^{1}J(^{31}P\text{-}^{195}Pt)$/Hz	2781	2767	2781	2787	2767	2780
^{77}Se:	δ/ppm	453	481	441	Not	474	454
	$^{1}J(^{77}Se\text{-}^{195}Pt)$/Hz	256	268	268	recorded	264	256
	avg. $^{2}J(^{77}Se\text{-}^{31}P)$/Hz	41	41	40		40	41
	$^{2}J(^{77}Se\text{-}^{31}P_{cis})$/Hz	-[a]	14	16		16	18
	$^{2}J(^{77}Se\text{-}^{31}P_{trans})$/Hz	-[a]	67	63		64	64
	$^{2}J(^{31}P\text{-}^{31}P)$/Hz	-[a]	20	20		19	18

[a] AA'X pattern not fully resolved.

The two ^{31}P-^{77}Se coupling constants ($^{2}J(^{77}Se\text{-}^{31}P_{trans})$ = 67 Hz (**1b**), 63 Hz (**1c**), 64 Hz (**2b,c**); $^{2}J(^{77}Se\text{-}^{31}P_{cis})$ = 14 Hz (**1b**), 16 Hz (**1c**, **2b**), 18 Hz (**2c**)) are very similar to those of $[Pd(Se_2C_{n+4}H_{2n+4})(PBu_3)_2]$[127] (avg. $^{2}J(^{77}Se\text{-}^{31}P_{trans})$ = 66 Hz, $^{2}J(^{77}Se\text{-}^{31}P_{cis})$ = 16 Hz). The calculated ^{31}P-^{31}P coupling constants are quite different however: $^{2}J(^{31}P\text{-}^{31}P)$ = 20 Hz (**1b,c**), 19 Hz (**2b**), 18 Hz (**2c**), *cf.* $^{2}J(^{31}P\text{-}^{31}P)$ = 44 Hz in $[Pd(Se_2C_{n+4}H_{2n+4})(PBu_3)_2]$. The calculated $^{2}J(^{77}Se\text{-}^{31}P_{trans})$ coupling constant of 86 Hz for compound **6c** is greater than those for **1b,c** and **2b,c**; this could be a direct result of the geometrical constraints placed on the $PtSe_2P_2$ core by the chelating phosphine. Although there is no crystal structure for **6c** the Pt-Se and Pt-P bond lengths of **5c** are shorter than those of **1b** and **1c** by approximately 0.01 and 0.03 Å respectively. The ^{77}Se chemical shifts of complexes **5c, 6c** and **7c** are not significantly different from those of **1c** and **2c** however. One point of note is that the ^{77}Se resonances of compounds **1b** and **2b** are at much lower field (approximately 30 ppm) than those of **1a**, **1c** and **2c**. This phenomenon is also observed in diselenolenes,[117,127] 1,2,3-selenadiazoles and 1,4-diselenins:[92] the number of carbon atoms in the aliphatic ring appears to have an influence on the electronic environment of the selenium atoms, with the C_7 ring giving lower field ^{77}Se NMR resonances than the C_6 and C_8 ring analogues. It is not clear why this is the case and whether it is limited to the C_6-C_8 ring sizes: syntheses of diselenolenes with a C_5 ring are highly unlikely to be successful (due to cyclopentyne being a very strained alkyne), and cyclononanone (an assumed precursor to cyclononeno-1,2,3-selenadiazole) is too expensive to warrant syntheses of diselenolenes with a C_9 ring. This effect of ring size upon chemical shift is also observed in the ^{13}C NMR of these compounds: the resonances of the aliphatic ring carbons are all at lower field for **1b** and **2b**. The resonances associated with the C=C group were weak, and as such the coupling constants associated with these peaks could not be determined.

Characterisation by FAB mass spectrometry (**1a-c, 2a-c**) and IR and UV-visible spectroscopy (**1b,c, 2b,c**) has also been carried out with the data presented in table 2.13. The mass spectra show a dominance of the $[Pt(PR_3)_2]^+$ ion indicating that cleavage of the Pt-Se bonds is relatively easy under mass spectrometry conditions. The colours of **1a-c** and **2a-c** (pale green) differ significantly from those of $[Pd(Se_2C_{n+4}H_{2n+4})(PBu_3)_2]$ and $[Pd_2(Se_2C_{n+4}H_{2n+4})_2(PBu_3)_2]$ (purple),[120] highlighting the sensitivity of the electronic properties of diselenolenes to the chemical

environment. The UV-visible spectra of the palladium diselenolenes show absorptions in the UV and the visible region, which are associated with a ligand to metal charge transfer (LMCT) band. Compounds **1b,c** and **2b,c** show no absorptions of significant intensity in the visible region, but do show large absorptions in the UV region. Since platinum is more difficult to reduce than palladium, it is assumed that the lowest energy LMCT band has been shifted into the UV region due to the higher energy associated with charge transfer to platinum. Unless we consider these complexes as diselenolates coordinated to an M^{2+} centre, then LMCT is not a wholly suitable description here; what is probably happening is that within the delocalised electron system of the diselenolene an electron is moving from a molecular orbital with a significant selenium component to one with a greater contribution from the metal. A comparison of the UV-visible spectra of $[Pd(Se_2C_8H_{12})(PBu_3)_2]$ and **2c** is shown in figure 2.18.

Table 2.13: Mass spectral, infrared and UV-Vis data for compounds **1a-c** and **2a-c**

		1a	**1b**	**1c**	**2a**	**2b**	**2c**
Mass Spectrum[a]	$[M]^+$	671 (100)	685 50)	699 (20)	839 (30)	853 (30)	867 (30)
	$[Pt(PR_3)_2]^+$	431 (70)	431 (100)	431 (100)	599 (100)	599 (100)	599 (100)
Infrared[b]		Not recorded	2959 (m)	2963 (m)	Not Recorded	2954 (s)	2952 (m)
			2915 (s)	2910 (s)		2916 (s)	2924 (s)
			1594 (w)	2840 (m)		2870 (m)	2837 (m)
			1440 (s)	1595(m)		1453 (m)	1459 (s)
			1354 (w)	1450 (s)		1405 (w)	1423 (w)
			1251 (w)	1415 (s)		1376 (w)	1378 (w)
			1211 (w)	1373 (w)		1349 (w)	1207 (w)
			1074 (w)	1223 (m)		1203 (m)	1125 (w)
			1029 (s)	1125 (w)		1092 (s)	1088 (m)
			997 (w)	1033 (s)		1047 (s)	1045 (w)
			757 (s)	880 (w)		1005 (w)	900 (s)
			726 (vs)	762 (s)		904 (s)	774 (s)
			635 (m)	720 (s)		891 (m)	720 (vs)
						773 (m)	610 (w)
						714 (s)	
UV-Vis[c]		Not Recorded	220 (26,400)	215 (26,300)	Not Recorded	220 (28,100)	215 (37,500)
			235 (29,500)	240 (29,200)		240 (36,900)	240 (37,500)
			320 (4500)	320 (4,700)		320 (5,100)	320 (5,500)

[a] *m/z* (%); recorded using FAB; figures are for isotopomers containing ^{195}Pt, ^{80}Se, ^{12}C, ^{1}H; expected isotope patterns were observed. [b] Selected bands (cm^{-1}) only. [c] λ_{max} (nm); ε (cm^{-1} M^{-1}) in parentheses; recorded in DCM solution (10^{-5} M).

Figure 2.18: UV-visible spectra of **2c** and the palladium analogue $[Pd(Se_2C_8H_{12})(PBu_3)_2]$ (not on same scale)

2c:

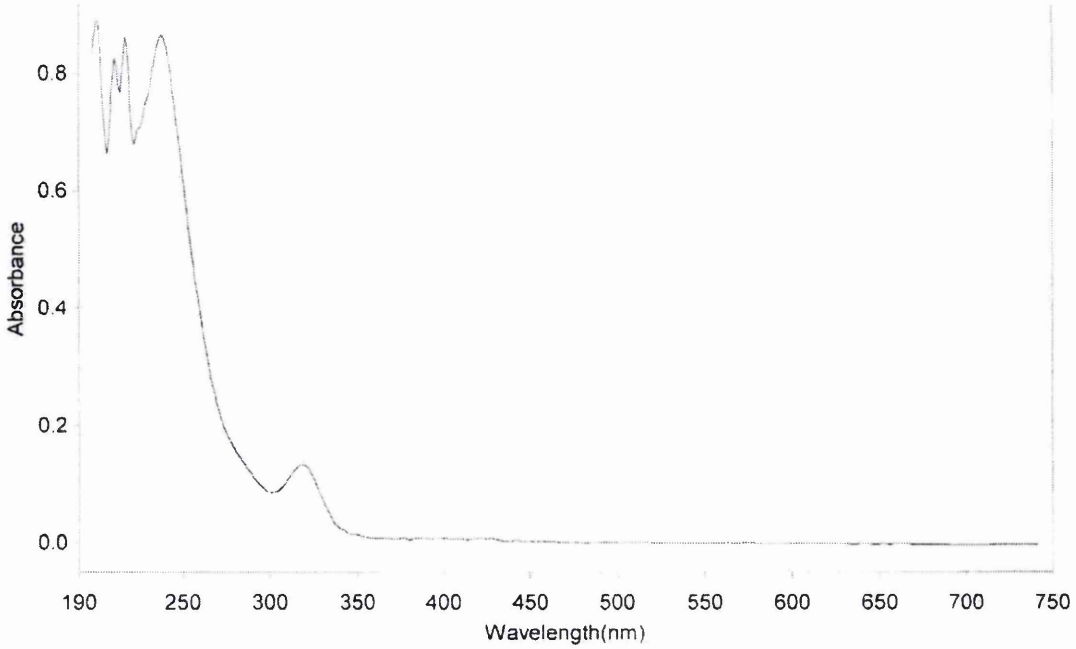

$[Pd(Se_2C_8H_{12})(PBu_3)_2]$:

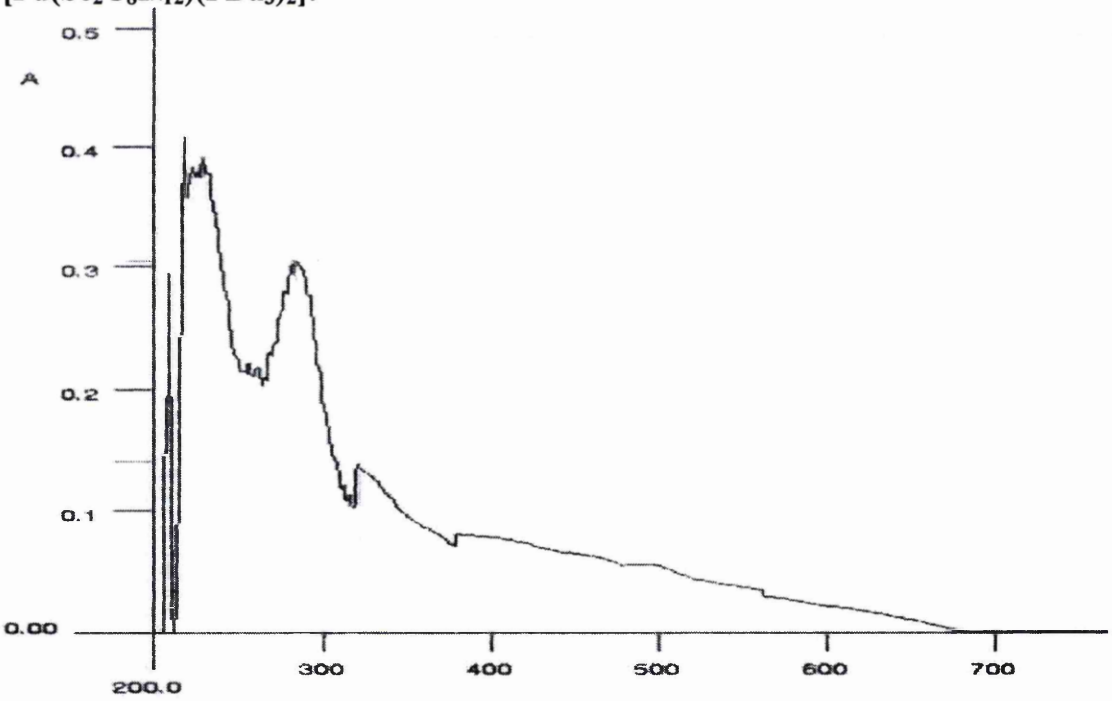

2.3 Attempted Syntheses of $[PtSe_4(PR_3)_2]$ (R = Et, Bu)

The synthesis of diselenolenes by reaction of metal polyselenides with activated alkynes was first reported by Bollinger and Rauchfuss for titanium diselenolenes.[153] Subsequent work by Ibers *et al.* and Mizobe and Hidea has shown this to be a viable route to tungsten and iridium diselenolenes respectively.[168,171] This is also a possible route to platinum diselenolenes. Morley *et al.* have reported that the tetraselenide $[PtSe_4(dppe)]$ can be synthesised from $[Pt(dppe)_2]$ or $[PtCl_2(dppe)]$ by treatment with elemental selenium or lithium polyselenide respectively (figure 2.19).

Figure 2.19:

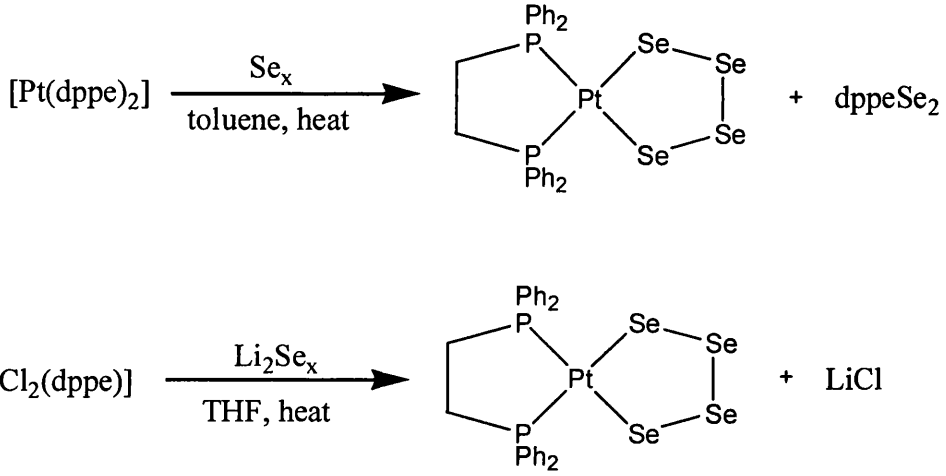

Subsequent reaction of this tetraselenide with the activated alkynes DMAD and DEAD yields diselenolenes of the type $[Pt\{Se_2C_2(CO_2R)_2\}(dppe)]$ (R = Me, Et; figure 2.20).[169,170,226]

Figure 2.20:

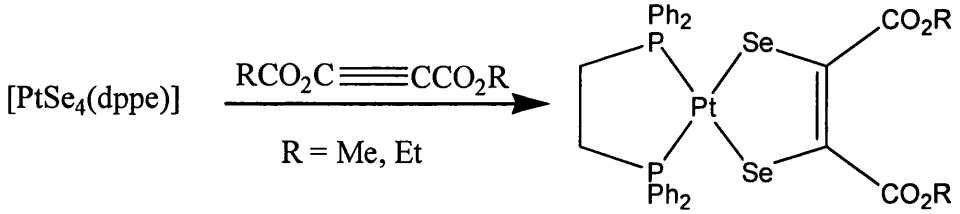

The applicability of this route to trialkylphosphine-substituted platinum complexes was investigated, following the methods documented in Mark Lewtas' thesis.[170] Firstly the reaction of $[Pt(C_2H_4)(PR_3)_2]$ (R = Et, Bu) with elemental selenium was investigated. It was found that stirring $[Pt(C_2H_4)(PR_3)_2]$ with a 10-fold excess of elemental grey selenium at room temperature or at reflux (dioxane/THF/toluene solvent mix) for varying periods of time gave black-brown solutions. After filtration and concentration of the liquors, brown residues were obtained; analysis of these residues by ^{31}P NMR spectroscopy showed only $P(Se)R_3$ signals.

The alternative route using *cis*-$[PtCl_2(PEt_3)_2]$ and lithium polyselenide was also attempted (*cis*-$[PtCl_2(PBu_3)_2]$ is more difficult to synthesise than *cis*-$[PtCl_2(PEt_3)_2]$ and so wasn't investigated). Treatment of elemental grey selenium with $LiBEt_3H$ (0.6 eq) in THF gave a purple solution (characteristic of Li_2Se_x); this was refluxed for 30 minutes, treated with a hot THF suspension of *cis*-$[PtCl_2(PEt_3)_2]$ and refluxed for a further 1 hour. The reaction was also carried out with prolonged reflux and at room temperature with overnight stirring, but in all cases ^{31}P NMR spectroscopic analysis showed only $P(Se)Et_3$.

It is not known if the product forms in these reactions and decomposes, or whether under these conditions PR_3 is extracted from the platinum starting material. What is known is that the success of this approach depends on the nature of the phosphine. It may be that the dppe has a stabilising effect as a chelating ligand, or that its lower basicity compared to the trialkylphosphines has an influence. The sensitivity of these reactions to the phosphine substituents is further exemplified by the reaction of $[Pt(PPh_3)_4]$ with elemental selenium, which gives the dinuclear Se-bridged species $[Pt_2(\mu\text{-}Se)_2(PPh_3)_4]$.[227]

Chapter 3

The Reactions of Cycloalkeno-1,2,3-thiadiazoles and Cycloalkeno-1,2,3-selenadiazoles with Platinum(0) Phosphine Complexes

3.1 Reactions of $[Pt(C_2H_4)(PR_3)_2]$ with Cycloalkeno-1,2,3-thiadiazoles

The chemistry of 1,2,3-thia- and 1,2,3-selenadiazoles was documented in the introduction; what is noticeable is that the chemistry of 1,2,3-thiadiazoles has been less explored, particularly in combination with the group 10 metals. To our knowledge there are no reports of the reactions of 1,2,3-thiadiazoles with platinum complexes; there has been a small amount of work on their reactions with palladium complexes.[120] Although the main focus of the work in this thesis is on the reactions of organoselenium compounds with platinum complexes, the lack of investigation in this area warranted an exploration of some organosulphur chemistry.

Refluxing $[Pt(C_2H_4)(PR_3)_2]$ (R = Et, Bu) with two equivalents of cyclohepteno- or cycloocteno-1,2,3-thiadiazole in a dioxane/THF/toluene mixture for one hour led to deep orange reaction mixtures. Subsequent column chromatography led to the isolation of compounds **8b,c** and **9b,c** as deep orange solids (figure 3.1).

Figure 3.1:

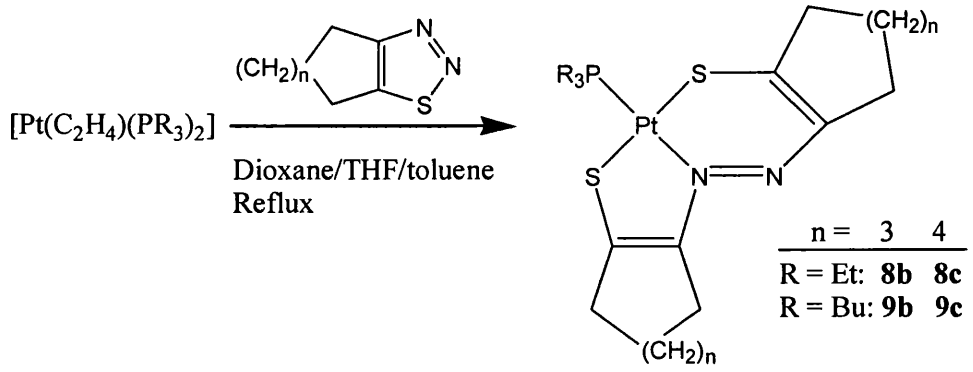

Compounds **8b,c** and **9b,c** are of the general formula $[PtL(PR_3)]$ where L is the ligand $SC(R^1)=C(R^2)N=NC(R^1)=C(R^2)S$ (R^1-R^2 = $(CH_2)_5$ or $(CH_2)_6$); this is the first example of this type of ligand containing sulphur. The ligand can be considered an alicyclic analogue of an azo dye, which may explain the intense colour of these complexes. The complexes are indefinitely stable in the solid state, but they have been observed to decompose upon prolonged standing in chloroform (evidenced by the solutions losing colour).

The proposed mechanism of the reaction is shown in figure 3.2: insertion of '$Pt(PR_3)_2$' into the S-N bond of a molecule of 1,2,3-thiadiazole is followed by addition of a thiaketocarbene fragment to this Pt(II) intermediate with loss of a trialkylphosphine to give the product. A similar mechanism has been proposed for the

synthesis of the analogous palladium complexes from cycloalkeno-1,2,3-selenadiazoles.[115,116]

Figure 3.2:

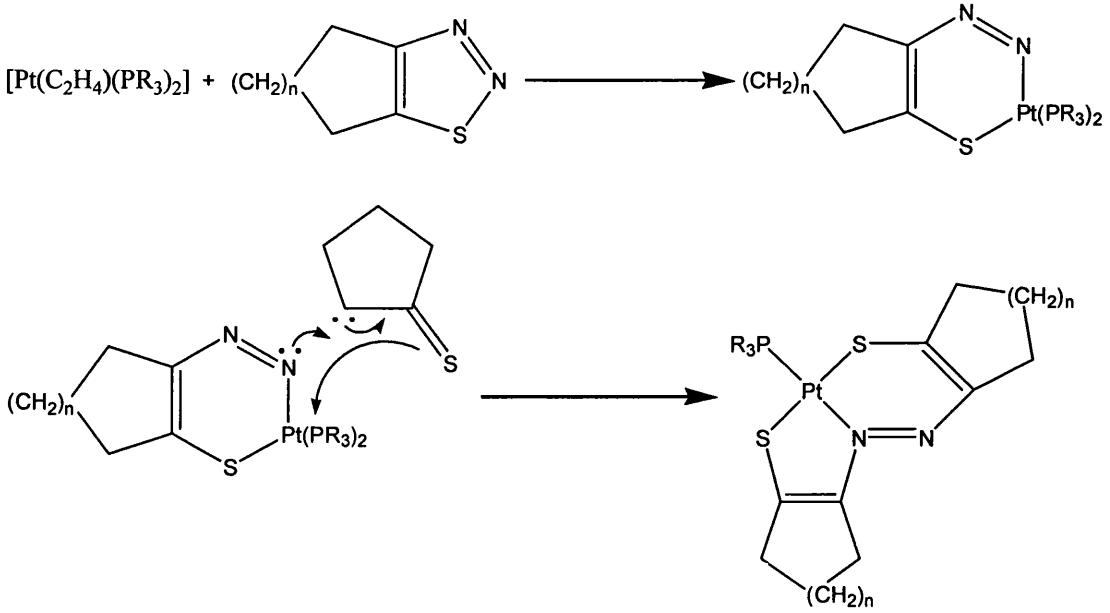

Both 1,2,3-thia- and 1,2,3-selenadiazoles *generally* react by elimination of dinitrogen to form thiaketocarbene and selenaketocarbene intermediates (figure 3.3), the fate of which decides the outcome of the reaction.[92,228] Addition of these ketocarbenes to another molecule of intact 1,2,3-thia/selenadiazole is (to our knowledge) unprecedented; hence it is unlikely there is coupling between thiaketocarbene and 1,2,3-thiadiazole followed by reaction with '$Pt(PR_3)_2$'.

Figure 3.3:

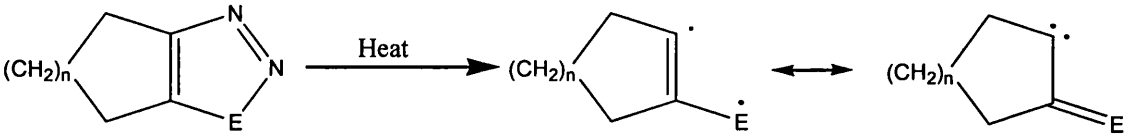

Attempts to synthesise the cyclohexeno- analogues of **8b,c** and **9b,c** were unsuccessful. This is attributed to the difficulty of removing dinitrogen from cyclohexeno-1,2,3-thiadiazole. Thiaketocarbenes are intermediates in the decomposition pathway of 1,2,3-thiadiazoles; thiaketocarbenes decompose *via* a radical mechanism to elemental sulphur and a substituted acetylene (figure 3.4).[92,228] Formation of cyclohexyne is not a favoured process due to the steric constraints placed upon it; this will limit the formation of the thiaketocarbene, which is necessary for the product to form.

Figure 3.4:

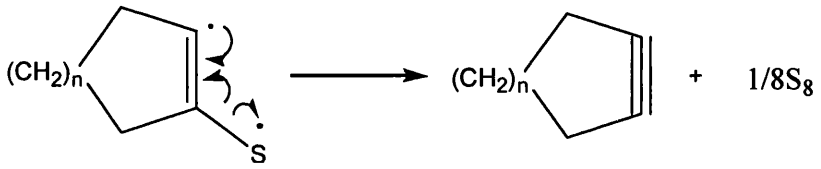

The compounds **8b,c** and **9b,c** are very soluble in most organic solvents. This hindered their crystallisation, but it was possible to obtain crystals of **8b**, **9b** and **9c** by slow evaporation of ethanol solutions of these compounds. The crystals of **8b** and **9b** were suitable for structure determination by X-ray diffraction. The crystal structure of **8b** is presented and discussed in chapter 6. The crystal structure of **9b** is shown in figure 3.5: thermal ellipsoids are drawn at 30% probability; hydrogen atoms are omitted for clarity. The diffraction data were collected with an Oxford Diffraction Xcalibur 3 CCD diffractometer, using graphite-monochromated MoK_α radiation (λ = 0.71069 Å). The structure was solved by direct methods using SIR 97[225] and heavy-atom procedures, with refinement by SHELXL 97.[223]

Table 3.1 shows the crystallographic data for **9b**, with some selected bond lengths and angles shown in table 3.2.

Figure 3.5: Crystal structure of **9b**

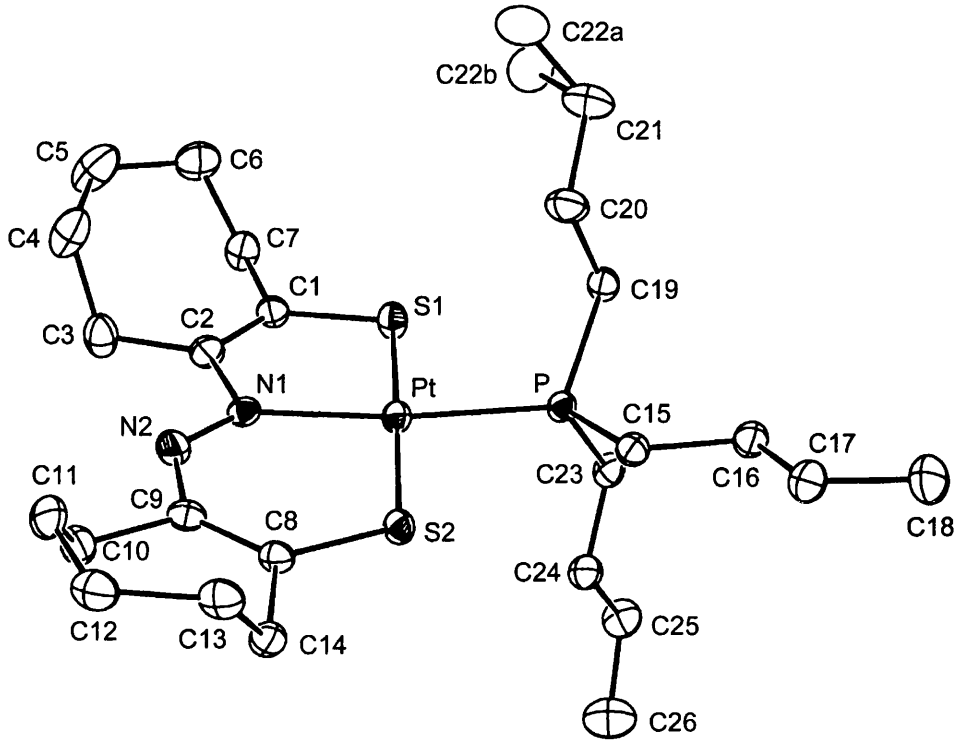

Table 3.1: Crystallographic data for **9b**

Empirical formula	$C_{26}H_{47}N_2PS_2Pt$
Formula weight	677.84
Crystal system	triclinic
Space group	P -1
Crystal dimensions (mm)	0.35 x 0.20 x 0.18
a/Å	10.096(3)
b/Å	12.555(4)
c/Å	12.914(4)
α/°	88.54(3)
β/°	68.15(3)
γ/°	73.89(3)
V/Å	1454.1(8)
Z	2
F(000)	684
D_{calc} (g cm^{-3})	1.548
μ (Mo-K_α/mm^{-1})	5.040
Temperature (K)	296
Reflections collected	16961
Independent reflections	8525
θ Range (°)	4.20-34.28
Reflect. with $I > 2\sigma(I)$	4616
No. of parameters	303
R_1; wR_2 [$I > 2\sigma(I)$]	0.0442; 0.1017
R_1; wR_2 (all data)	0.0762; 0.1091
GoF	0.841

It can be seen that **9b** consists of a slightly distorted square-planar PtS_2NP core with the phosphine *trans-* to the platinum-bound nitrogen of the ligand. The crystallographic sites are occupied by **9b** in one of two possible 'orientations' dependent on which nitrogen atom is bound to the platinum centre. It was found that there was a 2:1 ratio of these orientations in favour of the orientation shown in figure 5. This has also been observed for the analogous selenium and palladium-containing species [Pd{SeC(R^1)=C(R^2)N=NC(R^1)=C(R^2)Se}(PBu_3)] (R^1-R^2 = $(CH_2)_4$), where it was possible to resolve the structure showing both possible orientations of the ligand.[116] The twelve atoms associated with the π-system of the ligand (SC(C)=C(C)-N=N-C(C)=C(C)S) are coplanar, as was observed for the π-system of [Pd{SeC(R^1)=C(R^2)N=NC(R^1)=C(R^2)Se}(PBu_3)]. These twelve atoms do not lie in the same plane as the PtS_2NP unit, although the deviation is small with a dihedral angle of 1.2°. The Pt-S(1) bonds are approximately 0.04 Å longer than the Pt-S(2)

Table 3.2: Selected bond lengths and angles of compound **9b**

Bond lengths (Å)	
Pt-S (1)	2.271(2)
Pt-S (2)	2.228(2)
Pt-P	2.258(1)
Pt-N(2)	2.079(4)
N(1)-N(2)	1.252(6)
S(2)-C(8)	1.689(5)
S(1)-C(1)	1.719(6)
N(2)-C(9)	1.385(7)
N(1)-C(2)	1.438(7)
C(1)-C(7)	1.368(7)
C(2)-C(1)	1.344(8)
Bond angles (°)	
S(1)-Pt-S(2)	177.34(6)
S(2)-Pt-P	92.12(6)
S(2)-Pt-N(1)	94.13(13)
S(1)-Pt-P	88.67(6)
S(1)-Pt-N(1)	85.18(13)
P-Pt-N(1)	173.41(12)
Pt-S(2)-C(8)	110.48(20)
Pt-S(1)-C(1)	98.40(20)
Pt-N(1)-N(2)	131.34(37)
Pt-N(1)-C(2)	115.93(36)
S(2)-C(1)-C(9)	127.12(43)
C(9)-N(2)-N(1)	124.60(48)
N(2)-N(1)-C(2)	112.47(46)
N(1)-C(2)-C(1)	117.32(49)
S(1)-C(1)-C(2)	123.03(42)

bonds; this is comparable to the situation in the complex [Pt{SeC(COOEt)=C(Me)N=NC(Me)=C(COOEt)Se}(PPh_3)],[118] where the Pt-Se bond in the 5-membered ring is approximately 0.05 Å longer than the Pt-Se bond in the 6-membered ring. The average Pt-P and Pt-N(2) distances of 2.259 and 2.080(43) Å are comparable to those of [Pt{SeC(COOEt)=C(Me)N=NC(Me)=C(COOEt}Se)(PPh_3)] (2.260(1) and 2.071(5) Å respectively). The average N(1)-N(2) distances of 1.230 Å are shorter (*cf.* 1.295(7) Å); they are also shorter than the reported N=N distances for [Pd{SeC(R^1)=C(R^2)N=NC(R^1)=C(R^2)Se}(PBu_3)] of 1.29(3) and 1.26(4) Å. The effect of the presence of sulphur atoms instead of selenium may be the donation of less electron density to the π-system, resulting in less electron density at the nitrogens, and a shorter N=N bond. The average Pt-S bond lengths of 2.226 and 2.265 Å are of

a comparable length to that in the similar complex [Pt{PhSNC(MeC$_6$H$_4$)N=NC(MeC$_6$H$_4$)NSPh}(PPh$_3$)] (2.266(3) Å).[229]

The multinuclear NMR data for compounds **8b,c** and **9b,c** are shown in tables 3.3 and 3.4. The NMR data at room temperature confirm the structure of these complexes shown in figure 3.5. It is known that disorder due to a 'pedal motion' exists in crystals of stilbenes and azobenzenes.[230] This has also been observed in the crystallographic analysis of [Pd{SeC(R^1)=C(R^2)N=NC(R^1)=C(R^2)Se}(PBu$_3$)], and corresponds to the potential of the nitrogen atoms to interchange between a bonding and non-bonding state with respect to the palladium atom. A similar situation can be envisaged in **8b,c** and **9b,c** and is shown in figure 3.6:

Figure 3.6:

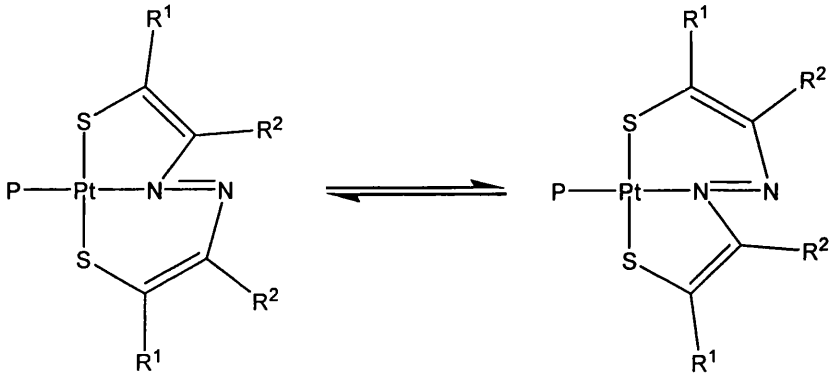

The NMR spectral data show that this process does not occur at room temperature on the NMR timescale, as each carbon in the two alicyclic rings gives a separate ^{13}C NMR resonance; if this process were occurring rapidly then one signal would be observed for each ring carbon *and* its 'equivalent' in the adjacent ring.

Table 3.3: ^{1}H and ^{13}C NMR spectroscopic data for complexes **8b,c** and **9b,c** in $CDCl_3$ solution

		8b	**8c**	**9b**	**9c**
^{1}H	CH_3	1.18 (9H, dt)[a]	1.18 (9H, dt)[a]	0.91 (9H, t)[a]	0.95 (9H, t)[a]
	CH_2P	2.15-2.21 (6H, m)	2.12-2.29 (6H, m)	2.06-2.22 (6H, m)	1.25-2.25 (6H, m)
	$CH_2CH_2CH_2P$			1.38-1.90(12H, m)	1.25-2.25 (12H, m)
	α-CH_2	3.10-3.50 (8H, m)	3.10-3.54 (8H,m)	3.06-3.51 (8H, m)	3.10-3.55 (8H, m)
	β,γ-CH_2	1.58-1.95 (12H, m)	1.26-1.92 (16H, m)	1.38-1.90 (12H, m)	1.25-2.25 (16H, m)
^{13}C	CH_3	8.5[b]	8.5[b]	14.4	14.4
	CH_2	17.8[c]	17.8[c]	26.5[c]	26.4[c]
	CH_2CH_2P	-	-	24.8	24.7
		-	-	24.2	24.6
	$C{=}C$	159.2[d]	155.9[d]	159.4[d]	155.8[d]
		147.9[e]	146.2[e]	148.0[e]	146.1[e]
		143.5[f]	143.1[f]	143.8[f]	143.2[f]
		134.8[g]	132.4[g]	134.8	133.8
	α-CH_2	43.1[h]	39.8[h]	43.2[h]	39.7[h]
		41.1[i]	38.1[i]	41.4[i]	38.1[i]
		38.2[j]	37.4[j]	38.5[j]	37.4[j]
		32.5	32.9	32.8	32.9
	β-CH_2	32.1	32.8	32.4	32.8
		28.3	32.6	28.5	32.6
		28.2	28.9	28.1	30.3
		27.9	28.1	27.8	28.9
	γ-CH_2	27.6	27.9	26.5	27.9
		25.8	27.2	26.0	27.2
			27.1		27.1
			26.7		26.7

[a] $^{3}J(^{1}H\text{-}^{1}H)$ = 7.6 Hz (**8b, 8c**), 7.2 Hz (**9b, 9c**), $^{3}J(^{1}H\text{-}^{31}P)$ = 16.8 Hz (**8b, 8c**); [b] ^{2}J ($^{13}C\text{-}^{31}P$) = 3 Hz, ^{3}J ($^{13}C\text{-}^{195}Pt$) = 16 Hz (**8b**), 14 Hz (**8c**); [c] ^{1}J ($^{13}C\text{-}^{31}P$) = 37 Hz (**8b, 8c**), 36 Hz (**9b, 9c**), ^{2}J ($^{13}C\text{-}^{195}Pt$) = 29 Hz (**8b, 8c**), 26 Hz (**9b, 9c**); [d] ^{2}J ($^{13}C\text{-}^{31}P$) = 2 Hz, ^{3}J ($^{13}C\text{-}^{195}Pt$) = 17 Hz (only resolved for **9c**); [e] ^{2}J ($^{13}C\text{-}^{195}Pt$) = 96 Hz (**8b**), 97 Hz (**8c, 9b**), 95 Hz (**9c**), ^{3}J ($^{13}C\text{-}^{31}P$) = 3 Hz; [f] ^{2}J ($^{13}C\text{-}^{195}Pt$) = 87 Hz (**8b, 9b**), 90 Hz (**8c, 9c**); [g] ^{3}J ($^{13}C\text{-}^{31}P$) = 6 Hz; [h] ^{3}J ($^{13}C\text{-}^{195}Pt$) = 44 Hz; [i] ^{3}J ($^{13}C\text{-}^{195}Pt$) = 46 Hz (**8b, 9b**), 42 Hz (**8c, 9c**); [j] ^{4}J ($^{13}C\text{-}^{31}P$) = 2 Hz (**8b, 9b** only), ^{3}J ($^{13}C\text{-}^{195}Pt$) = 34 Hz (**8b**), 33 Hz (**8c**), 35 Hz (**9b**), 37 Hz (**9c**).

Table 3.4: ^{31}P NMR spectroscopic data for complexes **8b,c** and **9b,c** in $CDCl_3$ solution

	8b	**8c**	**9b**	**9c**
δ/ppm	1.4	1.0	-6.5	-6.8
$^1J(^{31}P\text{-}^{195}Pt)$/Hz	3076	3062	3060	3063

To investigate whether fluxionality could be observed at higher temperatures a variable temperature NMR study was carried out. ^{1}H NMR spectra of compound **9b** (in d_6-DMSO) were run at room temperature, 60 °C, 80 °C and 100 °C; these spectra are shown in figure 3.7. It can be seen that in the regions δ = 1.1-1.8 and 2.2-3.3 ppm (where the aliphatic ring protons resonate) there is very little change upon increasing the temperature. The fact that this process is slow on the NMR timescale even at 100 °C, suggests that interconversion of the isomers requires a lot of energy.

The energy barrier of this interconversion in the analogous species [Pd{SeC(R^1)=C(R^2)N=NC(R^1)=C(R^2)Se}(PBu_3)] (R^1-R^2 = $(CH_2)_5$) was quantum mechanically calculated by Professor M. Di Vaira (University of Florence, Italy) to be approximately 30 kcal mol^{-1}; this is too high for interconversion of the isomers on the NMR timescale. Due to platinum being much less labile than palladium,[231] the energy barrier for this process in **8b,c** and **9b,c** should be higher, and preliminary calculations have indicated that this is the case. Therefore this isomerisation does not occur on the NMR timescale, even at elevated temperatures.

As was observed with the diselenolenes (chapter 2) the ^{13}C resonances of 7-membered aliphatic rings (in **8b** and **9b**) are at lower field than the corresponding 8-membered rings; this effect appears to be common to both cycloalkeno-1,2,3-thia- and cycloalkeno-1,2,3-selenadiazoles and their derivatives. The ^{1}H NMR spectra are relatively complex, as would be expected from the structure shown in figure 3.1, but four multiplets are typically observed at low field (δ = 3.06-3.51 ppm) which are assigned to the α-CH_2 groups.

The mass spectral, infrared and UV-visible data for **8b,c** and **9b,c** are shown in table 3.5.

Table 3.5: Mass spectral, infrared, and UV-visible data for complexes **8b,c** and **9b,c**

		8b	**8c**	**9b**	**9c**
Mass Spectrum[a]	$[M]^+$	593 (100)	621 (100)	677 (100)	705 (100)
Infrared[b] (cm^{-1})		2966 (w)	2963 (m)	2955 (w)	2956 (w)
		2916 (s)	2918 (s)	2919 (s)	2921 (s)
		2845 (m)	2846 (m)	2847 (m)	2847 (m)
		1558 (m)	1562 (m)	1559 (m)	1562 (m)
		1450 (m)	1440 (s)	1451 (m)	1440 (s)
		1425 (s)	1427 (s)	1428 (s)	1428 (s)
		1366 (m)	1355 (m)	1367 (m)	1355 (m)
		1208 (s)	1259 (m)	1209 (s)	1261 (m)
		1036 (s)	1072 (s)	1037 (s)	1071 (s)
		989 (m)	1032 (s)	990 (m)	1028 (m)
		954 (s)	979 (m)	955 (s)	905 (m)
		907 (m)	907 (m)	905 (m)	882 (m)
		765 (s)	766(s)	755 (m)	794 (m)
		730 (s)	732 (s)	734 (s)	723 (s)
		636 (m)	636 (w)	601 (s)	609 (m)
		600 (m)	608 (m)		
UV-Vis[c] (λ nm)		230 (35,200)	225 (39,400)	220 (32,800)	225 (34,400)
		455sh (8,600)	455sh (10,000)	455sh (8,000)	465sh (9,000)
		520 (15,600)	515 (15,600)	520 (15,000)	515 (13,700)

[a] *m/z* (%); recorded using FAB; figures are for isotopomers containing ^{195}Pt, ^{32}S, ^{14}N, ^{12}C, ^{1}H. [b] Selected bands (cm^{-1}) only, [c] λ_{max} (nm); ε (cm^{-1} M^{-1}) in parentheses; recorded in MeCN solution (10^{-5} M).

Figure 3.7: ^{1}H NMR spectra (δ = 0 – 3.5 ppm) of **9b** at room temperature, 60 °C, 80 °C and 100 °C

Room Temperature:

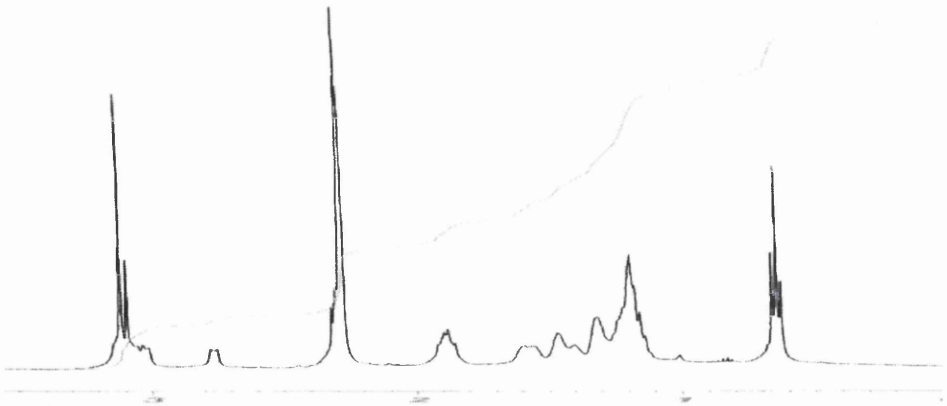

60 °C:

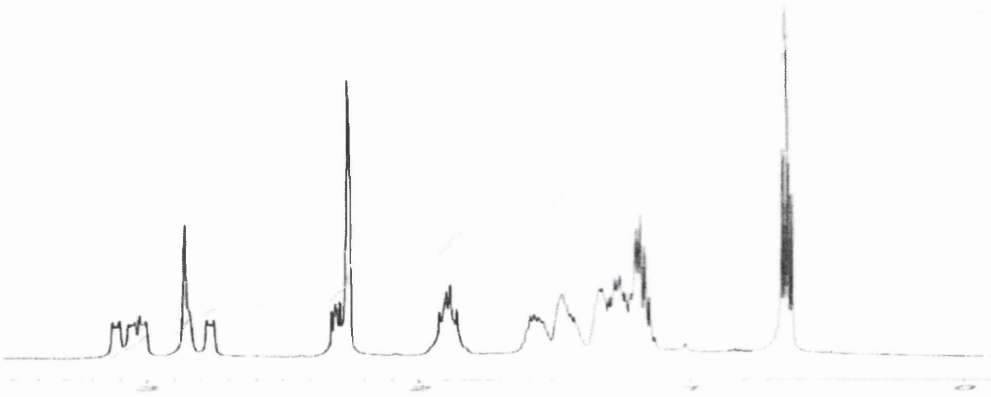

80 °C:

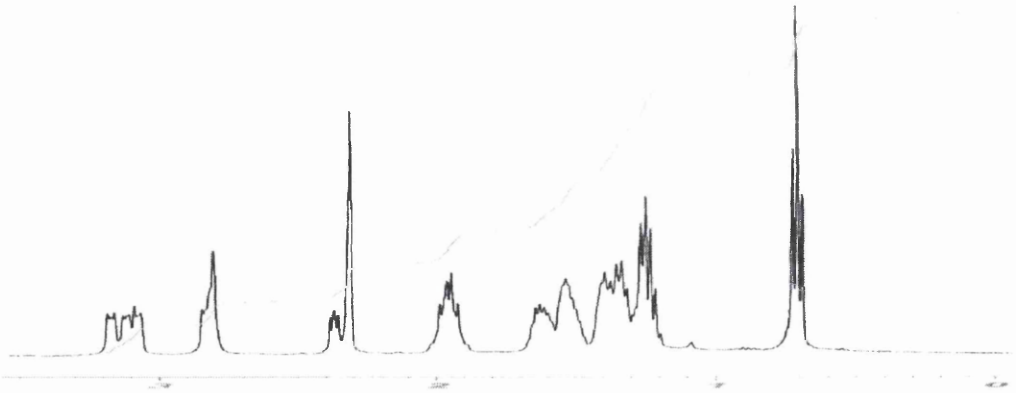

100 °C:

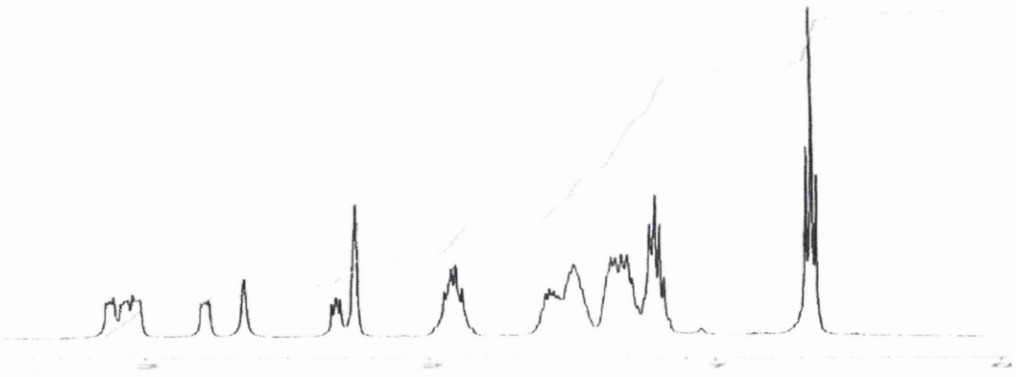

The mass spectra all show molecular ion peaks at 100% relative intensity, which suggests that these complexes are quite robust. Their intense orange colour is explained by the UV-visible spectra, which all show an intense, relatively broad absorption at $\lambda \sim 520$ nm with a shoulder at $\lambda \sim 460$ nm. The nature of the phosphine appears to play no part here and so the absorptions are assumed to be ligand based. The absorptions at $\lambda \sim 220$ nm *may* be attributed to a LMCT process as was observed with platinum diselenolenes (chapter 2). The intensities of the absorptions are greater than those found for $[Pd\{SeC(R^1)=C(R^2)N=NC(R^1)=C(R^2)Se\}(PR_3)]$ (R^1-$R^2 = (CH_2)_n$, n = 4, 5, 6; R = Et, Bu).[116]

3.2 Reactions of $[Pt(C_2H_4)(PR_3)_2]/[PtCl_2(PR_3)_2]$ with Cycloalkeno-1,2,3-selenadiazoles

The chemistry of 1,2,3-selenadiazoles with low-valent transition metal complexes has undergone more investigation than the corresponding 1,2,3-thiadiazole chemistry. In particular there have been two reports (chapter 1) of the reactions of 1,2,3-selenadiazoles with low-valent platinum complexes. The reaction of cycloocteno-1,2,3-selenadiazole with $[Pt(PPh_3)_4]$ was discussed in chapter 2. There has also been a report on the reaction of 4-methyl-5-ethoxycarbonyl-1,2,3-selenadiazole with $[Pt(PPh_3)_4]$ which gave the complex $[PtL(PPh_3)]$, where L is the ligand SeC(COOEt)=C(Me)N=NC(Me)=C(COOEt)Se.[118] These complexes are analogous to **8b,c** and **9b,c** and importantly, they have been shown to be selective catalysts in the hydrosilylation of terminal acetylenes.

It was found that the reaction of $[Pt(C_2H_4)(PR_3)_2]$ (R = Et, Bu) with cycloalkeno-1,2,3-selenadiazoles gives complexes of the type $[Pt(SeC_{n+4}H_{2n+4})(PR_3)_2]$ (n = 2, 3, 4); these reactions are discussed later on in this chapter. However, the reaction of a mix of $[Pt(C_2H_4)(PR_3)_2]/[PtCl_2(PR_3)_2]$ with cycloalkeno-1,2,3-selenadiazoles was found to give complexes of the type $[PtL(PR_3)]$ where L is the ligand $SeC(R^1)=C(R^2)N=NC(R^1)=C(R^2)Se$ (R^1-R^2 = $(CH_2)_n$; n = 4, 5, 6). These species are the selenium analogues of complexes **8b,c** and **9b,c** (figure 3.8). All reactions were carried out in refluxing dioxane/THF/toluene for one hour.

Figure 3.8:

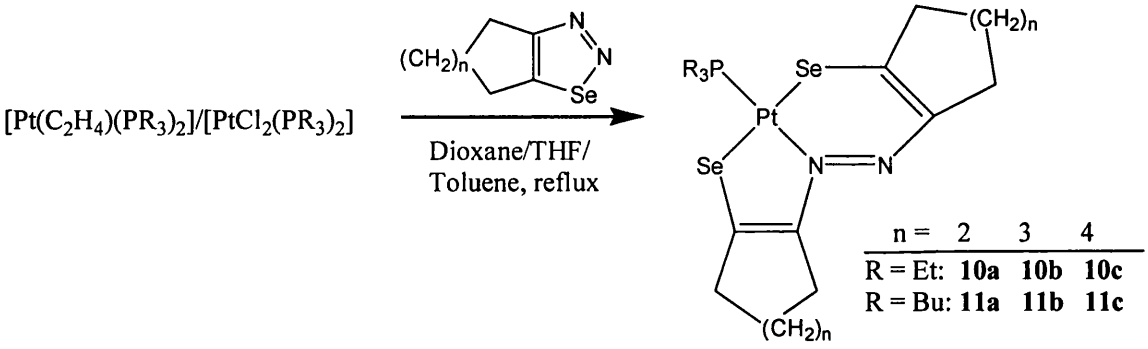

n =	2	3	4
R = Et:	**10a**	**10b**	**10c**
R = Bu:	**11a**	**11b**	**11c**

The mechanism for this reaction is unclear; investigation has shown that neither $[Pt(C_2H_4)(PR_3)_2]$ nor $[PtCl_2(PR_3)_2]$ is catalytic and the formation of **10a-c** and **11a-c** depends on a critical ratio of the platinum reagents. $[Pt(C_2H_4)(PR_3)_2]$ is synthesised by the addition of $NaC_{10}H_8$ to $[PtCl_2(PR_3)_2]$ under an ethene atmosphere, and the ratio of $[Pt(C_2H_4)(PR_3)_2]$ to $[PtCl_2(PR_3)_2]$ is determined by the amount of $NaC_{10}H_8$ added

to the reaction (figure 3.9). There are no reported methods precisely to determine the molarity of $NaC_{10}H_8$ solutions and complete conversion of $[PtCl_2(PR_3)_2]$ to $[Pt(C_2H_4)(PR_3)_2]$ is determined visually, by the solution keeping the green colour of the $NaC_{10}H_8$ for about 5 minutes before clearing. Unfortunately, because the molarity of the $NaC_{10}H_8$ solutions was unknown, it was not possible to determine the ideal ratio of $[Pt(C_2H_4)(PR_3)_2]$ to $[PtCl_2(PR_3)_2]$ for the formation of **10a-c** and **11a-c**. What is known is that approximately 1-1.5 equivalents of $NaC_{10}H_8$ are necessary: if there is a dominance of $[Pt(C_2H_4)(PR_3)_2]$ then formation of the compounds $[Pt(SeC_{n+4}H_{2n+4})(PR_3)_2]$ is the main reaction, and if there is a dominance of $[PtCl_2(PR_3)_2]$ then there is effectively no reaction. In fact (as would be expected) the syntheses of **10a-c** and **11a-c** were difficult to reproduce and the reactions often yielded no product.

Figure 3.9:

$$[PtCl_2(PR_3)_2] \xrightarrow[C_2H_4]{xNaC_{10}H_8} (x/2)[Pt(C_2H_4)(PR_3)_2] + (1-x/2)[PtCl_2(PR_3)_2]$$

$0 < x < 2$

This difference in reactivity of the cycloalkeno-1,2,3-selenadiazoles compared to the cycloalkeno-1,2,3-thiadiazoles is attributed to the ease with which 1,2,3-selenadiazoles lose dinitrogen to form selenaketocarbenes (figure 3.3); it is essential for the formation of **10a-c** and **11a-c** that one 1,2,3-selenadiazole molecule retains dinitrogen. It is believed that the presence of $[PtCl_2(PR_3)_2]$ somehow aids this dinitrogen retention; this is not necessary in the formation of **8b,c** and **9b,c** as the loss of dinitrogen from 1,2,3-thiadiazoles to form thiaketocarbenes requires much more energy.

Compounds **10a-c** and **11a-c** are deep purple in colour, the same as the palladium analogues $[Pd\{SeC(R^1)=C(R^2)N=NC(R^1)=C(R^2)Se\}(PR_3)]$.[116] Unfortunately it was not possible to obtain crystals of these complexes for an x-ray crystallographic study. Also due to the capricious nature of these reactions and difficulty in obtaining pure products some spectroscopic data have not been obtained. Tables 3.6 and 3.7 show the NMR spectroscopic data obtained for compounds **10a-c** and **11a-c**.

Table 3.6: ^{1}H and ^{13}C NMR spectroscopic data for complexes **10a-c** and **11a-c** in $CDCl_3$ solution

		10a	**10b**	**10c**	**11a**	**11b**	**11c**
^{1}H	CH_3	Not recorded	1.14 (9H, dt)[a]	1.14 (9H, dt)[a]	Not recorded	0.94 (9H, t)[a]	1.00-3.50
	CH_2P		2.00-2.32 (6H, m)	2.06-2.22 (6H, m)		2.08-2.17 (6H, m)	(51H, m)
	$CH_2CH_2CH_2P$					1.36-1.88 (12H, m)	
	α-CH_2		3.02-3.60 (6H, m)	3.02-3.60 (6H, m)		3.06-3.46 (6H, m)	
	α,β,γ-CH_2		1.41-1.96 (14H, m)	1.24-1.90 (18H, m)		1.36-1.88 (14H, m)	
^{13}C	CH_3	8.5[b]	8.3[b]	8.6[b]	14.1	14.0	14.0
	CH_2	17.8[c]	17.8[c]	17.9[c]	26.4[c]	26.3[c]	26.3[c]
	CH_2CH_2P	-	-	-	24.7[d]	24.4	24.4
	$CH_3CH_2CH_2$	-	-	-	25.5	24.3	24.2
	C=C	158.3[e]	163.2[e]	160.0[e]	158.1[e]	163.2[e]	159.9
		146.0[f]	150.9	149.3[f]	145.9[f]	151.0	149.1
		137.4[g]	139.5[g]	139.7[g]	137.6[g]	139.6	139.7[g]
		129.4	135.2	133.0	133.9	135.1	132.8
	α-CH_2	37.3[h]	41.4	40.3[h]	37.3	43.5[h]	40.2
		35.9[i]	39.0	39.2[i]	35.8	41.5[i]	39.1
		35.4	37.7	37.5	35.3	39.1[j]	37.3
		31.1[j]	31.8	32.7	31.0	32.2	32.6
	β-CH_2	26.2	30.6	32.5	26.3	32.0	32.4
		25.1	29.8	32.1	25.1	27.7	32.0
		24.3	27.7	30.5	24.2	27.3	30.4
		23.3	27.0	28.1	23.3	27.0	28.1
	γ-CH_2		25.1	27.8		25.3	28.0
			24.6	27.0		25.1	26.9
				27.0			26.8
				26.4			26.3

[a] $^{3}J(^{1}H\text{-}^{1}H)$ = 7.6 Hz (**10b,c**), 7.2 Hz (**11b**), $^{3}J(^{1}H\text{-}^{31}P)$ = 17.2 Hz (**10b**), 16.8 Hz (**10c**); [b] ^{2}J ($^{13}C\text{-}^{31}P$) = 3 Hz, ^{3}J ($^{13}C\text{-}^{195}Pt$) = 9 Hz (**10a,b**), 14 Hz (**10c**); [c] ^{1}J ($^{13}C\text{-}^{31}P$) = 37 Hz (**10a,c**), 38 Hz (**10b**), unresolved (**11a-c**), ^{2}J ($^{13}C\text{-}^{195}Pt$) = 20 Hz (**10a, 11c**), 29 Hz (**10b**), 31 Hz (**10c**), 16 Hz (**11a**), 24 Hz (**11b**); [d] ^{2}J ($^{13}C\text{-}^{31}P$) = 6 Hz; [e] ^{3}J ($^{13}C\text{-}^{31}P$) = 3 Hz (**10a-c, 11a**), 5 Hz (**11b**), ^{2}J ($^{13}C\text{-}^{195}Pt$) = not resolved (**10a,b**), 84 Hz (**10c**), 95 Hz (**11a**), 69 Hz (**11b**); [f] ^{2}J ($^{13}C\text{-}^{195}Pt$) = 80 Hz (**10a**), 75 Hz (**10c**), 84 Hz (**11a**); [g] ^{3}J ($^{13}C\text{-}^{31}P$) = 5 Hz (**10a, 11a**), 6 Hz (**10b,c, 11c**); [h] ^{3}J ($^{13}C\text{-}^{195}Pt$) = 32 Hz (**10a**), 29 Hz (**10c, 11b**); [i] ^{3}J ($^{13}C\text{-}^{195}Pt$) = 21 Hz (**10a**), 25 Hz (**10c**), 22 Hz (**11b**); [j] ^{3}J ($^{13}C\text{-}^{195}Pt$) = 15 Hz (**10a**), 32 Hz (**11b**).

Table 3.7: ^{31}P and ^{77}Se NMR spectroscopic data for **10a-c** and **11a-c** in $CDCl_3$ solution

		10a	**10b**	**10c**	**11a**	**11b**	**11c**
^{31}P:	δ/ppm	-1.1	-0.8	-1.6	-9.4	-9.2	-9.0
	$^{1}J(^{31}P\text{-}^{195}Pt)$/Hz	3029	3019	3013	2985	3003	3015
^{77}Se:	$\delta(Se_A)$/ppm	547	602	574	545	598	573
	$^{1}J(^{77}Se_A\text{-}^{195}Pt)$/Hz	235	244	240	230	240	234
	$^{2}J(^{77}Se_A\text{-}^{31}P)$/Hz	25	24	25	27	27	26
	$\delta(Se_B)$/ppm	299	308	310	302	325	316
	$^{1}J(^{77}Se_B\text{-}^{195}Pt)$/Hz	190	195	190	180	180	185
	$^{2}J(^{77}Se_B\text{-}^{31}P)$/Hz	21	21	20	20	20	21

The NMR spectral data confirm the structures of **10a-c** and **11a-c** as those shown in figure 3.8. The selenium atoms are inequivalent and give rise to two signals in the ^{77}Se NMR spectra; each of these signals is split by coupling to the phosphorus atom in the *cis-* position and has a ^{195}Pt satellite structure. As an example the ^{77}Se NMR spectrum of **10c** is shown in figure 3.10.

Figure 3.10: ^{77}Se NMR spectrum of **10c**

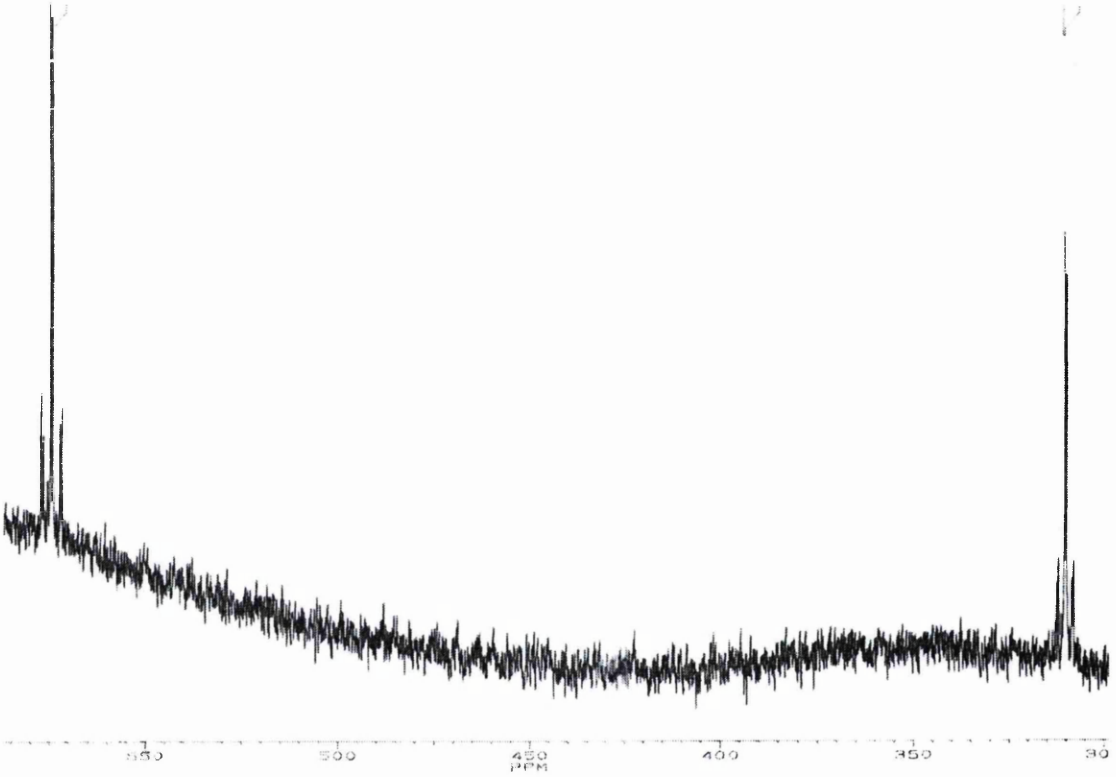

The $^{2}J(^{77}Se\text{-}^{31}P)$ coupling constants (avg. 23 Hz) are significantly larger than those observed in the analogous palladium species (9 Hz).[116] Generally in heterocyclic Pt(II) compounds with Pt-Se bonds the ^{77}Se resonances for 5-membered rings are at lower field than those of 6-membered rings;[232] therefore the resonance at $\delta \sim 575$ ppm is attributed to the selenium atom in the $PtSeC_2N$ ring, and the resonance at $\delta \sim 310$ ppm is attributed to the selenium atom in the $PtSeC_2N_2$ ring. This suggests that there is greater electron delocalisation in the 5-membered ring; indeed the δ values of the selenium in the 5-membered ring are comparable to those of selenophenes (δ = 513-717 ppm)[232] and platinum diselenolenes (δ = 441-481 ppm, chapter 2). In addition the $^{2}J(^{77}Se\text{-}^{31}P)$ coupling constants are approximately 5 Hz larger for the selenium in the 5-membered ring, which may be a result of this delocalisation. As in the ^{77}Se NMR

spectra of the diselenolenes (chapter 2) the resonance in the region δ = 550-600 ppm is observed at lower field for **10b** and **11b** compared to **10a,c** and **11a,c**; this increase in δ value appears to be indicative of the presence of a cyclohepteno-backboned species in most of the compounds studied. The ^{13}C NMR spectra show resonances for each individual carbon atom showing the structure in figure 3.8 to exist in solution; there is no evidence for an interconversion of isomers analogous to that shown in figure 3.6. As discussed for **8b,c** and **9b,c** this isomerisation has been calculated to be a high-energy process for the analogous palladium species, and therefore would not be expected to occur on the NMR timescale. Due to the capricious nature of the syntheses of complexes **10a-c** and **11a-c** and difficulties in purification, the data may not be as reliable as those for **8b,c** and **9b,c**, but some trends are apparent. The resonances for the carbon atoms of the PR_3 groups are similar in **8b,c**, **9b,c** and **10a-c**, **11a-c**, showing that the chalcogen present has little electronic effect on the phosphine group. The ring carbon atoms of compounds **10b** and **11b** exhibit lower field resonances than those of **10a,c** and **11a,c**, as has been observed in all compounds so far. The absence of some coupling constants, for example the $^{1}J(^{13}C\text{-}^{31}P)$ coupling constants for the CH_2P resonances, is attributed to the poor quality of some of the data obtained. The ^{1}H NMR data are quite complex as would be expected; in some cases due to difficulties with purification no useful information could be gained from the spectra (hence few peaks in the spectra are assigned) and the data are not reported. However through this complexity three well-spaced multiplets were observed at relatively low field (δ = 3.0-3.5 ppm) which are assigned to three of the α-CH_2 groups.

The mass spectral data of **10a-c** and **11a-c** are shown in table 3.8, together with the IR and UV-visible spectral data of **10b** and **11b**. Due to difficulties with obtaining pure material the IR and UV-visible spectra of **10a,c** and **11a,c** were not acquired. Small amounts of pure **10b** and **11b** were obtained by slow recrystallisation from ethanol solutions; the crystals obtained were very small and not suitable for an X-ray crystallographic investigation.

Table 3.8: Mass spectral data for compounds **10a-c**, **11a-c**, and infrared, UV-visible data for complexes **10b** and **11b**

	10a	**10b**	**10c**	**11a**	**11b**	**11c**
Mass Spectrum[a] $[M]^+$	661 (75)	689 (100)	717 (100)	745 (100)	773 (100)	801 (100)
Infrared[b] (cm^{-1})		2964 (w) 2916 (s) 2845 (m) 1564 (m) 1452 (s) 1434 (s) 1353 (m) 1255 (m) 1208 (s) 1034 (s) 975 (w) 951 (s) 907 (w) 765 (s) 729 (s) 642 (w) 587 (w)			2955 (m) 2919 (s) 2848 (s) 1566 (m) 1455 (s) 1436 (s) 1353 (m) 1255 (w) 1208 (s) 1093 (s) 1084 (s) 1061 (m) 1030 (w) 976 (w) 904 (m) 776 (m) 722 (s) 651 (w) 588 (m)	
UV-Vis[c] (λ nm)		225 (48,000) 495 (9,950) 545 (10,700)			230 (44,400) 495 (12,200) 545 (13,100)	

[a] *m/z* (%); recorded using FAB; figures are for isotopomers containing ^{195}Pt, ^{80}Se, ^{14}N, ^{12}C, ^{1}H. [b] Selected bands (cm^{-1}) only. [c] λ_{max} (nm); ε (cm^{-1} M^{-1}) in parentheses; recorded in MeCN solution (10^{-5} M).

The presence of molecular ion peaks in the mass spectral data, most of which are at 100% relative intensity, suggests that these complexes are quite robust; the molecular ion peaks all exhibit the expected isotope patterns. The UV-visible spectra explain the purple colour of these compounds. The absorptions in the visible region start at ~450 nm and finish at ~600 nm; because there is effectively no absorption in the 350-450 nm and 600–700 nm regions the compounds appear purple. The two peaks (495 and 545 nm) are shifted closer together than those of the palladium analogues (480 and 570 nm);[116] they are also more intense with average ε values of 11,000 and 12,000 $cm^{-1} M^{-1}$ compared to 1,550 and 2,100 $cm^{-1} M^{-1}$ for the palladium compounds. The UV-visible spectra differ quite markedly, in structure and position from those of **8b,c** and **9b,c**. In these complexes the two peaks in the visible region are of much different intensity; the higher energy peak is less intense and appears as a shoulder on the more intense peak. In addition these peaks are shifted to the blue region by approximately 25-30 nm compared to **10b** and **11b**. As a result these peaks tail off into the blue region of the spectrum; this explains why compounds **8b,c** and **9b,c** are orange-red in colour and **10a-c** and **11a-c** are purple. Figure 3.11 shows a comparison of the UV-visible spectra of **9b** and **11b**. Because changing from platinum to palladium does not have a dramatic effect on the UV-visible spectra, but changing the chalcogen atom does, the absorptions in the visible region of the spectra are assumed to be ligand-based.

Figure 3.11: UV-visible spectra of **9b** and **11b**

9b:

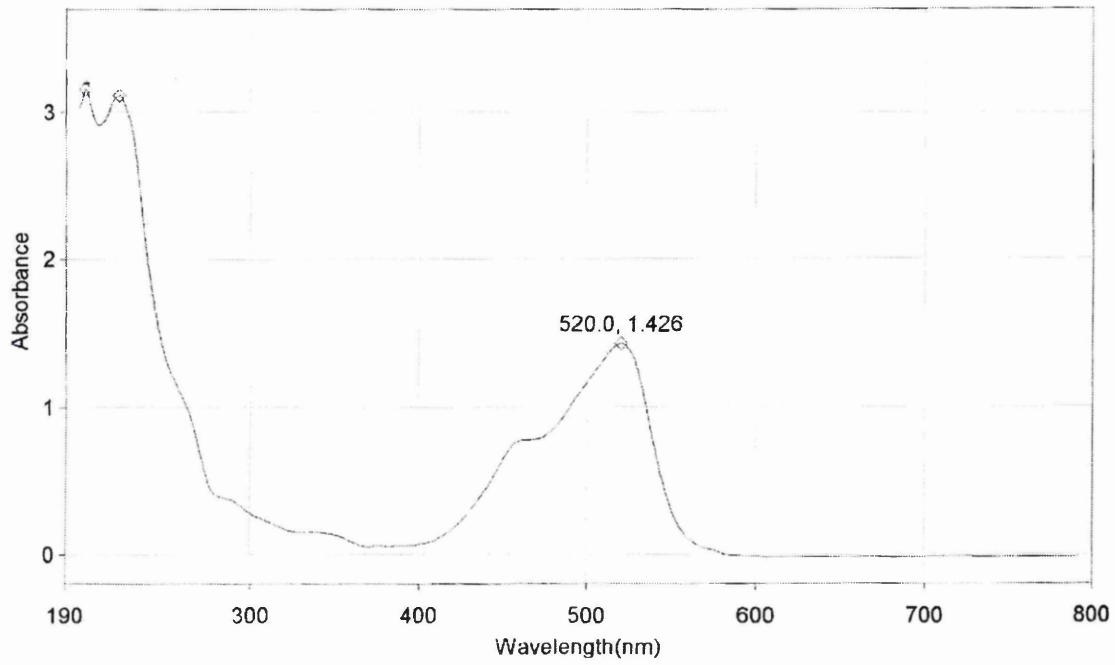

11b:

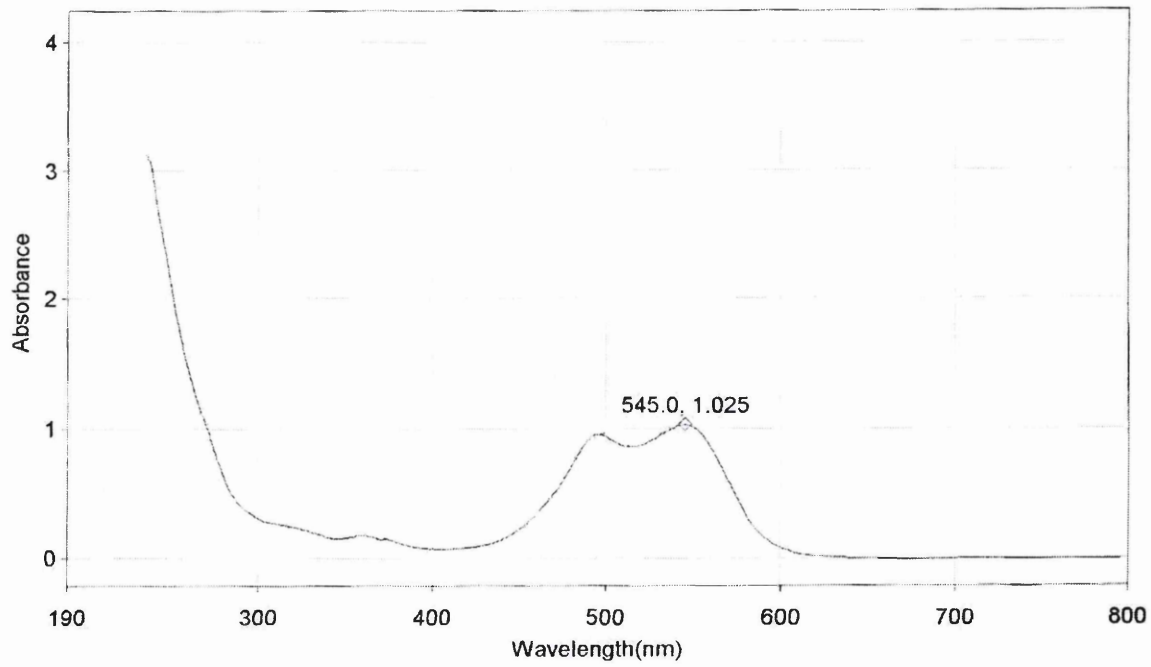

3.3 The Reaction of $[Pt(PPh_3)_4]$ with Cyclohexeno-1,2,3-selenadiazole

In chapter 2 the reaction of $[Pt(PPh_3)_4]$ with cyclohexeno-1,2,3-selenadiazole in refluxing toluene was discussed; it was found that this reaction gave a very poor yield (if any) of the expected diselenolene $[Pt(Se_2C_6H_8)(PPh_3)_2]$. It was noted that the reaction mixture sometimes became purple in colour. If the same reagents were stirred at room temperature for 2-4 days then a deep purple solution was formed. Concentration of the reaction mixture and subsequent column chromatography led to the isolation of a purple solid which was identified as $[PtL(PPh_3)]$ (L = $SeC(R^1)=C(R^2)N=NC(R^1)=C(R^2)Se$; R^1-R^2 = $(CH_2)_4$; 25% yield); this compound is analogous to **10a** and **11a** (figure 3.12).

Figure 3.12:

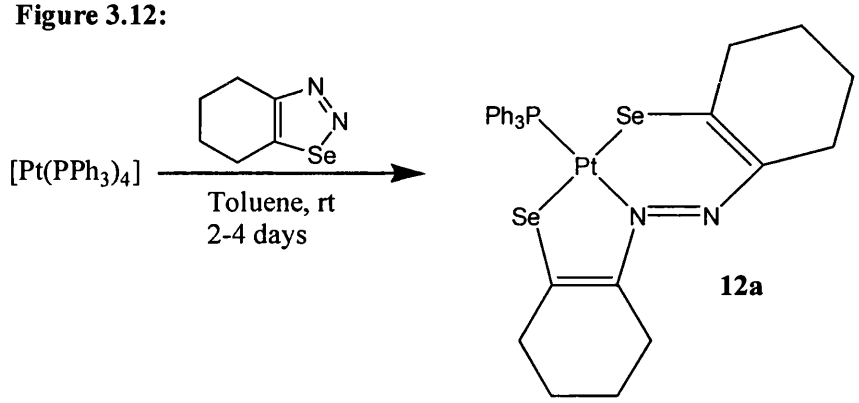

12a

It is also possible to synthesise **12a** using $[Pt(C_2H_4)(PPh_3)]$ as the starting material instead of $[Pt(PPh_3)_4]$. The compound has been characterised by ^{31}P and ^{77}Se NMR spectroscopy and mass spectrometry; these data are shown in table 3.9.

What is noticeable from the data is that the $^1J(^{77}Se\text{-}^{195}Pt)$ coupling constants are approximately 60 Hz less than those found for **10a-c** and **11a-c**, and the $^2J(^{77}Se\text{-}^{31}P)$ coupling constants are larger; this may be a direct result of the lower basicity of PPh_3 compared to PEt_3 and PBu_3. In addition the ^{77}Se resonances are at lower field; this could be due to PPh_3 withdrawing electron density from the $PtSe_2NP$ core.

Table 3.9: ^{31}P and ^{77}Se NMR spectroscopic ($CDCl_3$ solution) and mass spectral data for **12a**

^{31}P:	δ/ppm	9.9	Mass Spectrum (FAB):[a] $[M]^+$ 805 (100)
	$^1J(^{31}P\text{-}^{195}Pt)$/Hz	3262	
^{77}Se:	$\delta(Se_A)$/ppm	599	
	$^1J(^{77}Se_A\text{-}^{195}Pt)$/Hz	183	
	$^2J(^{77}Se_A\text{-}^{31}P)$/Hz	40	
	$\delta(Se_B)$/ppm	353	
	$^1J(^{77}Se_B\text{-}^{195}Pt)$/Hz	134	
	$^2J(^{77}Se_B\text{-}^{31}P)$/Hz	31	

[a] *m/z* (%); recorded using FAB; figures are for isotopomers containing ^{195}Pt, ^{80}Se, ^{14}N, ^{12}C, ^1H.

As reported in chapter 2 the reaction of $[Pt(PPh_3)_4]$ with cyclohepteno-1,2,3-selenadiazole in refluxing toluene gave $[Pt(Se_2C_7H_{10})(PPh_3)]$ in poor yield, but when the reaction was carried out at room temperature for several days a purple-red mixture was produced, from which small amounts of $[PtL(PPh_3)]$ (L = $SeC(R^1)=C(R^2)N=NC(R^1)=C(R^2)Se$; $R^1\text{-}R^2 = (CH_2)_5$) could be isolated after column chromatography. The purple solid shows a ^{31}P NMR resonance at δ = 10.3 ppm, $^1J(^{31}P\text{-}^{195}Pt) \sim 3200$ Hz and the FAB mass spectrum shows a peak at *m/z* = 833 (100%) confirming the synthesis of this species.

The reaction of $[Pt(PPh_3)_4]$ with cycloocteno-1,2,3-selenadiazole in toluene at room temperature gave an orange solution, in which there was no $[PtL(PPh_3)]$ (L = $SeC(R^1)=C(R^2)N=NC(R^1)=C(R^2)Se$; $R^1\text{-}R^2 = (CH_2)_6$) present. These reactions are believed to proceed via the mechanism proposed in figure 3.2 and they offer a good insight into how ring size affects the reactivity of these cycloalkeno-1,2,3-selenadiazoles. In these reactions it is critical that dinitrogen is retained by some of the 1,2,3-selenadiazole molecules; as has been discussed above dinitrogen is more difficult to remove from the cyclohexeno-1,2,3-selenadiazoles, due to the geometric constraints which would be placed on a resulting cyclohexyne species, whereas it is relatively easily removed from cycloocteno-1,2,3-selenadiazole as cyclooctyne is less strained. This explains why this reaction is successful for cyclohexeno-1,2,3-selenadiazole, less successful for cyclohepteno-1,2,3-selenadiazole and unsuccessful

for cycloocteno-1,2,3-selenadiazole. It also explains why, in the syntheses of the diselenolenes $[Pt(Se_2C_{n+4}H_{2n+4})(PPh_3)_2]$ (chapter 2), where dinitrogen loss is critical, the opposite trend exists *i.e.* the synthesis of $[Pt(Se_2C_8H_{12})(PPh_3)_2]$ is the most successful and the synthesis of $[Pt(Se_2C_6H_8)(PPh_3)_2]$ is the least successful.

The reaction of $[Pt(PPh_3)_4]$ with 4-phenyl-1,2,3-selenadiazole was also investigated. After stirring the reagents in toluene at room temperature for 3 days a purple reaction mixture was given; concentration and column chromatography led to the isolation of $[Pt\{SeC{=}C(Ph)N{=}NC(Ph){=}CSe\}(PPh_3)]$ as a purple solid (figure 3.13, 32% yield). The compound is air-sensitive and so was not thoroughly investigated (in view of the fact that **8b,c**, **9b,c**, **10a-c** and **11a-c** are air-stable). The ^{31}P NMR spectrum was recorded and showed a resonance at δ = 24.1 ppm, $^{1}J(^{31}P\text{-}^{195}Pt)$ = 3304 Hz which is atrributed to this compound.

Figure 3.13:

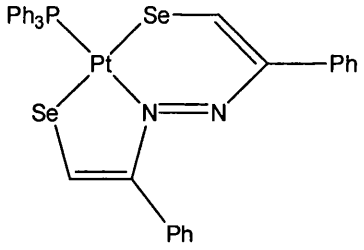

3.4 Reactions of $[Pt(C_2H_4)(PR_3)_2]$ with Cycloalkeno-1,2,3-selenadiazoles

In the previous sections of this chapter it was shown that complexes of the type $[PtL(PR_3)]$ (L = $EC(R^1)=C(R^2)N=NC(R^1)=C(R^2)E$; E = S, Se; R = Et, Bu) could be synthesised by the reaction of $[Pt(C_2H_4)(PR_3)_2]$ with cycloalkeno-1,2,3-thiadiazoles, or by the reaction of $[Pt(C_2H_4)(PR_3)_2]/[PtCl_2(PR_3)_2]$ with cycloalkeno-1,2,3-selenadiazoles. In the absence of sufficient $[PtCl_2(PR_3)_2]$, the reaction of $[Pt(C_2H_4)(PR_3)_2]$ (R = Et, Bu) with cycloalkeno-1,2,3-selenadiazoles in refluxing dioxane/THF/toluene gave complexes of the type $[Pt(SeC_{n+4}H_{2n+4})(PR_3)_2]$ (figure 3.14).

Figure 3.14:

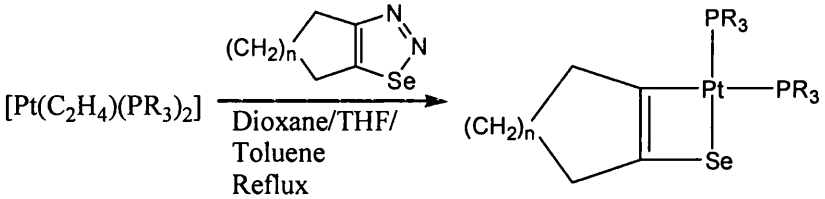

	n = 2	3	4
R = Et	**13a**	**13b**	**13c**
R = Bu	**14a**	**14b**	**14c**

This type of product has been observed previously (as has been well documented in the introduction) in the reaction of $[Pt(PPh_3)_4]$ with cycloocteno-1,2,3-selenadiazole, where the compound $[Pt(SeC_8H_{12})(PPh_3)_2]$ was one of the products.[114] The reaction of $[Co(\eta^5\text{-}C_5Me_5)(C_2H_4)_2]$ with cycloocteno-1,2,3-selenadiazole gives $[CoCp^*(SeC_8H_{12})L]$, where L is an intact selenadiazole molecule.[109] In addition the reaction of $[Fe_2(CO)_9]$ with various 1,2,3-thia- and 1,2,3-selenadiazoles results in the addition of the $Fe_2(CO)_6$ unit with loss of N_2 to give compounds with a C_2Fe_2E heterocycle.[99,100] In these examples the reaction was believed to proceed via the reaction of the low-valent metal species with a thia/selenaketocarbene and this could be the mechanism for the formation of **13a-c** and **14a-c**. However, given that insertion of '$Pt(PR_3)_2$' into the E-N bond is assumed to be a step in the formation of **8b,c**, **9b,c**, and possibly **10a-c** and **11a-c**, it is feasible that the mechanism involves insertion of '$Pt(PR_3)_2$' into the Se-N bond followed by dinitrogen elimination (both mechanisms are shown in figure 3.15). It is unclear which of these mechanisms is correct. Compound **14c** can be synthesised at room temperature if the reaction mixture is stirred for five days. This may suggest the reaction is dependent on the

formation of the selenaketocarbene (which is relatively slow at room temperature); alternatively this could be due to dinitrogen elimination from the PtN_2C_2Se species shown in figure 3.15 being a slow step. It is assumed that insertion of '$Pt(PR_3)_2$' into the N-Se bond should be relatively fast as the bond is relatively weak (the reactivity of 1,2,3-selenadiazoles is based on the easy cleavage of this bond); it is, however, entirely possible that this is the rate-limiting step.

Figure 3.15:

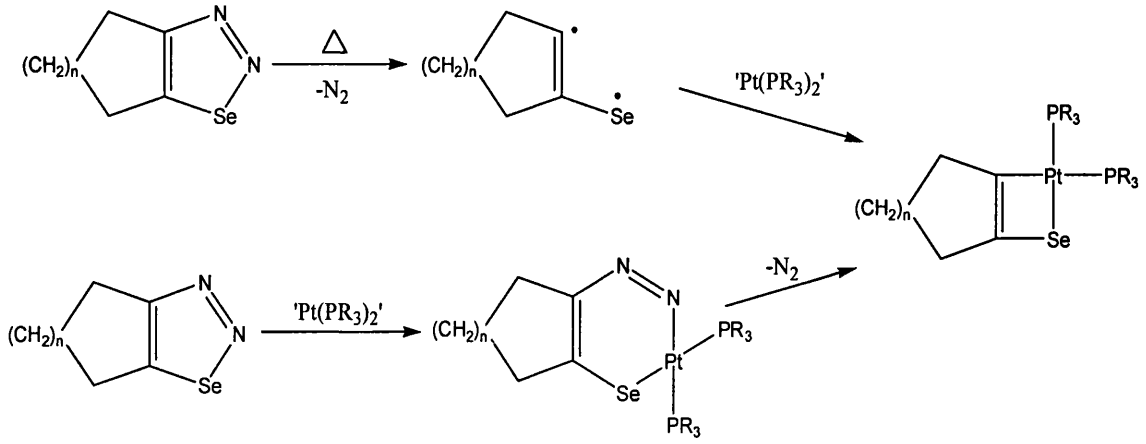

Filtration and concentration of solutions of **13a-c** and **14a-c** typically gave thick, deep red oils. It was necessary to analyse these under inert atmosphere conditions, as they are quite unstable; upon prolonged stirring the products decompose. This instability led to problems with purification; the compounds decomposed when column chromatography was attempted (even under inert atmosphere) and attempts at recrystallisation proved unsuccessful. Since only very crude products were obtained their characterisation is limited to ^{31}P and ^{77}Se NMR and mass spectral data; these are shown in table 3.10.

Table 3.10: ^{31}P and ^{77}Se NMR spectroscopic (d_6-benzene) and mass spectral data for **13a-c** and **14a-c**

		13a	**13b**	**13c**	**14a**	**14b**	**14c**
^{31}P:	$\delta(P_A)$/ppm	9.5	10.6	9.3	1.2	2.1	0.6
	$^1J(^{31}P_A\text{-}^{195}Pt)$/Hz	3351	3361	3360	3356	3368	3368
	$\delta(P_B)$/ppm	-0.5	-0.1	-1.2	-8.3	-7.8	-6.7
	$^1J(^{31}P_B\text{-}^{195}Pt)$/Hz	1813	1822	1810	1812	1800	1805
	$^2J(^{31}P_A\text{-}^{31}P_B)$/Hz	8	8	8	6	8	6
^{77}Se:	δ/ppm	-136	-101	-138	-140	-104	-140
	$^2J(^{77}Se\text{-}^{31}P_{trans})$/Hz	36	34	33	34	33	32
Mass Spectrum:[a]							
	$[M]^+$	591 (20)	605 (15)	619 (5)	-	773 (100)	788 (10)
	$[Pt(PR_3)_2]^+$	431 (20)	431 (15)	-	599 (100)	599 (85)	599 (25)

[a] *m/z* (%); recorded using FAB; figures are for isotopomers containing ^{195}Pt, ^{80}Se, ^{31}P, ^{12}C, ^1H.

What is immediately obvious from these data is the absence of ^{77}Se-^{195}Pt coupling in the ^{77}Se NMR spectra; it is unusual that this coupling is absent and it must be due to the particular electronic environment of selenium and platinum in these complexes. It is known that the magnitude of the coupling constant between two nucleii is dependent on a number of factors, including the amount of s-character the bond(s) between those nucleii have (the more s-character, the greater the coupling constant).[9] As the geometric constraints of the four-membered ring are likely to impose a C-Se-Pt bond angle close to 90°, the Pt-Se bond in **13a-c** and **14a-c** may have low s-character (it is probable that the Se orbitals involved are almost entirely p-based) which results in the ^{77}Se-^{195}Pt coupling constant being small enough not to be observed. The ^{77}Se NMR spectrum of $[Pt(SeC_8H_{12})(PPh_3)_2]$ has been recorded and shows a multiplet at δ = -13 ppm. The resonance was weak and difficult to analyse but it appears that there is ^{77}Se-^{195}Pt coupling and ^{77}Se-$^{31}P_{cis}$ coupling; this suggests that the type of phosphine present also has an influence.

The absence of observable ^{77}Se-$^{31}P_{cis}$ coupling in these species is not unexpected; it is typical for the ^{77}Se-$^{31}P_{cis}$ coupling to be much less than the ^{77}Se-$^{31}P_{trans}$ coupling, as was observed for the diselenolenes in chapter 2. The ^{77}Se NMR spectrum of **13c** is shown in figure 3.16 as an example. The ^{77}Se NMR resonances of **13a-c** and **14a-c** are at much higher field than any of the compounds discussed so far. This, and the absence of ^{77}Se-^{195}Pt coupling are a reflection of the unique chemical environment of selenium in these compounds. Again a lower field resonance is observed in the ^{77}Se NMR spectra of compounds **13b** and **14b** compared to **13a,c** and **14a,c**; this pattern is also observed in the ^{31}P NMR spectra of **13a-c** and **14a-c**. The lower field ^{31}P NMR resonances of **13a-c** and **14a-c** are attributed to the phosphorus nuclei *trans* to the selenium atom on the basis of their larger ^{31}P-^{195}Pt coupling constants. Generally platinum-phosphorus coupling constants are low (~ 1800 Hz) for phosphines *trans* to a Pt-C bond, and higher for phosphines *trans* to a Pt-X bond (X = chalcogen or halogen).[233]

The mass spectral data are quite poor reflecting the impurity of the material used, although it was possible to see the molecular ions (except for **14a**) all of which showed the correct isotope patterns. The low intensity of some of the molecular ions may be attributed to the instability of these compounds, which is why peaks for $[Pt(PR_3)_2]$ are observed.

Figure 3.16: ^{77}Se NMR spectrum of **13c**

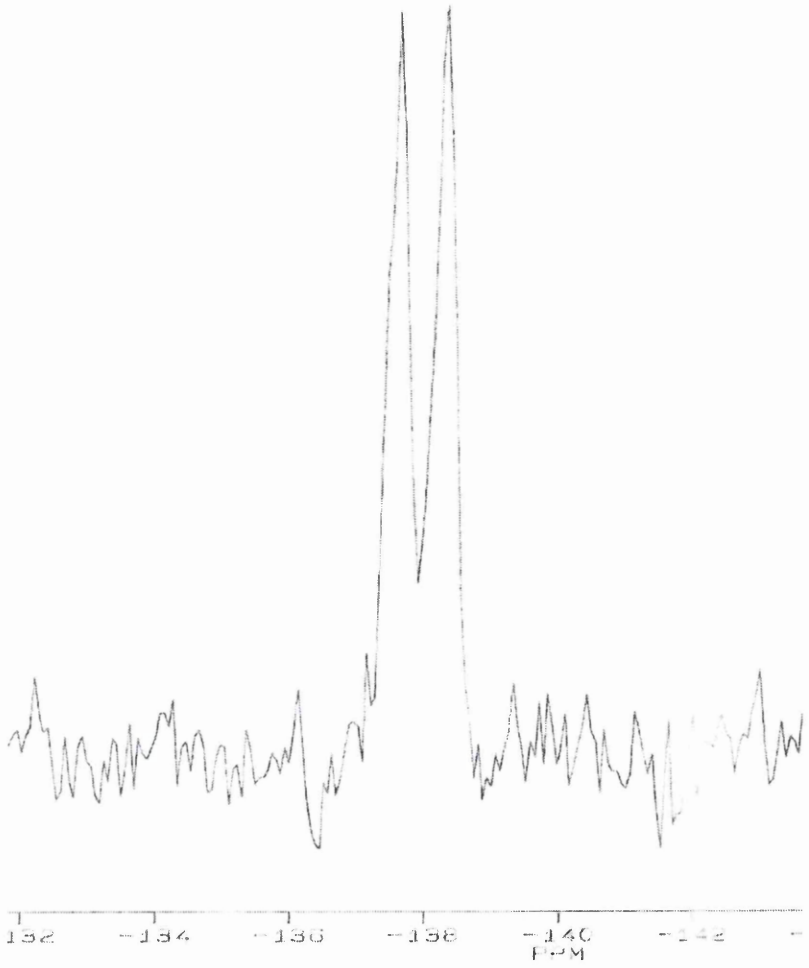

The reactions of $[Pt(C_2H_4)(L)]$ (L = dppm or dppe) with cycloocteno-1,2,3-selenadiazole were investigated to see if it was possible to synthesise the compounds $[Pt(SeC_8H_{12})(L)]$; these reactions were unsuccessful. The lack of success of these reactions may indicate that insertion of platinum into the Se-N bond is an important step in the mechanism of this reaction; 'PtL' fragments are less nucleophilic than '$Pt(PR_3)_2$' and so oxidative insertion will often not occur for 'PtL' where it does for '$Pt(PR_3)_2$' (mainly due to the greater basicity of trialkylphosphines). It may also indicate that phosphine dissociation/association plays a part; the fact that it is possible to synthesise $[Pt(SeC_8H_{12})(PPh_3)_2]$ means steric factors are unlikely to be affecting the outcome of the reaction.

Since it has been shown that bimetallic selenaketocarbene complexes can be formed with iron[99,100] and cobalt,[109] (figure 3.17) the reaction of cycloocteno-1,2,3-selenadiazole with a two-fold excess of $[Pt(C_2H_4)(PBu_3)_2]$ was attempted to see if an analogous platinum complex could be synthesised. The reaction yielded only $[Pt(SeC_8H_{12})(PBu_3)_2]$; this was perhaps to be expected. In this compound platinum would have to be in the +1 oxidation state; also the $Pt(PBu_3)_2$ moieties are large and it would be difficult to fit two of them into a 5-membered ring.

Figure 3.17:

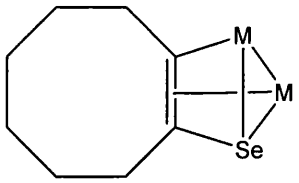

M = $Fe(CO)_3$, CoCp

3.5 Reactions of $[Pt(SeC_{n+4}H_{2n+4})(PR_3)_2]$ with MeI

Due to the difficulties in isolating and characterising **13a-c** and **14a-c** attempts were made to make a crystalline derivative and confirm its structure. The reaction with MeI was attempted as palladium diselenolenes have been successfully derivatised this way;[172] the reaction of dinuclear palladium diselenolenes with MeI gives mononuclear products of the type $[PdI\{Se(Me)C_{n+4}H_{2n+4}Se\}(PR_3)]$ via a bridge cleavage reaction (section 1.9).

Stirring **13a-c** and **14a-c** with an excess of MeI in a foil-covered flask overnight, followed by filtration and column chromatography led to the isolation of pink-purple oily solids. Based upon early spectral characterisations (and the chemistry observed for palladium diselenolenes) these products were believed to be $[PtI\{Se(Me)\ C_{n+4}H_{2n+4}\}(PR_3)]$ (figure 3.18).

Figure 3.18:

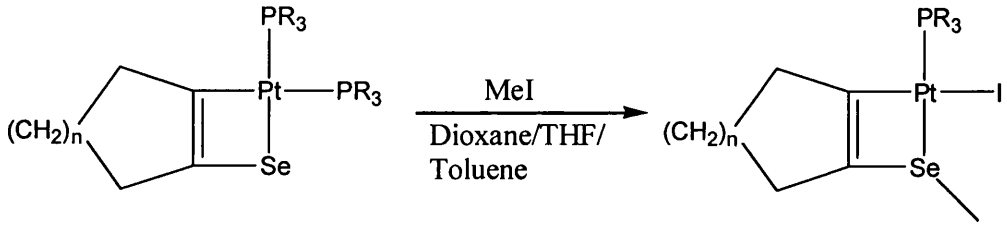

Upon further data collection it became apparent that there were two chemically and magnetically equivalent phosphorus atoms present. This suggested that oxidative addition of MeI to the Pt centre may have been occuring generating an octahedral species with the phosphines *trans* to one another. The reaction of **14c** with EtI was carried out and a ^{77}Se NMR spectrum recorded. The ^{77}Se chemical shift was 352 ppm, whereas with the analogous MeI product it was 235 ppm; this result suggested that alkylation of the selenium atom *not* the platinum atom occurs. It is therefore proposed that methylation of the selenium atom occurs with the iodide adding to the platinum to give a product with a square pyramidal geometry (figure 3.19). It has not been possible to deduce from the spectral data whether the selenium atom lies in an equatorial or axial position; the phosphine groups are *trans* to each other in both situations and are chemically and magnetically equivalent.

Compounds **15a-c** and **16a-c** have been isolated as pink-purple oily solids. They are very soluble in all organic solvents, which has unfortunately prevented the growth of crystals of these compounds. It has been possible to isolate these compounds in a relatively pure state by chromatographing 3-4 times; the most difficult part of the

purification is separating the compounds from the residual naphthalene present from the synthesis of **13a-c** and **14a-c**.

Figure 3.19:

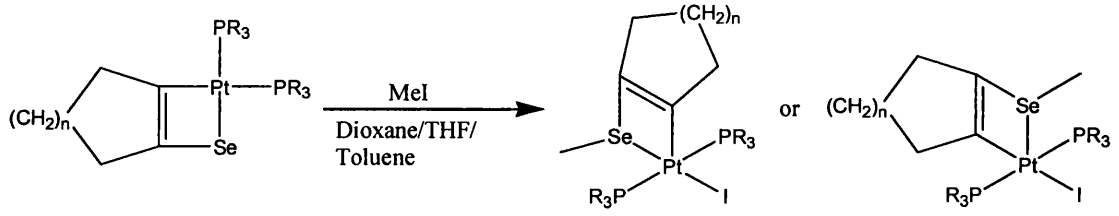

n =	2	3	4
R = Et:	**15a**	**15b**	**15c**
R = Bu:	**16a**	**16b**	**16c**

The formation of compounds **15a-c** and **16a-c** and not the products proposed in figure 3.18 suggests that the Pt-P bond in **13a-c** and **14a-c** is very strong and is not easily broken; this may be a result of the electronic properties of the $PtSeC_2$ system which were discussed above.

Compounds **15a-c** and **16a-c** have been characterised by multinuclear NMR spectroscopy and mass spectrometry; these data are presented in tables 3.11, 3.12 and 3.13. The NMR spectra are in accord with the structures proposed in figure 3.19. The ^{77}Se NMR resonance is split by the two equivalent phosphorus atoms into a triplet; the ^{77}Se and ^{195}Pt NMR spectra of **16a** are shown in figure 3.20 as an example. The ^{77}Se-^{195}Pt coupling constants of **15a-c** and **16a-c** are large and so the ^{195}Pt satellites are visible, unlike the situation in **13a-c** and **14a-c.** The presence of ^{77}Se-^{195}Pt coupling and the triplet structure in the ^{77}Se NMR spectra confirms that the selenium remains bound to platinum in these compounds. Were the reactions to proceed via methylation of Se followed by cleavage of the Se-Pt bond, most of the spectral data would be similar to **15a-c** and **16a-c**, but the ^{77}Se NMR data would show no ^{77}Se-^{195}Pt coupling and probably no ^{77}Se-^{31}P coupling. The ^{77}Se resonance is shifted downfield by more than 350 ppm compared to **13a-c** and **14a-c**. This shows that methylation has a big impact on the electronic environment of the selenium atom; not only is the electron density about selenium reduced (as evidenced by the change in chemical shift), but the character of the Se-Pt bonding is altered so the ^{77}Se-^{195}Pt coupling constant is increased by approximately 500 Hz. The C-Se-Pt bond angle must still be approximately 90°, but now the selenium atom has a 3-coordinate geometry (and is probably sp^2 hybridised); this obviously increases the s-character of the Se-Pt bond by a significant amount resulting in the relatively large ^{77}Se-^{195}Pt coupling constant.

Table 3.11: ^{1}H and ^{13}C NMR spectroscopic data for complexes **15a-c** in d_6-acetone solution

		15a	**15b**	**15c**
^{1}H	CH_3	1.06 (18H, dt)	1.05 (18H, dt)[a]	0.92 (18H, dt)[a]
	CH_2P	1.50-2.43 (12H, m)	1.95-2.18 (12H, m)	1.78-2.04 (12H, m)
	CH_3Se	1.50-2.43 (3H, m)[b]	1.78 (3H, s)	1.78-2.04 (3H, m)[b]
	α-CH_2	2.88-3.18 (4H, m)	2.28-2.68 (4H, m)	2.09-2.42 (4H, m)
	β-CH_2	1.50-2.43 (4H, m)	1.49-1.60 (4H, m)	1.25-1.45 (4H, m)
	γ-CH_2		1.61-1.69 (2H, m)	1.25-1.45 (4H, m)
^{13}C	CH_3	9.1[c]	9.2[c]	9.2[c]
	CH_2P	16.1[d]	16.7[d]	17.1[d]
	CH_3Se	3.2[e]	5.1[e]	4.6[e]
	$C=C$	136.8[f]	143.6[f]	140.6[f]
		122.2[g]	Not observed	126.0
	α-CH_2	40.2[h]	43.5[h]	41.2[h]
		32.9[i]	36.2[i]	32.8[i]
	β-CH_2	34.5	38.3	35.2
		30.3	30.7	30.5
	γ-CH_2		27.8	28.0
				26.3

[a] $^{3}J(^{1}H\text{-}^{1}H)$ = 8.0 Hz (**15a,c**), 7.6 Hz (**15b**), $^{3}J(^{1}H\text{-}^{31}P)$ = 16.0 Hz (**15a**), 16.8 Hz (**15b,c**); [b] singlet not distinguishable from aliphatic multiplet structure; [c] ^{3}J ($^{13}C\text{-}^{195}Pt$) = 26 Hz (**15a,c**), 21 Hz (**15b**); [d] AA'X system avg. J ($^{13}C\text{-}^{31}P$) = 17 Hz; [e] $^{1}J(^{13}C\text{-}^{77}Se)$ = 28 Hz (**15a**), 29 Hz (**15b**), 31 Hz (**15c**), ; [f] ^{2}J ($^{13}C\text{-}^{31}P$) = 9 Hz (**15a,b**), 7 Hz (**15c**); [g] ^{3}J ($^{13}C\text{-}^{31}P$) = 4 Hz; [h] ^{3}J ($^{13}C\text{-}^{195}Pt$) = 52 Hz (**15a**), 64 Hz (**15b,c**); [i] ^{2}J ($^{13}C\text{-}^{195}Pt$) = 66 Hz (**15a**), 78 Hz (**15b**), 68 Hz (**15c**).

Table 3.12: ^{1}H and ^{13}C NMR spectroscopic data for complexes **16a-c** in d_6-acetone solution

		16a	**16b**	**16c**
^{1}H	CH_3	0.80 (18H, t)[a]	0.81 (18H, t)[a]	0.80 (18H, t)[a]
	CH_2P	1.72-2.09 (12H, m)	1.91-2.09 (12H, m)	1.90-2.10 (12H, m)
	CH_2CH_2P	1.26-1.62 (12H, m)	1.25-1.63 (12H, m)	1.25-1.65 (12H, m)
	$CH_3CH_2CH_2$	1.26-1.62 (12H, m)	1.25-1.63 (12H, m)	1.25-1.65 (12H, m)
	CH_3Se	1.72-2.09 (3H, m)[b]	1.88 (3H, s)	1.90-2.10 (3H, m)[b]
	α-CH_2	2.15-2.50 (4H, m)	2.22-2.48 (4H, m)	2.29-2.60 (4H, m)
	β-CH_2	1.26-1.62 (4H, m)	1.25-1.63 (4H, m)	1.25-1.65 (4H, m)
	γ-CH_2		1.25-1.63 (2H, m)	1.25-1.65 (4H, m)
^{13}C	CH_3	14.7	14.4	14.7
	CH_2^P	24.1[c]	24.1[c]	24.9[c]
	CH_2CH_2P	25.4[d]	25.2[d]	25.4[d]
	$CH_3CH_2CH_2$	27.4	27.1	27.4
	CH_3Se	3.7	4.9	4.9
	$C{=}C$	138.2[e]	144.7[e]	142.0[e]
		122.7[f]	Not observed	126.4[f]
	α-CH_2	40.8[g]	43.9[g]	42.7[g]
		33.4[h]	36.6[h]	33.1[h]
	β-CH_2	34.8	38.0	35.4
		30.7	33.1	30.6
	γ-CH_2		28.1	28.4
				26.7

[a] $^{3}J(^{1}H\text{-}^{1}H)$ = 7.6 Hz (**16b,c**), 7.2 Hz (**16a**); [b] singlet not distinguishable from aliphatic multiplet structure; [c] AA'X system avg. J ($^{13}C\text{-}^{31}P$) = 17 Hz; [d] AA'X system, avg. J ($^{13}C\text{-}^{31}P$) = 7 Hz; [e] ^{2}J ($^{13}C\text{-}^{31}P$) = 8 Hz; [f] ^{3}J ($^{13}C\text{-}^{31}P$) = 4 Hz (**16a**), 5 Hz (**16c**); [g] ^{3}J ($^{13}C\text{-}^{195}Pt$) = 54 Hz (**16a**), 63 Hz (**16b**), 61 Hz (**16c**); [h] ^{2}J ($^{13}C\text{-}^{195}Pt$) = 71 Hz (**16a**), 77 Hz (**16b**), 61 Hz (**16c**).

Table 3.13: ^{31}P, ^{77}Se and ^{195}Pt (**15b, 16a** only) NMR spectroscopic (d_6-acetone solution) and mass spectral data for **15a-c** and **16a-c**

		15a	**15b**	**15c**	**16a**	**16b**	**16c**
^{31}P:	δ/ppm	7.7	7.5	9.0	0.2	-0.3	1.3
	$^{1}J(^{31}P\text{-}^{195}Pt)$/Hz	2817	2872	2869	2799	2857	2856
^{77}Se:	δ/ppm	217	244	229	220	256	235
	$^{1}J(^{77}Se\text{-}^{195}Pt)$/Hz	469	487	511	469	463	492
	$^{2}J(^{77}Se\text{-}^{31}P)$/Hz	4	5	5	4	5	5
^{195}Pt:	δ/ppm		-1835		-1797		
Mass Spectrum:[a]							
	$[M\text{-}I]^+$	606 (100)	620 (100)	634 (95)	774 (100)	788 (100)	802 (20)
	$[M\text{-}I\text{-}PR_3]^+$	-	502 (15)	516 (35)	572 (20)	586 (85)	600 (100)

[a] *m/z* (%); recorded using FAB; figures are for isotopomers containing ^{195}Pt, ^{80}Se, ^{31}P, ^{12}C, ^{1}H.

Figure 3.20: ^{77}Se and ^{195}Pt NMR spectra of **16a**

^{77}Se:

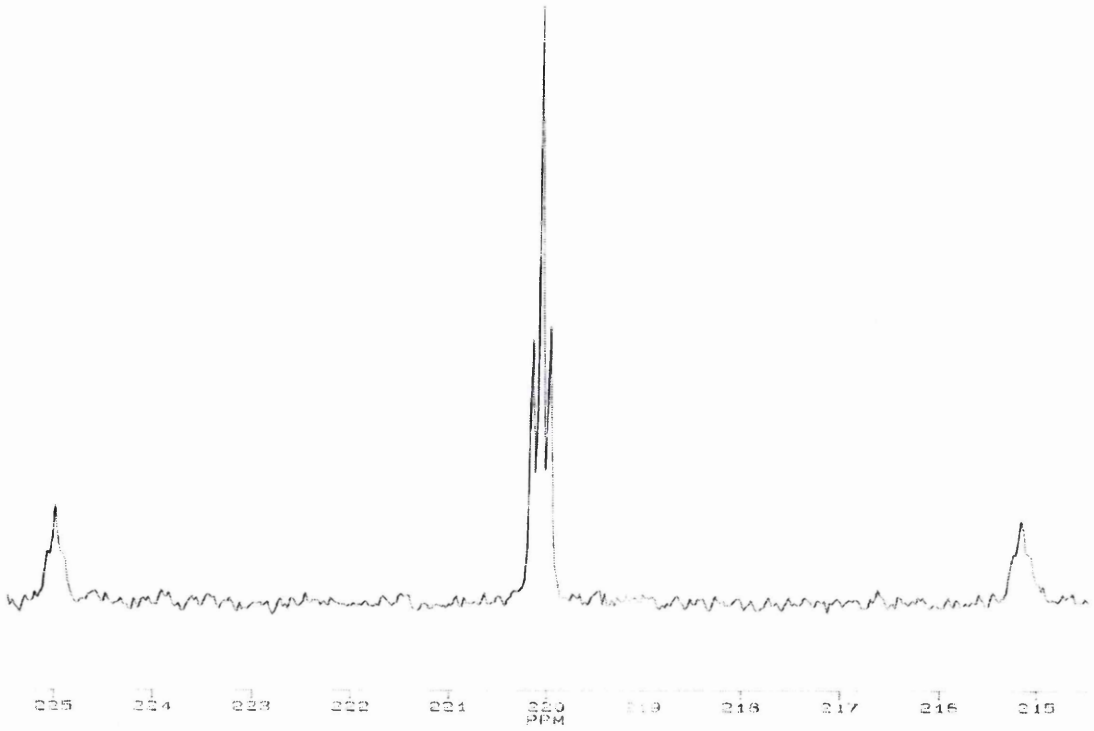

^{195}Pt:

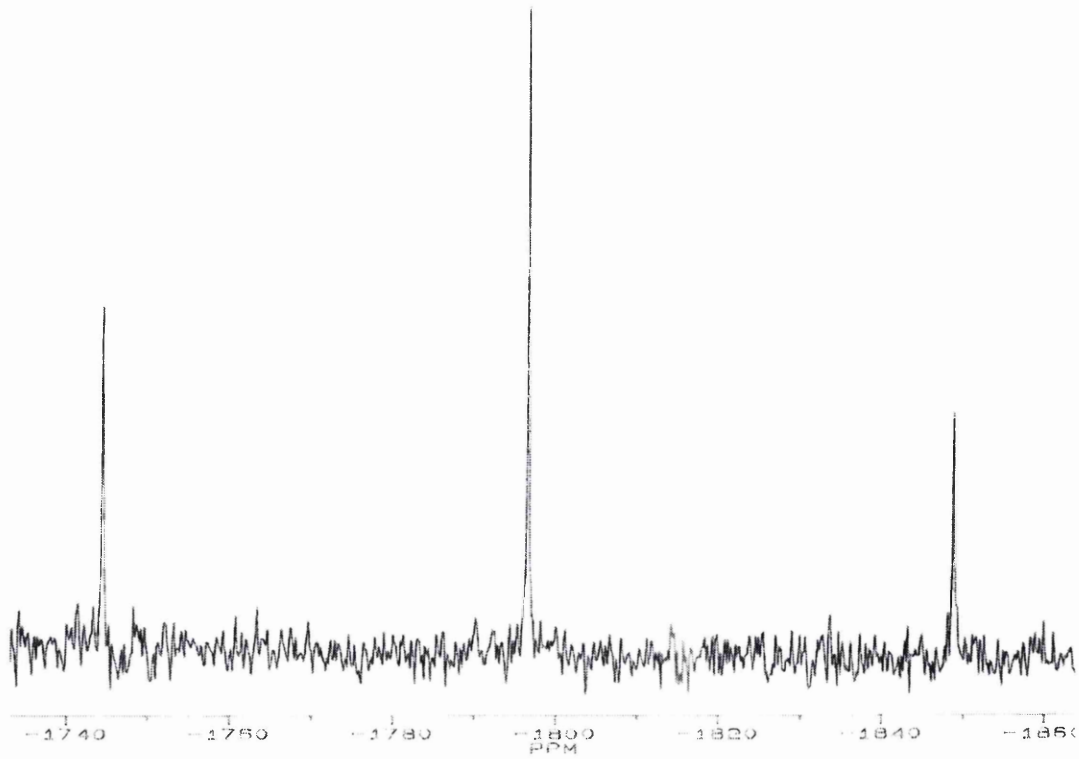

As expected the ^{77}Se chemical shifts of compounds **15b** and **16b** are at lower field than those of **15a,c** and **16a,c**; it appears also that the ^{77}Se-^{195}Pt coupling constant increases with the aliphatic ring size. The ^{195}Pt chemical shift of **16a** is at lower field than that of **15b**; although the compounds are not directly comparable it is believed that this is largely due to the differing phosphines present.

The ^{13}C and ^{1}H NMR data are fairly consistent; there are some data missing due to the difficulties in obtaining pure material. The chemical shift of the selenium-bound methyl group is quite low indicating that there is a lot of electron density about this group. As usual the chemical shifts of the ring carbon atoms in compounds **15b** and **16b** are at slightly lower field than in the other compounds, especially for the β-CH_2 groups. Although the ^{1}H spectra were complex, in most cases it was possible to pick out the α-CH_2 multiplets as their lower-field resonances separate them from the majority of the other peaks.

The mass spectra of the compounds all show high intensity (except **16c**) peaks corresponding to $[M\text{-}I]^+$. $[M]^+$ peaks were not observed at significant intensity; this suggests that the Pt-I bond in these complexes is relatively weak. The isotope patterns of the $[M\text{-}I]^+$ ions match the theoretical isotope patterns well.

It was found that **14c** would not react with dimethylsulphate (Me_2SO_4). This indicates that alkylation of the selenium atom *is* the critical step, and it is dependent on the strength of the alkylating group (Me_2SO_4 is a weaker methylating agent than MeI). This is also the case in the bridge cleavage reactions of palladium diselenolenes, where the first step of the reaction was proven to be alkylation of the selenium atom and not halogen-induced bridge cleavage.[172]

3.6 Reactions of $[PtI\{Se(Me)C_{n+4}H_{2n+4}\}(PR_3)_2]$ with $TlPF_6$

Since a crystallographic characterisation of compounds **15a-c** and **16a-c** was not possible, these compounds were further derivatised by reaction with $TlPF_6$. Stirring **15a-c/16a-c** with a slight excess of $TlPF_6$ in acetone for 2-3 days gave orange-red solutions with a fine yellow precipitate (TlI); filtration followed by concentration gave the orange-yellow oily solids **17a-c** and **18a-c** (figure 3.21).

Figure 3.21:

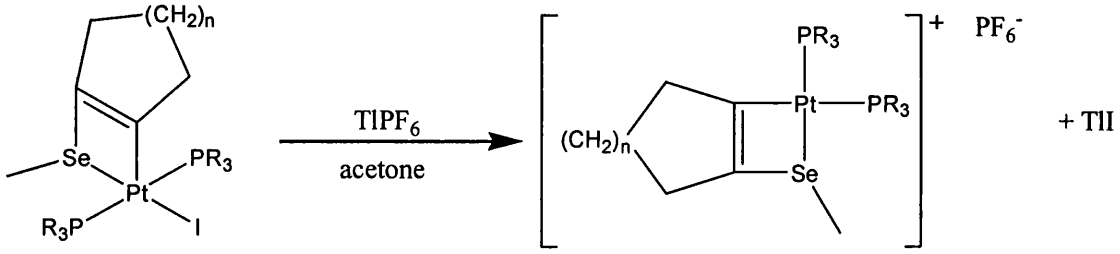

	n = 2	3	4
R = Et	**17a**	**17b**	**17c**
R = Bu	**18a**	**18b**	**18c**

The reactions proceeded as expected, iodide being extracted from **15a-c** and **16a-c** by Tl^+ to give $[Pt\{Se(Me)C_{n+4}H_{2n+4}\}(PR_3)_2]^+$ for which PF_6^- acts as the counterion. Compounds **17a-c** and **18a-c** have been characterised by multinuclear NMR spectroscopy and mass spectrometry; unfortunately at the time of writing no crystals of these compounds have been isolated and so an x-ray crystallographic study has not been carried out.

Tables 3.14, 3.15 and 3.16 show the NMR spectral and mass spectrometric data for compounds **17a-c** and **18a-c**. The NMR data are consistent with the proposed structures; the phosphines are not chemically equivalent and give rise to separate peaks in the ^{31}P, ^{13}C and ^{1}H NMR spectra. As for compounds **13a-c** and **14a-c** the phosphine *trans* to the selenium atom is assumed to give rise to larger coupling constants; this phosphorus (shown in figure 3.22) is assigned as P_A.

Figure 3.22:

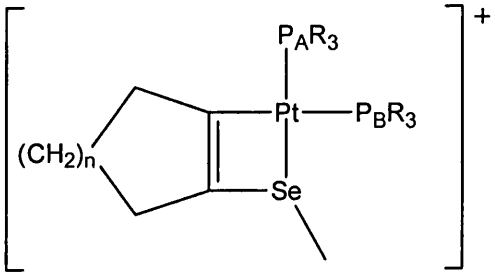

Table 3.14: ^{1}H and ^{13}C NMR spectroscopic data for complexes **17a-c** in d_6-acetone solution

		17a	**17b**	**17c**
^{1}H	CH_3	0.98-1.16 (18H, m)	1.04 (9H, dt)[a]	1.05 (9H, dt)[a]
			1.10 (9H, dt)[a]	1.15 (9H, dt)[a]
	CH_2P	1.80-2.41 (12H, m)	1.80-2.65 (m, 12H)	1.83-2.14 (12H, m)
	CH_3Se	1.80-2.41 (3H, m)[b]	1.99 (3H, s)	1.83-2.14 (3H, m)[b]
	α-CH_2	1.80-2.41 (4H, m)	1.80-2.65 (4H, m)	2.30-2.61 (4H, m)
	β-CH_2	1.40-1.70 (4H, m)	1.25-1.65 (4H, m)	1.29-1.59 (4H, m)
	γ-CH_2		1.25-1.65 (2H, m)	1.29-1.59 (4H, m)
^{13}C	CH_3(A)	8.8[c]	8.0[c]	8.5[c]
	CH_3(B)	8.3[d]	7.3[d]	7.9[d]
	CH_2P(A)	17.4[e]	16.2[e]	16.8[e]
	CH_2P(B)	16.7[f]	15.8[f]	16.4[f]
	CH_3Se	16.0[g]	15.6[g]	16.0[g]
	$C=C$	136.3[h]	137.6[h]	138.1[h]
		121.8[i]	Not observed	Not observed
	α-CH_2	38.8[j]	42.5[j]	36.7[j]
		32.4[k]	32.5	29.7
	β-CH_2	33.2[l]	35.0[l]	31.0[l]
		30.9	30.6	26.7
	γ-CH_2		26.4	26.0
				25.6

[a] $^{3}J(^{1}H\text{-}^{1}H)$ = 7.6 Hz, $^{3}J(^{1}H\text{-}^{31}P)$ = 16.4 Hz; [b] singlet not distinguishable from aliphatic multiplet structure; [c] ^{2}J ($^{13}C\text{-}^{31}P$) = 3 Hz (**17a,c**), 2 Hz (**17b**), ^{3}J ($^{13}C\text{-}^{195}Pt$) = 31 Hz (**17a,b**), 32 Hz (**17c**); [d] ^{3}J ($^{13}C\text{-}^{195}Pt$) = 14 Hz (**17a**), 16 Hz (**17b,c**); [e] ^{1}J ($^{13}C\text{-}^{31}P$) = 36 Hz (**17a**), 35 Hz (**17b,c**), ^{3}J ($^{13}C\text{-}^{31}P$) = 2 Hz (**17a**), not resolved (**17b,c**), ^{2}J ($^{13}C\text{-}^{195}Pt$) = 41 Hz (**17a**), 42 Hz (**17b**), 43 Hz (**17c**); [f] ^{1}J ($^{13}C\text{-}^{31}P$) = 29 Hz (**17a-c**), ^{2}J ($^{13}C\text{-}^{195}Pt$) = 36 Hz (**17a**), not resolved (**17b,c**); [g] $^{1}J(^{13}C\text{-}^{77}Se)$ = 20 Hz (**17a**), not resolved (**17b,c**), ^{3}J ($^{13}C\text{-}^{31}P$) = 2 Hz (**17a**), 3 Hz (**17b,c**); [h] ^{2}J ($^{13}C\text{-}^{31}P$) = 3 Hz (**17a,b**), not resolved (**17c**), ^{1}J ($^{13}C\text{-}^{195}Pt$) = 123 Hz (**17a**), 119 Hz (**17b**), 105 Hz (**17c**); [i] ^{2}J ($^{13}C\text{-}^{195}Pt$) = 8 Hz; [j] ^{3}J ($^{13}C\text{-}^{31}P$) = not resolved (**17a**), 7 Hz (**17b**), 8 Hz (**17c**), ^{3}J ($^{13}C\text{-}^{195}Pt$) = 57 Hz (**17a**), 54 Hz (**17b**), 58 Hz (**17c**); [k] ^{2}J ($^{13}C\text{-}^{195}Pt$) = 66 Hz (**17a**); [l] ^{3}J ($^{13}C\text{-}^{195}Pt$) = 12 Hz (**17a**), 14 Hz (**17b**), 13 Hz (**17c**).

Table 3.15: ^{1}H and ^{13}C NMR spectroscopic data for complexes **18a-c** in d_6-acetone solution

		18a	**18b**	**18c**
^{1}H	CH_3	0.82 (9H, t)[a]	0.83 (9H, t)[a]	0.83 (9H,t)[a]
		0.82 (9H, t)[a]	0.82 (9H, t)[a]	0.82 (9H, t)[a]
	CH_2P	1.73-2.38 (12H, m)	1.28-2.15 (12H, m)	1.80-2.12 (12H, m)
	CH_2CH_2P	1.28-1.72 (12H, m)	1.28-2.15 (12H, m)	1.29-1.75 (12H, m)
	$CH_3CH_2CH_2$	1.28-1.72 (12H, m)	1.28-2.15 (12H, m)	1.29-1.75 (12H, m)
	CH_3Se	1.73-2.38 (3H, m)[b]	1.28-2.15 (3H, m)[b]	1.80-2.12 (3H, m)[b]
	α-CH_2	1.73-2.38 (4H, m)	2.28-2.45 (4H, m)	2.32-2.85 (4H, m)
	β-CH_2	1.28-1.72 (4H, m)	1.28-2.15 (4H, m)	1.29-1.75 (4H, m)
	γ-CH_2		1.28-2.15 (2H, m)	1.29-1.75 (4H, m)
^{13}C	CH_3(A)	15.0	13.6	13.5
	CH_3(B)	15.0	13.6	13.5
	CH_2P(A)	26.0[c]	24.7[c]	24.6[c]
	CH_2P(B)	25.0[d]	Not observed	24.4[d]
	CH_2CH_2P(A)	25.7[e]	24.4[e]	24.1[e]
	CH_2CH_2P (B)	25.5[f]	24.3[f]	24.3[f]
	$CH_3CH_2CH_2$	28.2	26.9	26.7
	CH_3Se	17.7[g]	16.8[g]	16.5[g]
	$C=C$	137.7[h]	138.7[h]	142.0
		121.7	122.1	126.4
	α-CH_2	37.0[i]	43.6[i]	36.9[i]
		32.5	33.5	30.0
	β-CH_2	34.7[j]	35.9[j]	31.3[j]
		28.8	29.4	27.8
	γ-CH_2		29.1	26.2
				25.9

[a] $^{3}J(^{1}H\text{-}^{1}H)$ = 7.2 Hz (**18a,c**), 7.6 Hz (**18b**); [b] singlet not distinguishable from aliphatic multiplet structure; [c] ^{1}J ($^{13}C\text{-}^{31}P$) = 26 Hz (**18a**), 29 Hz (**18b**), 28 Hz (**18c**); [d] ^{1}J ($^{13}C\text{-}^{31}P$) = 22 Hz (**18a**), 25 Hz (**18b**), 17 Hz (**18c**); [e] ^{2}J ($^{13}C\text{-}^{31}P$) = 18 Hz (**18a**), 14 Hz (**18b**), 15 Hz (**18c**); [f] ^{2}J ($^{13}C\text{-}^{31}P$) = 17 Hz (**18a**), 14 Hz (**18b**). 13 Hz (**18c**); [g] ^{3}J ($^{13}C\text{-}^{31}P$) = 2 Hz (**18a**), 3 Hz (**18b,c**); [h] ^{2}J ($^{13}C\text{-}^{31}P$) = 3 Hz (**18a,b**), ^{1}J ($^{13}C\text{-}^{195}Pt$) = 123 Hz (**18a**), 118 Hz (**18b**); [i] ^{3}J ($^{13}C\text{-}^{31}P$) = not resolved (**18a**), 8 Hz (**18b**), 7 Hz (**18c**), ^{3}J ($^{13}C\text{-}^{195}Pt$) = 60 Hz (**18a**), 54 Hz (**18b**), 45 Hz (**18c**); [j] ^{3}J ($^{13}C\text{-}^{195}Pt$) = 14 Hz (**18a**), 13 Hz (**18b, 18c**).

Table 3.16: ^{31}P, ^{77}Se NMR spectroscopic (d_6-acetone solution) and mass spectral data for **17a-c** and **18a-c**

		17a	**17b**	**17c**	**18a**	**18b**	**18c**
^{31}P:[a]	$\delta(P_A)$/ppm	13.8	14.4	13.1	5.0	5.9	4.4
	$^1J(^{31}P_A\text{-}^{195}Pt)$/Hz	3740	3680	3725	3720	3740	3737
	$\delta(P_B)$/ppm	0.0	-0.8	0.1	-7.7	-8.5	-7.4
	$^1J(^{31}P_B\text{-}^{195}Pt)$/Hz	1906	1894	1902	1895	1895	1894
^{77}Se:	δ/ppm	-152	-118	-143	-151	-116	-143
	$^1J(^{77}Se\text{-}^{195}Pt)$/Hz	79	97	96	81	98	102
	$^2J(^{77}Se\text{-}^{31}P_{trans})$/Hz	87	84	86	87	85	86
Mass Spectrum:[b]							
	$[M]^+$	606 (100)	620 (100)	634 (100)	774 (100)	788 (100)	802 (100)
	$[PF_6]^-$	145 (100)	145 (100)	145 (100)	145 (100)	145 (100)	145 (100)

[a] All ^{31}P NMR spectra showed a resonance at δ = -144.1 ppm corresponding to PF_6^-. [b] *m/z* (%); recorded using ESI (cone voltage = 20 V) in positive and negative ion modes; figures are for isotopomers containing ^{195}Pt, ^{80}Se, ^{31}P, ^{19}F ^{12}C, ^1H.

The ^{77}Se NMR resonances of **17a-c** and **18a-c** are split into doublets by coupling to the *trans* phosphorus atom. The ^{77}Se-$^{31}P_{trans}$ coupling constants are much larger than were observed for **13a-c** and **14a-c**, but the ^{77}Se-$^{31}P_{cis}$ coupling constants are still too small to be resolved; figure 3.23 shows the ^{77}Se NMR of **18b** as an example. The ^{77}Se NMR resonances are at high field, in a similar region to those of **13a-c** and **14a-c**; the ^{77}Se NMR resonances of compounds **15a-c** and **16a-c** were at much lower field. Unlike those of **13a-c** and **14a-c** the ^{77}Se spectra of **17a-c** and **18a-c** do show ^{77}Se-^{195}Pt coupling (figure 3.23) although the value is small compared to **15a-c** and **16a-c** (~ 90 Hz compared to ~ 475 Hz). The ^{77}Se-$^{31}P_{trans}$ coupling constants are fairly consistent for each of the compounds, but the ^{77}Se-^{195}Pt coupling constants do seem to increase upon increasing the size of the aliphatic ring. Typically lower field resonances are observed for **17b** and **18b**. The ^{77}Se NMR spectra of compounds **13a-c, 14a-c, 15a-c, 16a-c, 17a-c** and **18a-c** have shown how even slight changes in structure can greatly change the electronic environment of the selenium atom; these changes would not have been revealed in as great a detail by any other spectroscopic technique.

The ^{31}P NMR spectra are as expected and are very similar to those of **13a-c** and **14a-c**; the ^{31}P-^{195}Pt coupling constants are slightly larger, which could be a result of the decreased electron density in **17a-c** and **18a-c**. The ^{31}P-^{31}P coupling was not resolved; as the PF_6^- resonance dominates the ^{31}P NMR spectra, the phosphine signals are relatively weak and no splitting was observed.

The ^{13}C data are fairly consistent and are similar to those of **15a-c** and **16a-c**. One noticeable difference however, is that the chemical shift of the selenium-bound methyl group is higher (by approximately 10 ppm) indicating that there is a loss of electron density about this group upon removal of I^-. As usual the carbon atoms in the aliphatic rings of **17b** and **18b** resonate at slightly lower field. As has been observed previously, although the ^{1}H spectra were complex in most cases it was possible to pick out the α-CH_2 multiplets as their lower-field resonances separate them from the majority of the other peaks.

Figure 3.23: ^{77}Se NMR spectrum of **18b**

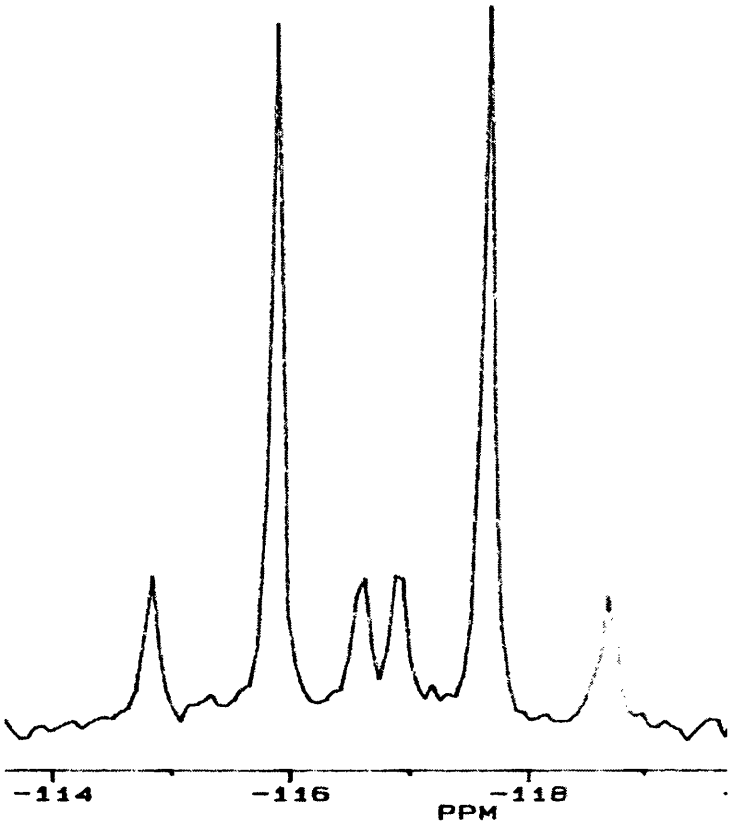

The ESI (electrospray ionisation) mass spectra all show $[M]^+$ peaks with 100% relative intensity in the positive ion spectra at a cone voltage of 20 V. The high intensities of these peaks could be attributed to the relatively 'soft' conditions used; at higher cone voltages (50 and 90 V) fragmentation occurs, typically with loss of a phosphine at 50 V, and extensive breakdown of the molecules at 90 V. There is no evidence of iodine in either the positive or negative ion spectra; this confirms that the reaction proceeds as shown in figure 3.21.

Although crystallographic characterisation of compounds **15a-c, 16a-c, 17a-c** and **18a-c** has not been possible, the multinuclear NMR spectroscopic and mass spectral data provide enough evidence to confirm the proposed structures for **13a-c** and **14a-c** (figure 3.14).

Chapter 4

The Syntheses, Reactions and Characterisation of Some Complexes Derived from Selenophene

4.1 The Reactions of $[Pt(C_2H_4)(PR_3)_2]$ with Selenophene

In chapter 1 the reactions of selenophenes with low-valent transition metal complexes were discussed; those with group 6, 7, 8 and 9 metals have been well covered, but the investigation of reactions with Ni, Pd and in particular Pt has been limited. To our knowledge the reaction of $[Pt(C_2H_4)(PPh_3)_2]$ with selenophene activated by $Mn(CO)_3^+$ is the only reported reaction of a *bis*-phosphine platinum(0) complex with a selenophene.[217] Oxidative addition of the C-Se bond to Pt(0) occurs to give the selenaplatinacycle $[Mn(CO)_3(\eta^5\text{-}\{Pt(SeC_4H_4)(PPh_3)_2\})]^+$; the '$Pt(PPh_3)_2$' fragment is a relatively weak nucleophile and activation of the C-Se bond (through electron withdrawal) of selenophene by $Mn(CO)_3^+$ is necessary for the reaction to proceed.

Stirring $[Pt(C_2H_4)(PR_3)_2]$ (R = Et, Bu) with selenophene in dioxane/THF at 50 °C overnight followed by column chromatography (**19**) or crystallisation (**20**) led to the isolation of the selenaplatinacycles $[Pt(SeC_4H_4)(PR_3)_2]$ (figure 4.1) as yellow (**19**) or orange (**20**) solids.

Figure 4.1:

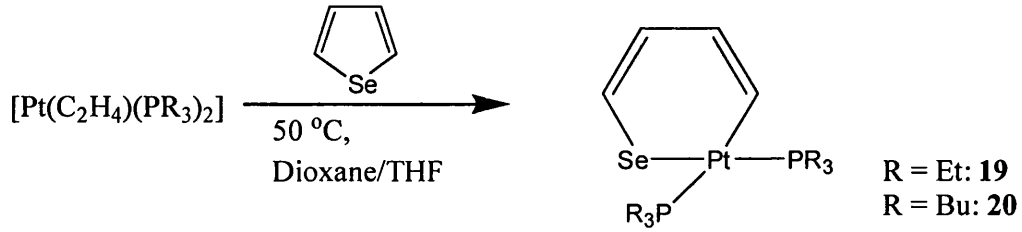

The reaction proceeds via oxidative addition of the C-Se bond of selenophene to the '$Pt(PR_3)_2$' moieties; due to the greater basicity of PEt_3 and PBu_3 compared to PPh_3 '$Pt(PR_3)_2$' is sufficiently nucleophilic for the reaction to proceed without activation of the C-Se bond. Analogous reactions have also been attempted using $[Pt(C_2H_4)(L)]$ (L = dppm, dppe) and selenophene. That these were not successful is attributed to the 'Pt(L)' moieties having a comparable nucleophilicity to '$Pt(PPh_3)_2$'; the reaction should not be affected by steric factors here (i.e. the reactions should proceed with activated selenophene).

It was possible to purify **20** by recrystallisation from hexane; these crystals were suitable for an x-ray diffraction study. The molecular structure is shown in figure 4.2; thermal ellipsoids are drawn at 30% probability and hydrogens are omitted for clarity. The crystal data are summarised in table 4.1, with selected bond lengths and angles listed in table 4.2. Diffraction data were collected on an Oxford Diffraction Excalibur

3 CCD diffractometer with Mo-K_α radiation (λ = 0.71069 Å); structure solution was by SIR 97[225] with refinement by SHELXL 97.[223]

Table 4.1 Crystallographic data for **20**

Empirical formula	$C_{28}H_{58}P_2SePt$
Formula weight	730.73
Crystal system	orthorhombic
Space group	F 2dd
Crystal dimensions (mm)	0.70 x 0.18 x 0.14
a/Å	10.280(1)
b/Å	31.707(3)
c/Å	42.304(3)
α/°	90.00
β/°	90.00
γ/°	90.00
V/Å	13789(2)
Z	16
F(000)	5888
D_{calc} (g cm^{-3})	1.408
μ (Mo-K_α/mm^{-1})	5.232
Temperature (K)	295
Reflections collected	22996
Independent reflections	6350
θ Range (°)	4.28-29.12
Reflect. with $I > 2\sigma(I)$	4382
No. of parameters	310
R_1; wR_2 [$I > 2\sigma(I)$]	0.0532; 0.1370
R_1; wR_2 (all data)	0.0764; 0.1511
GoF	1.014

Figure 4.2: Crystal Structure of **20**

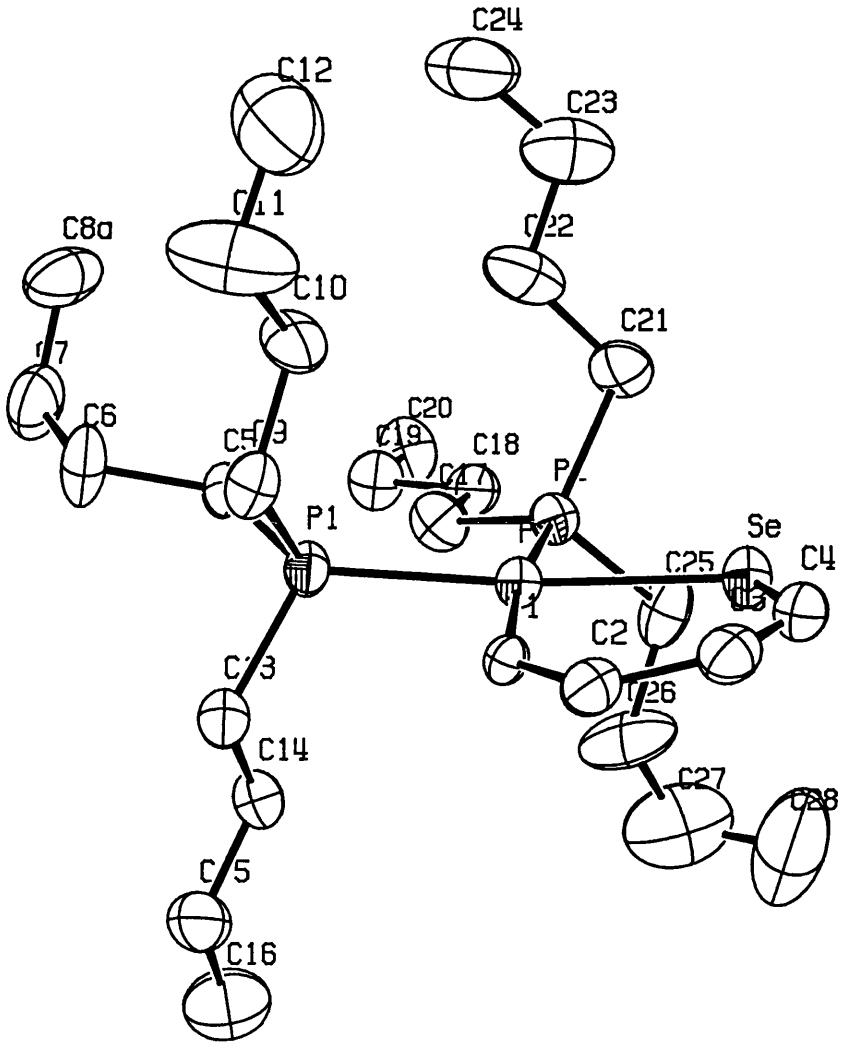

Table 4.2: Selected bond lengths and angles of compound **20**

Bond Lengths (Å)	
Pt-Se	2.4270(8)
Pt-C(1)	2.096(6)
Pt-P(1)	2.276(2)
Pt-P(2)	2.355(2)
Se-C(4)	1.824(13)
Bond Angles (°)	
Se-Pt-C(1)	89.28(15)
Se-Pt-P(1)	169.72(7)
Se-Pt-P(2)	84.70(6)
P(1)-Pt-P(2)	102.32(7)
P(1)-Pt-C(1)	84.25(16)
P(2)-Pt-C(1)	172.48(15)
Pt-C(1)-C(2)	135.51(51)
Pt-Se-C(4)	108.85(28)

Dihedral angle between $PtSeCP_2$ plane and Se-C(1) plane = 8.7°

The geometry about the platinum(II) centre is distorted square-planar. The P(1)-P(2) angle of 102.32° is assumed to be greater than 90° due to steric repulsion of the bulky PBu_3 groups; this angle is larger than that seen in thiaplatinacycles with PEt_3 ligands (*ca.* 98°),[210] probably due to the larger size of PBu_3. The Se-Pt distance of 2.427(0) Å is comparable with the Pt-Se distance in $[Mn(CO)_3(\eta^5\text{-}\{Pt(SeC_4H_4)(PPh_3)_2\})]^+$ (2.421(9) Å),[217] although the P-Pt-Se angles are less (169.72 and 84.70° compared to 171.61 and 86.82°); this correlates with the smaller P-Pt-P angle (96.79°) in $[Mn(CO)_3(\eta^5\text{-}\{Pt(SeC_4H_4)(PPh_3)_2\})]^+$. The Pt-Se distance is *ca.* 0.1 Å bigger than the Pt-S distance in analogous thiaplatinacycles,[210] as expected given the larger size of the selenium atom compared to sulphur. The C(1)-Pt-Se angle of 89.28° is similar to that of $[Pt\{SCHC(Cl)CHCH\}(PEt_3)_2]$ (89.84°),[210] but quite different from that of $[Mn(CO)_3(\eta^5\text{-}\{Pt(SeC_4H_4)(PPh_3)_2\})]^+$ (85.55°); this may be due to the smaller P-Pt-P angle in this species or the influence of the $Mn(CO)_3^+$ moiety. The Se-C(4)-C(3)-C(2)-C(1) component of the selenaplatinacycle is essentially planar; the platinum atom deviates from this plane and the dihedral angle of the Se-C(4)-C(3)-C(2)-C(1) and Se-Pt-C(1) planes is 8.7°. Deviation of platinum from this plane is typical of this type of complex,[210,217] and angles ranging from 1.3° ($[Pt(SCHC(Cl)CHCH)(PEt_3)_2]$) to 37.5° ($[Pt\{SC_3H_3C(NO_2)\}(PEt_3)_2]$[210] have been observed. The deviation of platinum from the selenophene plane indicates that, even though this is a 6π-electron system

like the diselenolenes discussed in chapter 2, there is not extensive electron delocalisation about the $PtSeC_4$ ring system. In the case of compounds **19** and **20** the steric factors favouring a non-planar $PtSeC_4$ ring outweigh the electronic benefits of a six-membered delocalised ring system.

Tables 4.3 and 4.4 show the multinuclear NMR data for compounds **19** and **20**, which are consistent with the proposed structures. The phosphines are not chemically equivalent and give rise to separate peaks in the ^{31}P, ^{13}C and ^{1}H NMR spectra. As in chapter 3 the phosphine *trans* to the selenium atom is assumed to give rise to larger coupling constants; this phosphorus (shown in figure 4.3) is designated P_A.

Figure 4.3:

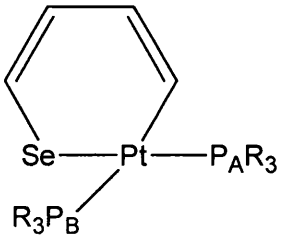

Table 4.3: ^{1}H and ^{13}C NMR spectroscopic data for **19** and **20** in d_6-acetone solution

		19	**20**
^{1}H	*CH*$_3$	0.81-0.93 (18H, m)	0.70 (18H, t)[a]
	CH$_2$P	1.75-1.89 (12H, m)	1.71-1.88 (12H, m)
	CH$_3$*CH*$_2$CH$_2$	-	1.13-1.45 (12H, m)
	CH$_2$CH$_2$P	-	1.13-1.45 (12H, m)
	CH(1)-*CH*(4)	6.50-7.40 (4H, m)	6.44-7.73 (4H, m)
^{13}C	*C*H$_3$(1)	8.5[b]	13.9
	*C*H$_3$(2)	8.4[c]	13.8
	*C*H$_2$P(1)	16.8[d]	24.6[d]
	*C*H$_2$P(2)	16.9[e]	24.7[e]
	*C*H$_2$CH$_2$P(1)	-	27.0[f]
	*C*H$_2$CH$_2$P(2)	-	26.9[g]
	CH$_3$*C*H$_2$CH$_2$	-	25.1
	C(1)	131.0[h]	130.5[h]
	C(2)	128.4[i]	128.4[i]
	C(3)	121.8	121.8
	C(4)	112.0[j]	112.0[j]

[a] $^{3}J(^{1}H\text{-}^{1}H)$ = 7.2 Hz; [b] $^{3}J(^{13}C\text{-}^{195}Pt)$ = 25 Hz; [c] $^{3}J(^{13}C\text{-}^{195}Pt)$ = 14 Hz; [d] $^{1}J(^{13}C\text{-}^{31}P)$ = 32 Hz (**19**), 13 Hz (**20**), $^{3}J(^{13}C\text{-}^{31}P)$ = 2 Hz (**19**), $^{2}J(^{13}C\text{-}^{195}Pt)$ = 31 Hz (**19**); [e] $^{1}J(^{13}C\text{-}^{31}P)$ = 27 Hz (**19**), 13 Hz (**20**), $^{2}J(^{13}C\text{-}^{195}Pt)$ = 13 Hz (**19**); [f] $^{3}J(^{13}C\text{-}^{195}Pt)$ = 23 Hz; [g] $^{3}J(^{13}C\text{-}^{195}Pt)$ = 13 Hz; [h] $^{2}J(^{13}C\text{-}^{31}P_{trans})$ = 98 Hz (**19**), 99 Hz (**20**), $^{3}J(^{13}C\text{-}^{31}P_{cis})$ = 9 Hz (**19**), 10 Hz (**20**); [i] $^{2}J(^{13}C\text{-}^{195}Pt)$ = 106 Hz; [j] $^{2}J(^{13}C\text{-}^{31}P_{trans})$ = 7 Hz, $^{3}J(^{13}C\text{-}^{31}P_{cis})$ = 3 Hz.

Table 4.4: ^{31}P and ^{77}Se NMR spectroscopic data for **19** and **20** in d_6-acetone solution.

		19	**20**
^{31}P:	$\delta(P_A)$/ppm	10.4	2.9
	$^1J(^{31}P_A\text{-}^{195}Pt)$/Hz	3190	3157
	$\delta(P_B)$/ppm	-0.8	-8.4
	$^1J(^{31}P_B\text{-}^{195}Pt)$/Hz	1732	1693
	$^2J(^{31}P_A\text{-}^{31}P_B)$/Hz	15	14
^{77}Se:	δ/ppm	303	294
	$^1J(^{77}Se\text{-}^{195}Pt)$/Hz	171	169
	$^2J(^{77}Se\text{-}^{31}P_{trans})$/Hz	71	70
	$^2J(^{77}Se\text{-}^{31}P_{cis})$/Hz	48	49

The ^{77}Se NMR spectra are as expected with Se the X part of an AMX pattern, so a doublet of doublets, due to splitting by the chemically inequivalent phosphines is observed. Figure 4.4 shows the ^{77}Se NMR spectrum of **20**; the AMX structure is very clear due to the relatively large values of the $^{77}Se\text{-}^{31}P$ coupling constants. The $^{77}Se\text{-}^{31}P_{trans}$ coupling constants are comparable to those of the diselenolenes **1a-c** and **2b,c** discussed in chapter 2, but the $^{77}Se\text{-}^{31}P_{cis}$ coupling constants are much larger (49 Hz *cf* 14-18 Hz). Indeed they are by far the largest $^{77}Se\text{-}^{31}P_{cis}$ coupling constants of any of the compounds discussed in this thesis; this is attributed to the unique chemical environment of the selenaplatinacycles. The ^{195}Pt satellites are clearly visible in the spectra from which we can obtain the $^{77}Se\text{-}^{195}Pt$ coupling constants; these are approximately 100 Hz lower than the $^{77}Se\text{-}^{195}Pt$ coupling constants of the diselenolenes **1a-c** and **2b,c**. In addition the chemical shifts of **19** and **20** are much lower than those of the diselenolenes ($\delta \sim 300$ ppm *cf* $\delta \sim 460$ ppm); this is believed to be due to the lack of electron delocalisation around the selenaplatinacycles compared to the diselenolenes (as discussed above). The ^{31}P NMR spectra are as expected; the lower field resonances are attributed to the phosphine *trans* to the selenium on the basis of the greater $^{31}P\text{-}^{195}Pt$ coupling constant.[233] The same protocol has been used in the assignment of the carbon and hydrogen atoms of the phosphines. The ^{13}C NMR spectra are as expected; due to low intensity (C(1)-C(4)) or overlap (PBu_3) some of the $^{13}C\text{-}^{195}Pt$ and $^{13}C\text{-}^{31}P$ coupling constants could not be established, but a resonance for every carbon atom was present. The ^1H NMR spectra were quite complex (especially in the olefinic region) but were of sufficient quality to confirm the structures of **19** and **20**.

Figure 4.4: ^{77}Se NMR spectrum of **20**

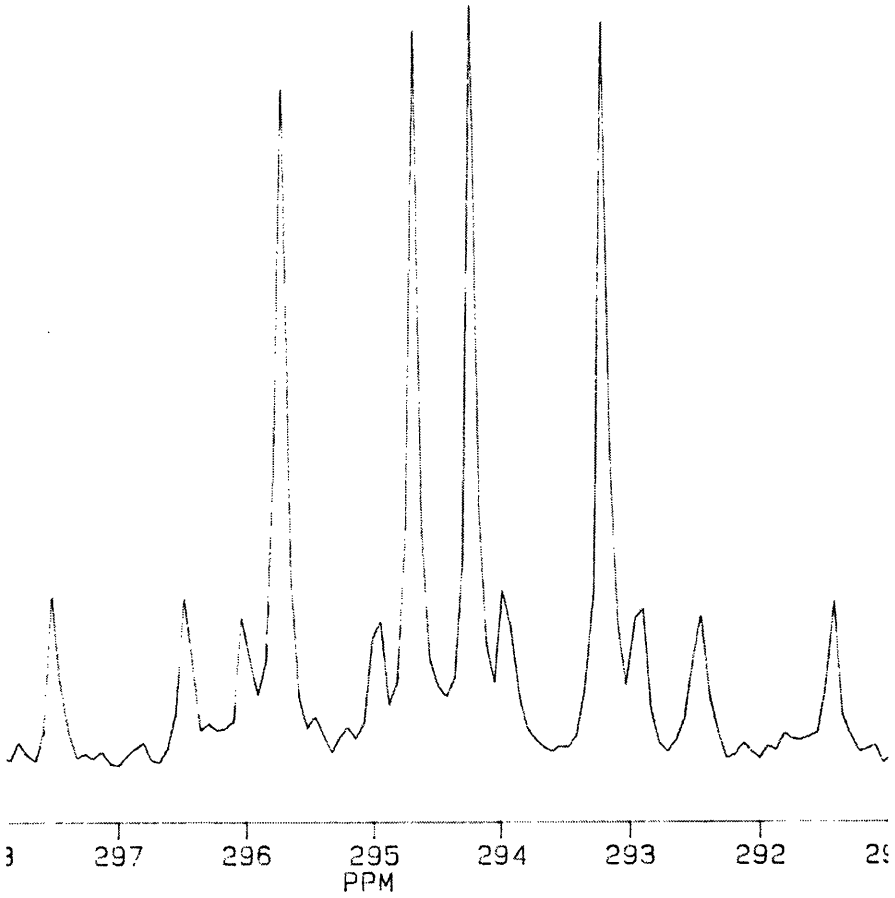

Table 4.5 shows the mass spectral data for **19** and **20** and the infrared and UV-visible spectroscopic data for **20**. Purification of compound **19** was difficult and material suitable for infrared and UV-visible spectroscopic analysis was not obtained.

The low relative intensity of the molecular ion peaks compared to the $[Pt(PR_3)_2]^+$ peaks suggest that **19** and **20** are not very stable; this was perhaps to have been expected. In general the main aim of investigations into the reactions of low-valent transition metals with thiophenes and selenophenes, is to find catalysts for the removal of chalcogens from chemical feedstocks.[196] It is thus a key requirement of these reactions that the products are not too thermodynamically stable to facilitate further reaction. In the mass spectrum of **20** there is a small cluster at m/z = 667-680 (7 %) which *may* correspond to $[PtSe(PBu_3)_2]^+$, but it is not of high enough intensity to suggest deselenation is a major process here.

Table 4.5: Mass spectral data for **19** and **20** and infrared and UV-visible spectroscopic data for **20**

		19	**20**
Mass Spectrum[a]	$[M]^+$	563 (30)	731 (25)
	$[Pt(PR_3)_2]^+$	431 (100)	599 (100)
Infrared[b]		Not recorded	2954 (s) 2927 (s) 2870 (m) 1462 (m) 1418 (w) 1377 (m) 1206 (w) 1160 (w) 1087 (m) 1050 (w) 967 (w) 905 (m) 784 (s) 723 (m) 643 (s)
UV-Vis[c]		Not Recorded	230 (15,700) 280 (10,700) 350sh (4,300)

[a] *m/z* (%); recorded using FAB; figures are for isotopomers containing ^{195}Pt, ^{80}Se, ^{31}P, ^{12}C, ^{1}H; expected isotope patterns were observed. [b] Selected bands (cm^{-1}) only. [c] λ_{max} (nm); ε (cm^{-1} M^{-1}) in parentheses; recorded in DCM solution (10^{-5} M).

The UV-visible spectrum of **20** explains the orange colour of the compound: the major absorbance bands are in the UV region of the spectrum, but there is a shoulder at 350 nm that tails off into the visible. The intensity of absorption drops to a very low value at approximately 400 nm, but doesn't drop to zero until approximately 600 nm; the fact that there is no absorption in the 600-800 nm region gives rise to the orange colour of this compound.

4.2 Reactions of [Pt(SeC$_4$H$_4$)(PBu$_3$)$_2$] (20)

Some reactions of **20** were investigated. There is a report of the thiaplatinacycle [Pt{*C,S*-(CH=CHC$_6$H$_4$S)}(PMe$_3$)$_2$] reacting with a slight excess of dppe to give [Pt{*C,S*-(CH=CHC$_6$H$_4$S)}(dppe)];[234] the reaction is presumably driven by the chelate effect. A similar reaction with **20** was attempted. Compound **20** was stirred with an excess of dppe in toluene for 3 days; during this time the pale yellow reaction mixture darkened. Subsequent analysis by ^{31}P NMR spectroscopy showed no starting material or product with a ^{31}P-^{195}Pt couple to be present.

In chapter 1 (section 1.6.3) the insertion of S or Se into the Co-C bond of [Co(η^5-C$_5$R$_5$)(SeC$_8$H$_{12}$)] (R = H or Me) was documented;[110,111] a similar reaction was attempted with compound **20** in an attempt to synthesise a product of the type shown in figure 4.5. This type of compound could be considered a vinylogue of diselenolenes.

Figure 4.5:

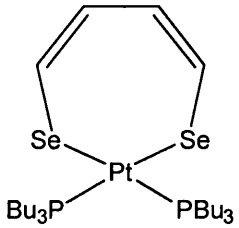

Stirring **20** with 2.5 equivalents of elemental grey selenium in toluene under an argon atmosphere at 80 °C for 15 minutes gave a dark brown reaction mixture; analysis by ^{31}P NMR spectroscopy showed mostly SePBu$_3$. These results suggest that compound **20** is not very stable: in solution 'Pt(PBu$_3$)$_2$' and selenophene may be in equilibrium with **20** (figure 4.6), and in the presence of oxygen or selenium 'Pt(PBu$_3$)$_2$' reacts with loss of EPBu$_3$ (E = O, Se) driving the equilibrium to the left with loss of the product.

Figure 4.6:

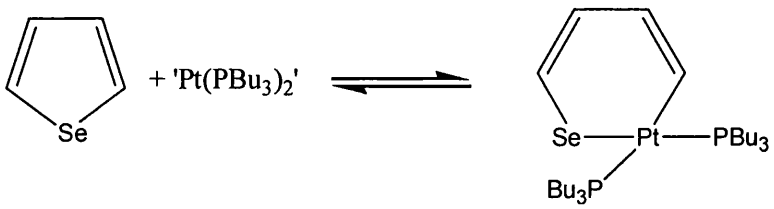

Compound **19** is less stable than **20** and is lost quickly in air-exposed solution (whereas **20** is stable enough to be crystallised from an air-exposed solution). This is

presumably a steric effect: PEt_3 is more easily oxidised than PBu_3, meaning it is removed from the equilibrium shown in figure 4.6 more quickly.

4.3 Miscellaneous Reactions

The reactions of $[Pt(C_2H_4)(PR_3)_2]$ with thiophene and 2,5-diphenyltellurophene have been investigated; along with the reactions of low-valent palladium phosphine complexes with thiophene and selenophene, these reactions are documented below.

4.3.1 Reactions of $[Pt(C_2H_4)(PR_3)_2]$ with Thiophene and 2,5-Diphenyltellurophene

Although the reactions of '$Pt(PEt_3)_2$' with thiophenes are well documented,[213,214,216,234] there are (to our knowledge) no reports of the reactions of '$Pt(PBu_3)_2$' with thiophenes. $[Pt(C_2H_4)(PBu_3)_2]$ was stirred with thiophene overnight at room temperature and at 70 °C; in both cases subsequent column chromatography led to the isolation of a yellow oil, the ^{31}P NMR spectra of which showed equal intensity peaks at δ = 3.3 ppm ($J(^{31}P\text{-}^{195}Pt)$ = 3084 Hz) and δ = -7.6 ppm ($J(^{31}P\text{-}^{195}Pt)$ = 1643 Hz). The FAB mass spectrum of the product obtained from the reaction carried out at 70 °C showed peaks at *m/z* = 599 (100%) and 683 (10%) corresponding to $[Pt(PBu_3)_2]^+$ and $[Pt(SC_4H_4)(PBu_3)_2]^+$ respectively. So it appears a thiaplatinacycle (figure 4.7) has been synthesised, but the yield was low (5-10%) and the reaction was therefore not investigated further.

Figure 4.7:

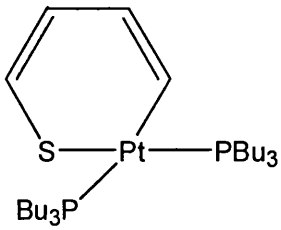

The reactions of $[Pt(C_2H_4)(PR_3)_2]$ (R = Et, Bu) with 2,5-diphenyltellurophene were also investigated; 2,5-diphenyltellurophene was used as it is more stable than tellurophene and its synthesis is relatively straightforward.[235] The reactions were carried out under the same conditions used to synthesise **19** and **20** substituting selenophene with 2,5-diphenyltellurophene. The yellow reaction mixtures were filtered, concentrated and analysed by ^{31}P NMR spectroscopy under an argon atmosphere; these analyses showed peaks at δ = 2.9 ppm ($J(^{31}P\text{-}^{195}Pt)$ = 1992, 3125 Hz) and δ = -4.0 ppm ($J(^{31}P\text{-}^{195}Pt)$ = 2205, 3125 Hz) for R = Et and Bu respectively. These peaks are attributed to the telluraplatinacycle shown in figure 4.8, assuming in

both cases that the ^{31}P chemical shifts of the two inequivalent phosphines are accidentally degenerate.

Figure 4.8:

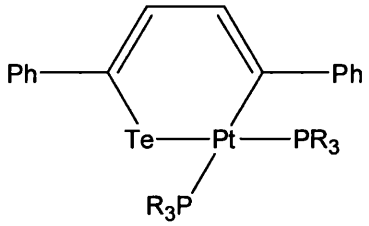

Unfortunately purification of these telluraplatinacycles was not possible by column chromatography. When allowed to stand in solution the deposition of 2,5-diphenyltellurophene occurs indicating that an equilibrium similar to that in figure 4.6 exists and it is biased to the left.

4.3.2 Reactions of Palladium(0) Phosphine Complexes with Selenophene

Since palladium diselenolenes analogous to the platinum diselenolenes discussed in chapter 2 can be synthesised from *in situ* generated '$Pd(PR_3)_2$',[120,126,169] an investigation into whether this was a viable method for insertion of Pd into selenophene was carried out. Under Ar a mixture of $[Pd_2(dba)_3]$.dba and PR_3 (R = Et, Bu) in toluene was treated with selenophene and stirred at 50 °C overnight. The reactions were attempted several times, but unfortunately none of the desired selenapalladacycles were isolated and spectroscopic analysis showed, if they were present it was in very small amounts. The reason for this could be due to the lability of palladium compared to platinum, resulting in an unstable selenapalladacycle forming, which quickly returns to starting materials. Alternatively '$Pd(PR_3)_2$' may not be a strong enough nucleophile to insert into the C-Se bond of selenophene; as discussed previously the nucleophilicity of the metal centre is critical to the success of the reaction.

Chapter 5

The Reactions of Compounds Containing an Se-Se bond with Zerovalent Platinum and Palladium Trialkylphosphine Complexes

5.1 The Reactions of $(PhSe)_2$ and $(FcSe)_2$ with $[Pt(C_2H_4)(PR_3)_2]$ and with $[Pd_2(dba)_3].dba/PR_3$ (R = Et, Bu)

In chapter 1 the reactions of various diaryl diselenides with low-valent platinum and palladium complexes were briefly discussed; the main focus of the research has been on triphenylphosphine derivatives. The reaction of diphenyl diselenide with $[Pt(C_2H_4)(PPh_3)_2]$ or $[Pt(PPh_3)_4]$ gives *trans*-$[Pt(SePh)_2(PPh_3)_2]$;[141,142] the reaction with $[Pd(PPh_3)_4]$ gives the dinuclear compound $[Pd_2(\mu_2\text{-}SePh)_2(SePh)_2(PPh_3)_2]$.[236] Similar trends are observed in the reactions of $[M(PPh_3)_4]$ (M = Pt, Pd) with *bis*-(2-thienyl) diselenide where the products are *trans*-$[Pt(SeTh)_2(PPh_3)_2]$ (Th = 2-thienyl) and $[Pd_2(\mu_2\text{-}SeTh)_2(SeTh)_2(PPh_3)_2]$.[143] Although there are reports of the reactions of ferrocenyl selenolates with platinum and palladium complexes,[237,176] there is only one report of oxidative addition of $(FcSe)_2$ (Fc = $[Fe(\eta^5\text{-}C_5H_5)(\eta^5\text{-}C_5H_4)]$) and that concerns a ruthenium complex.[238] There are no reports of the reactions of $(PhSe)_2$ with platinum(0) trialkylphosphine complexes to produce complexes of the type *trans*-$[Pt(SeR')(PR_3)_2]$ (R = Et, Bu); although there is a report of the synthesis of *trans*-$[Pd(SePh)_2(PBu_3)_2]$, it was prepared by the reaction of $[PdCl_2(PBu_3)_2]$ with NaSePh.[239] With this in mind the reactions of $[Pt(C_2H_4)(PR_3)_2]$ with $(R'Se)_2$ (R' = Ph, Fc) and the reactions of $[Pd_2(dba)_3].dba/PR_3$ with $(FcSe)_2$ were investigated.

Stirring $[Pt(C_2H_4)(PR_3)_2]$ and $(R'Se)_2$ in a dioxane/THF mixture overnight, followed by column chromatography led to the isolation of the compounds *trans*-$[Pt(SePh)_2(PR_3)_2]$ (**21a,b**, yellow solids) and *trans*-$[Pt(SeFc)_2(PR_3)_2]$ (**22a,b**, orange solids) as shown in figure 5.1.

Figure 5.1:

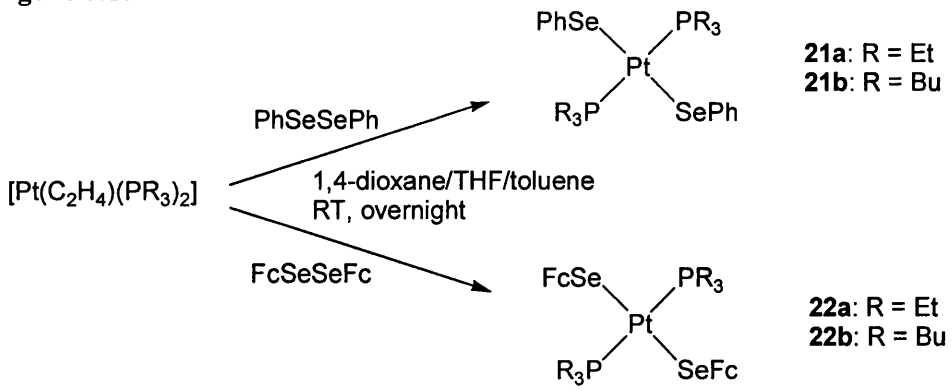

Similarly the reaction of a $[Pd_2(dba)_3].dba/PR_3$ mixture with $(FcSe)_2$ in toluene at room temperature overnight, followed by precipitation by hexane and filtration led to

the isolation of the compounds *trans*-$[Pd(SeFc)_2(PR_3)_2]$ (**23a,b**, red/orange solids) as shown in figure 5.2.

Figure 5.2:

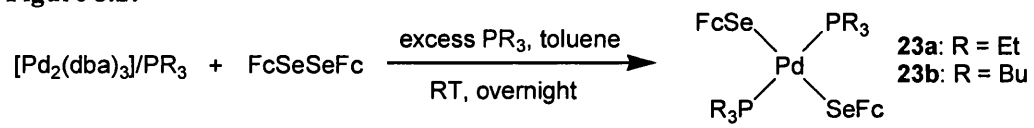

A $[Pd_2(dba)_3]$.dba/PR_3 mixture is used as the precursor in the palladium reactions as there are no reported syntheses of $[Pd(C_2H_4)(PR_3)_2]$ (R = Et, Bu) and our attempts to prepare these complexes have been unsuccessful. In the syntheses of **23a,b** an excess of phosphine was used; the synthesis of compounds of the type $[Pd_2(\mu_2\text{-}SePh)_2(SePh)_2(PR_3)_2]$ by using a palladium to phosphine ratio of 1:1 was attempted under the same conditions. Brown reaction mixtures were given and chromatographic purification or precipitation with hexane gave brown solids; analysis by ^{31}P NMR spectroscopy showed many peaks and recrystallisation was unsuccessful. These reactions obviously do not proceed cleanly and isolation of any products is difficult, so they were pursued no further.

Only the *trans*- isomers of **21a,b**, **22a,b** and **23a,b** are isolated. There is no evidence for the presence of the *cis*- isomers; this is attributed to the steric influence of the bulky phosphine substituents which are further apart in the *trans*-isomers. The initial formation of the *cis*- isomers cannot be ruled out; it is possible that they form and then isomerise to the *trans*- isomers. It has been reported that the reaction of $[Pt(C_2H_4)(PPh_3)_2]$ with $(PhSe)_2$ gives *cis*-$[Pt(SePh)_2(PPh_3)_2]$ which isomerises to *trans*-$[Pt(SePh)_2(PPh_3)_2]$ at room temperature in solution;[240] the same isomerisation has been reported for *cis*-$[Pt(SePh)_2(PPh_3)_2]$ generated from the reaction of *cis*-$[PtCl_2(PPh_3)_2]$ with NaSePh.[241,242]

Crystals of **21a, 21b** and **22a** suitable for an x-ray diffraction study were obtained by recrystallisation from toluene/hexane at –20 °C; the results of this study are presented in chapter 6. One point of note from this study is that the unit cell of **21a** contains both the *syn*- and *anti*- stereoisomers (figure 5.3). The unit cells of **21b** and **22b** showed only the *anti*-isomer.

Figure 5.3: *Syn-* and *anti-* isomers of **21a**

***Syn*-isomer:**

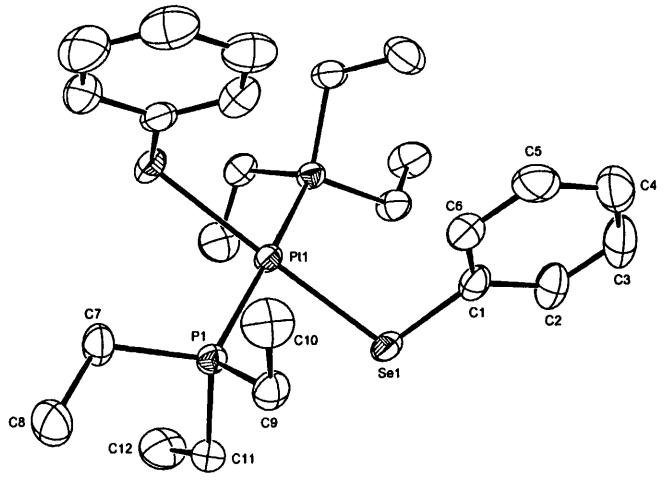

***Anti*-isomer:**

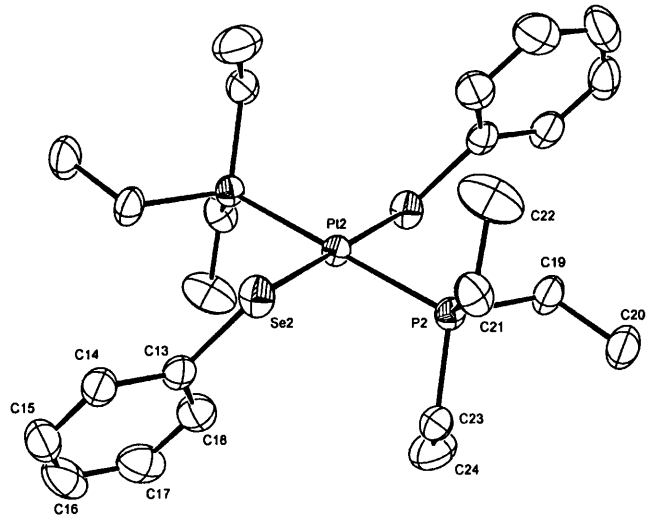

Interconversion of these isomers via pyramidal inversion of the selenium atom is a process that has been well studied[44] and is generally fast in solution, so the individual isomers are often not shown upon spectroscopic analysis, especially where simple monodentate selenolate ligands are present.

The multinuclear NMR spectroscopic data for **21a,b**, **22a,b** and **23a,b** are presented in tables 5.1 and 5.2.

Table 5.1: ^{1}H and ^{13}C NMR spectroscopic data for **21a,b**, **22a,b**, **23a,b** in d_6-benzene solution

Compound		**21a**	**21b**	**22a**	**22b**	**23a**	**23b**
δ(^{1}H)	CH_3	0.90 (18H, dt)[a]	0.84 (18H, t)[b]	1.00 (18H, dt)[a]	0.96 (18H, t)[b]	0.99 (18H, dt)[a]	1.07 (18H, t)[b]
	CH_2P	1.94-2.05 (12H, m)	1.20-1.30 (12H, m)	1.83-1.97 (12H, m)	1.36-1.48 (12H, m)	1.80-1.89 (12H, m)	1.37-1.50 (12H, m)
	$CH_3CH_2CH_2$		1.42-1.53 (12H, m)		1.48-1.60 (12H, m)		1.46-1.58 (12H, m)
	CH_2CH_2P		2.04-2.14 (12H, m)		1.97-2.06 (12H, m)		1.91-1.99 (12H, m)
	C_6H_5 (*o/p*)	6.94-7.07 (6H, m)	6.93-7.08 (6H, m)				
	C_6H_5 (*m*)	7.97-8.02 (4H, m)	7.99-8.03 (4H, m)				
	C_5H_4			3.96-3.99 (4H, m)	3.98-4.02 (4H, m)	3.97-4.00 (4H, m)	3.98-4.01 (4H, m)
				4.48-4.51 (4H, m)	4.52-4.55 (4H, m)	4.48-4.51 (4H, m)	4.51-4.54 (4H, m)
	C_5H_5			4.19 (10H, s)	4.24 (10H, s)	4.22 (10H, s)	4.25 (10H, s)
δ(^{13}C)	CH_3	8.2[c]	14.0	8.8[c]	14.3	8.9	14.2
	CH_2P	14.5[d]	23.6[d]	15.3[d]	23.0[d]	15.9[d]	24.0[d]
	$CH_3CH_2CH_2$		27.0		27.2		27.6
	CH_2CH_2P		24.6[e]		24.8[e]		25.0[e]
	i-C_6H_5	133.7[g]	134.1[g]				
	o-C_6H_5	139.4[h]	139.7[h]				
	m-C_6H_5	127.9	128.1				
	p-C_6H_5	123.4	123.6				
	C_5H_4			78.9[i]	78.1[i]	79.4[i]	79.5[i]
				75.3	75.7	75.5	76.1
				67.6	68.3	67.5	67.9
	C_5H_5			70.4	70.4	70.2	70.5

[a] $^{3}J(^{1}H\text{-}^{1}H)$ = 7.6 Hz (**21a, 22a, 23a**), $^{3}J(^{31}P\text{-}^{1}H)$ = 16.0 Hz (**21a**, **22a**), 16.4 Hz (**23a**); [b] $^{3}J(^{1}H\text{-}^{1}H)$ = 7.2 Hz (**21b, 23b**), 7.6 Hz (**22b**); [c] $^{3}J(^{195}Pt\text{-}^{13}C)$ = 19 Hz (**21a**), 21 Hz (**22a**); [d] virtual triplet, avg. $J(^{31}P\text{-}^{13}C)$ = 18 Hz (**21a**), 17 Hz (**21b, 22a, 22b**), 14 Hz (**23a**), 13 Hz (**23b**); [e] virtual triplet, avg. $J(^{31}P\text{-}^{13}C)$ = 7 Hz; [g] $^{2}J(^{195}Pt\text{-}^{13}C)$ = 38 Hz (**21a**), 37 Hz (**21b**); [h] $^{3}J(^{195}Pt\text{-}^{13}C)$ = 26 Hz (**21a**), not resolved (**21b**); [i] $^{3}J(^{31}P\text{-}^{13}C)$ = not resolved (**22a**), 2 Hz (**22b**, **23a**), 3 Hz (**23b**).

Table 5.2: ^{31}P and ^{77}Se NMR spectroscopic data for **21a,b**, **22a,b** and **23a,b** in d_6-benzene solution

	Compound	**21a**	**21b**	**22a**	**22b**	**23a**	**23b**
^{31}P:	δ/ppm	19.7	12.6	19.4	11.7	22.4	14.5
	$^{1}J(^{195}Pt\text{-}^{31}P)$/Hz	2479	2469	2610	2605	-	-
^{77}Se:	δ/ppm	78	82	-47	-38	-20	-12
	$^{1}J(^{195}Pt\text{-}^{77}Se)$/Hz	106	98	225	235	-	-
	$^{2}J(^{77}Se\text{-}^{31}P)$/Hz	7	6	11	12	6	8

The NMR spectroscopic data are in accord with the proposed structures, based on the assumption that there is rapid interconversion of the *syn-* and *anti-* isomers (via pyramidal inversion at the selenium atom or rotation of the metal-selenium bond); this is usual for monodentate selenolates.[44] The chemically and magnetically equivalent environments of the two phosphorus nuclei in each compound give rise to a triplet in the ^{77}Se NMR spectra (as an example figure 5.4 shows the ^{77}Se NMR spectrum of **22b**); the satellite structure due to ^{77}Se-^{195}Pt coupling is of course not present in **23a,b**. The ^{77}Se NMR chemical shift and the ^{77}Se-^{195}Pt and ^{77}Se-^{31}P coupling constants are predominantly determined by the nature of the selenium substituent; the ^{77}Se NMR chemical shifts of **22a,b** and **23a,b** are at much higher field than **21a,b** indicating that the ferrocenyl substituents contribute more electron density to the selenium than phenyl groups do. The ^{77}Se-^{195}Pt and ^{77}Se-^{31}P coupling constants for **22a,b** are approximately two times greater than those of **21a,b**, which may be a direct result of this greater electron density provided by the ferrocenyl groups. The nature of the phosphine substituent has less of an effect, but it is clear that the PBu_3 substituted compounds have higher ^{77}Se NMR chemical shifts than their PEt_3 substituted analogues; this trend is reversed in the ^{31}P NMR spectra of these compounds.

The ^{13}C and ^{1}H NMR are as expected; in the ^{13}C NMR spectra there is a slight increase in the chemical shifts of the phosphine carbon atoms of **22a,b** and **23a,b** compared to **21a,b** attributed to the presence of ferrocenyl selenolate ligands instead of phenyl selenolate ligands.

Compounds **21a,b**, **22a,b**, and **23a,b** have also been characterised by FAB mass spectrometry, UV-visible and infrared spectroscopies; these data are shown in tables 5.3 and 5.4.

Figure 5.4: ^{77}Se NMR spectrum of **22b**

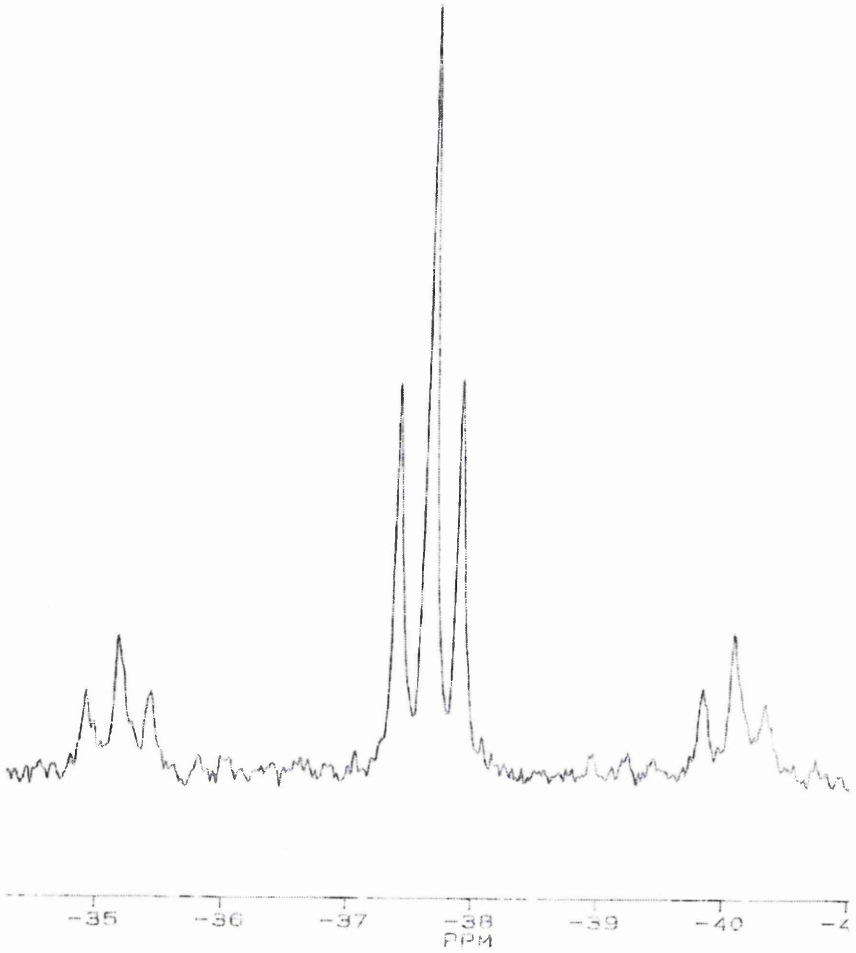

The mass spectra of all the complexes show a molecular ion peak, although in most cases it is weak and peaks corresponding to the loss of selenolate ligands are more intense. It is notable that compounds **21a**, **22a** and **23a** only showed ion peaks corresponding to the loss of one selenolate ligand, whereas compounds **21b**, **22b** and **23b** show peaks corresponding to the loss of one and two selenolate ligands; this indicates that the selenolate ligands may be more tightly bound in the compounds with PEt_3 ligands.

The differing colours of the phenylselenolate (**21a,b**) and ferrocenylselenolate (**22a,b**, **23a,b**) complexes are explained by the UV-visible spectra. The ferrocenylselenolate ligands of **22a,b** and **23a,b** give rise to absorptions in the visible region at approximately 465 nm, explaining the orange-red colour of these compounds. These absorption bands are absent in the spectra of **21a,b**, which are yellow in colour, presumably due to the absorption at 350 nm tailing off into the visible region. The UV-visible spectra of **22a,b** and **23a,b** are similar and thus so

are the colours of these compounds; this is in contrast to what has been observed in the case of neutral ferrocenyl selenide ligands.[243] Investigation of the related complexes [MCl(ECHR'CHR'NMe_2)(PR_3)] (M = Pd or Pt; E = S, Se or Te; R' = H or Me; R_3 = Me_2Ph, *etc.*) has shown their highest wavelength absorption bands to be ligand (E) to ligand (PR_3) charge transfer based; this is not the case with **21a,b** , **22a,b** and **23a,b**.

Table 5.3: Mass and UV-visible spectral data for compounds **21a,b**, **22a,b** and **23a,b**

		21a	**21b**	**22a**	**22b**	**23a**	**23b**
Mass Spectrum[a]	$[M]^+$	745 (30)	913 (15)	961 (10)	1129 (10)	872 (3)	1040 (3)
	[M-SeR']	588 (100)	756 (40)	696 (20)	864 (60)	607 (25)	775 (40)
	$[Pt(PR_3)_2]^+$		599 (100)		599 (100)		510 (45)
UV-Vis[b]		215 (60,000)		215 (54,000)		215 (41,200)	215 (35,000)
		225 (42,500)	230 (47,000)	225 (49,000)	225 (41,500)	220 (33,700)	225 (23,600)
		250 (38,000)	250 (34,000)	255 (45,000)	255 (34,700)	250 (26,000)	250 (27,600)
		295 (32,500)	295 (31,200)	310sh (19,600)	315sh (15,900)	335 (18,500)	335 (60,000)
		350sh (4,400)	345sh (5,800)			395sh (5,000)	400sh (12,300)
				465sh (2,120)	460sh (2650)	470sh (2,300)	470 (8,700)

[a] *m/z* (%); recorded using FAB; figures are for isotopomers containing ^{195}Pt or ^{106}Pd, ^{80}Se, ^{56}Fe, ^{12}C, ^{1}H; expected isotope patterns were observed.
[b] λ_{max} (nm); ε (cm^{-1} M^{-1}) in parentheses; recorded in DCM solution (2 x 10^{-5} M); sh = shoulder.

Table 5.4: Infrared spectral data for compounds **21a,b**, **22a,b** and **23a,b**

	21a	**21b**	**22a**	**22b**	**23a**	**23b**
Infrared[a]	2960 (w)	2951 (s)	2957 (w)	2951 (w)	2957 (m)	2954 (m)
(cm^{-1})	2926 (w)	2925 (s)	2933 (m)	2930 (m)	2930 (m)	2925 (m)
	2870(w)	2868 (m)	2870 (m)	2850 (m)	2870 (w)	2861 (m)
	1571 (s)	1573 (s)		1689 (m)		
	1467 (w)	1465 (s)	1446 (m)	1458 (m)	1447 (m)	1462 (m)
	1448 (m)	1454 (w)	1403 (m)	1407 (w)	1404 (m)	1406 (m)
	1413 (m)	1403 (w)	1376 (m)		1377 (m)	1376 (w)
	1374 (m)	1375 (w)	1361 (w)	1356 (w)	1342 (w)	1358 (w)
		1357 (w)	1256 (m)	1295 (w)	1254 (w)	1261 (w)
	1255 (w)	1263 (w)	1234 (vw)	1230 (vw)	1233 (w)	1226 (w)
	1238 (w)	1227 (vw)	1138 (w)	1139 (w)	1138 (m)	1140 (m)
	1152 (vw)	1091 (m)	1102 (m)	1091 (w)	1102 (s)	1102 (m)
	1066 (s)	1068 (m)	1057 (w)			1090 (m)
	1031 (s)	1046 (m)	1033 (s)	1046 (vw)	1032 (vs)	1047 (w)
	1019 (s)	1021 (m)	1016 (s)		1017 (s)	1014 (m)
	1002 (w)	1000 (w)	1002 (s)	999 (w)	1003 (s)	998 (m)
	894 (w)	899 (s)	885 (w)	898 (w)		903 (w)
		889 (m)	872 (m)	871 (m)	873 (vs)	874 (m)
		790 (m)	807 (s)	803 (s)	808 (vs)	808 (s)
	760 (vs)	771 (m)	764 (s)	781 (s)	766 (vs)	789 (m)
	734 (vs)	731 (vs)			730 (vs)	
	720 (vs)	719 (s)	723 (s)	716 (s)		722 (m)
	691 (vs)	690 (s)				
	666 (s)	667 (m)	665 (vw)	657 (s)	666 (vs)	657 (vw)
	628 (m)	616(w)	636 (w)		634 (w)	

[a] Selected bands only.

5.2 The Reactions of $(PhTe)_2$ and $(FcTe)_2$ with $[Pt(C_2H_4)(PR_3)_2]$ and with $[Pd_2(dba)_3]$.dba/PR_3 (R = Et, Bu)

Since the syntheses of **21a,b** , **22a,b** and **23a,b** were relatively straightforward, the analogous tellurium chemistry was investigated. The reactions of $[Pt(C_2H_4)(PR_3)_2]$ (R = Et, Bu) with $(R'Te)_2$ (R' = Ph, Fc) in dioxane/THF overnight at room temperature, followed by column chromatography led to the isolation of yellow (R = Ph) or orange (R = Fc) solids believed to contain $[Pt(TeR')_2(PR_3)_2]$ (Figure 5.5).

Figure 5.5:

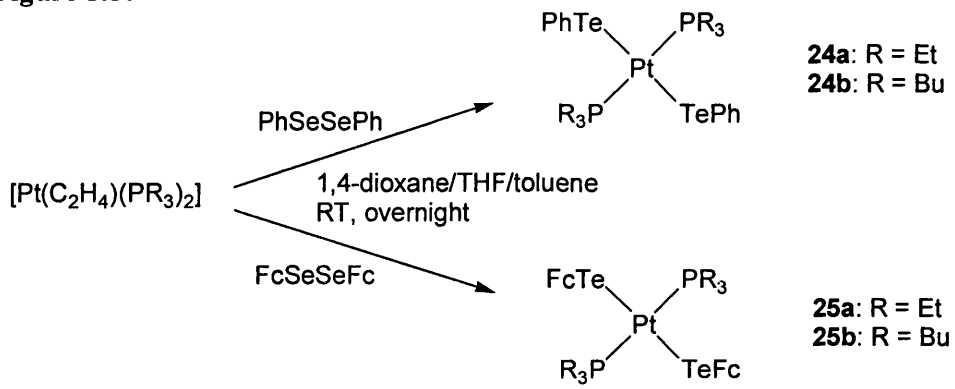

Unfortunately only **25b** was isolated in sufficient purity for a multinuclear NMR spectroscopic and mass spectral analysis; compounds **24a** and **25a** decompose rapidly upon isolation even when stored under an inert atmosphere indicating that *bis*(triethylphosphine)platinum tellurolate complexes are not stable. The NMR spectra of compound **24b** indicated that there were many species present; the mass spectra showed a number of high mass peaks indicating that some or all of these species may be of high nuclearity. The NMR spectral and mass spectrometric data for **25b** are shown in table 5.5.

The data are in accord with the proposed structure for **25b**; again there is no spectral evidence for the *cis*- isomer. The data correlate well with those of **22b**, although in **25b** the ^{13}C NMR chemical shifts are approximately 2 ppm greater than in **22b**. The ^{125}Te NMR spectrum shows a triplet with ^{195}Pt satellites, as was observed in the ^{77}Se NMR spectrum of **22b**. As expected the ^{125}Te-^{195}Pt and ^{125}Te-^{31}P coupling constants are much larger than the ^{77}Se-^{195}Pt and ^{77}Se-^{31}P coupling constants for **22b**; this is an effect of the difference in the gyromagnetic ratios of ^{77}Se and ^{125}Te (5.115 and –8.497 10^7 rad. T^{-1} s^{-1} respectively).[76]

Table 5.5: ^{1}H, ^{13}C, ^{31}P, ^{125}Te NMR spectroscopic and mass spectral data for **25b** in d_6-benzene solution

NMR spectra:

$\delta(^{1}H)$	CH_3	0.97 (18H, t)[a]
	CH_2P	1.95-2.22 (12H, m)
	$CH_3CH_2CH_2$	1.35-1.69 (12H, m)
	CH_2CH_2P	1.35-1.69 (12H, m)
	C_5H_4	3.97-4.08 (4H, m)
		4.50-4.63 (4H, m)
	C_5H_5	4.17-4.30 (10H, m)
$\delta(^{13}C)$	CH_3	14.9
	CH_2P	27.2[b]
	$CH_3CH_2CH_2$	28.4
	CH_2CH_2P	25.3[c]
	C_5H_4	80.4[d]
		Not observed
		70.3
	C_5H_5	71.1
$\delta(^{31}P)$		6.2[e]
$\delta(^{125}Te)$		-10[f]

Mass spectrum[g]

$[M]^+$	1223 (5)
$[M\text{-}Fc]^+$	1038 (25)
$[M\text{-}TeFc]^+$	911 (100)
$[Pt(PBu_3)_2]^+$	599 (55)

[a] $^{3}J(^{1}H\text{-}^{1}H)$ = 7.2 Hz; [b] virtual triplet, avg. $J(^{31}P\text{-}^{13}C)$ = 17 Hz; [c] virtual triplet, avg. $J(^{31}P\text{-}^{13}C)$ = 7 Hz; [d] $^{3}J(^{31}P\text{-}^{13}C)$ = not resolved; [e] $^{1}J(^{31}P\text{-}^{195}Pt)$ = 2556 Hz; [f] $^{1}J(^{125}Te\text{-}^{195}Pt)$ = 1283 Hz, $^{1}J(^{125}Te\text{-}^{31}P)$ = 30 Hz; [g] *m/z* (%); recorded using FAB; figures are for isotopomers containing ^{195}Pt, ^{128}Te, ^{56}Fe, ^{31}P, ^{12}C, ^{1}H; expected isotope patterns were observed.

The mass spectral data shows a weak $[M]^+$ peak with strong $[M\text{-}TeFc]^+$ and $[Pt(PBu_3)_2]^+$ peaks; this suggests that the Pt-Te bonds are quite weak and may go some way to explaining why only **25b** has been successfully isolated.

The reactions of a $[Pd_2(dba)_3]$.dba/PR_3 mixture with $(R'Te)_2$ in toluene at room temperature overnight, followed by chromatography or precipitation from hexane, gave dark coloured solids for which the spectral data were poor, and no products could be identified. It is apparent that the reactions of diaryl ditellurides with low-

valent platinum and palladium phosphine complexes are quite different from those of diaryl diselenides. The differences could be attributed to an instability of complexes of the type $[M(TeR')_2(PR_3)_2]$ (which is probably the case for **24a,b** and **25a**), or it may be that the reaction is following different paths, giving rise to different products. It has been reported in a study of the reactions of $(PhE)_2$ (E = Se, Te) with $[Pd(PPh_3)_4]$ in dichloromethane, that where E = Se, the product is $[Pd_2(\mu_2\text{-}SePh)_2(SePh)_2(PPh_3)_2]$, and where E = Te a mixture of products is given, including the polynuclear compound $[Pd_6Cl_2Te_4(TePh)_2(PPh_3)_6]$.[236] It may be that a similar situation exists here.

5.3 The Reactions of $(FcSe)_2$ and $(FcTe)_2$ with $[Pt(PPh_3)_4]$

The reactions of $(FcE)_2$ (E = Se, Te) with $[Pt(PPh_3)_4]$ had not been previously explored and so these reactions were investigated. Stirring $[Pt(PPh_3)_4]$ with $(FcE)_2$ in toluene at room temperature overnight followed by filtration led to the isolation of a yellow (E = Se) or red (E= Te) solid. These solids were very insoluble in organic solvents and water, which prevented their analysis by NMR spectroscopy, but it was possible to obtain mass spectral data for them. These data confirmed the structure of the product where E = Se to be *trans*-$[Pt(SeFc)_2(PPh_3)_2]$ (**26**, figure 5.6), but the mass spectral data where E = Te showed several high mass peaks, none of which could be assigned. This suggests that (as was observed previously) the tellurium reactions proceed via a different path and these were not pursued.

Figure 5.6:

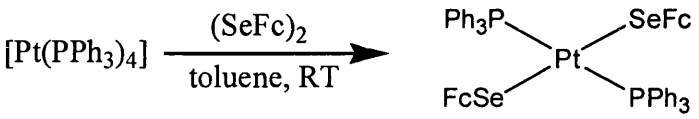

26

Table 5.6 shows the mass spectral data for **26**.

Table 5.6: Mass spectral data for **26**

$[M]^+$	1249 (50)
$[M\text{-}PPh_3]^+$	987 (100)
$[Pt(PPh_3)_2]^+$	719 (80)

[a] *m/z* (%); recorded using FAB; figures are for isotopomers containing ^{195}Pt, ^{80}Se, ^{56}Fe, ^{31}P ^{12}C, ^{1}H; expected isotope patterns were observed.

The structure of **26** has also been indirectly proven by derivatisation: stirring **26** with an excess of PBu_3 in toluene for 3 days gave an orange solution. Concentration of this solution and analysis by ^{31}P NMR spectroscopy showed two peaks, one due to $OPBu_3$ and one at δ = 11.7 ppm ($^1J(^{31}P\text{-}^{195}Pt)$ = 2606 Hz) which can be attributed to **22b**, showing that phosphine exchange has occurred and that the structure assigned to **26** is correct.

5.4 The Reactions of *bis*-Benzo-1,2-diselenin with $[Pt(C_2H_4)(PR_3)_2]$ and with $[Pd_2(dba)_3]$.dba/PR_3 (R = Et, Bu)

The syntheses of compounds **21a,b**, **22a,b** and **23a,b** showed the oxidative addition of Se-Se bonds to zerovalent platinum and palladium phosphine complexes to be a viable synthetic method; the investigation was therefore extended to the reactions of *bis*-benzo-1,2-diselenin (figure 5.7).

Figure 5.7:

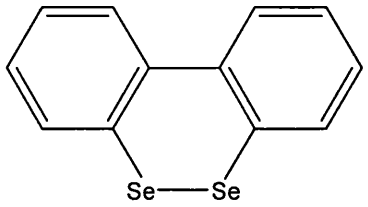

The reactions of low-valent transition metal complexes with some cyclic compounds containing Se-Se bonds were discussed in the introduction. There are (to our knowledge) no reports of the reactions of low-valent transition metal complexes with 1,2-diselenins; there is however a report of the reaction of diacenaphtho[1,2-c:1',2'-e]-1,2-dithiin with $[Pt(COD)_2]$, which gives $[Pt(S_2C_{24}H_{12})(COD)]$ via oxidative addition of the S-S bond to the zerovalent platinum centre.[132]

5.4.1 The Syntheses of $[Pt(Se_2C_{12}H_8)(PR_3)_2]$ and $[Pd(Se_2C_{12}H_8)(PR_3)_2]$

The reaction of $[Pt(C_2H_4)(PR_3)_2]$ (R = Et, Bu) with *bis*-benzo-1,2-diselenin in a dioxane/THF/toluene mixture at room temperature overnight, followed by column chromatography led to the isolation of **27a** (yellow solid) and **27b** (orange solid) as shown in figure 5.8.

Figure 5.8:

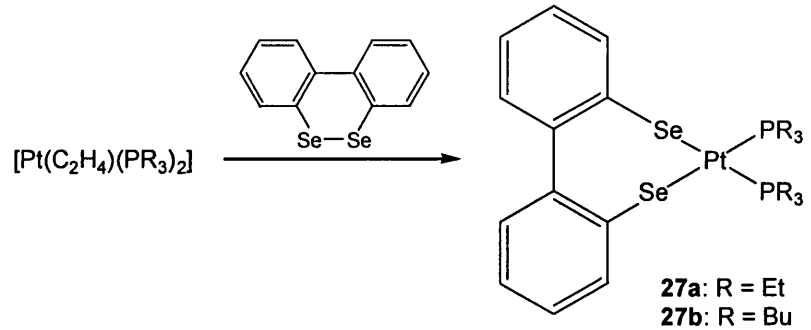

Similarly, stirring a mixture of $[Pd_2(dba)_3]$.dba and excess PR_3 in toluene followed by treatment with *bis*-benzo-1,2-diselenin at room temperature overnight, then addition

of hexane and filtration, led to the isolation of **28a** and **28b** both of which are red solids (figure 5.9).

Figure 5.9:

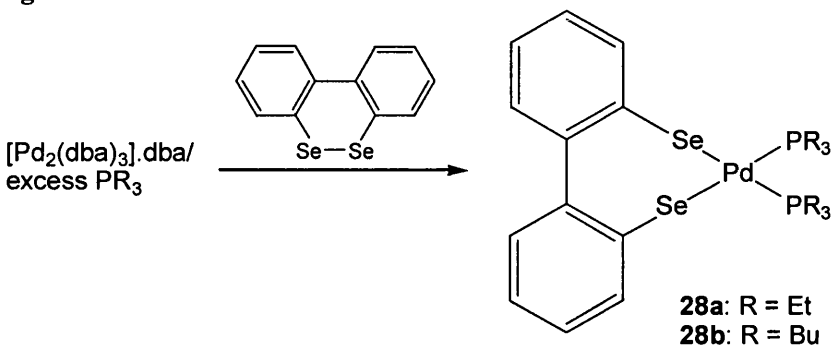

Crystals of **27a,b** and **28a** suitable for an x-ray diffraction study were obtained by recrystallisation from hexane/toluene at –20 °C. The structure of **27a** was established whilst at the University of Florence and so is discussed in detail in chapter 6. Diffraction data were collected on an Oxford Diffraction Excalibur 3 CCD diffractometer with Mo-Kα radiation (λ = 0.71069 Å); structure solution was by SIR 97[225] with refinement by SHELXL 97.[223]

The structures of **27b** and **28a** are shown in figures 5.10 and 5.11; thermal ellipsoids are drawn at 30% probability and hydrogens are omitted for clarity. Crystal data and selected bond lengths and angles (with **27a**) are shown in tables 5.7 and 5.8.

Figure 5.10: Crystal structure of **27b**

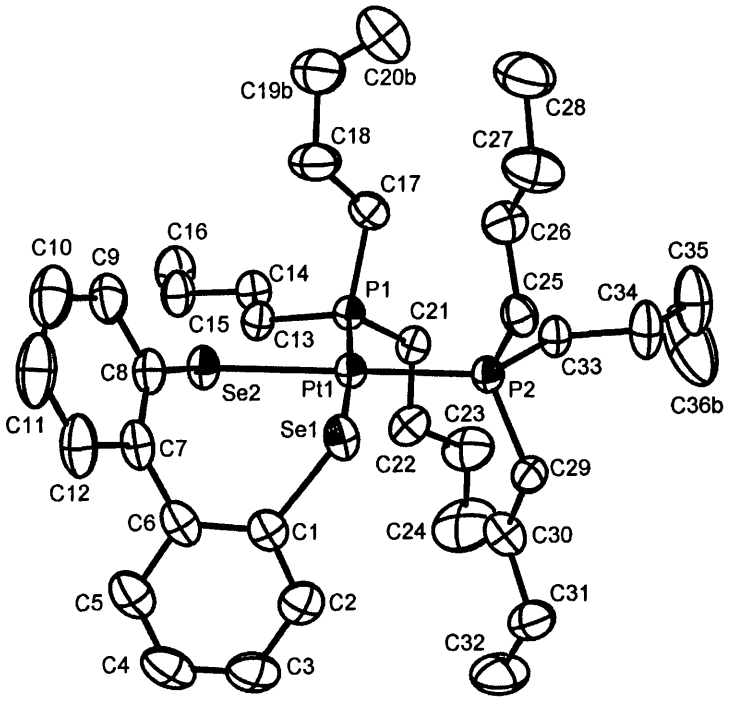

Figure 5.11: Crystal structure of **28a**

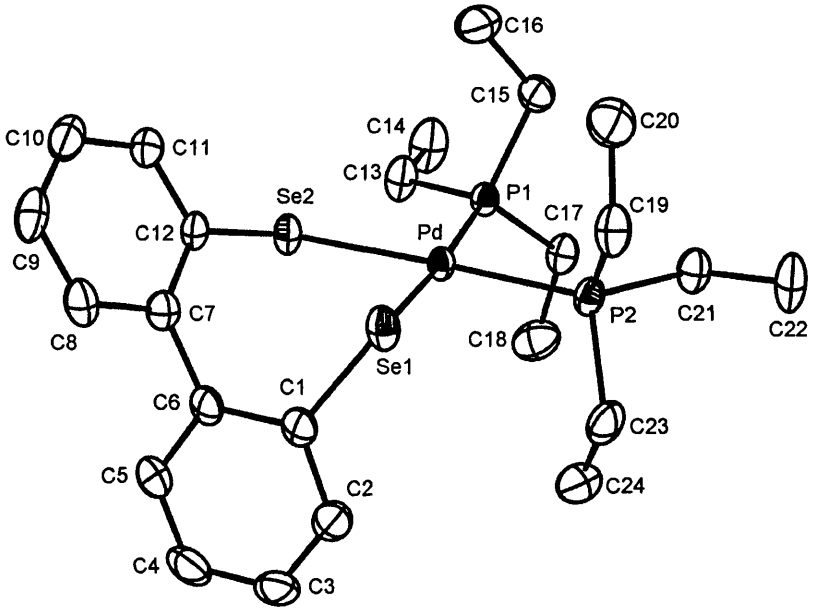

Table 5.7: Crystallographic data for compounds **27a,b** and **28a**

Compound	**27a**	**27b**	**28a**
Empirical formula	$C_{24}H_{38}P_2Se_2Pt.C_{3.5}H_4$	$C_{36}H_{62}P_2Se_2Pt$	$C_{24}H_{38}P_2Se_2Pd.C_{3.5}H_4$
Formula weight	787.6	909.5	698.9
Crystal system	triclinic	triclinic	triclinic
Space group	P -1	P -1	P -1
Crystal size (mm)	0.40 x 0.30 x 0.25	0.40 x 0.30 x 0.25	0.40 x 0.30 x 0.30
a/Å	9.794(1)	13.237(1)	9.861(1)
b/Å	11.457(1)	15.209(1)	11.460(1)
c/Å	14.197(2)	20.486(1)	14.226(1)
α/°	80.67(1)	103.07(1)	81.09(1)
β/°	69.16(1)	95.92(1)	68.71(1)
γ/°	88.15(1)	91.16(1)	86.25(1)
V/Å	1469.0(3)	3992.0(4)	1489.8(3)
Z	2	2	2
F(000)	766	1816	702
D_{calc} (g cm^{-3})	1.78	1.514	1.568
μ (Mo-K_α/mm^{-1})	7.37	5.440	3.21
Temperature (K)	293	293	293
Reflections collected	5890	36044	14310
Independent reflections	4719	14813	5767
θ Range (°)	4.13-26.37	3.81-25.68	4.13-26.37
Reflect. with $I > 2\sigma(I)$	4423	9281	3919
No. of parameters	310	807	320
R_1; wR_2 [$I > 2\sigma(I)$]	0.0293; 0.0577	0.0268; 0.0469	0.0268; 0.0548
R_1; wR_2 (all data)	0.0415; 0.0613	0.0612; 0.0502	0.0519; 0.0586
GoF	0.941	0.846	0.904

Table 5.8: Selected bond lengths and angles for compounds **27a,b** and **28a**

Compound	**27a**	**27b**	**28a**
Bond lengths (Å)			
M-Se(1)	2.4873(6)	2.4767(5)	2.4807(5)
M-Se(2)	2.4613(6)	2.4631(5)	2.4531(5)
M-P(1)	2.302(1)	2.291(1)	2.3291(8)
M-P(2)	2.300(1)	2.289(1)	2.3277(8)
Se(1)-C(1)	1.926(5)	1.936(4)	1.9268(31)
Se(2)-C(8)	1.926(4)	1.929(4)	
Se(2)-C(12)			1.9263(28)
Bond angles (°)			
Se(1)-M-Se(2)	89.94(2)	88.00(2)	90.34(2)
Se(2)-M-P(1)	87.57(3)	87.78(3)	87.01(2)
P(1)-M-P(2)	98.29(4)	99.91(4)	98.52(3)
P(2)-M-Se(1)	84.15(3)	84.29(3)	84.03(2)
Se(1)-M-P(1)	175.25(3)	175.76(3)	175.13(2)
Se(2)-M-P(2)	174.07(3)	171.54(3)	174.28(2)
M-Se(1)-C(1)	100.41(14)	101.54(10)	100.28(9)
M-Se(2)-C(8)	113.19(13)	112.56(11)	113.44(8)
Dihedral angles (°)			
Between phenyl rings			
C1-C6 and C7-C12	64.18(13)	53.90(13)	64.65(8)
Between MSe_2P_2 plane and			
phenyl ring C1-C6	79.04(11)	77.09(10)	79.28(8)
phenyl ring C7-C12	58.06(10)	62.95(12)	57.96(7)

The crystal structure of compound **27b** does not contain a toluene solvate molecule like those of **27a** and **28a**; it does, however, share the same space group (P -1). There are two molecules in the asymmetric unit; the data reported are for the molecule shown in figure 3.10. The compound contains a square-planar $PtSe_2P_2$ core with a *cis-* geometry imposed by the chelating diselenolate ligand; the butyl and biphenyl groups protrude significantly from this plane. The square plane is slightly asymmetric with one Pt-Se bond approximately 0.01 Å longer than the other (the deviation is larger in **27a**, where a difference of approximately 0.02 Å is observed) and the P-Pt-Se angles differing by 3°. A similar distortion has been observed in platinum diselenolenes (chapter 2) and dithiolenes.[169] The Pt-P and Pt-Se bond lengths are very similar to those found in *cis*-$[Pt(SePh)_2(PPh_3)_2]$,[241] but the Se-Pt-Se angle is significantly smaller (88.00° *vs* 95.10°), probably as a result of the constraint imposed by the $Se_2C_{12}H_8$ ligand; interestingly the angle is also significantly smaller than the S-Pt-S angle of $[Pt(S_2C_{24}H_{12})(COD)]$ (94.02°).[132] The dihedral angle of the biphenyl group (53.9°) lies between the values found for $[Pt(S_2C_{24}H_{12})(COD)]$ (45.6°) and **27a** (64.2°). The Pt-Se and Pt-P bond lengths of **27b** are slightly shorter than those of **27a**; this could be the influence of PBu_3 compared to PEt_3, with PBu_3 perhaps contributing more electron density to the Pt centre, or the disorder which was found in the butyl chains affecting the bond lengths and angles.

Compound **28a** has a structure isomorphous to that of **27a**; it similarly contains a $PdSe_2P_2$ square-planar core with a *cis-* geometry enforced by the $Se_2C_{12}H_8$ ligand. The ethyl and biphenyl groups protrude from the plane; the dihedral angle of the biphenyl group is very similar to that of **27a** and much greater than that found in $[Pt(S_2C_{24}H_{12})(COD)]$ (45.6°). Like **27a,b** the square plane is slightly asymmetric, with the Pd-Se bonds and P-Pd-Se angles differing by 0.03 Å and 3° respectively. Similar distortions have been observed in the crystal structures of palladium diselenolenes.[127] The Pd-Se bond lengths are similar to those found in $[Pd(SePh)_2(dppe)]$,[244] although the Pd-P bond lengths are approximately 0.05 Å longer (avg. 2.328 Å *vs* avg. 2.279 Å) and the Se-Pd-Se angle is significantly smaller (90.3° *vs* 99.1°). The angle is however almost identical to the Se-Pt-Se angle of **27a** and similar to that of **27b**, showing it to be constrained by the $Se_2C_{12}H_8$ ligand. The bond lengths and angles of **28a** are almost identical to those of **27a**; this can be attributed to the isomorphous structures of these compounds. The M-P bond lengths are approximately 0.02 Å longer in **28a**, due to the (slightly) smaller atomic radius of

Pt compared to Pd. Compounds **27a,b** and **28a,b** can be considered vinylogues of diselenolenes, but **27a,b** and **28a,b** do not exhibit an analogous electron delocalisation in the $PtSe_2C_4$ ring as evidenced by the distortion of the ring. In order for there to be significant electron delocalisation the ring would have to lie in the same plane as both the benzene rings of the biphenyl group and this is obviously not favoured.

The multinuclear NMR spectroscopic data for **27a,b** and **28a,b** are shown in tables 5.9 and 5.10.

The data are in accord with the proposed structures. The ^{77}Se nucleus is the X part of an AA'X system (due to the inequivalent magnetic environments of the phosphorus nuclei), and the spectrum should consist of five lines; these are observed for **27a,b** and the ^{77}Se NMR spectrum of **27a** is shown in figure 5.12 as an example. For **27a,b** the ^{77}Se-$^{31}P_{cis}$ coupling constants have been calculated to be 11 Hz (**27a**) and 27 Hz (**27b**), and the ^{77}Se-$^{31}P_{trans}$ coupling constants have been calculated to be 90 Hz (**27a**) and 104 Hz (**27b**). These *cis*- coupling constants are similar in magnitude to those found for platinum diselenolenes (chapter 2) and $[Pt(SeC_4H_4)(PBu_3)_2]$ (chapter 4), but the *trans*- coupling constants are greater (for example the ^{77}Se-$^{31}P_{trans}$ coupling constants for $[Pt(Se_2C_7H_{10})(PEt_3)_2]$ and $[Pt(SeC_4H_4)(PBu_3)_2]$ are 67 Hz and 70 Hz respectively); the complex $[Pt\{Fe(\eta^5\text{-}C_5H_4Se)_2\}(PBu_3)_2]$ is reported to have a ^{77}Se-$^{31}P_{trans}$ coupling constant of 84 Hz.[176] These values indicate that the ^{77}Se-$^{31}P_{trans}$ coupling constants may be dependent on the size of the Se-Pt heterocycle with increased ring size leading to increased values of ^{77}Se-$^{31}P_{trans.}$. Although $[Pt\{Fe(\eta^5\text{-}C_5H_4Se)_2\}(PBu_3)_2]$ can be formally considered to contain an 8-membered heterocyclic ring, the presence of the ferrocenyl backbone alters the geometry enough to make the ^{77}Se-$^{31}P_{trans}$ coupling constant lower than those of **27a,b**. The lack of electron delocalisation around the $PtSe_2C_4$ ring in these compounds is further evidenced by the ^{77}Se NMR chemical shifts of **27a,b** and **28a,b** which are approximately 200 ppm less than the ^{77}Se NMR chemical shifts of platinum diselenolenes (chapter 2) and palladium diselenolenes.[120,127]

Table 5.9: ^{1}H and ^{13}C NMR spectroscopic data for **27a,b** and **28a,b** in $CDCl_3$ (**27a**), d_6-benzene (**27b**) or d_6-acetone (**28a,b**) solution

		27a	**27b**	**28a**	**28b**
$\delta(^{1}H)$	CH_3	1.10 (18H, dt)[a]	0.87 (18H, t)[b]	1.04 (18H, dt)[a]	0.93 (18H, t)[b]
	CH_2P	1.89-2.18 (12H, m)	1.23-1.37 (12H, m)	1.69-1.90 (12H, m)	1.35-1.66 (12H, m)
	$CH_3CH_2CH_2$		1.37-1.58 (12H, m)		1.35-1.66 (12H, m)
	CH_2CH_2P		1.79-2.08 (12H, m)		1.90-2.11 (12H, m)
	$C_{12}H_8$	6.95-7.01 (2H, m)	6.95-7.06 (2H, m)	6.65-6.73 (2H, m)	6.89-6.94 (2H, m)
		7.13-7.18 (2H, m)	7.10-7.21 (2H, m)	6.75-6.84 (2H, m)	7.00-7.05 (2H, m)
		7.18-7.23 (2H, m)	7.25-7.34 (2H, m)	6.89-7.03 (2H,m)	7.15-7.21 (2H,m)
		7.66-7.71 (2H, m)	8.10-8.20 (2H, m)	7.40-7.48 (2H, m)	7.65-7.69 (2H, m)
$\delta(^{13}C)$	CH_3	9.2[c]	14.4	8.7	13.9
	CH_2P	17.4[d]	25.4[d]	17.1[d]	24.9[d]
	$CH_3CH_2CH_2$		27.4		27.3
	CH_2CH_2P		24.9[e]		24.8[e]
	$C_{12}H_8$:				
	C(6)	151.4	152.3	151.7	151.7
	C(2)	137.4[f]	137.9[f]	137.6	135.8
	C(1)	135.4[g]	136.3[g]	138.2	137.6
	C(3,4,5)	128.9	129.5	128.3	128.4
		127.2	127.1	126.7	126.7
		126.4	126.3	126.0	125.9

[a] $^{3}J(^{1}H\text{-}^{1}H)$ = 7.6 Hz, $^{3}J(^{1}H\text{-}^{31}P)$ = 16.4 Hz; [b] $^{3}J(^{1}H\text{-}^{1}H)$ = 7.2 Hz (**27b**), 7.6 Hz (**28b**); [c] $^{3}J(^{13}C\text{-}^{195}Pt)$ = 23 Hz; [d] complex multiplet; [e] virtual triplet, avg. $J(^{13}C\text{-}^{31}P)$ = 7 Hz; [f] $^{3}J(^{13}C\text{-}^{195}Pt)$ = 13 Hz (**27a**), 16 Hz (**27b**); [g] $^{2}J(^{13}C\text{-}^{195}Pt)$ = 34 Hz (**27a**), 33 Hz (**27b**).

Table 5.10: ^{31}P and ^{77}Se NMR spectroscopic data for **27a,b** and **28a,b** in $CDCl_3$ (**27a**), d_6-benzene (**27b**) or d_6-acetone (**28a,b**) solution

	27a	**27b**	**28a**	**28b**
^{31}P: δ/ppm	7.0	12.4	12.4	3.8
$^{1}J(^{31}P\text{-}^{195}Pt)$/Hz	2885	2851	-	-
^{77}Se: δ/ppm	217	231	316	314
$^{1}J(^{77}Se\text{-}^{195}Pt)$/Hz	168	165	-	-
avg. $^{2}J(^{77}Se\text{-}^{31}P)$/Hz	49[a]	65[a]	39	25

[a] Analysis of AA'X system gives: $^{2}J(^{77}Se\text{-}^{31}P_{cis})$ = 11 (**27a**), 27 (**27b**) Hz ; $^{2}J(^{77}Se\text{-}^{31}P_{trans})$ = 90 (**27a**), 104 (**27b**) Hz; $^{2}J(^{31}P\text{-}^{31}P)$ = 35 (**27a**), 24 (**27b**) Hz.

Figure 5.12 : ^{77}Se NMR spectrum of **27a** (arrow shows ^{1}J (^{77}Se-^{195}Pt))

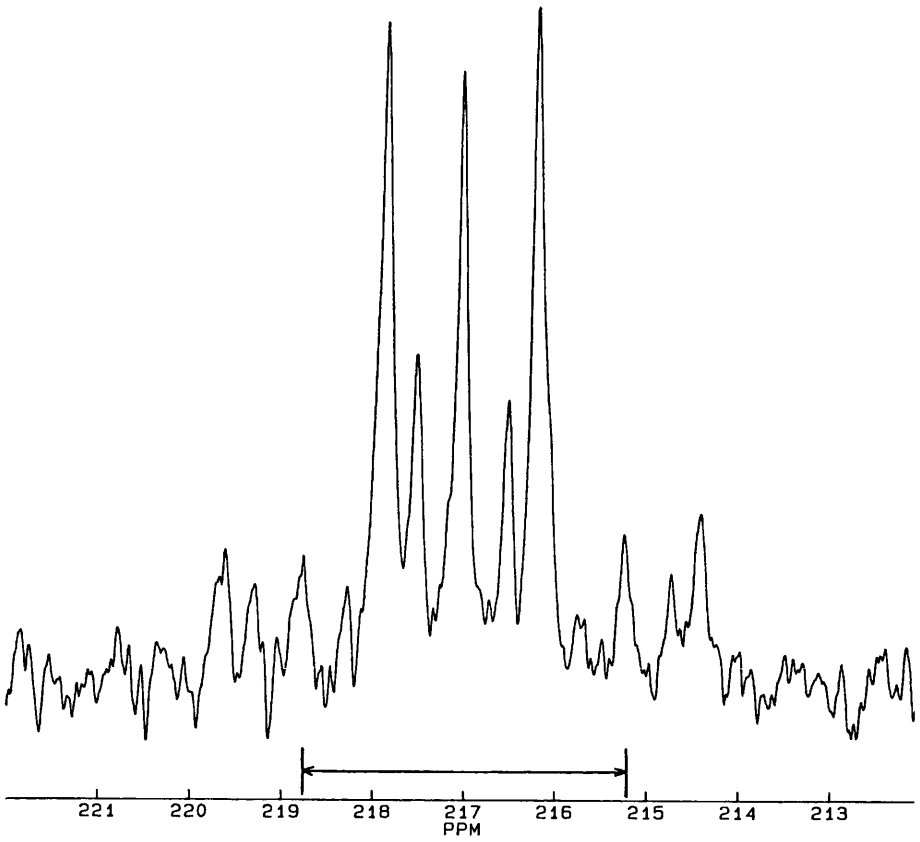

For the palladium complexes **28a,b** the weakest two lines in the ^{77}Se NMR spectrum were not observed and so only an average value of ^{2}J(^{77}Se-^{31}P) could be obtained. It has been observed that solutions of **28a** have limited stability and will decompose over several hours; the long acquisition time of ^{77}Se NMR spectra means that this decomposition becomes significant and is observed in these spectra. The decomposition process is discussed further in the next section.

The ^{31}P, ^{13}C and ^{1}H NMR spectra of **27a,b** and **28a,b** are in accord with the proposed structures. In the ^{13}C NMR spectra the signals for *C*H$_2$P are complex multiplets; they do not have the expected AA'X structure and peak overlap complicates their appearance. There are only six signals for the $Se_2C_{12}H_8$ ligand indicating that, in solution, the benzene groups are equivalent, probably through pyramidal inversion of the selenium atoms. It has been possible to assign the C(1), C(2) and C(6) atoms of the ligand (numbering based on figures 5.10 and 5.11). The C(1) and C(6) signals are of lower intensity with the relatively large ^{2}J(^{13}C-^{195}Pt) coupling constant for one of the signals facilitating differentiation of the CSe (C(1)) and quaternary (C(6)) carbons. The C(2) group is assigned based on the presence of a small ^{3}J(^{13}C-^{195}Pt) coupling and

an intensity comparable to the other CH signals. In the case of **28a,b** C(1) and C(2) were distinguished by running ^{13}C DEPT NMR spectra of these compounds. It is worthy of not that in **28a,b** the C(1) resonances are at lower field than the C(2) resonances, whereas the opposite is true for **27a,b**.

Compounds **27a,b** and **28a,b** have been further characterised by FAB mass spectrometry, infrared and UV-visible spectroscopy; these data are shown in table 5.11.

Table 5.11 Mass spectral, IR and UV-Vis data for compounds **27a,b** and **28a,b**

		27a	**27b**	**28a**	**28b**
Mass Spectrum[a]	$[M]^+$	743 (30)	911 (30)	654 (15)	822 (5)
	$[M - SeC_{12}H_8]^+$	511 (100)	679 (30)	422 (70)	590 (15)
	$[Pd/Pt(PR_3)_2]^+$		599 (100)	342 (100)	510 (45)
Infrared[b]		2963 (w)	2955 (s)	2963 (w)	2952 (m)
		2915 (w)	2929 (s)	2915 (w)	2916 (m)
			2870 (m)	2870 (w)	2850 (m)
		1444 (m)	1477 (m)	1443 (m)	1447 (m)
		1408 (m)	1416 (m)	1407 (m)	1407 (w)
		1377(w)	1377 (m)	1377 (w)	1295 (w)
		1244 (w)	1208 (w)	1240 (m)	1188 (m)
			1088 (m)		1091 (w)
		1031 (s)	1072 (m)	1030 (vs)	1046 (vw)
		978 (w)	1003 (m)	1001 (w)	999 (w)
			935 (w)	939 (vw)	913 (w)
			896 (m)		871 (m)
		768 (s)	781 (w)	767 (vs)	781 (s)
		751 (s)	743 (s)	750 (vs)	743 (s)
		717 (s)	721 (s)	711 (vs)	716 (s)
			654 (w)	627 (w)	657 (s)
UV-Vis[c]		240 (55,000)	240 (28,000)	230 (64,700)	225 (31,000)
				335 (25,000)	330 (21,000)

[a] *m/z* (%); recorded using FAB; figures are for isotopomers containing ^{106}Pd or ^{195}Pt, ^{80}Se, ^{56}Fe, ^{12}C, ^{1}H; expected isotope patterns were observed.
[b] selected bands only (cm^{-1}), [c] λ_{max} (nm); ε (cm^{-1} M^{-1}) in parentheses; recorded in CH_2Cl_2 solution (2×10^{-5} M).

The FAB mass spectra of **27a,b** and **28a,b** all show ions corresponding to the loss of a $SeC_{12}H_8$ fragment; this is similar to the behaviour of $[Pt(S_2C_{24}H_{12})(COD)]$ which decomposes upon heating to 80 °C for 3 hours to $SC_{24}H_{12}$ and [PtS(COD)] (figure 5.13).[132] A similar reaction was attempted with **27a**. A toluene solution of **27a** was heated to 80 °C overnight; subsequent analysis of the sample by ^{31}P NMR spectroscopy showed that no decomposition had taken place. This may be due to the phosphine groups having a greater stabilising effect than COD; indeed the $[MSe(PR_3)_2]^+$ peaks in the mass spectra are more intense for **27a** and **28a** than for **27b** and **28b**, suggesting that PBu_3 has a greater stabilising effect than PEt_3. If this is the case then the stability of these complexes is quite sensitive to the ancillary ligands.

Figure 5.13:

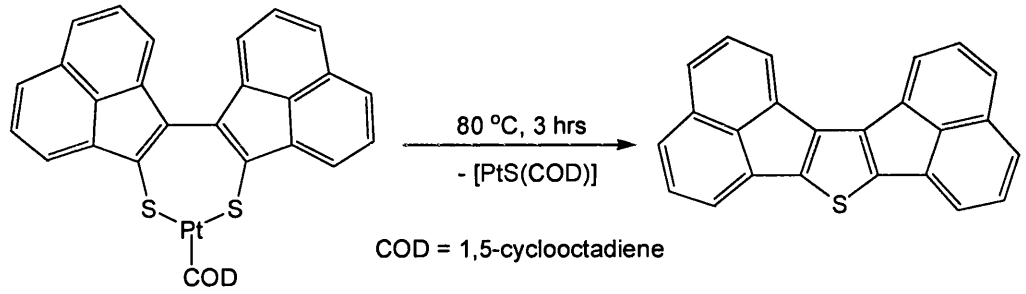

The UV-visible data explain the differences in colour of **27a,b** and **28a,b**. An absorption band at ~ 330 nm in **28a,b** tails off into the visible region and results in the red colour of these compounds; this band is absent in **27a,b** so these compounds are yellow/orange in colour. If this band is LMCT-based then it would be expected at a lower wavelength for the platinum complexes due to the greater difficulty in reducing platinum compared to palladium; a similar situation was encountered in the UV-visible spectra of platinum and palladium diselenolenes (chapter 2).

5.4.2 The Syntheses of $[Pd_2(Se_2C_{12}H_8)_2(PR_3)_2]$

The dinuclear compounds $[Pd_2(Se_2C_{12}H_8)_2(PR_3)_2]$ (R = Et, Bu) can be synthesised by a method analogous to that for **28a,b** if the Pd/PR_3 stoichiometric ratio used is 1:1. Stirring a mixture of $[Pd_2(dba)_3].dba$ and two equivalents of PR_3 in toluene followed by treatment with *bis*-benzo-1,2-diselenin at room temperature overnight, then addition of hexane and filtration, led to the isolation of **29a** and **29b** both of which are red solids (figure 5.14).

Figure 5.14:

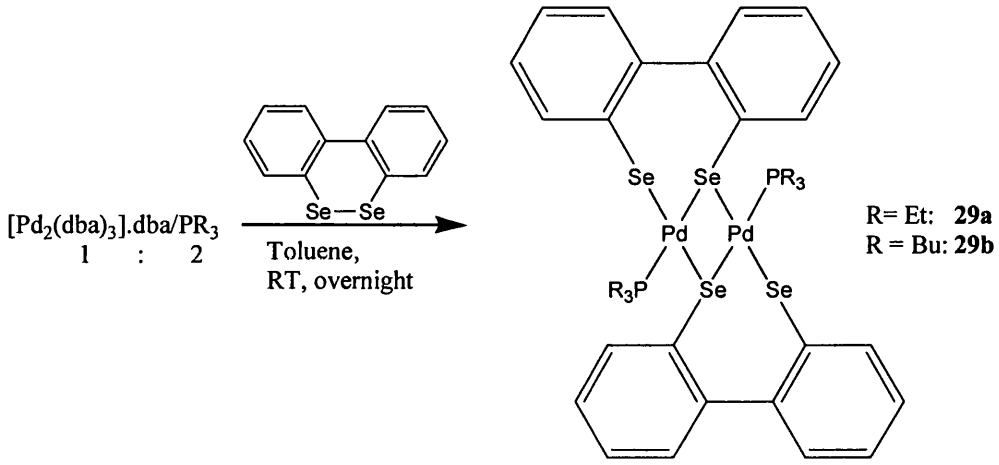

It has been found that **29a** will form from **28a** (in addition to some other unidentified decomposition products) in chloroform and acetone solutions that have been exposed to air (figure 5.15). The reaction may be driven by the formation of $OPEt_3$; it has been found that in the presence of excess PEt_3, under an inert atmosphere the conversion of **28a** to **29a** is suppressed. Upon prolonged stirring of **29b** with an excess of PBu_3 there was no formation of **28b**, however. This suggests that the condensation reaction is irreversible.

Figure 5.15:

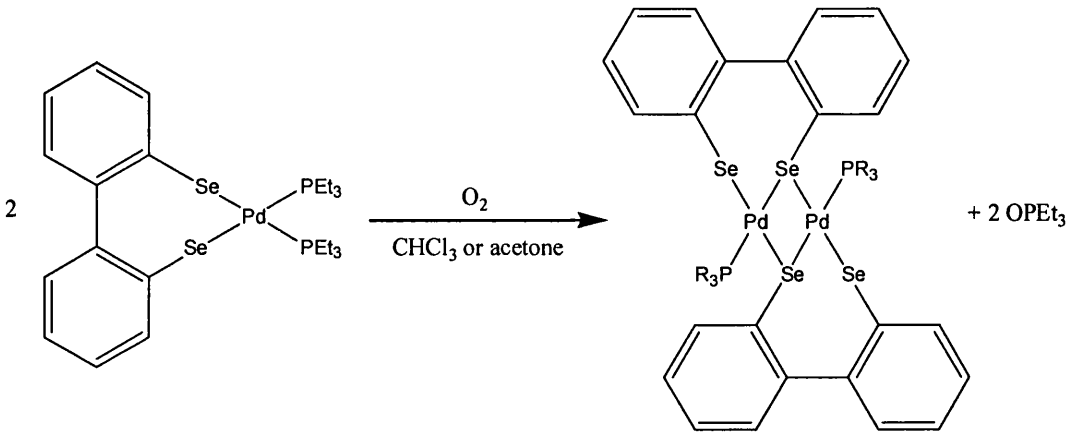

These condensation reactions have been proposed to occur in the synthesis of $[M(\mu_2\text{-SeTh})_2(SeTh)_2(PPh_3)_2]$ (Th = 2-thienyl),[143] and be involved in the formation of the polynuclear compounds of the type $[Pd_6Cl_2Te_4(TePh)_2(PPh_3)_6]$.[236]

Crystals of **29a** suitable for an x-ray diffraction study were obtained from a toluene solution of **28a** at –20 °C; the results of this study are presented in chapter 6. One point of note is the orientation of the biphenyl groups. Figure 5.16 shows the crystal structure of **28a** with the phosphine groups and hydrogens removed (generated using the Mercury program, version 1.4.1, thermal ellipsoids at 30% probability); it can be seen that both ligands have a *DL*- configuration and that the bridging Se-C bonds both point 'downwards'. A different isomer can be envisaged where one of the bridging Se-C bonds points 'downwards' and the other 'upwards' with respect to the $Pd_2Se_4P_2$ plane.

Figure 5.16: Crystal structure of **29a** with phosphine groups removed

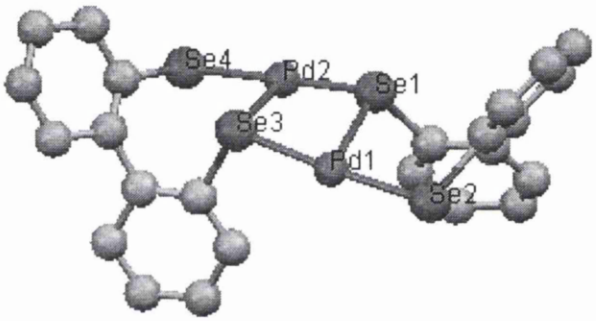

The multinuclear NMR spectroscopic data for **29a,b** are shown in tables 5.12 and 5.13. The NMR spectra of **29a** showed two equivalent species to be present which are assigned as the isomers proposed above; these isomers could be distinguished by the intensities of their signals in the NMR spectra with the most intense assigned as **29a**(1). The interconversion of these isomers would rely on the pyramidal inversion of two Se atoms and therefore is assumed to be a relatively slow process; hence both isomers are seen in the NMR spectra.

Table 5.12: ^{1}H and ^{13}C NMR spectroscopic data for **29a,b** in $CDCl_3$ solution

		29a(1)	**29a**(2)	**29b**
δ(^{1}H)	CH_3	1.00 (18H, dt)[a]	0.91 (18H, dt)[a]	0.73 (18 H, t)[b]
	CH_2P	1.45-1.81 (12H, m)	1.45-1.81 (12H, m)	1.17-1.59 (12 H, m)
	$CH_3CH_2CH_2$			1.17-1.59 (12 H, m)
	CH_2CH_2P			1.17-1.59 (12 H, m)
	$C_{12}H_8$	6.98-7.40 (12H, m)	6.98-7.40 (12H, m)	6.90-7.31 (12H, m)
		7.87-7.92 (2H, m)	7.97-8.01 (2H,m)	7.97-8.03 (2H, m)
		8.65-8.70 (2H, m)	8.65-8.70 (2H, m)	8.71-8.76 (2H,m)
δ(^{13}C)	CH_3	8.7	8.5	13.9
	CH_2P	15.5[c]	14.8[c]	22.3[c]
	$CH_3CH_2CH_2$			26.5
	CH_2CH_2P			24.4[d]
	$C_{12}H_8$:			
	$C(C)_3$	150.5	149.4	149.2
	$C(C)_3$	146.2	145.5	145.2
	CSe	135.2	133.5	133.5
	CSe	130.6	129.8	129.6
		137.8	137.7	137.0[e]
		129.6	129.9	129.7
		128.7	129.6	129.3
		127.6	127.8	127.7[f]
		127.2	126.6	127.5
		127.0	-	126.4

[a] $^{3}J(^{1}H\text{-}^{1}H)$ = 7.6 Hz , $^{3}J(^{1}H\text{-}^{31}P)$ = 16.8 Hz; [b] $^{3}J(^{1}H\text{-}^{1}H)$ = 7.6 Hz; [c] $^{1}J(^{13}C\text{-}^{31}P)$ = 27 Hz (**29a**(1), **29b**), 28 Hz (**29a**(2)), $^{3}J(^{13}C\text{-}^{77}Se)$ = 20 Hz (**29a**(1)), 24 Hz (**29a**(2)), not observed (**29b**); [d] $^{2}J(^{13}C\text{-}^{31}P)$ = 14 Hz; [e] $^{3}J(^{13}C\text{-}^{31}P)$ 7 Hz; [f] $^{3}J(^{13}C\text{-}^{31}P)$ = 6 Hz.

Table 5.13: ^{31}P and ^{77}Se NMR spectroscopic data for **29a,b** in $CDCl_3$ solution

	29a(1)	**29a**(2)	**29b**
^{31}P: δ/ppm	16.2	20.2	11.5
^{77}Se: δ/ppm terminal	369 (s)	345 (s)	340 (s)
bridging	-216 (dd)	-251 (dd)	-249 (dd)
$^{2}J(^{77}Se\text{-}^{31}P_{cis})$/Hz	14	14	11
$^{2}J(^{77}Se\text{-}^{31}P_{trans})$/Hz	119	114	109

The NMR data are in accord with the structures proposed in figure 5.14. The presence of two isomers for **29a** and not **29b** suggests that the phosphine has a large influence on the chemistry of these compounds; the presence of the butyl chains may be sterically hindering the formation of the second isomer of **29b** (which would involve a large movement of the biphenyl groups) so that only one isomer is observed. Two signals are observed in the ^{77}Se NMR spectra corresponding to the terminal and bridging selenium atoms. The terminal selenium atom resonances are apparent singlets as the $^{2}J(^{77}Se\text{-}^{31}P_{cis})$ coupling is too small to be resolved; however both the $^{2}J(^{77}Se\text{-}^{31}P_{cis})$ and $^{2}J(^{77}Se\text{-}^{31}P_{trans})$ coupling constants are resolved for the bridging selenium atoms. As was the case for **27a** and **27b** the *cis*- ^{77}Se-^{31}P coupling constants of **29a** (14 Hz) and **29b** (11 Hz) are similar to those of platinum diselenolenes (chapter 2) and $[Pt(SeC_4H_4)(PBu_3)_2]$ (chapter 4), but the *trans*- ^{77}Se-^{31}P coupling constants (**29a,** avg. 117 Hz; and **29b,** 109Hz) are much larger. Both the *cis*- and *trans*- ^{77}Se-^{31}P coupling constants are close in value to those of the dinuclear palladium diselenolenes $[Pd_2(Se_2C_{n+4}H_{2n+4})(PBu_3)_2]$ (9 Hz and avg. 111 Hz),[120,127] which also have a $Pd_2Se_4P_2$ core. There is a large difference in the chemical shifts of the terminal ($\delta_{avg.}$ = 350 ppm) and bridging ($\delta_{avg.}$ = -239 ppm) selenium atoms, which suggests that there is a lot more electron density around the bridging selenium atom. This is in contrast to the situation encountered in dinuclear palladium diselenolenes where the chemical shifts of the terminal and bridging selenium atoms are close in value ($\delta_{avg.}$ = 488 ppm terminal and 417 ppm bridging). The difference may be attributable to the delocalised electron system of the dinuclear palladium diselenolenes, which is not present in **29a** and **29b**.

The ^{31}P NMR spectra show the expected singlets. Because there are two resonances in the ^{31}P NMR spectrum of **29a** corresponding to different isomers a variable temperature ^{31}P NMR study was carried out to investigate their possible interconversion. ^{31}P NMR spectra of **29a** were recorded at 40, 60, 80 and 100 °C; it was found that the peaks did not merge and so any interconversion process is slow on the NMR timescale. It was observed that the peak attributed to **29a**(2) did appear to grow in intensity until at 100 °C the peaks were equal in intensity, but upon standing at room temperature the peak dropped to its original intensity. Stirring the NMR sample at 70 °C for 3 days did not increase the relative intensity of the peak attributed to **29a**(2).

The ^{13}C and ^{1}H NMR spectra are in agreement with the structures proposed. The ^{13}C NMR spectra show only nine or ten of the expected twelve resonances for the $Se_2C_{12}H_8$ ligand. It is unclear why this is the case; it may be attributed to signal overlap although none of the signals had an unusually high intensity. The two lowest field signals are assigned to the quaternary carbons due to their lower intensity; this was further confirmed by DEPT NMR spectra in which these peaks were absent; these spectra also facilitated identification of the CSe signals. As was observed in **27a,b** and **28a,b** the CSe signals are at relatively high field (compared to the $C(C)_3$ signals), it is not known why this is the case. Unfortunately no ^{13}C-^{77}Se coupling was observed presumably due to the low intensity of the signals. The presence of a peak at approximately 145 ppm in the ^{13}C NMR spectra of **29a,b** provides a method for distinguishing these compounds from **28a,b**. The ^{1}H NMR spectrum of **29a** was difficult to interpret due to signal overlap of the two isomers present; this is reflected in the broad ranges reported for some of the resonances.

Compounds **29a,b** have also been characterised by mass spectrometry and infrared and UV-visible spectroscopy; these data are presented in table 5.14.

In the mass spectra of **29a,b** the loss of $SeC_{12}H_8$ fragments is observed; in both cases the $[M\text{-}2SeC_{12}H_8]^+$ ion is dominant suggesting that the loss of $SeC_{12}H_8$ is a relatively easy process under mass spectral conditions. The $[M\text{-}2SeC_{12}H_8]^+$ ion is more intense for **29a** than **29b**; this is similar to the behaviour of **27a,b** and **28a,b** and suggests that PBu_3 has a greater stabilising effect than PEt_3. The thermal decomposition of these complexes has not been investigated. The UV-visible spectra are analogous to those of **28a,b** with the absorption band at ~335 nm tailing into the visible region, giving rise to the red colour of these compounds. The absorption is more intense for **29a,b** and it is observed that **29a,b** are deeper red than **28a,b**.

Table 5.14: Mass spectral, IR and UV-visible spectroscopic data for compounds **29a,b**

		29a	**29b**
Mass Spectrum[a]	$[M]^+$	1070 (45)	1240 (50)
	$[M - SeC_{12}H_8]^+$	838 (17)	-
	$[M - 2SeC_{12}H_8]^+$	606 (100)	776 (50)
Infrared[b]		2963 (w)	2953 (w)
		2934 (w)	2926 (m)
		2873 (w)	2867 (m)
		1446 (m)	1446 (m)
		1414 (m)	1415 (m)
		1373 (vw)	1377 (w)
		1249 (w)	1251 (vw)
		1099 (w)	1092 (m)
		1028 (s)	1048 (m)
		1001 (vw)	1001 (vw)
		980 (m)	903 (m)
		763 (s)	764 (m)
		747 (vs)	730 (vs)
		728 (vs)	721 (vs)
		692 (s)	652 (m)
		653 (w)	
UV-Vis[c]		230 (76,600)	230 (116,000)
		330 (105,800)	335 (43,750)

[a] *m/z* (%); recorded using FAB; figures are for isotopomers containing ^{106}Pd, ^{80}Se, ^{56}Fe, ^{31}P, ^{12}C, ^{1}H; expected isotope patterns were observed.
[b] selected bands only (cm^{-1}).
[c] λ_{max} (nm); ε (cm^{-1} M^{-1}) in parentheses; recorded in CH_2Cl_2 solution (2×10^{-5} M).

The synthesis of platinum analogues of **29a,b** has not been investigated; it may be possible to synthesise this type of compound using a $[Pt_2(dba)_3]$.dba/PR_3 mixture as a precursor instead of $[Pt(C_2H_4)(PR_3)_2]$.

The Reactions of $(FcSe)_2$ and *bis*-Benzo-1,2-diselenin with $[Pt(C_2H_4)(L)]$ (L = dppm, dppe)

The reactions of $[Pt(C_2H_4)(L)]$ (L = dppm, dppe) with $(FcSe)_2$ and *bis*-benzo-1,2-diselenin were briefly investigated to see if the reactions were feasible, and to compare the properties of any products with those of the compounds already synthesised. Stirring $[Pt(C_2H_4)(L)]$ with $(FcSe)_2$ or *bis*-benzo-1,2-diselenin in a dioxane/THF mixture followed by precipitation with hexane and filtration led to the isolation of yellow orange solids (figure 5.17).

Figure 5.17:

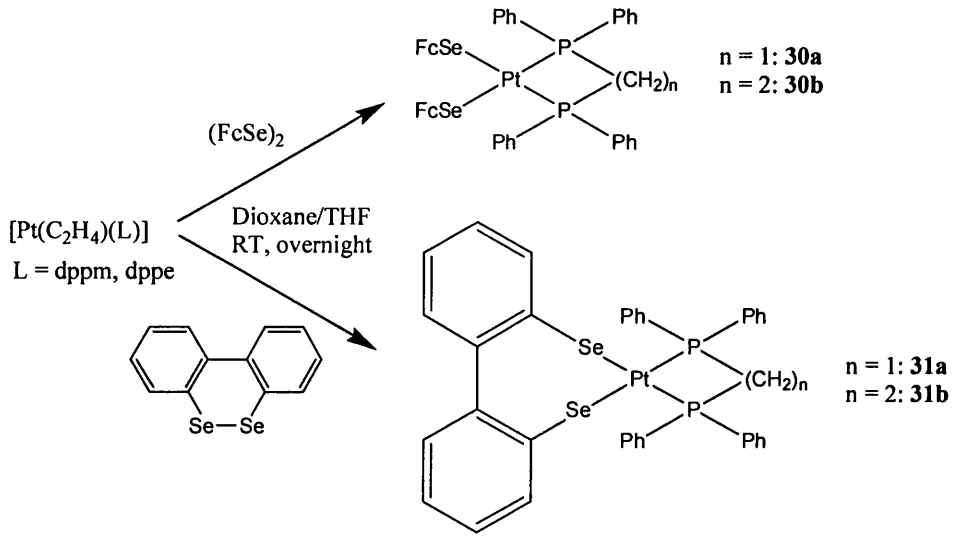

Compounds **30a,b** and **31a,b** were poorly soluble in most organic solvents; in addition they were not very pure and purification by either column chromatography or repeated reprecipitations was unsuccessful. The spectral data of these compounds were therefore limited to ^{31}P NMR spectroscopy and mass spectrometry; these data are shown in table 5.15.

The data are in accord with the proposed structures, and it is likely that these compounds have formed, but due to the lack of success in purification, these reactions were pursued no further. The insolubility of these types of compounds may be attributed to the aryl substituents on the phosphine, as the reactions of $[Pt(PPh_3)_4]$ with $(FcE)_2$ (E = Se, Te) also gave very insoluble products.

Table 5.15: ^{31}P NMR spectroscopic ($CDCl_3$) and mass spectral data for **30a,b** and **31a,b**

		30a	**30b**	**31a**	**31b**
^{31}P:	δ/ppm	-53.0	45.6	-51.8	45.4
	$^{1}J(^{195}Pt\text{-}^{31}P)$/Hz	2485	2824	2396	2846
Mass spectrum:[a]	$[M]^+$	1109 (5)	1123 (15)	Not	905 (5)
	$[M\text{-}SeFc]^+$	844 (10)	858 (100)	recorded	
	$[M\text{-}SeC_8H_{12}]^+$				673 (85)

[a] *m/z* (%); recorded using FAB; figures are for isotopomers containing ^{106}Pd, ^{80}Se, ^{56}Fe, ^{31}P, ^{12}C, ^{1}H; expected isotope patterns were observed.

Chapter 6

An X-ray Crystallographic Study of Some Organometallic and Coordination Compounds

6.1 X-Ray Crystallography

One of the fundamental quests of the chemist is to gain knowledge of the structure of materials: x-ray crystallography is a technique which can provide this information. Determination of a crystal structure provides the precise spatial arrangements of atoms in that crystal; from this, information such as connectivity, bond lengths, angles and stereochemistry can be obtained. In addition it often provides conclusive proof of the structure of a compound.

Here is provided a (very) basic overview of x-ray crystallography; for a more thorough consideration the reader is referred to the texts by Massa[245] and Clegg.[246]

X-ray crystallography differs from most spectroscopic techniques as, instead of measuring the absorption or emission of radiation, the diffraction of the x-ray radiation is measured. X-ray radiation lies in the region of the electromagnetic spectrum which has a similar wavelength to that of interatomic bond distances (1-3 Å, 1 Å = 100 pm). By directing x-ray radiation at a crystal the lattice will convert (through interference) this radiation (with no change in wavelength) into a number of observable reflections (the diffraction pattern); hence this part of the technique is called x-ray diffraction. From this diffraction pattern the ordering of the atoms in the crystal can be deduced.

In order to understand and interpret these interference phenomena, it is necessary to know what exactly a crystal is: Massa[245] provides a good description. 'A "crystal" is a solid object in which a basic pattern of atoms is repeated over and over in all three dimensions. In order to describe the structure of a crystal, it is thus only necessary to know the simplest repeating "motif" and the lengths and directions of the three vectors which together describe its repetition in space.' Thus if each molecule were represented by a point, the crystal structure is a regular array of points, equivalent to each other by translation; this is the *lattice*. The smallest repeating volume of the lattice is the unit cell, characterised by the three vectors *a, b, c,* (the lattice constants) and by the three angles α, β, γ (figure 6.1). The positions of atoms within the unit cell are given in terms of fractional coordinates (*x, y, z*), which describe fractions of the lattice constants (*a, b, c* respectively).

Figure 6.1:

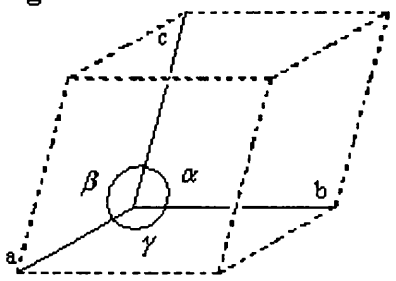

Due to restrictions imposed by rotational and reflectional symmetry there are seven possible types of crystal called the seven crystal systems. Table 6.1 shows these systems and the restrictions on their cell dimensions.

Table 6.1: The seven crystal systems and restrictions

Crystal System	**Restrictions**
Triclinic	none
Monoclinic	$\alpha = \gamma = 90°$
Orthorhombic	$\alpha = \beta = \gamma = 90°$
Tetragonal	$a = b, \alpha = \beta = \gamma = 90°$
Trigonal, hexagonal	$a = b, \alpha = \beta = 90°, \gamma = 120°$
Cubic	$a = b = c, \alpha = \beta = \gamma = 90°$

The most basic unit cells are those in which a lattice point exists at each vertex (primitive unit cells). It is often possible to expand these to larger cells (of 2, 3 or 4 times the volume), which correspond to crystal systems of higher symmetry. These systems can have lattice points centred on the faces or in the middle of the cell and when added to the six primitive lattices, give rise to the fourteen Bravais lattices. Computer programs have been developed which can check if transformation of a unit cell to one of higher symmetry is possible. As well as translation, rotation, reflection and inversion symmetries, crystals can also exhibit glide planes and screw axes, which correspond to reflection-translation and rotation-translation symmetry operations. The symmetry elements of a crystal are regularly arranged in space in accordance with the lattice translational symmetry; there are 230 possible arrangements of these symmetry elements, which give rise to the 230 *space groups*. These space groups can be found in the *International Tables for Crystallography,* Volume A.[247]

We now consider the interaction of x-ray radiation with the crystal. A beam of monochromatic (usually Mo-K_α, or Cu-K_α) radiation is directed at the crystal and the

diffracted radiation collected by a photographic plate, point counter or CCD area detector. The resulting diffraction pattern should ideally be a pattern of relatively well-defined spots, formed by the various 'reflections' of the radiation. The geometry, symmetry and intensity of these spots (and the absence of spots) can then be used to determine the unit cell, space group and subsequently the positions of the atoms in the crystal. To understand this, we need to consider what happens when radiation is diffracted by a row of regularly spaced objects (figure 6.2). The scattered radiation will have zero intensity due to destructive interference of the individual scattered rays, unless they are all in phase.

Figure 6.2:

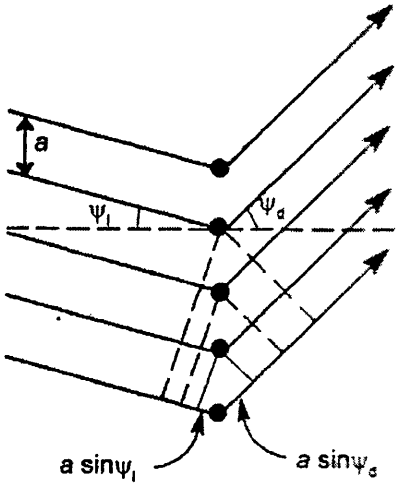

For the waves to be in phase the differences in their path lengths must be equal to whole numbers of wavelengths, and so for rays scattered by two adjacent points: PD = a $\sin\psi_i$ + a $\sin\psi_d$ = $h\lambda$ (PD = path difference, i = incident beam, d = diffracted beam, h = integer). Expansion of this consideration to a three-dimensional lattice gives rise to the integers k and l, corresponding to the b and c axes respectively. These *hkl* indices can be used to label the spots observed in the diffraction pattern. An alternative description, derived by W. L. Bragg, requires the use of only one equation, the *Bragg equation*. Bragg showed that by appropriate orientation of the crystal relative to the x-ray beam, the diffracted beam could be considered a reflection from parallel lattice planes, passing through lattice points. A plane is defined by the *hkl* integers which specify its position relative to the three unit cell edges; the spacing between the planes is determined by the lattice geometry (figure 6.3).

Figure 6.3:

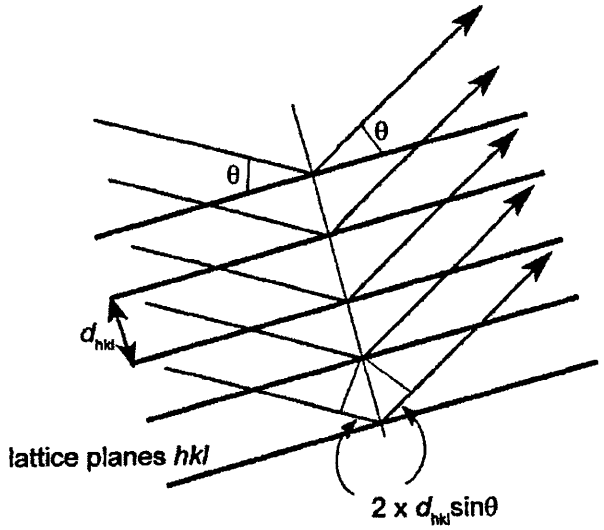

It is from this that the Bragg equation is derived: PD = $2d_{hkl}\sin\theta = n\lambda$. By considering planes with small spacing, n can be set to 1 and often the Bragg equation is used in the form $2d_{hkl}\sin\theta = \lambda$. Using the Bragg equation each diffracted beam can be labelled with its three indices and its net scattering angle calculated. Rearrangement of the Bragg equation shows an inverse relationship between sinθ and d_{hkl}; thus there is an inverse relationship between the diffraction pattern and the crystal lattice.

Since the diffraction phenomena observed are mainly due to the interaction of the x-ray radiation with electrons, then the intensities in the diffraction pattern are essentially the Fourier transform of the electron density in the unit cell. Therefore, by carrying out Fourier transforms of the diffraction pattern intensities, a picture of the electron density in the unit cell, and hence atomic positions can be gained. This can (after refinement) provide the molecular structure of the crystal analysed. It should be re-iterated that this is a very basic overview of x-ray crystallography and for thorough accounts the reader should consult the references given.

6.2 Crystal Structure Determinations

The remainder of this chapter deals with the actual crystal structure determinations carried out. In all cases crystals were mounted on a glass fibre and secured with superglue. Diffraction data were collected on an Oxford Diffraction Xcalibur 3 CCD diffractometer using monochromated Mo-K_α (λ = 0.7109 Å) radiation (exceptions are discussed). Data collection was carried out using the Oxford Diffraction software package, CrysAlisCCD (version 1.5); data reduction was carried out using the Oxford Diffraction software package, CrysAlisRED (version 1.5). All graphics were generated using ORTEP-3.[248]

6.3 Crystal Structure Determinations of *trans*-[Pt(SePh)$_2$(PR$_3$)$_2$] (R = Et, Bu), *trans*-[Pt(SeFc)$_2$(PBu$_3$)$_2$] and [Pt(Se$_2$C$_{12}$H$_8$)(PEt$_3$)$_2$]

6.3.1 Crystal Structure Determinations of *trans*-[Pt(SePh)$_2$(PBu$_3$)$_2$] (21b) and *trans*-[Pt(SeFc)$_2$(PBu$_3$)$_2$] (22b)

Pale green crystals of **21b** were obtained by recrystallisation from toluene/hexane at –20 °C; from these a prism with dimensions 0.20 x 0.20 x 0.10 mm was chosen for analysis. The crystal had a few smaller crystals ('passengers') stuck to its surface. The crystal gave a poor diffraction pattern, only exhibiting low angle reflections with a powder diffraction pattern evident. After a short data acquisition the UM TTT command (which proposes possible unit cells, based on analysis of the diffraction pattern) in the Oxford Diffraction software package, CrysAlisCCD (version 1.5), suggested a triclinic unit cell with dimensions: a = 8.67(4) Å, b = 10.24(5) Å, c = 12.31(8) Å, α = 77.63(6)°, β = 85.64(6)°, γ = 81.9(4)°, V = 1052 Å^3. A full data acquisition was carried out, after which the UM TTT command proposed the same triclinic cell. The data were reduced and processed with absorption correction using SADABS,[249] ABSPACK (Oxford Diffraction software) and ABSPACK with a shape correction; SADABS gave the best R_{int} value. The structure was solved by direct methods using SIR 97[225] and refined using SHELXL 97.[223] In the structure refinement it was necessary to apply a SHEL command due to a large number of unobserved reflections in the original data set. This command limits the reflections considered to a certain θ range (in this case θ values corresponding to values of d between 20 and 1.1 Å). There were found to be no extinction effects. The space group is P –1 with half a molecule in the asymmetric unit (the minimum group of atoms whose positions, together with those generated by the symmetry operations of the space group generate the complete contents of the unit cell), with the Pt atom lying on an inversion centre. It was necessary to impose a restraint on the thermal parameters of C1 and all non-hydrogen atoms were anisotropically refined. The hydrogen atoms were added in calculated positions and constrained. Table 6.2 shows the crystallographic data obtained for **21b** (and **22b**). Figure 6.4 shows the crystal structure of **21b**; thermal ellipsoids are drawn at 30% probability, and hydrogens are omitted for clarity.

Table 6.2: Crystallographic data for **21b** and **22b**

Compound	**21b**	**22b**
Empirical formula	$C_{18}H_{30}PSePt_{0.5}$	$C_{22}H_{36}PSeFePt_{0.5}$
Formula weight	455.91	563.83
Crystal system	triclinic	triclinic
Space group	P -1	P -1
a/Å	8.483(6)	10.577(2)
b/Å	10.335(7)	10.645(2)
c/Å	12.246(9)	10.866(2)
α/°	77.63(6)	99.95(1)
β/°	85.64(6)	100.99(1)
γ/°	83.43(6)	91.748(1)
V/Å	1040.3(13)	1180.39
Z	2	2
F(000)	456	564
D_{calc} (g cm^{-3})	1.455	1.586
μ (Mo-K_α/mm^{-1})	5.22	5.20
Temperature (K)	293	293
Reflections collected	5961	5997
Independent reflections	1610	4451
θ Range (°)	4.32-18.84	4.42-26.02
Reflect. with $I > 2\sigma(I)$	964	3969
No. of parameters	187	233
R_1; wR_2 [$I > 2\sigma(I)$]	0.0717; 0.1648	0.0309; 0.0769
R_1; wR_2 (all data)	0.0918; 0.1797	0.0305; 0.0796
GoF	0.931	1.108

Figure 6.4: 21b

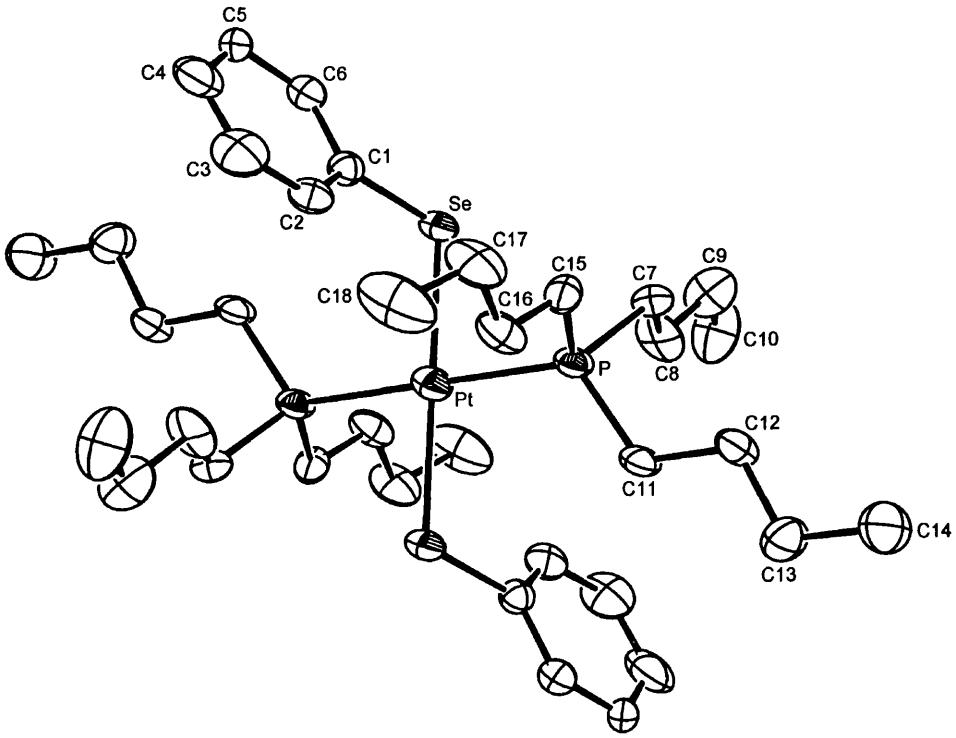

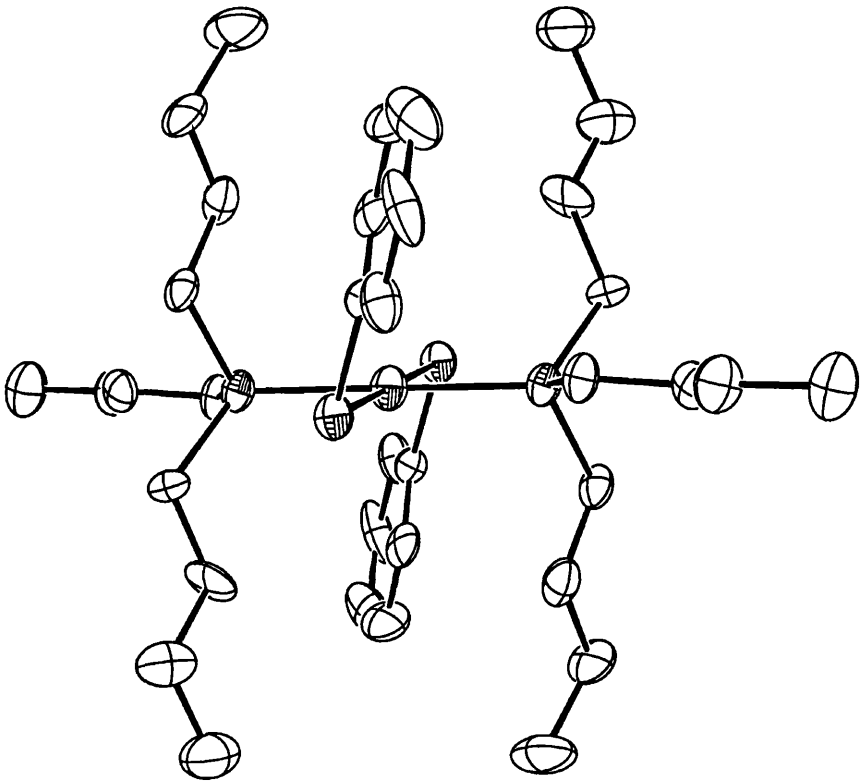

Orange crystals of **22b** were obtained by recrystallisation from toluene/hexane at –20 °C; from these a prism with dimensions 0.40 x 0.35 x 0.22 mm was chosen for analysis. After a short data acquisition the UM TTT command suggested a monoclinic face-centred (mC) cell with dimensions: a = 14.74(1) Å, b = 15.19(1) Å, c = 10.85(2) Å, α = 90.0°, β = 105.0(1)°, γ = 90.0°, V = 2345 Å^3. The alternative UM F command (Oxford Diffraction software package, CrysAlisCCD (version 1.5)), however, suggested a triclinic cell, which could be transformed into the monoclinic cell described above. A full data acquisition was carried out and a data reduction performed according to the suggested monoclinic face-centred cell. Subsequent attempts to solve the structure by direct methods failed; the monoclinic cell volume was apparently too small to host more than two molecules, and this would have imposed too high a symmetry on the molecule. The data were reduced according to the triclinic cell proposed (table 6.2), with subsequent processing with absorption correction using SADABS and ABSPACK with a shape correction. The structure was solved by direct methods using SIR 97 and refined using SHELXL 97, with the ABSPACK corrected data used in the final cycles. There was found to be no extinction. As for **21b**, the space group is P –1 with half a molecule in the asymmetric unit, and the Pt atom lying on an inversion centre. All non-hydrogen atoms were anisotropically refined; the hydrogen atoms were added in calculated positions and constrained. Table 6.2 shows the crystallographic data obtained for **22b** (and **21b**). Figure 6.5 shows the crystal structure of **22b**; thermal ellipsoids are drawn at 30% probability, and hydrogens are omitted for clarity.

Table 6.3 shows some of the bond lengths and angles of **21a** (discussed later), **21b** and **22b**. Since the asymmetric units of the complexes contain half a molecule the $PtSe_2P_2$ core is highly symmetric. The Pt-Se bond lengths are of comparable length (2.452 Å for **21a**, 2.463 Å for both **21b** and **22b**), and longer than in the related complex *trans*-$[Pt(SePh)_2(PPh_3)_2]$[240] (avg. 2.418 Å), though a similar length is observed in the complex *trans*-$[Pt(SeTh)_2(PPh_3)_2]$[143] (avg. 2.464 Å). The Pt-P bond lengths of **21a,b** and **22b** are comparable to those of *trans*-$[Pt(SeTh)_2(PPh_3)_2]$ (2.311 and 2.316 Å *cf.* avg. 2.315 Å) and longer than those of *trans*-$[Pt(SePh)_2(PPh_3)_2]$ (avg. 2.29 Å). The Se-Pt-P angles of **21a,b** (avg 93.5 and 86.5°) are similar to those observed in *trans*-$[Pt(SePh)_2(PPh_3)_2]$ (avg 94.6

and 86.0°) which can be attributed to the similarities of the complexes. The angles are closer to 90° in **22b** (91.56 and 88.44°), whereas in *trans*-[$Pt(SeTh)_2(PPh_3)_2$] they are observed to deviate most significantly from 90° (avg 96.4 and 85.9°). The differences in these values can probably be attributed to the different steric influences of the substituents.

Table 6.3: Selected bond lengths and angles for **21a,b** and **22b**

Compound	**21a**	**21b**	**22b**
Bond lengths (Å)			
Pt-Se(1)	2.4522(8)	2.4627(28)	2.4631(6)
Pt-P(1)	2.311(2)	2.311(6)	2.316(1)
Se(1)-C(1)	1.893(9)	1.890(23)	
Se(1)-C(13)			1.902(4)
Bond angles (°)			
Se(1)-Pt-Se(2)	180.	180.	180
Se(1)-Pt-P(1)	86.29(5)	93.39(16)	91.56(3)
Se(1)-Pt-P(2)	93.71(5)	86.61(16)	88.44(3)
P(1)-Pt-P(2)	180	180	180
Pt-Se(1)-C(1)	104.56(25)	104.85(73)	
Pt-Se(1)-C(13)			102.74(14)

Note that the angles Pt-Se(1)-C(1) and Pt-Se(1)-C(13) refer to the same angle (see figures 4 and 5).

Figure 6.5: 22b

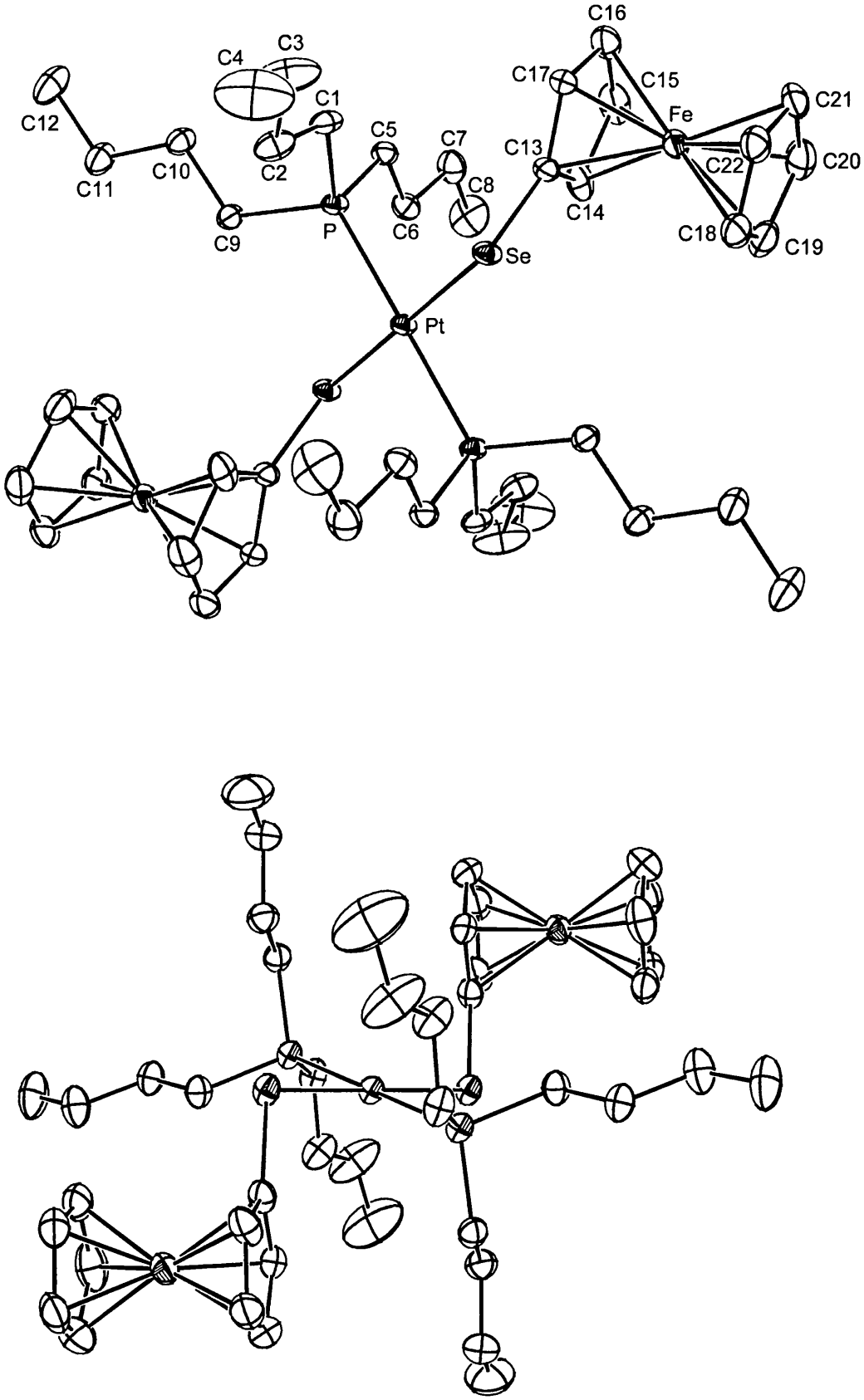

6.3.2 Crystal Structure Determination of [Pt($Se_2C_{12}H_8$)(PEt_3)$_2$] (27a)

Although the preparation of **27a** was similar to that of **21b** and **22b**, the product has a *cis-* geometry enforced by the $Se_2C_{12}H_8$ ligand. Pale yellow crystals of **27a** were obtained by recrystallisation from toluene/hexane at –20 °C; from these a prism with dimensions 0.40 x 0.30 x 0.25 mm was chosen for analysis. After a short data acquisition, both the UM F and UM TTT commands suggested a triclinic cell with dimensions: a = 9.79(1) Å, b = 11.44(1) Å, c = 14.17(1) Å, α = 80.7(1)°, β = 69.3(1)°, γ = 86.1(1)°, V = 1465 Å^3. A full data acquisition was carried out and was consistent with the proposed cell. The data were reduced and processed with absorption correction using SADABS and ABSPACK with a shape correction. The structure was solved by direct methods using SIR 97, and refined using SHELXL 97 with the SADABS data giving the best results in the final refinement cycles. It was necessary to use a SHEL command to limit the data considered (0.8 < d < 20 Å). There was found to be no extinction, and anisotropic refinement was applied to all non-hydrogen atoms. Hydrogens were added in calculated positions and were constrained. The space group is P –1 with one molecule of **27a** and half a molecule of toluene in the asymmetric unit. The toluene molecule lies partly disordered, around an inversion centre. This caused problems with the refinement; three different models were refined to see which gave the best result.

1. A model with three ring carbons and a methyl group, with the methyl group weighted 0.5.
2. A model with a complete, rigid benzene ring, weighted 0.5. The ring lies in proximity of the inversion centre with its mirror image.
3. A model with three benzene carbons around the inversion centre suitably restrained and no methyl group.

The third model showed - through difference Fourier transformations - that there is practically no trace of the methyl group (indicating a higher disorder than first thought). When the presence of the methyl group was 'forced', then the model oscillated; it was not possible to add fractional methyl groups (models 2 and 3), as well as hydrogens to each benzene carbon. Model 2 proved to give the best results, allowing a refinement with no damping factor necessary (in cases where a structure is difficult to refine, a damping factor allows the program to suppress oscillations and divergences, but the use of this factor leads to a less accurate result). At a later date

the whole toluene molecule was refined based on the toluene methyl group being partly hidden by the molecule of **27a**. The data presented are of this (better) refinement.

Table 6.4 shows the crystallographic data for **27a** and figure 6.6 shows the crystal structure; thermal ellipsoids are drawn at 30% probability, and hydrogens are omitted for clarity.

Table 6.4: Crystallographic data for compound **27a**

Empirical formula	$C_{24}H_{38}P_2Se_2Pt.C_{3.5}H_4$
Formula weight	787
Crystal system	triclinic
Space group	P -1
a/Å	9.794(1)
b/Å	11.457(1)
c/Å	14.197(2)
α/°	80.67(1)
β/°	69.16(1)
γ/°	86.15(1)
V/Å	1469.0(3)
Z	2
F(000)	766
D_{calc} (g cm^{-3})	1.78
μ (Mo-K_α/mm^{-1})	7.37
Temperature (K)	293
Reflections collected	5890
Independent reflections	4719
θ Range (°)	4.13-26.37
Reflect. with $I > 2\sigma(I)$	4423
No. of parameters	310
R_1; wR_2 [$I > 2\sigma(I)$]	0.0287; 0.0524
R_1; wR_2 (all data)	0.0410; 0.0558
GoF	0.936

The calculated bond lengths and angles of **27a** are shown in table 6.5. Like **21b** and **22b**, compound **27a** contains a square-planar $PtSe_2P_2$ core, although here a *cis*-geometry is exhibited. The ethyl groups and biphenyl ring protrude significantly from the plane. The dihedral angle of the biphenyl group of 64.1° is greater than that in the

Figure 6.6: 27a

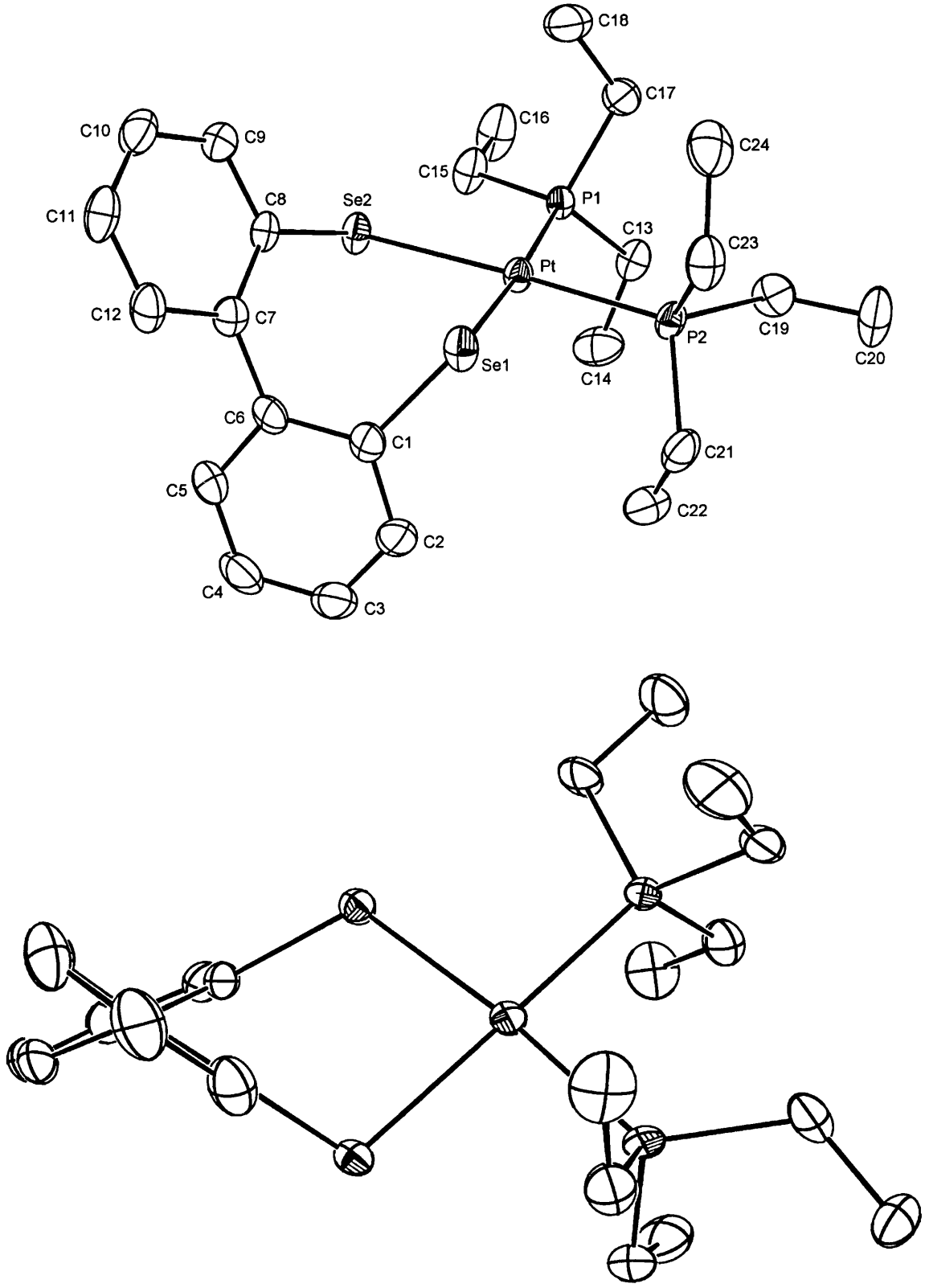

analogous complex [Pt($S_2C_{24}H_{12}$)(COD)] (45.6°);[132] this may be due to the greater size of Se compared to S, allowing the ligand more flexibility. The square plane is slightly asymmetric: one Pt-Se bond is approximately 0.02 Å longer than the other and the P-Pt-Se angles differ by 3°. This contrasts with the symmetry observed in **21b** and **22b**; however, similar distortions have been observed in platinum diselenolenes (see chapter 2) and dithiolenes.[169] The Pt-P and Pt-Se bond lengths (avg. 2.30 and 2.47 Å respectively) are almost identical to those found in *cis*-[Pt($SePh)_2(PPh_3)_2$] (avg. 2.29 and 2.47 Å respectively),[241] but the Se-Pt-Se angle is significantly more acute (89.94° *vs* 95.10°) reflecting the constraint imposed by the $Se_2C_{12}H_8$ ligand; as expected, a similar value (94.02°) is observed in [Pt($S_2C_{24}H_{12}$)(COD)].

Table 6.5: Selected bond lengths and angles for compound **27a**

Bond lengths (Å)	
Pt-Se(1)	2.4873(6)
Pt-Se(2)	2.4613(6)
Pt-P(1)	2.302(1)
Pt-P(2)	2.299(1)
Se(1)-C(1)	1.926(5)
Se(2)-C(8)	1.925(4)
Bond angles (°)	
Se(1)-Pt-Se(2)	89.94(2)
Se(1)-Pt-P(1)	175.24(3)
Se(1)-Pt-P(2)	84.16(3)
Se(2)-Pt-P(2)	174.08(3)
Se(2)-Pt-P(1)	87.55(3)
P(1)-Pt-P(2)	98.29(4)
Pt-Se(1)-C(1)	100.47(14)
Pt-Se(2)-C(8)	113.18(13)

6.3.3 Crystal Structure Determination of *trans*-[Pt(SePh)$_2$(PEt$_3$)$_2$] (21a)

The crystal structure determination of **21a** warrants an extended discussion, as it took several attempts, with various models examined which eventually proved inaccurate, before the final structure was accurately determined. In the first analysis undertaken, it was possible to obtain an approximate model of the crystal structure of **21a**. Yellow crystals of **21a** were obtained by recrystallisation from toluene/hexane at –20 °C; from these a small crystal (ill-formed) of dimensions 0.30 x 0.25 x 0.15 mm was chosen for analysis. The intial diffraction pattern was poor and showed what were believed to be split reflections. After a short data acquisition the UM TTT command suggested an orthorhombic unit cell with dimensions: a = 9.20(1) Å, b = 10.11(1) Å, c = 14.95(1) Å, α = 90.0°, β = 90.0°, γ = 90.0°, V = 1390 Å^3. A long data acquisition was carried out and the same unit cell proposed; the data were reduced according to this unit cell with a scan width of 1.2 (an arbitrary value, which should reduce errors caused by the poor diffraction pattern). Subsequent attempts to solve the structure by direct methods failed.

The structure determination was reattempted using a crystal from a different batch; the crystal was a fragment cut from a larger crystal, and had the dimensions 0.40 x 0.35 x 0.40 mm. Although this crystal was, visually, of better quality than the last, the diffraction pattern was very similar; however after a short data collection the UM TTT command suggested a triclinic cell of dimensions: a = 8.81(1) Å, b = 9.04(1) Å, c = 10.23(1) Å, α = 63.3(1)°, β = 74.5(1)°, γ = 88.2(1)°, V = 699 Å^3. After a long data acquisition, the UM TTT command showed two possible triclinic cells, the one detailed above and another with double the volume and dimensions: a = 9.069(3) Å, b = 11.538(3) Å, c = 15.204(3) Å, α = 81.15(2)°, β = 71.96(2)°, γ = 68.66(2)°, V = 1407 Å^3. This second triclinic cell was only found by using a threshold intensity of 2000 in the peak-hunting command (i.e. looking for reflections in the diffraction pattern of intensity 2000 or above); the first cell was found using threshold intensities of 3000-10000. The data were reduced according to a triclinic cell, with subsequent processing with absorption correction using SADABS and ABSPACK with a shape correction. The structure was solved by direct methods with SIR 97 and refined as far as possible by SHELXL 97; the

larger cell was used, as solution with the smaller cell was not possible. The space group of this model is P 1, and there are two molecules in the cell, which are apparently not symmetry related. The R values are high (for data with $I > 2\sigma(I)$: $R_1 = 0.0985$; $wR_2 = 0.2591$), so, although chemically meaningful at the time, from a crystallographic point of view the model was not satisfactory. Figure 6.7 shows the model obtained; thermal ellipsoids are drawn at 20% probability.

Figure 6.7: 21a (first model)

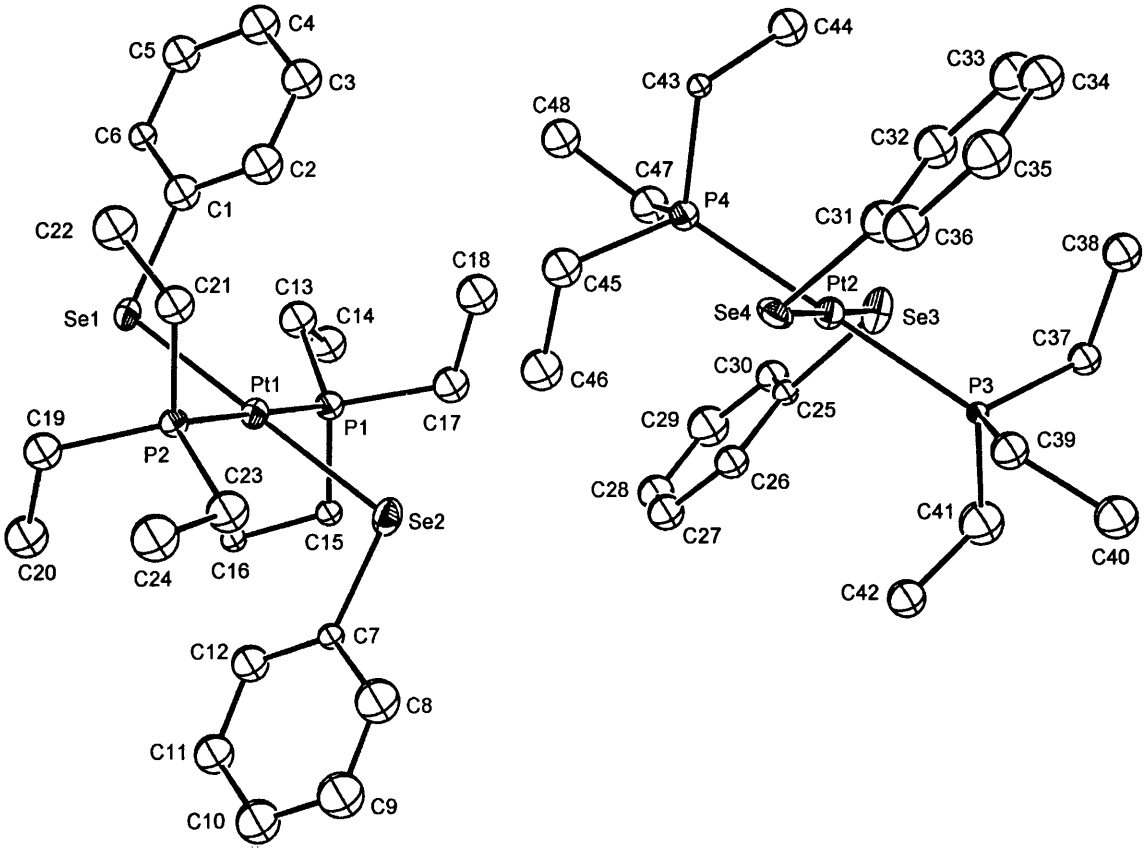

At a later date, recrystallisation of **21a** from hexane/DCM at –20 °C gave large yellow crystals of **21a**. From one of these crystals, a smaller fragment with dimensions 0.30 x 0.30 x 0.30 mm was cut and analysed. Initial analysis was carried out using Cu-K_α radiation (λ = 1.5418 Å), due to Mo-K_α radiation being unavailable. A model was established using these data of a triclinic cell with dimensions: a = 9.047(1) Å, b = 9.195(1) Å, c = 39.903(4) Å, α = 83.38(1)°, β = 83.67(1)°, γ = 59.39(1)°, V = 2832.7 Å^3. The presence of the long c-axis results in the closely spaced spots observed in the diffraction pattern. The space group was P –1, with one molecule and two half-molecules (both with Pt on an inversion centre) in the unit cell. The model could not be refined due to problems with negative temperature factors, which are associated with the use of Cu-K_α radiation. The structure was then conclusively determined using Mo-K_α radiation. After an initial short data acquisition, the UM TTT command proposed the same cell as observed in the Cu-K_α radiation experiment. A long data acquisition was carried out, with the CCD detector set a distance of 80 mm from the crystal (normally 50 mm), to allow a good separation of the closely spaced spots in the diffraction pattern. When the data acquisition was complete, the UM TTT command proposed a monoclinic cell with double the volume: a = 15.533(2) Å, b = 9.168(1) Å, c = 39.852(3) Å, α = 90.00°, β = 97.76(1)°, γ = 90.00°, V = 5623.1 Å^3. The data were reduced according to this cell, with absorption correction processing carried out using SADABS and ABSPACK with no shape correction. The structure was solved by direct methods using SIR 97 and refined using SHELXL 97. It was necessary to apply a small correction for extinction (using the EXTI command with a final value of 0.000181); the SADABS corrected data were found to give the best results. The space group is the face-centred monoclinic C 2/c; there are 2 half-molecules in the asymmetric unit, one of which lies on an inversion centre and the other on a two-fold axis. Hydrogen atoms were added in calculated positions and were constrained. Table 6.6 shows the crystallographic data obtained for **21a**; selected bond lengths and angles for the molecule lying on the inversion centre are shown in table 6.3. Figure 6.8 shows the crystal structure of **21a**: both molecules are shown (*not* as they are orientated in the unit cell!), thermal ellipsoids are drawn at 30% probability and hydrogens are omitted for clarity. The SePh groups exemplify the different symmetries of the two

molecules: inversion symmetry shown by the molecule with one SePh group pointing 'up' and one 'down', and the two-fold axis symmetry shown by the molecule with both SePh groups pointing 'up'.

Table 6.6: Crystallographic data for **21a**

Empirical formula	$C_{24}H_{40}P_2Se_2Pt$
Formula weight	743.51
Crystal system	monoclinic
Space group	C 2/c
a/Å	15.533(2)
b/Å	9.168(1)
c/Å	39.852(3)
α/°	90.00
β/°	97.76(1)
γ/°	90.00
V/Å	5623.2(9)
Z	8
F(000)	2880
D_{calc} (g cm^{-3})	1.773
μ (Mo-K_α/mm^{-1})	7.702
Temperature (K)	293
Reflections collected	7301
Independent reflections	5744
θ Range (°)	4.17-26.37
Reflect. with $I > 2\sigma(I)$	4641
No. of parameters	271
R_1; wR_2 [$I > 2\sigma(I)$]	0.0466; 0.0835
R_1; wR_2 (all data)	0.0585; 0.0897
GoF	1.126

Figure 6.8: 21a (final model)

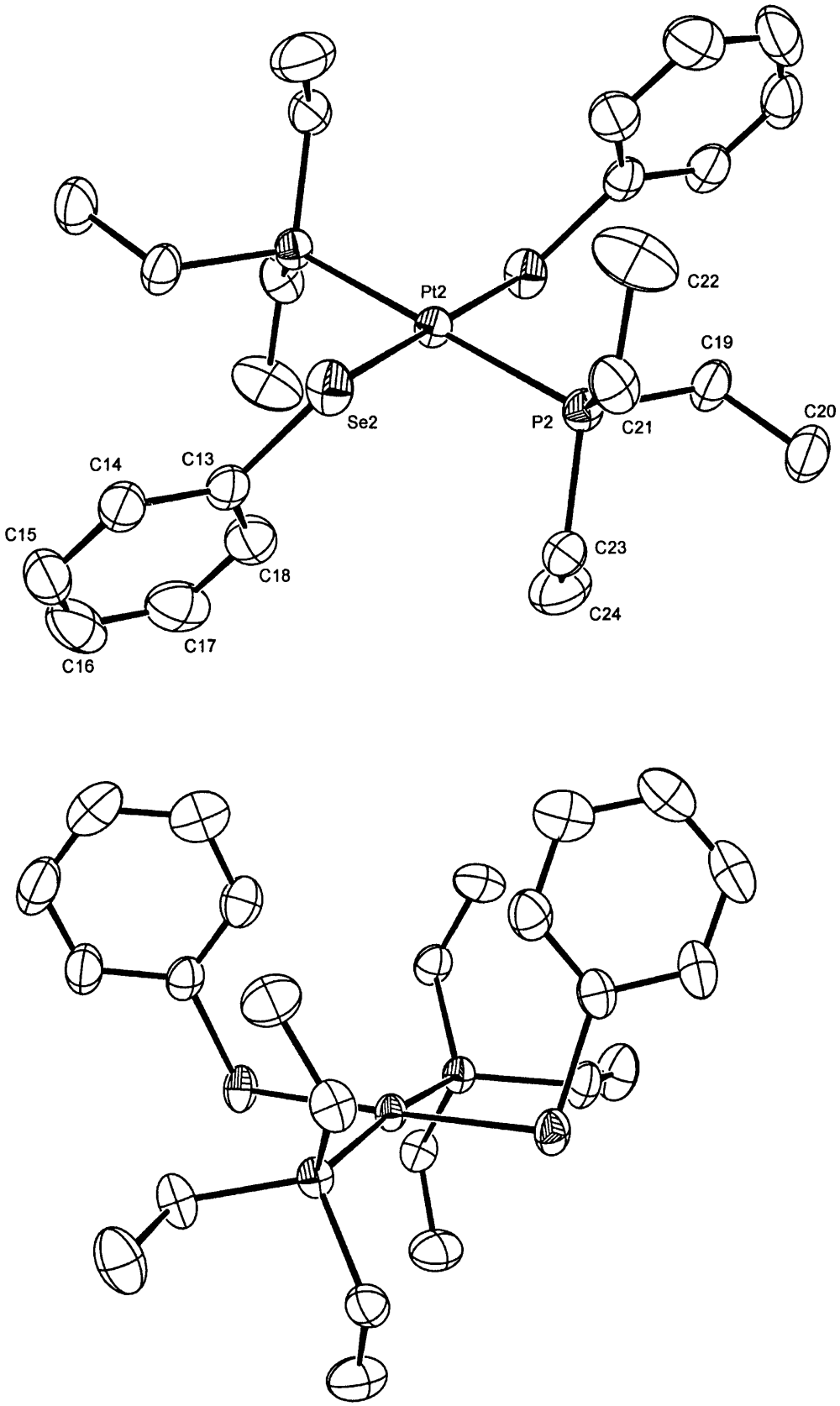

6.4 Crystal Structure Determination of $[Pd_2(Se_2C_{12}H_8)_2(PEt_3)_2]$ and Partial Crystal Structure Determination of *trans*-$[Pd(SeFc)_2(PBu_3)_2]$

In the reaction of $[Pd_2(dba)_3].dba$, PEt_3 and $Se_2C_{12}H_8$, NMR spectral evidence suggested the formation of both a mononuclear and a dinuclear product. We were able to obtain crystals of the dinuclear product and its crystal structure was established. The partial crystal structure determination of a related palladium compound is also described in this section.

6.4.1 Crystal Structure Determination of $[Pd_2(Se_2C_{12}H_8)_2(PEt_3)_2]$ (29a)

Orange-red crystals of **29a** were obtained by recrystallisation from toluene/hexane at –20 °C; from these a prism with dimensions 0.40 x 0.30 x 0.20 mm was selected for analysis. After a short data collection, two alternative unit cells (both orthorhombic) were proposed; the UM F command proposed a cell with dimensions: a = 7.49(1) Å, b = 12.37(1) Å, c = 21.60(1) Å, α = 90.0°, β = 90.0°, γ = 90.0°, V = 2001 Å^3; whereas the UM TTT command proposed a cell twice as big, with dimensions: a = 12.37(1) Å, b = 14.96(1) Å, c = 21.64(1) Å, α = 90.0°, β = 90.0°, γ = 90.0°, V = 4007 Å^3 (note the doubled a axis becomes b by convention). A long data acquisition was carried out and the data reduced. The first solution was attempted using the cell proposed by UM F. Analysis of the *hkl* indices suggested a *0kl* condition for $k + l$, pointing toward P $nm2_1$ or P nmm as possible space groups. Attempted solutions using these space groups failed and the data were corrected (SADABS, ABSPACK with shape correction) according to the larger cell. The structure was solved by direct methods using SHELXS 97[7] in the space group P 2_1nb, and refined using SHELXL 97, with the ABSPACK corrected data yielding better results. There was found to be no extinction. All non-hydrogen atoms were anisotropically refined; hydrogens were added in calculated positions and constrained. The "enantiomeric" structure was refined also and found to have slightly worse R-values. It was difficult to assign an absolute configuration, as reflected by a Flack parameter of 0.5 (the Flack parameter is used where inversion twinning is possible; a Flack value of 0

indicates the refined structure is correct, whereas a value of 1 indicates the inverse structure is true; a value of 0.5 indicates a 1:1 ratio of both structures). This high value of the Flack parameter is attributed to the essentially centrosymmetric pattern of the heavy atoms present.

Table 6.7 shows the crystallographic data for **29a.** Figure 6.9 shows the crystal structure: thermal ellipsoids are drawn at 20% probability, and hydrogens are omitted for clarity. Also included is a picture of the packing to show the essentially centrosymmetric pattern of the heavy atoms.

Table 6.7: Crystallographic data for **29a**

Empirical formula	$C_{36}H_{46}P_2Se_4Pd_2$
Formula weight	1069.31
Crystal system	orthorhombic
Space group	P 2_1nb
a/Å	12.373(1)
b/Å	14.962(1)
c/Å	21.642(1)
α/°	90.00
β/°	90.00
γ/°	90.00
V/Å	4006.5(5)
Z	4
F(000)	2080
D_{calc} (g cm^{-3})	1.773
μ (Mo-K_α/mm^{-1})	4.635
Temperature (K)	293
Reflections collected	19325
Independent reflections	8001
θ Range (°)	4.00-26.37
Reflect. with $I > 2\sigma(I)$	3894
No. of parameters	403
R_1; wR_2 [$I > 2\sigma(I)$]	0.0432;0.0879
R_1; wR_2 (all data)	0.0984;0.1028
GoF	0.845

Table 6.8 shows some selected bond lengths and angles of **29a**. The Pd_2Se_2 core exhibits a hinged arrangement (20.6(1)° dihedral angle between square planes), as is observed in $[Pd_2(Se_2C_8H_{12})_2(PPh_3)_2]$[117] (75.6(1)°); a coplanar arrangement is also possible and is observed in the complexes $[Pd_2(SePh)_4(PPh_3)_2]$,[236]

$[Pd_2\{\mu\text{-}\eta^1\text{-}Fe(\eta^5\text{-}C_5H_4Se)_2\}_2(PBu_3)_2]$[176] and $[Pd_2(\eta^3\text{-}C_3H_5)_2\{Ph_2P(O)NP(Se)Ph_2\text{-}Se\}_2]$.[250] The $PdSe_3P$ square planes are slightly distorted, probably as a result of the geometry imposed by the chelating ligand.

Figure 6.9: 29a

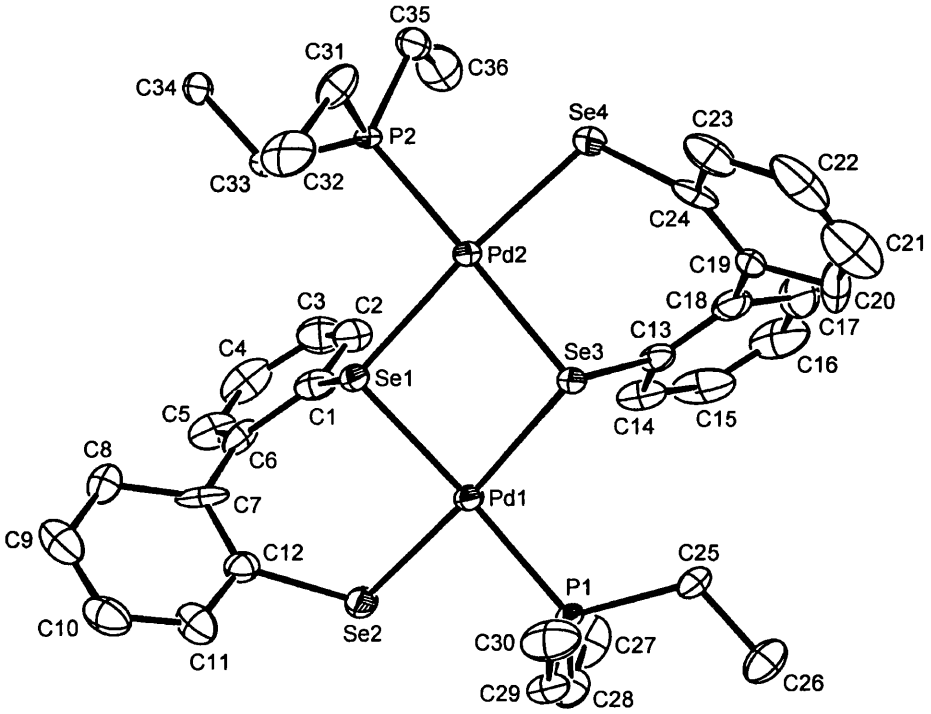

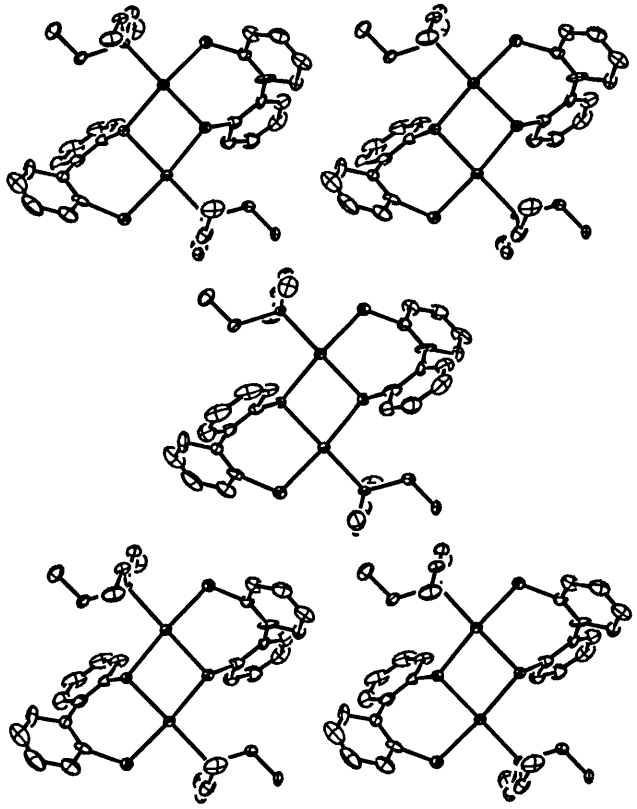

Table 6.8: Selected bond lengths and angles for **29a**

Bond lengths (Å)	
Pd(1)-Se(1)	2.460(2)
Pd(1)-Se(2)	2.432(2)
Pd(1)-Se(3)	2.446(2)
Pd(1)-P(1)	2.298(4)
Pd(2)-Se(1)	2.464(2)
Pd(2)-Se(3)	2.454(2)
Pd(2)-Se(4)	2.435(2)
Pd(2)-P(2)	2.280(4)
Se(1)-C(1)	1.907(14)
Se(2)-C(12)	1.938(14)
Se(3)-C(13)	1.939(14)
Se(4)-C(24)	1.949(16)
Bond angles (°)	
Se(1)-Pd(1)-Se(2)	92.76(7)
Se(1)-Pd(1)-P(1)	171.85(12)
Se(1)-Pd(1)-Se(3)	82.80(4)
Se(1)-Pd(2)-P(2)	97.31(10)
Se(1)-Pd(2)-Se(4)	174.10(7)
Se(1)-Pd(2)-Se(3)	82.55(4)
Se(2)-Pd(1)-Se(3)	175.56(7)
Se(2)-Pd(1)-P(1)	87.40(9)
Se(3)-Pd(1)-P(1)	96.99(10)
Se(3)-Pd(2)-P(2)	173.88(12)
Se(3)-Pd(2)-Se(4)	92.03(6)
Se(4)-Pd(2)-P(2)	87.83(10)
Pd(1)-Se(1)-Pd(2)	94.41(7)
Pd(1)-Se(3)-Pd(2)	95.03(7)
Pd(1)-Se(1)-C(1)	97.01(41)
Pd(1)-Se(2)-C(12)	107.35(36)
Pd(1)-Se(3)-C(13)	106.25(43)
Pd(2)-Se(3)-C(13)	97.30(39)
Pd(2)-Se(4)-C(24)	108.09(35)
Pd(2)-Se(1)-C(1)	109.44(47)

Dihedral angles for **29a**: 60.48° and 60.54° between phenyl rings for C1-C6/C7-C12 and C13-C18/C19-C24 respectively. The rings C1-C6 and C7-C12 form dihedral angles with the Pd(1)Se(1)Se(2)Se(3)P(1) plane of 79.13° and 65.23° respectively; The rings C13-C18 and C19-C24 form dihedral angles with the Pd(2)Se(1)Se(3)Se(4)P(2) plane of 80.34° and 65.69° respectively.

There is only a small variation in the Pd-Se bridging bond lengths (2.446(2)-2.464(2) Å), whereas in the complexes $[Pd_2(Se_2C_8H_{12})_2(PPh_3)_2]$ and

$[Pd_2\{\mu\text{-}\eta^1\text{-}Fe(\eta^5\text{-}C_5H_4Se)_2\}_2(PBu_3)_2]$ larger variations in bond lengths are observed (2.459(1)-2.492(1) Å and 2.413(4)-2.489 Å respectively). The terminal Pd-Se bonds are almost equal in length (avg. 2.434 Å); this is also observed in the complexes $[Pd_2(Se_2C_8H_{12})_2(PPh_3)_2]$ (avg. 2.385 Å) and $[Pd_2\{\mu\text{-}\eta^1\text{-}Fe(\eta^5\text{-}C_5H_4Se)_2\}_2(PBu_3)_2]$ (avg. 2.454 Å). The bond angles of the Pd(1) and Pd(2) square planes differ slightly (as previously mentioned the molecule is not quite centrosymmetric), with the maximum difference occuring between the Se(1)-Pd-P(1) and Se(3)-Pd-P(2) bond angles (171.8(1)° and 173.9(1)° respectively). The Se-Pd-Se bridging angles are less than 90° (82.80(4)° and 82.55(4)°), but this is expected: $[Pd_2\{\mu\text{-}\eta^1\text{-}Fe(\eta^5\text{-}C_5H_4Se)_2\}_2(PBu_3)_2]$ and $[Pd_2(SePh)_4(PPh_3)_2]$ both exhibit bridging angles of approximately 84.1°, and $[Pd_2(Se_2C_8H_{12})_2(PPh_3)_2]$ has very acute bridging angles of an average 77.7°. Perhaps to compensate for this Pd-Se-Pd angles larger than 90° are observed (94.41(7)° and 95.03(7)°); similar angles were observed in $[Pd_2(SePh)_4(PPh_3)_2]$ (95.89(4)°), but in $[Pd_2(Se_2C_8H_{12})_2(PPh_3)_2]$ the angles are much less than 90° (avg. 77.8°), which may be a corollary of the greater dihedral angle between the Pd square planes than in **29a**. The dihedral angles formed by the phenyl groups in the chelating ligands are both approximately 60° which is slightly less than that observed in **27a** (approximately 64°).

6.4.2 Partial Crystal Structure Determination of *trans*-$[Pd(SeFc)_2(PBu_3)_2]$ (23b)

It was possible to obtain an approximate model for the structure of **23b**. Brown crystals of **23b** were obtained by recrystallisation from toluene/hexane at –20 °C; from these a small crystal of dimensions 0.35 x 0.20 x 0.15 mm was chosen for analysis. Although the diffraction pattern appeared to be good, after a short data collection there was difficulty with the cell determination. The UM F command consistently failed, and the UM TTT command consistently suggested a cell with dimensions: a = 10.48(1) Å, b = 11.11(1) Å, c = 12.04(1) Å, α = 71.9(1)°, β = 63.6(1)°, γ = 82.9(1)°, V = 1194 Å^3, but this cell was based on only ~ 50% of the measured reflections (no matter what threshold intensity was set). A long data acquisition was run, but the situation was the same, although now the cell was proposed with a greater degree of precision (a = 10.478(3) Å, b = 11.112(3) Å, c = 12.044(3) Å, α = 71.88(2)°, β = 63.61(2)°, γ = 82.85(2)°, V = 1193.8 Å^3); it is

worthy of note that the reciprocal lattice is poor. The data were reduced and processed with absorption correction using SADABS and ABSPACK with a shape correction. Attempts to solve by direct methods using SIR 97 and SHELXS 97 failed. The structure was 'solved' using Patterson methods, with the Pd atom assumed to lie on an inversion centre in the P –1 space group (with half a molecule in the asymmetric unit); the VECT command was used to place the Pd vector at the origin. The model was resolved as far as possible with a final R_1 value of approximately 0.16. A second attempt at data reduction using a scan width of 2.0 (the standard width used is 0.8) was attempted, but this failed. The width is the parameter for the amount of the diffraction pattern the program reads at a time: for example, if a pattern has a lot of small, closely spaced reflections, then it is best to use a shorter width so the program will 'see' all of the spots; alternatively, for a poor diffraction pattern, then using a larger width may help to eliminate anomalous reflections. The model is believed to suffer from poor quality data rather than other sorts of errors; this may be resolved by analysis of other crystals, should they become available.

Figure 6.10 shows the structure resolved: thermal ellipsoids are drawn at 20% probability; hydrogen atoms were not included in this model.

Figure 6.10: 23b

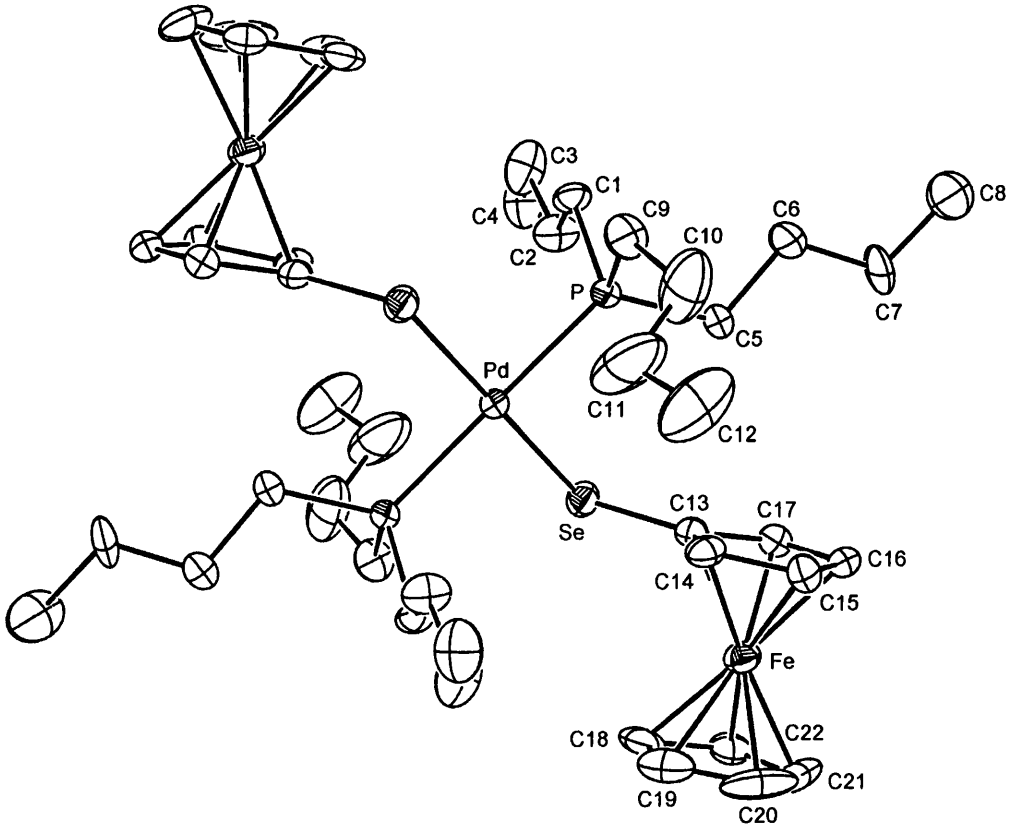

6.5 Crystal Structure Determination of [Pt{SC(R^1)=C(R^2)N=NC(R^1)=C(R^2)S}(PEt_3)] (R^1-R^2 = $(CH_2)_5$) (8b)

The high solubility of **8b** in all solvents made its recrystallisation difficult, but it was possible to obtain small dark orange crystals by recrystallisation from ethanol at –20 °C. From these a rhombohedron of dimensions 0.30 x 0.20 x 0.30 mm was selected for analysis. The diffraction pattern exhibited closely spaced spots; this suggested the presence of a long cell axis, or possibly a poor quality crystal. After a short data collection the UM TTT command suggested a monoclinic cell with dimensions: a = 12.91(1) Å, b = 10.24(1) Å, c = 17.79(1) Å, α = 90.0°, β = 99.1(1)°, γ = 90.0°, V = 2318 Å^3. A long data acquisition was carried out and the UM TTT command proposed the original cell (albeit slightly more refined) and a cell three times as big, with dimensions: a = 12.922(12) Å, b = 10.247(1) Å, c = 52.957(5) Å, α = 90.00°, β = 94.82(1)°, γ = 90.00°, V = 6987 Å^3. A data reduction according to the first cell was carried out, but all subsequent attempts at structure solution using these data failed. It was decided that the larger cell may be correct (it correlates with the closely spaced spots), and a second long data collection was carried out with the CCD detector set at a distance of 80 mm (standard setting: 50 mm); an increased detector distance increases the distance between spots in the diffraction pattern, making it easier for the program to distinguish individual spots. Applying the UM TTT command to these data gave the larger cell, although the dimensions differ slightly: a = 12.912(1) Å, b = 10.241(1) Å, c = 52.886(1) Å, α = 90.00°, β = 94.84(1)°, γ = 90.00°, V = 6968.7 Å^3. Data reduction was carried out and absorption correction processing carried out using SADABS and ABSPACK with and without a shape correction. The structure was solved by direct methods using SIR 97, and refined using SHELXL 97, with the SADABS corrected data giving the best result. There was found to be no extinction present, and data from a reduction with a scan width of 1.2 (compared to 0.8) gave no improvement. The space group is P 2_1/c with three independent molecules in the asymmetric unit (12 in the unit cell). There was found to be disorder in the C_7 ring of one of the molecules; it was necessary to refine this as two independent and complementary

rings with several geometric restraints. It was also necessary to apply restraints to S-C, N-C and C-C bonds, due to the large thermal motion present. Hydrogen atoms were added in calculated positions and were constrained; an attempt to allow free rotation of methyl groups (using code 137 in SHELXL 97) offered no improvement.

Table 6.9 shows the crystallographic data for **8b** and figure 6.11 shows the crystal structure(s). The figure shows the molecule with disorder in the C_7 ring (thermal ellipsoids 10%) and one of the molecules with no disorder (thermal ellipsoids 20%); hydrogen atoms are omitted for clarity.

Table 6.9: Crystallographic data for **8b**

Empirical formula	$C_{20}H_{35}N_2PS_2Pt$
Formula weight	593.68
Crystal system	monoclinic
Space group	P 2_1/c
a/Å	12.922(1)
b/Å	10.247(1)
c/Å	52.957(5)
α/°	90.00
β/°	94.82(1)
γ/°	90.00
V/Å	3070.2(6)
Z	4
F(000)	3528
D_{calc} (g cm^{-3})	1.693
μ (Mo-K_α/mm^{-1})	6.280
Temperature (K)	293
Reflections collected	86055
Independent reflections	14060
θ Range (°)	3.90-26.37
Reflect. with $I > 2\sigma(I)$	9885
No. of parameters	770
R_1; wR_2 [$I > 2\sigma(I)$]	0.0627; 0.1352
R_1; wR_2 (all data)	0.0885; 0.1468
GoF	1.088

Figure 6.11: 8b

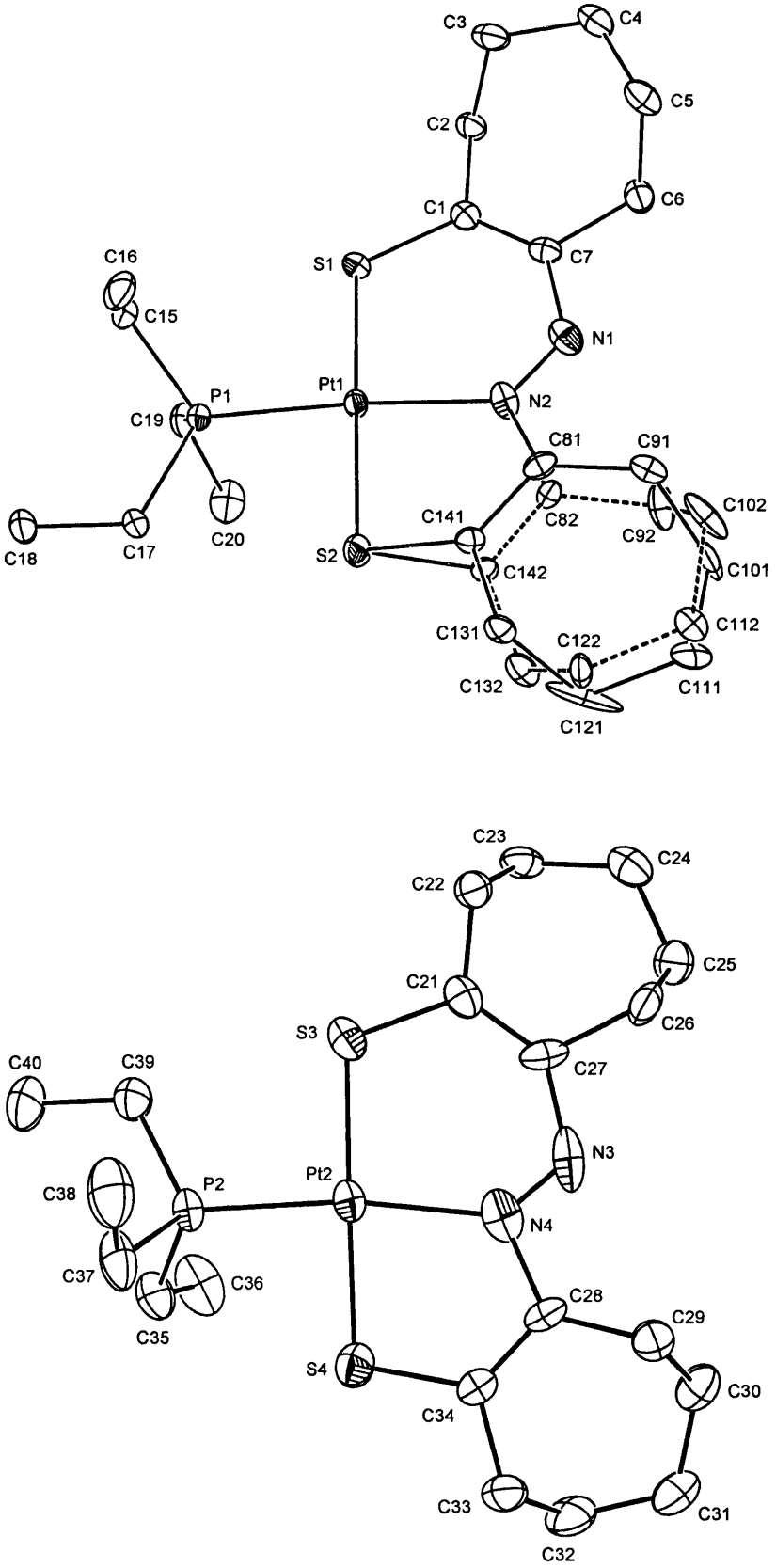

One interesting feature, shown in figure 6.12, is the configuration of the C_7 rings in the three molecules of the asymmetric unit. Viewing these molecules from the side shows one to have a 'boat' conformation, one to have a 'chair' conformation, and in the molecule with a disordered ring both conformations are observed. It is important to note that the figure does not reflect the relative orientation of these molecules in the asymmetric unit.

Table 6.10 shows some selected bond lengths and angles of **8b.** Because there are three slightly different molecules in the asymmetric unit there are three sets of data, molecules I, II and III; note that molecule I contains the disordered C_7 ring, which has been considered as two rings i and ii. Data for **9b** have also been included for comparitive purposes.

The molecule consists of a PtS_2NP core which is approximately square planar as would be expected, with the phosphine *trans-* to the platinum-bound nitrogen of the ligand. The square plane is slightly asymmetric with an average difference between P-Pt-S angles of 2.92° within each molecule, probably a result of the shape of the ligand. There are two possible orientations of the ligand, dependent on which nitrogen is coordinated to platinum; the ratio of these in the crystal of **9b** analysed was found to be 2:1. A similar property has been observed for the analogous palladium species $[Pd\{SeC(R^1)=C(R^2)N=NC(R^1)=C(R^2)Se\}(PBu_3)]$ (R^1-R^2 = $(CH_2)_4$),[116] for which the structure was resolved showing both possible orientations of the ligand. The twelve atoms associated with the π-system of the ligand (SC(C)=C(C)-N=N-C(C)=C(C)S) are not coplanar, as was observed for the π-system of $[Pd\{SeC(R^1)=C(R^2)N=NC(R^1)=C(R^2)Se\}(PBu_3)]$. The Pt-S(2) bonds are approximately 0.04 Å longer than Pt-S(1); this is comparable to the situation in the complex $[Pt\{SeC(COOEt)=C(Me)N=NC(Me)=C(COOEt)Se\}(PPh_3)]$,[118] where the Pt-Se bond in the 5-membered ring is approximately 0.05 Å longer than the Pt-Se bond in the 6-membered ring. This is probably a result of the strain in the 5-membered ring, preventing the sulphur atom from getting as close to platinum, as it can in the 6-membered ring. The average Pt-P and Pt-N(2) distances of 2.259 and 2.080 Å are comparable to those of

Figure 6.12: Different conformations of **8b** in the asymmetric unit

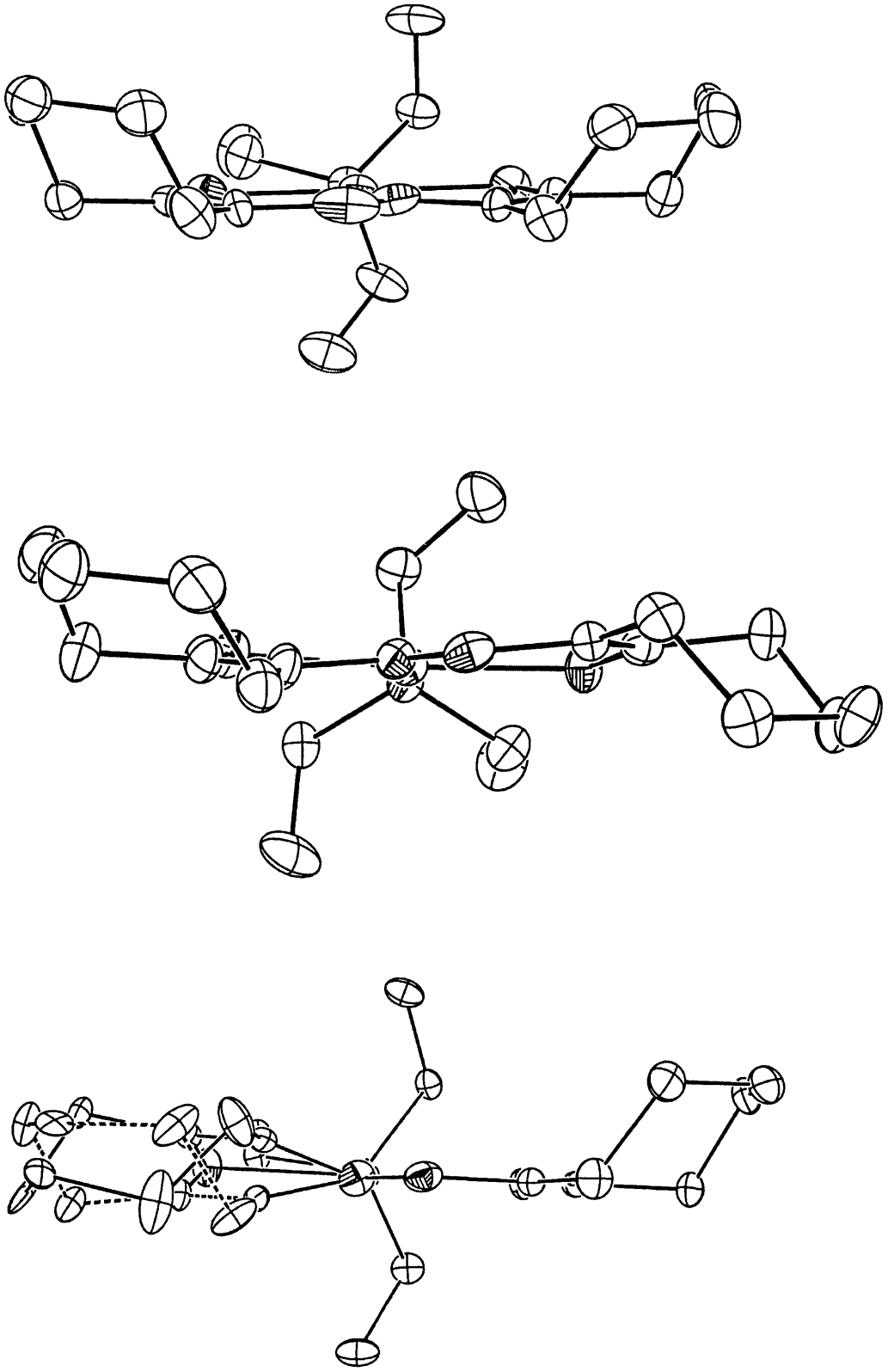

Table 6.10: Selected bond lengths and angles of **8b** (**I**, **II**, and **III**), and **9b***

Compound	**I**	**II**	**III**	**9b**
Bond lengths (Å)				
Pt-S (1)	2.234(3)	2.223(4)	2.227(3)	2.228(2)
Pt-S (2)	2.261(3)	2.254(4)	2.279(3)	2.271(2)
Pt-P	2.257(3)	2.259(3)	2.261(3)	2.258(1)
Pt-N(2)	2.092(1)	2.120(11)	2.057(8)	2.079(4)
N(1)-N(2)	1.214(13)	1.181(13)	1.253(11)	1.252(6)
S(1)-C(1)	1.699(10)	1.705(10)	1.700(9)	1.689(5)
S(2)-C(14)	1.716(16)i/1.731(15)ii	1.717(10)	1.711(10)	1.719(6)
N(1)-C(7)	1.454(8)	1.463(8)	1.450(7)	1.385(7)
N(2)-C(8)	1.463(8)i/1.464(8)ii	1.467(8)	1.456(7)	1.438(7)
C(1)-C(7)	1.344(15)	1.358(15)	1.342(13)	1.368(7)
C(8)-C(14)	1.378(32)i/1.359(25)ii	1.362(15)	1.334(15)	1.344(8)
Bond angles (°)				
S(1)-Pt-S(2)	179.39(11)	178.75(12)	176.35(12)	177.34(6)
S(1)-Pt-P	88.34(10)	92.47(12)	90.40(10)	92.12(6)
S(1)-Pt-N(2)	96.14(30)	96.22(29)	94.81(22)	94.13(13)
S(2)-Pt-P	92.23(10)	88.77(12)	91.04(10)	88.67(6)
S(2)-Pt-N(2)	83.29(30)	82.55(29)	83.92(22)	85.18(13)
P-Pt-N(2)	175.51(30)	171.26(29)	174.14(23)	173.41(12)
Pt-S(1)-C(1)	109.14(45)	108.57(47)	109.86(39)	110.48(20)
Pt-S(2)-C(14)	98.78(68)i/100.85(61)ii	101.38(42)	98.64(40)	98.40(20)
Pt-N(2)-N(1)	130.39(92)	134.05(90)	132.49(64)	131.34(37)
Pt-N(2)-C(8)	117.17(1.22)i/116.42(94)ii	119.36(80)	117.78(67)	115.93(36)
S(1)-C(1)-C(7)	126.96(94)	124.76(99)	127.94(83)	127.12(43)
C(7)-N(1)-N(2)	123.71(1.11)	117.49(1.04)	123.00(81)	124.60(48)
N(1)-N(2)-C(8)	108.46(1.41)i/112.64(1.19)ii	106.56(1.07)	109.68(83)	112.47(46)
N(2)-C(8)-C(14)	112.57(1.75)i/116.87(1.34)ii	112.70(1.00)	114.76(93)	117.32(49)
S(2)-C(14)-C(8)	123.78(1.35)i/120.10(1.19)ii	123.90(83)	123.95(81)	123.03(42)

* In the diagram of **9b** the numbering differs (due to different times of analysis). The following list shows the atom number in the table with the atom number in the figure in parentheses: S1(S2), C1(C8), C7(C9), N1(N2), N2(N1), C8(C2), C14(C1), S2(S1).

[Pt{SeC(COOEt)=C(Me)N=NC(Me)=C(COOEt)Se}(PPh_3)] (2.260(1) and 2.071(5) Å respectively). The average N(1)-N(2) distances of 1.230 Å are shorter (*cf* 1.295(7) Å); they also shorter than the reported N=N distances for [Pd{SeC(R^1)=C(R^2)N=NC(R^1)=C(R^2)Se}(PBu_3)] (R^1-R^2 = $(CH_2)_4$) of 1.29(3) and 1.26(4) Å. The average Pt-S bond lengths of 2.226 and 2.265 Å are of a comparable length to those in the similar complex [Pt{PhSNC(MeC_6H_4)N-NC(MeC_6H_4)NSPh}(PPh_3)] (2.266(3) Å).[229]

6.6 Crystal Structure Determination of [PtCl{FcSe(CH$_2$)$_3$Se(CH$_2$)$_3$SeFc}][PF$_6$]

The compound **[PtCl{FcSe(CH$_2$)$_3$Se(CH$_2$)$_3$SeFc}][PF$_6$]** was prepared and recrystallised by Su Jing as reported in her PhD thesis.[251] Recrystallisation by ether diffusion into a solution of **[PtCl{FcSe(CH$_2$)$_3$Se(CH$_2$)$_3$SeFc}][PF$_6$]** in acetone gave orange plates, from which a smaller plate of dimensions 0.48 x 0.34 x 0.04 mm was cut and analysed. The diffraction pattern was good; after a short data acquisition the UM F command proposed a monoclinic cell with dimensions: a = 20.01(1) Å, b = 7.62(1) Å, c = 20.18(1) Å, α = 90.0°, β = 97.6(1)°, γ = 90.0°, V = 3051 Å^3. A long data acquisition was carried out and the UM F command proposed the same cell (albeit slightly refined); the UM TTT command proposed a different cell, but in view of the reliability of UM F (at the time of analysis) compared to UM TTT, this was ignored. The data were reduced and processed with absorption correction using SADABS and ABSPACK with and without a shape correction. The structure was solved by direct methods using SIR 97 and refined using SHELXL 97; it was found that the ABSPACK data with a shape correction gave the best results. There was found to be a small extinction, which was corrected (using EXTI command with a final value of 0.000374); it was also necessary to eliminate one reflection (*hkl* = -3 0 23), to damp oscillations in the model. In addition it was necessary to apply soft restraints to the anisotropic thermal parameters of four ferrocenyl carbons. The space group is P 2$_1$/c with one [PtCl{FcSe(CH$_2$)$_3$Se(CH$_2$)$_3$SeFc}]$^+$ cation and PF$_6^-$ in the asymmetric unit. All non-hydrogen atoms were refined anisotropically; hydrogens were added in their calculated positions and restrained.

Table 6.11 shows the crystallographic data for **[PtCl{FcSe(CH$_2$)$_3$Se(CH$_2$)$_3$SeFc}][PF$_6$]**. Figure 6.13 shows the crystal structure (cation only); thermal ellipsoids are drawn at 30% probability and hydrogen atoms are omitted for clarity.

Table 6.11: Crystallographic data for compound **[PtCl{FcSe(CH$_2$)$_3$Se(CH$_2$)$_3$SeFc}][PF$_6$]**

Empirical formula	$C_{26}H_{30}ClFe_2Se_3PtPF_6$
Formula weight	1066.59
Crystal system	monoclinic
Space group	P $2_1/c$
a/Å	20.049(2)
b/Å	7.631(1)
c/Å	20.181(2)
α/°	90.00
β/°	97.54(1)
γ/°	90.00
V/Å	3060.9(6)
Z	4
F(000)	2016
D_{calc} (g cm^{-3})	2.315
μ (Mo-K$_\alpha$/mm^{-1})	9.255
Temperature (K)	293
Reflections collected	41961
Independent reflections	6203
θ Range (°)	4.06-26.37
Reflect. with $I > 2\sigma(I)$	5182
No. of parameters	362
R_1; wR_2 [$I > 2\sigma(I)$]	0.0480; 0.1045
R_1; wR_2 (all data)	0.0603; 0.1142
GoF	1.124

Table 6.12 shows some selected bond lengths and angles for **[PtCl{FcSe(CH$_2$)$_3$Se(CH$_2$)$_3$SeFc}][PF$_6$]**. As expected the $PtSe_3Cl$ core is square planar, although it is slightly distorted. The Pt-Se bond *trans*- to Cl is slightly shorter (2.370(1) Å) than the Pt-Se bonds *cis*- to Cl (average 2.415 Å); this is attributed to SeR having a greater *trans*-effect than Cl^-, possibly due to its greater π-acceptor properties. This effect is also observed in the cation $[(PdCl)_2([24]aneSe_6)]^{2+}$,[61] although the Pd-Se$_{cis}$ bond lengths are slightly longer (avg. Pd-Se$_{cis}$ = 2.428 Å, avg. Pd-Se$_{trans}$ = 2.368 Å). The Pt-Se$_{trans}$ bond lengths are similar to the Pt-Se bond lengths found in $[Pt([16]aneSe_4)]^{2+}$ (avg. 2.419 Å).[60] The Se-C bond lengths of the aliphatic part of the ligand are fairly consistent (avg. 1.963 Å) and are similar to those found in $[(PdCl)_2([24]aneSe_6)]^{2+}$ (avg 1.95 Å). The Se-C bonds lengths of the ferrocenyl part of the ligand are shorter (avg. 1.902 Å). There is a deviation from the ideal square planar geometry, probably as a result of the shape of the ligand; the Se(1)-Pt-Se(3)

Figure 6.13: $[PtCl\{FcSe(CH_2)_3Se(CH_2)_3SeFc\}]^+$

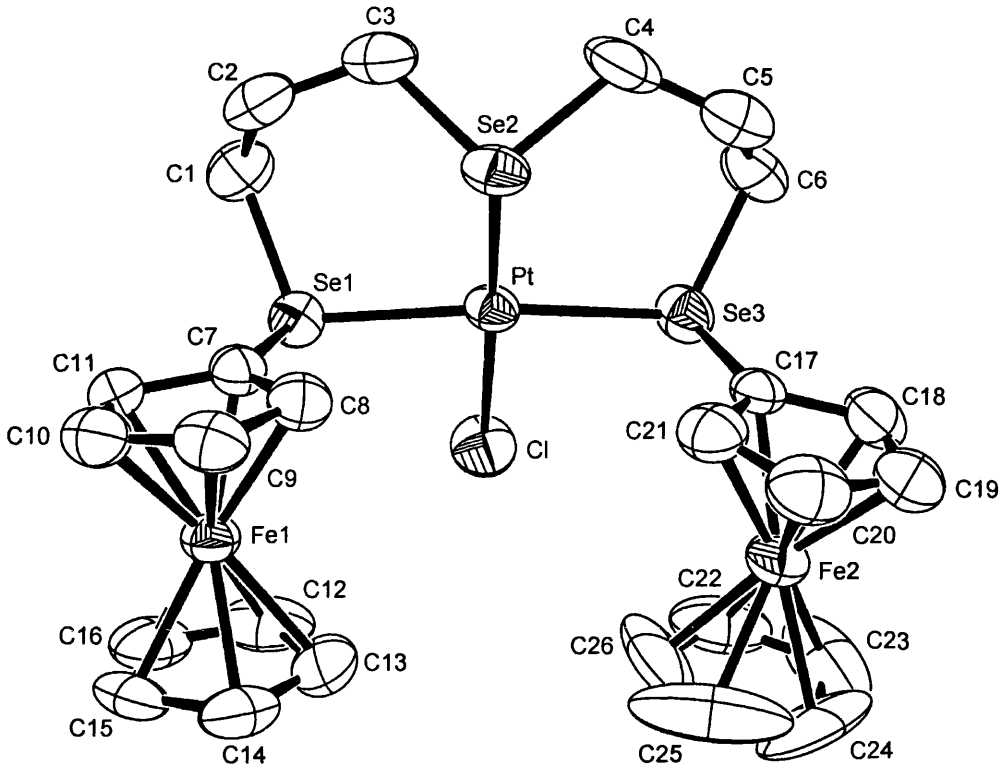

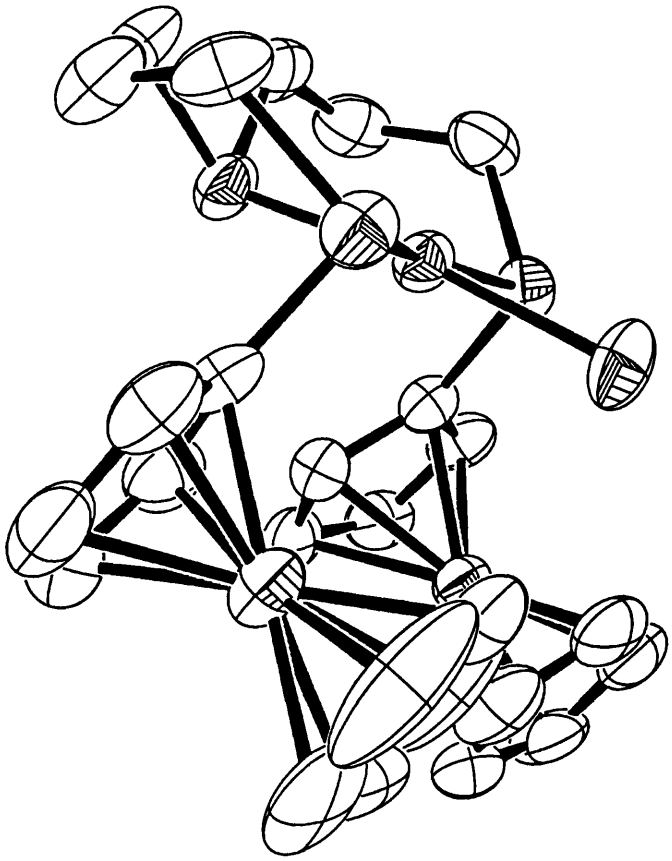

Table 6.12: Selected bond lengths and angles for **[PtCl{FcSe(CH$_2$)$_3$Se(CH$_2$)$_3$SeFc}][PF$_6$]**

Bond lengths (Å)	
Pt-Se(1)	2.412(1)
Pt-Se(2)	2.3701)
Pt-Se(3)	2.416(1)
Pt-Cl	2.316(2)
Se(1)-C(1)	1.960(9)
Se(1)-C(7)	1.901(8)
Se(2)-C(3)	1.959(10)
Se(2)-C(4)	1.971(9)
Se(3)-C(6)	1.965(10)
Se(3)-C(17)	1.903(9)
C(1)-C(2)	1.489(13)
C(2)-C(3)	1.515(14)
C(4)-C(5)	1.493(15)
C(5)-C(6)	1.496(16)
Bond angles (°)	
Se(1)-Pt-Se(2)	94.17(3)
Se(1)-Pt-Se(3)	167.77(3)
Se(1)-Pt-Cl	83.90(7)
Se(2)-Pt-Se(3)	97.40(3)
Se(2)-Pt-Cl	172.96(7)
Se(3)-Pt-Cl	85.08(7)
Pt-Se(1)-C(1)	106.72(30)
Pt-Se(1)-C(7)	107.17(23)
Pt-Se(2)-C(3)	108.08(30)
Pt-Se(2)-C(4)	110.10(35)
Pt-Se(3)-C(6)	110.11(33)
Pt-Se(3)-C(17)	106.05(24)
Se(1)-C(1)-C(2)	115.63(59)
Se(2)-C(3)-C(2)	115.37(62)
Se(2)-C(4)-C(5)	114.72(73)
Se(3)-C(6)-C(5)	115.80(72)

angle is significantly less than 180° (167.77(3)°), and the Se(1)-Pt-Se(2) and Se(2)-Pt-Se(3) angles deviate significantly from 90° (94.17(3) and 97.40(3)° respectively). Similar effects are observed in $[(PdCl)_2([24]aneSe_6)]^{2+}$ (the equivalent Se(1)-Pt-Se(3) angle is 170.3° (avg), the other Se-Pt-Se angles lie in the range 90.7 to 97.8°), whereas in $[Pt([16]aneSe_4)]^{2+}$ the platinum has an almost square planar geometry (the equivalent Se(1)-Pt-Se(3) angle *is* 180°, the other Se-Pt-Se angles lie in the range 88.8 to 91.2°); this is attributed to the high symmetry of the $[16]aneSe_4$ ligand.

6.7 Crystal Structure Determinations of $FcSe(CH_2)_3SeFc$ and $[M\{FcE(CH_2)_3EFc\}(CO)_4]$

The compounds **$FcSe(CH_2)_3SeFc$** and **$[M\{FcE(CH_2)_3EFc\}(CO)_4]$** (M = Mo, E = Se; M = Cr, W, E = Te) were synthesised and recrystallised by Su Jing as reported in her PhD thesis.[251]

6.7.1 Crystal Structure Determination of $FcSe(CH_2)_3SeFc$

Pale yellow plates of **$FcSe(CH_2)_3SeFc$** were obtained by ether diffusion into an acetone solution of $[Cr\{FcSe(CH_2)_3SeFc\}(CO)_4]$ (it was originally intended to obtain crystals of this compound, not the ligand); from one of these plates a fragment with dimensions 0.60 x 0.40 x 0.10 mm was cut and analysed. After a short data acquisition, both the UM F and UM TTT commands suggested a triclinic cell with dimensions: a = 5.85(1) Å, b = 12.08(2) Å, c = 15.89(1) Å, α = 108.2(1)°, β = 94.1(1)°, γ = 92.1(1)°, V = 1061 Å^3. A long data acquisition was carried out, after which the same cell was suggested (albeit slightly refined). The data were reduced according to this cell with absorption correction processing by SADABS and ABSPACK without a shape correction. The structure was solved by direct methods using SIR 97, with refinement using SHELXL 97; the SADABS data gave better results and were used in the final refinement. There was found to be no extinction. It was necessary to apply restraints to all C-C bonds, but this had no adverse effects on the R values. The space group is P -1 with one molecule in the asymmetric unit; the initial solution gave an asymmetric unit containing the $FcSe(CH_2)_3Se$ unit of one molecule and the Fc unit of the other. This was resolved by translating the Fc unit by applying the symmetry operation -x, -y, -z. All non-hydrogen atoms were anisotropically refined; hydrogen atoms were added in calculated positions and were constrained.

Table 6.13 shows the crystallographic data for **$FcSe(CH_2)_3SeFc$.** Figure 6.14 shows the crystal structure; thermal ellipsoids are drawn at 30% probability.

Table 6.13: Crystallographic data for compound **$FcSe(CH_2)_3SeFc$**

Empirical formula	$C_{23}H_{24}Fe_2Se_2$
Formula weight	570.04
Crystal system	triclinic
Space group	P -1
a/Å	5.875(1)
b/Å	12.077(2)
c/Å	15.905(2)
α/°	108.13(1)
β/°	94.07(1)
γ/°	92.25(1)
V/Å	1067.5(3)
Z	2
F(000)	564
D_{calc} (g cm^{-3})	1.773
μ (Mo-K_α/mm^{-1})	4.774
Temperature (K)	293
Reflections collected	10574
Independent reflections	4281
θ Range (°)	4.33-26.37
Reflect. with $I > 2\sigma(I)$	2220
No. of parameters	248
R_1; wR_2 [$I > 2\sigma(I)$]	0.0541; 0.1231
R_1; wR_2 (all data)	0.0877; 0.1371
GoF	0.870

Some selected bond lengths and angles of **$FcSe(CH_2)_3SeFc$** are shown in table 6.14. It can be seen that the molecule is not completely symmetrical, with significant differences in the Se-C distances of the aliphatic chain (1.995(7) and 1.979(6) Å), although the Se-C distances for the Fc groups differ less (1.872(6) and 1.879(6) Å), and as expected are shorter.

Figure 6.14: $FcSe(CH_2)_3SeFc$

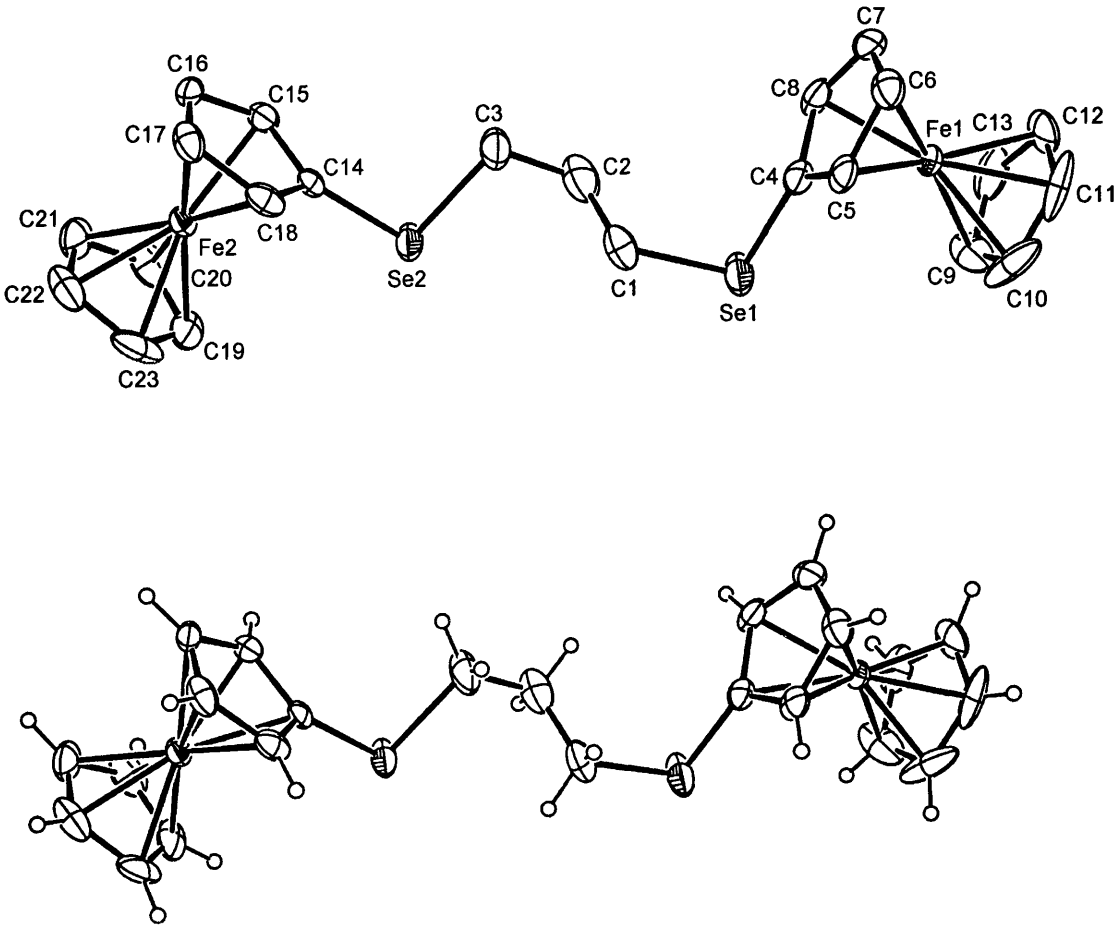

Table 6.14: Selected bond lengths and angles for **$FcSe(CH_2)_3SeFc$**

Bond lengths (Å)	
Se(1)-C(1)	1.995(7)
Se(2)-C(3)	1.979(6)
Se(1)-C(4)	1.872(6)
Se(2)-C(14)	1.879(6)
Bond angles (°)	
C(1)-Se(1)-C(4)	97.32(30)
C(3)-Se(2)-C(14)	97.73(27)

6.7.2 Crystal Structure Determinations of [M{FcE(CH$_2$)$_3$EFc}(CO)$_4$]

The crystal structure determinations of **[M{FcE(CH$_2$)$_3$EFc}(CO)$_4$]** (M = Mo: E = Se; M = Cr, W: E = Te) were relatively straightforward, as it was possible to use the model from a previous determination of [Mo{FcTe(CH$_2$)$_3$TeFc}(CO)$_4$]. The model was of a monoclinic P 2_1/c unit cell with approximate dimensions: a = 15 Å, b = 12 Å, c = 15 Å, α = 90°, β = 102°, γ = 90°, V = 2800 Å^3, with one molecule of [Mo{FcTe(CH$_2$)$_3$TeFc}(CO)$_4$] in the asymmetric unit.

Dark orange crystals of **[Mo{FcSe(CH$_2$)$_3$SeFc}(CO)$_4$]** were obtained by ether diffusion into an acetone solution of **[Mo{FcSe(CH$_2$)$_3$SeFc}(CO)$_4$]**; from these a prism with dimensions 0.60 x 0.50 x 0.30 mm was chosen for analysis. After a short data collection the UM TTT command proposed an orthorhombic unit cell with dimensions: a = 18.47(1) Å, b = 23.83(2) Å, c = 12.46(1) Å, α = 90.0°, β = 90.0°, γ = 90.0°, V = 5484 Å^3. After a long data acquisition the same cell was proposed, but this turned out to be unsuitable, mainly due to problems with systematic absences. The data were revisited and using the UM F command with a threshold limit of 10,000 gave the correct cell: a = 15.030(3) Å, b = 12.468(3) Å, c = 15.066(3) Å, α = 90.00°, β = 104.46(2)°, γ = 90.00°, V = 2733.9 Å^3. The data were reduced according to this cell with absorption correction processing using SADABS. Application of the model to the SADABS-corrected data and refinement using SHELXL 97 quickly gave a low R value. It was necessary to correct for extinction (final value – 0.001986); all non-hydrogen atoms were anisotropically refined; hydrogen atoms were added in calculated positions, riding. Figure 6.15 shows the structure of **[Mo{FcSe(CH$_2$)$_3$SeFc}(CO)$_4$]**; thermal ellipsoids are drawn at 30% probability; hydrogen atoms are omitted for clarity. The crystal data are shown in table 6.15.

Orange crystals of **[Cr{FcTe(CH$_2$)$_3$TeFc}(CO)$_4$]** were obtained by ether diffusion into an acetone solution of **[Cr{FcTe(CH$_2$)$_3$TeFc}(CO)$_4$]**; from these a prism with dimensions 0.40 x 0.40 x 0.25 mm was cut from a larger crystal and analysed. After a short data collection the UM TTT command again proposed an orthorhombic cell with the dimensions: a = 18.86(1) Å, b = 23.96(1) Å, c = 12.39(1) Å, α = 90.0°, β = 90.0°, γ = 90.0°, V = 5595 Å^3. The UM F command, on the other hand proposed the monoclinic cell: a = 15.18(1) Å, b = 12.39 (1) Å, c = 15.31(3) Å , α = 90.00°, β =

103.6(1)°, γ = 90.00°, V = 2798 Å^3. A long data acquisition was carried out. Data reduction based on the orthorhombic cell resulted in an unacceptable R_{int} value of 0.5, so this route was not pursued. Data reduction according to the monoclinic unit cell was carried out, with absorption correction processing using SADABS and ABSPACK without a shape correction. The data were applied to the model with refinement by SHELXL 97; as with **[Mo{FcSe(CH$_2$)$_3$SeFc}(CO)$_4$]** the SADABS data gave the best results. There were found to be no extinction effects; all non-hydrogen atoms were anisotropically refined; hydrogen atoms were added in calculated positions, riding. The structure is shown in figure 6.16: thermal ellipsoids are drawn at 30% probability; hydrogen atoms are omitted for clarity. The crystal data are shown in table 6.15.

Dark orange crystals of **[W{FcTe(CH$_2$)$_3$TeFc}(CO)$_4$]** were obtained by ether diffusion into an acetone solution of **[W{FcTe(CH$_2$)$_3$TeFc}(CO)$_4$]**; from these a prism with dimensions 0.30 x 0.20 x 0.15 mm was cut from a larger crystal and analysed. After a short data collection the UM F command proposed the monoclinic cell: a = 15.23(1) Å, b = 12.45(1) Å, c = 15.39(1) Å, α = 90.0°, β = 103.2(1)°, γ = 90.0°, V = 2841 Å^3. A long data acquisition was carried out after which the UM F command proposed the same cell (albeit slightly refined). The data were reduced according to this cell, with absorption correction processing using SADABS and ABSPACK without a shape correction. The data were applied to the model with refinement by SHELXL 97; as in the previous examples the SADABS data gave the best results. No extinction effects were found to be present; all non-hydrogen atoms were anisotropically refined; hydrogens were added in calculated positions, riding. The structure is shown in figure 6.17: thermal ellipsoids are drawn at 30% probability. The crystal data are shown in table 6.15, and selected bond lengths and angles for all three complexes are shown in tables 6.16 and 6.17, along with those for the complex [Mo{FcTe(CH$_2$)$_3$TeFc}(CO)$_4$] (previously determined), for comparative purposes.

Figure 6.15: [Mo{FcSe(CH$_2$)$_3$SeFc}(CO)$_4$]

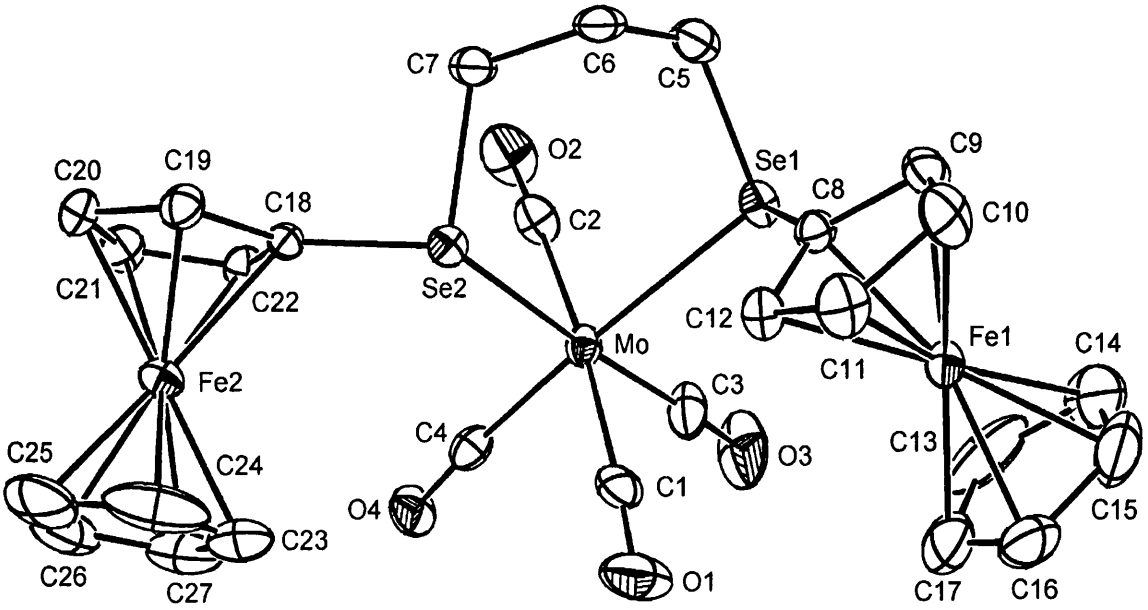

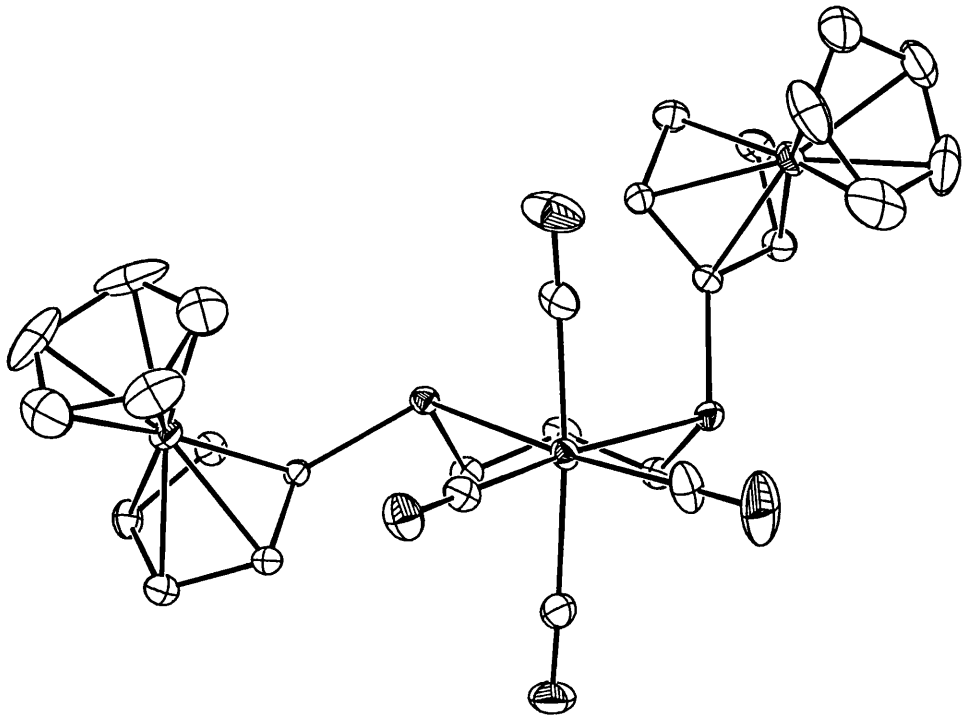

Figure 6.16: [Cr{FcTe(CH$_2$)$_3$TeFc}(CO)$_4$]

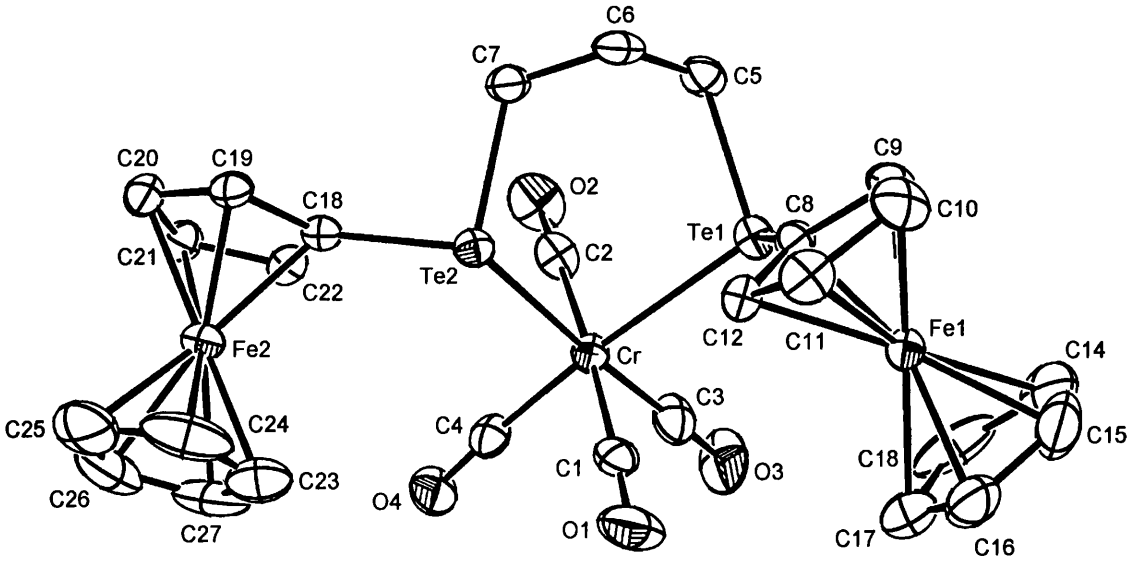

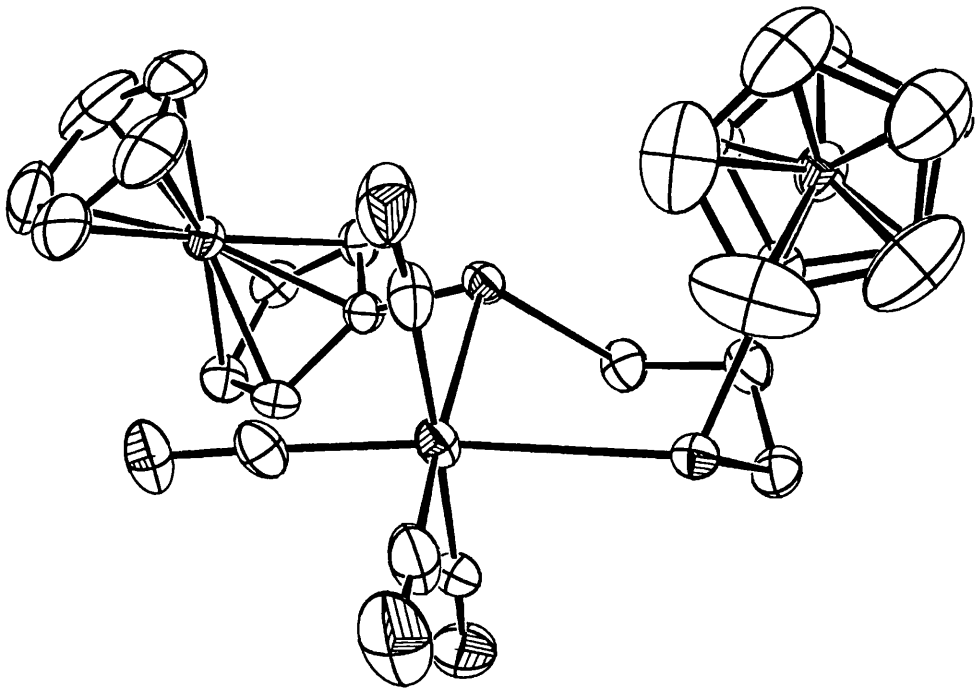

Figure 6.17: [W{FcTe(CH$_2$)$_3$TeFc}(CO)$_4$]

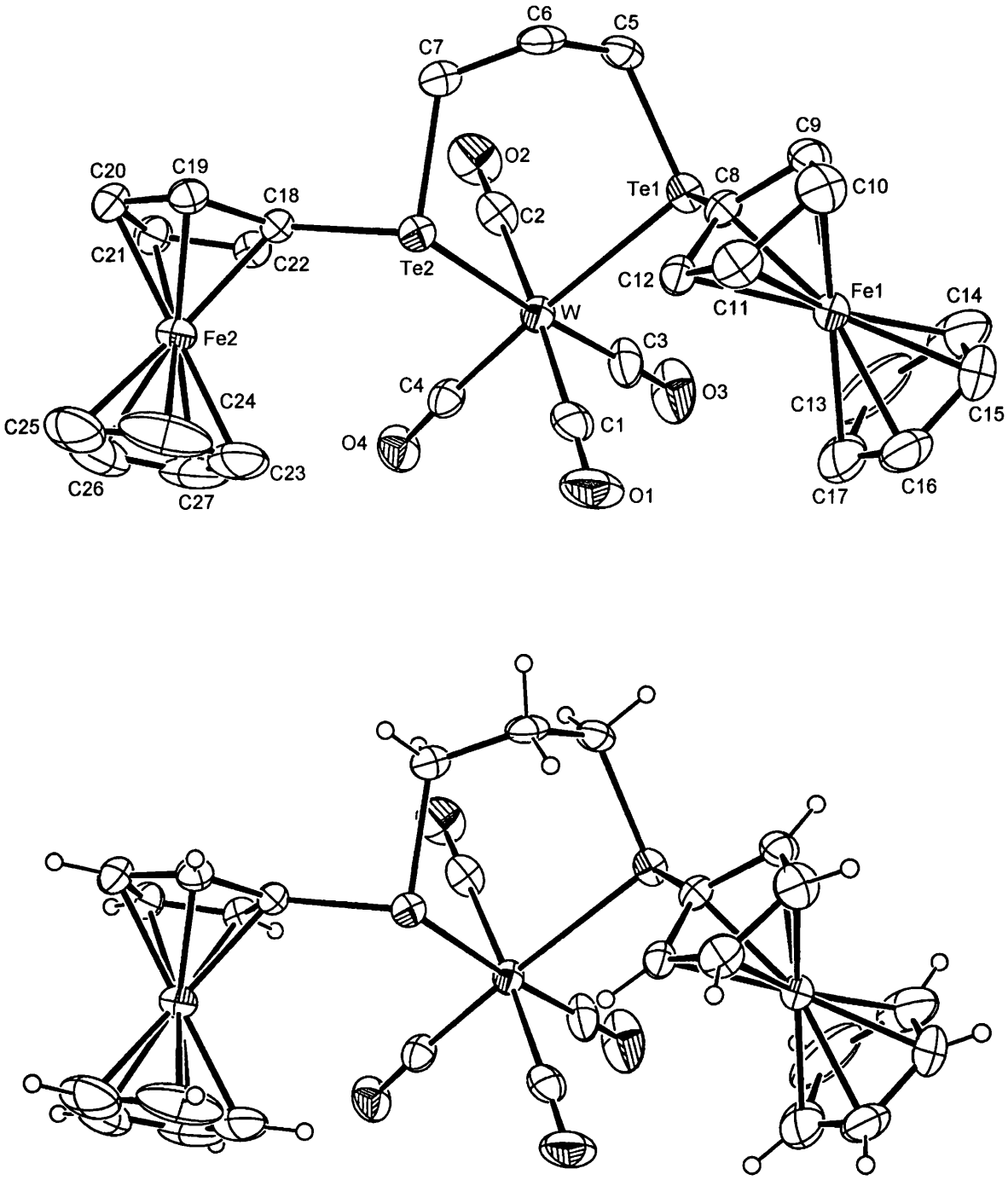

Table 6.15: Crystallographic data for compounds **[M{FcE(CH$_2$)$_3$EFc}(CO)$_4$]** (M = Mo: E = Se; M = Cr, W: E = Te)

Compound	**[Mo{FcSe(CH$_2$)$_3$SeFc}(CO)$_4$]**	**[Cr{FcTe(CH$_2$)$_3$TeFc}(CO)$_4$]**	**[W{FcTe(CH$_2$)$_3$TeFc}(CO)$_4$]**
Empirical formula	$C_{27}H_{24}Fe_2O_4Se_2Mo$	$C_{27}H_{24}Fe_2O_4Te_2Cr$	$C_{27}H_{24}Fe_2O_4Te_2W$
Formula weight	778.02	831.36	963.21
Crystal system	monoclinic	monoclinic	monoclinic
Space group	P 2_1/c	P 2_1/c	P 2_1/c
a/Å	15.030(3)	15.186(1)	15.254(1)
b/Å	12.468(3)	12.369(1)	12.476(1)
c/Å	15.066(3)	15.335(1)	15.396(1)
α/°	90.00	90.00	90.00
β/°	104.46(2)	103.55(1)	103.19(1)
γ/°	90.00	90.00	90.00
V/Å	2733.8(1)	2800.3(3)	2852.7(3)
Z	4	4	4
F(000)	1520	1592	1792
D_{calc} (g cm^{-3})	1.890	1.972	2.243
μ (Mo-K$_\alpha$/mm^{-1})	4.193	3.476	7.061
Temperature (K)	293	293	293
Reflections collected	12969	27464	28246
Independent reflections	5330	5680	5803
θ Range (°)	4.42-26.02	4.30-26.37	2.9-18.8
Reflect. with $I > 2\sigma(I)$	3311	4320	4336
No. of parameters	326	325	326
R_1; wR_2 [$I > 2\sigma(I)$]	0.0480; 0.1045	0.0320; 0.0600	0.0305; 0.0656
R_1; wR_2 (all data)	0.0603; 0.1142	0.0522; 0.0634	0.0428; 0.0688
GoF	0.832	1.015	0.977

Table 6.16: Selected bond lengths (Å) for **[M(FcE(CH$_2$)$_3$EFc)(CO$_4$)]** (M = Mo: E = Se; M = Cr, Mo, W: E = Te)

Compound	[Mo{FcSe(CH$_2$)$_3$SeFc}(CO$_4$)]	[Cr{FcTe(CH$_2$)$_3$TeFc}(CO$_4$)]	[Mo{FcTe(CH$_2$)$_3$TeFc}(CO$_4$)]	[W{FcTe(CH$_2$)$_3$TeFc}(CO$_4$)]
M-C(1)	1.999(5)	1.870(5)	2.009(5)	2.006(7)
M-C(2)	2.033(5)	1.893(5)	2.041(5)	2.039(6)
M-C(3)	1.941(5)	1.818(5)	1.943(5)	1.943(6)
M-C(4)	1.957(5)	1.836(5)	1.967(4)	1.967(6)
C(1)-O(1)	1.141(5)	1.154(5)	1.146(5)	1.151(7)
C(2)-O(2)	1.132(5)	1.140(6)	1.143(5)	1.137(7)
C(3)-O(3)	1.143(5)	1.160(6)	1.155(5)	1.157(7)
C(4)-O(4)	1.147(5)	1.157(5)	1.156(5)	1.153(6)
M-E(1)	2.6649(7)	2.6555(7)	2.7988(8)	2.7903(4)
M-E(2)	2.6751(7)	2.6661(7)	2.8093(8)	2.8013(4)
E(1)-C(5)	1.956(4)	2.165(4)	2.165(4)	2.162(5)
E(2)-C(7)	1.973(4)	2.161(4)	2.170(4)	2.153(5)
E(1)-C(8)	1.900(4)	2.101(4)	2.101(4)	2.098(5)
E(2)-C(18)	1.893(4)	2.088(4)	2.089(4)	2.096(5)

Table 6.17: Selected bond angles (°) for **[M(FcE(CH$_2$)$_3$EFc)(CO$_4$)]** (M = Mo: E = Se; M = Cr, Mo, W: E = Te)

Compound	[Mo{FcSe(CH$_2$)$_3$SeFc}(CO$_4$)]	[Cr{FcTe(CH$_2$)$_3$TeFc}(CO$_4$)]	[Mo{FcTe(CH$_2$)$_3$TeFc}(CO$_4$)]	[W{FcTe(CH$_2$)$_3$TeFc}(CO$_4$)]
E(1)-M-E(2)	86.51(2)	88.75(2)	87.46(3)	87.48(1)
E(1)-M-C(1)	96.21(12)	94.00(13)	94.01(12)	93.87(15)
E(1)-M-C(2)	89.23(13)	88.59(14)	88.47(12)	88.24(16)
E(1)-M-C(3)	88.96(14)	87.17(15)	88.13(13)	87.47(17)
E(1)-M-C(4)	174.05(12)	173.89(14)	174.47(12)	174.40(15)
E(2)-M-C(1)	89.14(14)	88.39(15)	88.69(15)	88.28(18)
E(2)-M-C(2)	90.63(13)	89.12(14)	89.00(13)	89.02(17)
E(2)-M-C(3)	174.66(14)	175.20(16)	175.15(14)	174.48(17)
E(2)-M-C(4)	99.21(12)	97.24(13)	97.88(12)	97.87(15)
M-C(1)-O(1)	174.76(39)	176.32(41)	177.22(40)	176.88(54)
M-C(2)-O(2)	177.82(43)	177.97(44)	179.38(45)	178.44(58)
M-C(3)-O(3)	177.44(44)	178.44(46)	178.55(49)	177.93(55)
M-C(4)-O(4)	175.40(37)	175.29(38)	176.08(36)	176.41(47)
M-E(1)-C(5)	108.93(13)	108.20(12)	107.41(11)	107.54(14)
M-E(2)-C(7)	106.34(13)	105.17(12)	104.23(11)	104.47(15)
M-E(1)-C(8)	113.36(12)	111.78(11)	111.03(10)	111.09(13)
M-E(2)-C(18)	111.04(11)	110.03(10)	108.59(10)	108.41(13)
C(5)-E(1)-C(8)	95.63(17)	92.76(15)	93.07(14)	92.57(18)
C(7)-E(2)-C(18)	94.98(16)	92.00(15)	93.03(15)	92.81(19)

The complexes [M{FcE(CH_2)$_3$EFc}(CO)$_4$] exhibit the expected octahedral geometry about the metal atom, although the octahedron is slightly distorted, probably due to the 'bite angle' of the ligand (the E-M-E angle is on average 87.5°). The C-O distances are affected by the ligand: it is observed that in all of the complexes, the C-O distances *trans-* to the chalcogen are, on average, 0.068 Å longer than the C-O distances *cis-* to the chalcogen atoms. Similar effects have been observed in the complexes *cis*-[W{($MeSeC_5H_4$)$_2$Fe}(CO)$_4$],[252] [Cr{MeSe(CH_2)$_2$SeMe}(CO)$_4$][253] and [W(xyte)(CO)$_4$] (xyte = 1,2-*bis*(methyltelluromethyl)benzene):[254] all M-C bonds *trans-* to a chalcogen are observed to be shorter (on average by 0.063 Å) than the M-C bonds *cis-* to a chalcogen; this is attributed to the chalcogen's weaker *trans-* effect compared with CO. The M-E distances are observed to vary with M and E as expected, so average distances of 2.67, 2.66, and 2.80 Å are observed for Mo-Se, Cr-Te, and M-Te (M = Mo, W) respectively; the similar lengths of Mo-Te and W-Te are attributed the similar atomic radii of Mo and W, due to the lanthanoid contraction.[255] The E-M-E angles are similar in all complexes (average 87.5°), and are similar to the E-M-E angles of *cis*-[W{($MeSeC_5H_4$)$_2$Fe}(CO)$_4$] (86.3°) and [Cr{MeSe(CH_2)$_2$SeMe}(CO)$_4$] (86.59(5)°); a much greater angle is observed in [W(xyte)(CO)$_4$] (95.69(3)°) which is attributed to the rigidity of the xyte ligand. The M-E-$C_{aliphatic}$ angles are also similar in all the complexes with average values of 107.88° (M-E(1)-C(5)) and 104.88° (M-E(2)-C(7)).

6.8 Crystal Structure Determination of *trans*-[$PdCl_2(\eta^1$-$FcSeCH_2SeFc)_2$]

***trans*-[$PdCl_2(\eta^1$-$FcSeCH_2SeFc)_2$]** was synthesised and recrystallised by Su Jing as reported in her PhD thesis.[251] Recrystallisation from DCM/MeCN gave dark brown, rhombohedral crystals, from which a crystal with dimensions 0.40 x 0.40 x 0.25 mm was selected for analysis. Initially a model was determined using Cu-K_α radiation (due to the unavailability of Mo-K_α radiation). After a short data acquisition the UM TTT command proposed a monoclinic cell with dimensions: a = 9.86(1) Å, b = 19.27(1) Å, c = 10.82(1) Å, α = 90.0°, β = 99.2(1)°, γ = 90.0°, V = 2029 Å^3. A full data acquisition was carried out, after which the UM TTT command proposed the same cell (albeit slightly refined). The data were reduced and processed with absorption correction using SADABS and ABSPACK with no shape correction. The structure was solved by direct methods using SIR 97 and refined using SHELXL 97; the refinement was limited by negative temperature factors (due to the use of Cu-K_α radiation). The space group of this model was found to be P 2_1/a with half a molecule in the asymmetric unit; the Pd atom lies on an inversion centre.

At a later date a data acquisition was carried out using Mo-K_α radiation; after both short and full data acquisitions, both the UM TTT and UM F commands proposed the cell given above. The data were reduced with processing for absorption correction by SADABS and ABSPACK without a shape correction. Using the model established above, with these data, it was possible quickly to refine the structure using SHELXL 97 (the SADABS data gave the best result). There was found to be no extinction, but it was necessary to apply a SHEL command due to a high number of unobserved reflections (0.8 < d < 20 Å). The hydrogen atoms were added in calculated positions, and were constrained.

Table 6.17 shows the crystallographic data for ***trans*-[$PdCl_2(\eta^1$-$FcSeCH_2SeFc)_2$]**. Figure 6.18 shows the crystal structure: thermal ellipsoids are drawn at 30% probability; hydrogens are omitted for clarity.

Table 6.17: Crystallographic data for ***trans*-[$PdCl_2(\eta^1$-$FcSeCH_2SeFc)_2$]**

Empirical formula	$C_{21}H_{20}ClFe_2Se_2Pd_{0.5}$
Formula weight	630.64
Crystal system	monoclinic
Space group	P 2_1/a
a/Å	9.851(1)
b/Å	19.226(2)
c/Å	10.791(1)
α/°	90.00
β/°	99.24(1)
γ/°	90.00
V/Å	2017.2(3)
Z	4
F(000)	1224
D_{calc} (g cm^{-3})	2.077
μ (Mo-K_α/mm^{-1})	5.614
Temperature (K)	293
Reflections collected	20154
Independent reflections	4095
θ Range (°)	4.32-26.36
Reflect. with $I > 2\sigma(I)$	3157
No. of parameters	241
R_1; wR_2 [$I > 2\sigma(I)$]	0.0277;0.0600
R_1; wR_2 (all data)	0.0387;0.0638
GoF	0.981

Table 6.18 shows some selected bond lengths and angles of ***trans*-[$PdCl_2(\eta^1$-$FcSeCH_2SeFc)_2$]**. The $PdCl_2Se_2$ core is square planar as would be expected for Pd(II), although it is slightly distorted. The Pd-Se bond lengths of 2.4351(4) Å are very similar to those of *trans*-[$PdCl_2\{(C_4H_3S)SeMe\}_2$] (2.439(2) Å)[30] but longer than the Pd-S bond lengths of *trans*-[$PdCl_2(\eta^1$-$PhSCH_2SPh)_2$] (2.329(1) Å);[36] this is attributed to the greater size of Se compared to S. The Pd-Cl distance of 2.2965(8) Å is similar to that found in *trans*-[$PdCl_2(\eta^1$-$PhSCH_2SPh)_2$] (2.292(1) Å); the Pd-Cl distance in *trans*-[$PdCl_2\{(C_4H_3S)SeMe\}_2$] is slightly shorter (2.263(6) Å). The Se(1)-Pd-Cl angle of 85.93(3)° is approximately 10° less than those of *trans*-[$PdCl_2\{(C_4H_3S)SeMe\}_2$] and *trans*-[$PdCl_2(\eta^1$-$PhSCH_2SPh)_2$] (96.3(2) and 95.3(1)° respectively), although the Se-Pd-Cl angle to the opposite Se atom is 94.07°, which accounts for this discrepancy. The Pd-Se(1)-C(1) and Se(1)-C(1)-Se(2) angles of 102.54(10) and 111.06(16)° are comparable to those

Figure 6.18: $[PdCl_2(\eta^1\text{-}FcSeCH_2SeFc)_2]$

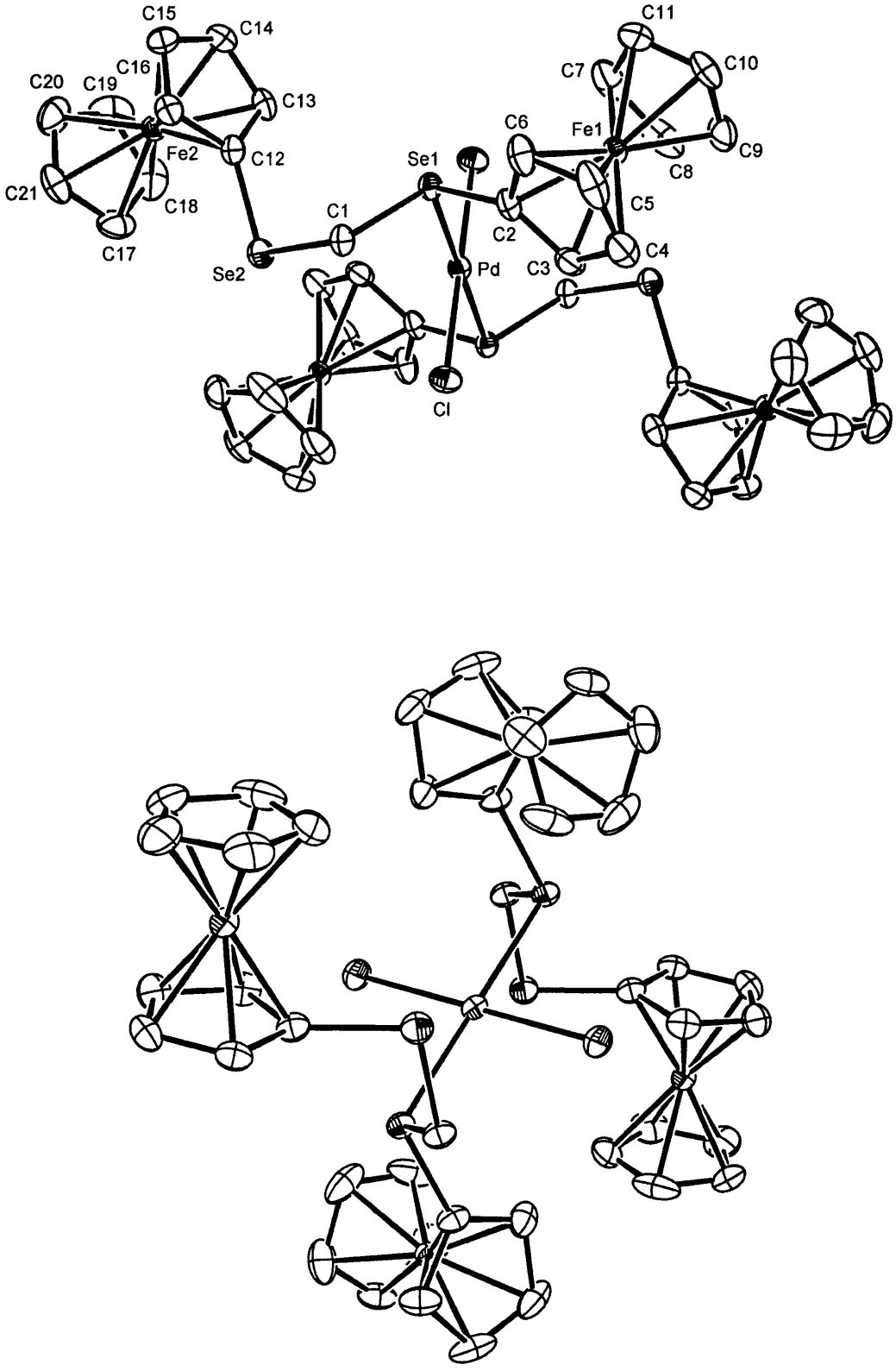

Table 6.18: Selected bond lengths and angles for **[$PdCl_2(\eta^1$-$FcSeCH_2SeFc)_2$]**

Bond lengths (Å)	
Pd-Se(1)	2.4351(4)
Pd-Cl	2.2965(8)
Se(1)-C(1)	1.950(3)
Se(1)-C(2)	1.907(3)
Se(2)-C(1)	1.931(3)
Se(2)-C(12)	1.898(4)
Bond angles (°)	
Se(1)-Pd-Se(1)	180.00(2)
Se(1)-Pd-Cl	85.93(3)
Pd-Se(1)-C(1)	102.54(10)
Pd-Se(1)-C(2)	106.85(11)
Se(1)-C(1)-Se(2)	111.06(16)
C(1)-Se(1)-C(2)	99.36(13)
C(1)-Se(2)-C(12)	100.66(14)

found in *trans*-[$PdCl_2(\eta^1$-$PhSCH_2SPh)_2$] (104.5(1) and 113.2(2)°). The Pd-Se(1)-C(2) angle (106.85(11)°) differs from the same angles in *trans*-[$PdCl_2\{(C_4H_3S)SeMe\}_2$] (101.5(6)°) and *trans*-[$PdCl_2(\eta^1$-$PhSCH_2SPh)_2$] (110.8(1)°); this is attributed to differences in the steric influences of the ligands.

6.9 Partial Crystal Structure Determination of [$PdCl_2${$FcSe(CH_2)_2SeFc$}]

It was possible to obtain a partial structure determination of **[$PdCl_2${$FcSe(CH_2)_2SeFc$}]**; this compound was synthesised and recrystallised by Su Jing as reported in her PhD thesis.[251] Recrystallisation from DCM/MeCN gave small dark brown plates of **[$PdCl_2${$FcSe(CH_2)_2SeFc$}]**; one of these plates of dimensions 0.35 x 0.14 x 0.06 mm was chosen for analysis. After a short data acquisition the UM TTT command suggested several different cells, dependent on the peak threshold selected. A full data acquisition was carried out, after which time the UM TTT command consistently suggested the monoclinic cell: a = 28.552(8) Å, b = 8.524(2) Å, c = 9.621(3) Å, α = 90.0°, β = 107.57(3)°, γ = 90.0°, V = 2232.3 Å^3. The data were reduced according to this cell with absorption correction processing by SADABS and ABSPACK without a shape correction. The structure was solved using SIR 97 and refined as far as possible using SHELXL 97. The SADABS data gave the best results, but the R values remain high; this can probably be attributed to poor data. Initial solution in the space group C c appeared to give the correct result, but this model proved very difficult to refine. It was later established that the correct space group is C 2/c (monoclinic face-centred), with half a molecule in the asymmetric unit and the Pd atom lying on a two-fold rotation axis. Hydrogens were added in calculated positions and constrained. The final R_1 value of 0.13 could not be improved, so, though the model is chemically meaningful, it is not satisfactory from a crystallographic point of view. The model is shown in figure 6.19: thermal ellipsoids are at 30% probability; hydrogens are omitted for clarity,

Figure 6.19: $[PdCl_2\{FcSe(CH_2)_2SeFc\}]$

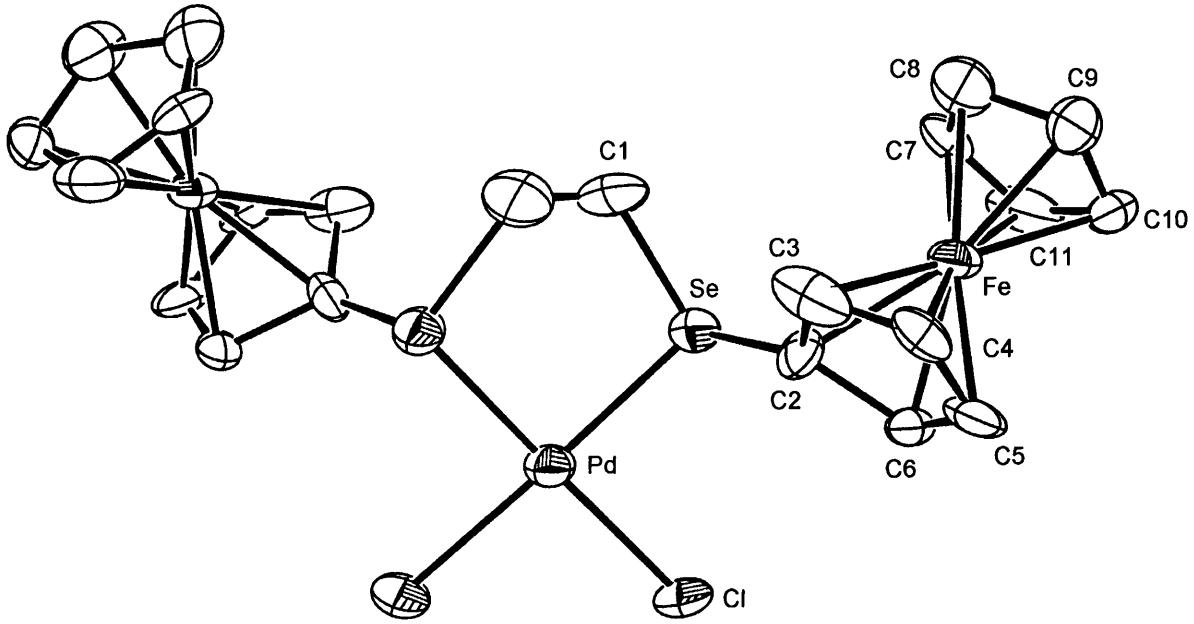

Chapter 7

Experimental Details

7.1 Experimental Details

All reactions were performed using standard Schlenk techniques under an atmosphere of dry argon; the majority of procedures followed were taken from 'Advanced Practical Inorganic and Metalorganic Chemistry'.[256] Dry solvents, when required were distilled over molten potassium (benzene, hexane, THF), molten sodium (1,4-dioxane, toluene, xylene), CaH_2 ($CHCl_3$, DCM, MeCN) or magnesium alkoxide (MeOH, EtOH). Solvents were degassed by repeated boiling under reduced pressure followed by saturation with inert gas.

^1H, ^{13}C and ^{31}P NMR spectra were recorded using a Bruker AC400 with tetramethylsilane as internal standard (^1H, ^{13}C) or 85% phosphoric acid as external standard (^{31}P). ^{77}Se and ^{125}Te NMR spectra were recorded on a Bruker WM250 with dimethyl selenide or dimethyl telluride respectively as external standards. All ^{13}C, ^{31}P, ^{77}Se and ^{125}Te NMR spectra were ^1H decoupled. IR spectra were recorded using a Perkin-Elmer Spectrum One FTIR spectrometer with ATR. UV-visible spectra were recorded on a Unicam UV300 spectrometer using quartz cuvettes; due to the small amounts of pure material available the UV-visible spectral data are subject to an error in the range 1-10%. Mass spectra were recorded by the EPSRC Mass Spectrometry Service Centre using fast atom bombardment (FAB) or electrospray ionisation (ESI).

X-ray structural analyses not reported in chapter 6 were carried out by Prof. Massimo Di Vaira at the University of Florence; crystals were mounted on a glass fibre and analysed using an Oxford Diffraction Xcalibur 3 CCD diffractometer.

Cycloalkeno-1,2,3-selenadiazoles,[92] cycloalkeno-1,2,3-thiadiazoles,[94] *bis*-cycloalkeno-1,4-diselenins,[120] $(FcSe)_2$,[257] $(FcTe)_2$,[258] *bis*-benzo-1,2-diselenin,[129] 2,5-diphenyltellurophene,[235] $[Pt(PPh_3)_4]$,[259] $[PtCl_2(PEt_3)_2]$,[260] $[PtCl_2(PBu_3)]$[261] and $[Pd_2(dba)_3].dba$[262] were synthesised by literature procedures (slightly adapted in some cases). Platinum and palladium salts were obtained on loan from Johnson Matthey plc; $P(i\text{-}C_5H_{11})_3$ and $(PhSe)_2$ were obtained from laboratory sources; PEt_3 and $TlPF_6$ were obtained from Strem Chemicals Inc.; cyclohexanone, cycloheptanone, cyclooctanone, dppm, dppe, dppp, ethene, EtI, $LiBEt_3H$, MeI, naphthalene, PBu_3, $P(OMe)_3$, potassium, selenium, selenophene, sodium and thiophene were obtained from Aldrich Chemical Company. All chemicals were used as supplied.

Standard safety procedures were followed as outlined in the University of Wales Swansea, Chemistry Department safety handbook.

7.2 Synthetic Procedures

Synthesis of 1c, 2c, 3c and 4c

Under argon in a pre-dried Schlenk tube, $[Pt(Se_2C_8H_{12})(PPh_3)_2]$ (50 mg, 0.05 mmol) was slurried in dry toluene (4 mL); the slurry was treated with 1 mL of PEt_3 (**1c**), PBu_3 (**2c**), $P(i\text{-}C_5H_{11})_3$ (**3c**) or $P(OMe)_3$ (**4c**) and stirred at approximately 70 °C for 3 days. After this time a green/yellow solution had formed. This was concentrated *in vacuo* and the residue chromatographically separated on Al_2O_3 with toluene/EtOAc (1:1) elution (**1c** and **2c** only); collection of the green/yellow fraction and subsequent concentration *in vacuo* gave **1c** (green solid, 32 mg, 93% yield) or **2c** (green solid, 40 mg, 90% yield). **3c** and **4c** were isolated as green/yellow oils due to the presence of excess phosphine or phosphite respectively.

Synthesis of 5c, 6c and 7c

Under argon in a pre-dried Schlenk tube, a mixture of $[Pt(Se_2C_8H_{12})(PPh_3)_2]$ (60 mg, 0.06 mmol) and dppm (230 mg, 0.6 mmol), dppe (240 mg, 0.6 mmol) or dppp (250 mg 0.6 mmol) in dry toluene (8 mL) was heated to 90 °C for 4 days. After this time a green solution had formed. This was concentrated *in vacuo,* and the residue chromatographically separated on alumina with toluene/DCM (1:1) elution; collection of the green fraction and subsequent concentration *in vacuo* gave **5c** (green solid, 44 mg, 86% yield), **6c** (green solid, 36 mg, 69% yield) or **7c** (green solid, 36 mg, 68%). Crystals of **5c** suitable for an x-ray diffraction study were obtained from a hexane/DCM solution at –20 °C.

Synthesis of 1a-c and 2a-c

All experiments were carried out according to the following general procedure. Under argon $[PtCl_2(PR_3)_2]$ (0.4 mmol; R = Et, Bu) was taken up in 1,4-dioxane (20 mL) and the solution degassed. This solution was put under an ethene atmosphere and treated dropwise with $NaC_{10}H_8$ (~ 0.12 M solution in THF), complete conversion to $[Pt(C_2H_4)(PR_3)_2]$ being evidenced by the solution holding the green colour for approximately 2-3 minutes before clearing. The ethene atmosphere was replaced with an argon atmosphere, and the reaction mixture was treated with a solution of *bis*-cycloalkeno-1,4-diselenin (0.6 mmol) in degassed toluene (8 mL). The reaction mixture was refluxed for 1 hr after which time it was pale green in colour;

concentration *in vacuo* gave an green oil, which was purified by column chromatography on alumina with a 3:1 mixture of toluene and ethyl acetate. Collection of the pale green band gave **1b,c** and **2b,c** as analytically pure green solids, and **1a** and **2a** as impure products. Yields: **1a**: 201 mg, 75%, **1b**: 218 mg, 80%, **1c**: 192 mg, 69% **2a**: 178 mg, 53%, **2b**: 201 mg, 59%, **2c**: 218 mg, 63%. Crystals of **1b** and **1c** suitable for an x-ray diffraction study were obtained by recrystallisation from toluene/hexane at –20 °C.

Synthesis of 8b,c and 9b,c

All experiments were carried out according to the following general procedure. Under argon $[PtCl_2(PR_3)_2]$ (0.4 mmol; R = Et, Bu) was taken up in 1,4-dioxane (20 mL) and the solution degassed. This solution was put under an ethene atmosphere and treated dropwise with $NaC_{10}H_8$ (~ 0.12 M solution in THF), complete conversion to $[Pt(C_2H_4)(PR_3)_2]$ being evidenced by the solution holding the green colour for approximately 2-3 minutes before clearing. The ethene atmosphere was replaced with an argon atmosphere, and the reaction mixture was treated with a solution of cycloalkeno-1,2,3-thiadiazole (1.2 mmol) in degassed toluene (8 mL). The reaction mixture was refluxed for 1 hr after which time it was deep orange in colour; concentration *in vacuo* gave an orange oil, which was repeatedly purified by column chromatography on alumina with a 1:1 mixture of toluene and hexane. Collection and concentration of the orange band gave **8b,c** and **9b,c** as analytically pure orange solids. Yields (based on Pt): **8b**: 71 mg, 30%, **8c**: 65 mg, 26%, **9b**: 81 mg, 30%, **9c**: 116 mg, 41%. Crystals of **8b** and **9b** suitable for an x-ray diffraction study were obtained by recrystallisation from EtOH at –20 °C.

Synthesis of 10a-c and 11a-c

All experiments were carried out according to the following general procedure. Under argon $[PtCl_2(PR_3)_2]$ (0.4 mmol; R = Et, Bu) was taken up in 1,4-dioxane (20 mL) and the solution degassed. This solution was put under an ethene atmosphere and treated dropwise with $NaC_{10}H_8$ (8 mL of an estimated 0.08 M solution in THF), to give a cloudy white reaction mixture. The ethene atmosphere was replaced with an argon atmosphere, and the reaction mixture was treated with a solution of cycloalkeno-1,2,3-selenadiazole (1.2 mmol) in degassed toluene (8 mL). The reaction mixture was refluxed for 1 hr after which time it was deep purple in colour;

concentration *in vacuo* gave a purple oil, which was repeatedly purified by column chromatography on alumina with a 1:1 mixture of toluene and hexane. Collection and concentration of the purple band gave **10b,c** and **11b,c** as analytically pure solids and **10a**, **11a** as reasonably pure solids. Yields (based on Pt) **10a**: 132 mg, 50%, **10b**: 118 mg, 43%, **10c**: 29 mg, 10%, **11a**: 134 mg, 45%, **11b**: 46 mg, 15%, **11c**: 54 mg, 17%.

Synthesis of 12a

Under argon, $[Pt(PPh_3)_4]$ (200 mg, 0.16 mmol) and cyclohexeno-1,2,3-selenadiazole (50 mg, 0.27 mmol) were taken up in dry toluene (5 mL), giving a yellow slurry which was stirred at room temperature for 4 days. After this time a purple solution had formed; concentration *in vacuo*, followed by column chromatography (Al_2O_3/toluene) and collection and concentration of the purple band gave **12a** as a purple solid (21 mg, 16% yield).

Synthesis of 13a-c and 14a-c

All experiments were carried out according to the following general procedure. Under argon $[PtCl_2(PR_3)_2]$ (0.4 mmol; R = Et, Bu) was taken up in 1,4-dioxane (20 mL) and the solution degassed. This solution was put under an ethene atmosphere and treated dropwise with $NaC_{10}H_8$ (~ 0.12 M solution in THF), complete conversion to $[Pt(C_2H_4)(PR_3)_2]$ being evidenced by the solution holding the green colour for approximately 2-3 minutes before clearing. The ethene atmosphere was replaced with an argon atmosphere; the reaction mixture was then treated with a solution of cycloalkeno-1,2,3-selenadiazole (0.3 mmol) in dry, degassed toluene (2 mL) and refluxed for 1 hr, during which time it changed colour from orange to red. The cooled reaction mixture was filtered under an argon atmosphere and concentrated to give **13a-c** and **14a-c** as red/orange oils. As purification of these compounds was unsuccessful no yields were recorded.

Synthesis of 15a-c and 16a-c

All experiments were carried out according to the following general procedure. Under argon $[PtCl_2(PR_3)_2]$ (0.4 mmol; R = Et, Bu) was taken up in 1,4-dioxane (20 mL) and the solution degassed. This solution was put under an ethene atmosphere and treated dropwise with $NaC_{10}H_8$ (~ 0.12 M solution in THF), complete conversion to $[Pt(C_2H_4)(PR_3)_2]$ being evidenced by the solution holding the green colour for

approximately 2-3 minutes before clearing. The ethene atmosphere was replaced with an argon atmosphere; the reaction mixture was treated with cycloalkeno-1,2,3-selenadiazole (0.3 mmol) in dry, degassed toluene (2 mL), refluxed for 1 hr then allowed to cool to room temperature. The flask was covered in foil; the reaction mixture was treated with MeI (0.5 mL) and stirred at room temperature overnight. After this time a pink/orange solution had formed with a fine white solid present (NaI); this was filtered through a pad of celite (1 cm) and concentrated to a pink/purple residue. Repeated chromatographic purification on alumina with hexane/toluene (1:0 to 2:1 gradient) elution, and collection and concentration of the pink/purple bands gave **15a-c** and **16a-c** as analytically pure pink/purple oily solids. It is necessary to carry out chromatographic purification of these compounds until they are free of residual naphthalene. Yields: **15a**: 90 mg, 31%, **15b**: 200 mg, 67%, **15c**: 149 mg, 49%, **16a**: 198 mg, 55%, **16b**: 150 mg, 41%, **16c**: 78 mg, 21%.

Synthesis of 17a-c and 18a-c

All experiments were carried out according to the following general procedure. Compounds **15a-c** and **16a-c** (0.1 mmol) were taken up in acetone (5 mL) and treated with $TlPF_6$ (39 mg, 0.11 mmol); the resulting yellow/orange slurries were stirred at room temperature for 2-3 days. After this time the reaction mixtures were filtered through a pad of celite (1 cm) and the red liquors were concentrated to give **17a-c** and **18a-c** as analytically pure red oily solids. Yields: **17a**: 68 mg, 90%, **17b**: 70 mg, 91%, **17c**: 74 mg, 95%, **18a**: 83 mg, 90%, **18b**: 86 mg, 92%, **18c:** 85 mg, 90%.

Synthesis of 19 and 20

Both experiments were carried out according to the following general procedure. Under argon $[PtCl_2(PR_3)_2]$ (0.4 mmol; R = Et, Bu) was taken up in 1,4-dioxane (20 mL) and the solution degassed. This solution was put under an ethene atmosphere and treated dropwise with $NaC_{10}H_8$ (~ 0.12 M solution in THF), complete conversion to $[Pt(C_2H_4)(PR_3)_2]$ being evidenced by the solution holding the green colour for approximately 2-3 minutes before clearing. The ethene atmosphere was replaced with an argon atmosphere and the reaction mixture was treated with selenophene (1.6 mL of a 5% v/v toluene solution). The reaction mixture was stirred at 50 °C overnight, then filtered under argon; the filtrate was concentrated to give the products as brown oils. Compound **19** was purified by column chromatography and isolated as a yellow

oil (200 mg, 89% yield). Compound **20** was purified by recrystallisation from hexane to give analytically pure brown needles (76 mg, 26% yield).

Synthesis of 21a,b and 22a,b

Experiments were carried out according to the following general procedure. Under argon $[PtCl_2(PR_3)_2]$ (0.4 mmol; R = Et, Bu) was taken up in 1,4-dioxane (20 mL) and the solution degassed. An ethene atmosphere was introduced, and the solution treated dropwise with $NaC_{10}H_8$ (~0.12 M solution in THF), until the green colour held for approximately 2-3 minutes before clearing. The ethene atmosphere was replaced with argon, and a solution of the diselenide ($(PhSe)_2$, 0.13 g, or $(FcSe)_2$, 0.21 g; 0.4 mmol) in degassed toluene (8 mL) was added. After stirring at room temperature overnight, concentration *in vacuo* gave a yellow or orange solid, which was purified by column chromatography on alumina with toluene/hexane elution. Collection of the coloured band and recrystallisation at -20 °C from toluene/hexane gave **21a** (yellow, 30 mg, 38% yield), **21b** (yellow, 140 mg, 38% yield), **22a** (orange, 40 mg, 32% yield) and **22b** (orange, 50 mg, 35% yield). Yields are based on $[PtCl_2(PR_3)_2]$; conversion to $[Pt(C_2H_4)(PR_3)_2]$ may not be 100%.

Synthesis of 23a,b

Under argon $[Pd_2(dba)_3]$.dba (0.06 g, 0.05 mmol) was taken up in dry toluene (5 mL). The resulting purple solution was treated with PR_3 (0.1 mL) and the reaction mixture allowed to stir for 5 minutes, after which time it was brown/yellow in colour. $(FcSe)_2$ (0.05 g, 0.1 mmol) was then added. After stirring at room temperature overnight, concentration *in vacuo* followed by treatment with hexane resulted in the precipitation of brown/orange solids. Filtration followed by recrystallisation from toluene/hexane at -10 °C gave **23a** (orange, 50 mg, 57% yield) and **23b** (red, 30 mg, 33% yield).

Synthesis of 24a,b and 25a,b

Experiments were carried out according to the following general procedure. Under argon $[PtCl_2(PR_3)_2]$ (0.4 mmol; R = Et, Bu) was taken up in 1,4-dioxane (20 mL) and the solution degassed. An ethene atmosphere was introduced, and the solution treated dropwise with $NaC_{10}H_8$ (~0.12 M solution in THF), until the green colour held for approximately 2-3 minutes before clearing. The ethene atmosphere was replaced with argon, and a solution of the ditelluride ($(PhTe)_2$, 0.16 g, or $(FcTe)_2$, 0.25 g; 0.4 mmol)

in degassed toluene (8 mL) was added. After stirring at room temperature overnight, concentration *in vacuo* gave a yellow or orange solid, which was purified by column chromatography on alumina with toluene/hexane elution. Collection of the coloured band gave **24a** (orange, >100% yield due to impurities), **24b** (orange, 385 mg, 96% yield), **25a** (orange, 380 mg, 90% yield) and **25b** (orange, 400 mg, 82% yield). Yields are based on $[PtCl_2(PR_3)_2]$; conversion to $[Pt(C_2H_4)(PR_3)_2]$ may not be 100%.

Synthesis of 26

Under argon $[Pt(PPh_3)_4]$ (124 mg, 0.1 mmol) and $(FcSe)_2$ (53 mg, 0.1 mmol) were taken up in dry toluene (5 mL) and the resulting red solution was stirred at room temperature overnight. After this time the solution was filtered and the orange solid (**26**) washed with toluene and dried *in vacuo* (60 mg, 48% yield).

Synthesis of 27a,b

Under argon $[PtCl_2(PR_3)_2]$ (0.4 mmol; R = Et, Bu) was taken up in 1,4-dioxane (20 mL) and the solution degassed. An ethene atmosphere was introduced, and the solution treated dropwise with $NaC_{10}H_8$ (~0.12 M solution in THF), complete conversion to $[Pt(C_2H_4)(PR_3)_2]$ being evidenced by the green colour holding for approximately 2-3 minutes before clearing. The ethene atmosphere was replaced with argon, and a solution of $Se_2C_{12}H_8$ (0.12 g, 0.4 mmol) in degassed toluene (8 mL) was added. After stirring at room temperature overnight, concentration *in vacuo* gave a yellow or orange solid, which was purified by column chromatography on alumina with toluene/hexane elution. Collection of the coloured band and recrystallisation at -20 °C from toluene/hexane gave **27a** (yellow, 150 mg, 50% yield) and **27b** (orange, 200 mg, 55% yield).

Synthesis of 28a,b and 29a,b

Under argon $[Pd_2(dba)_3]$.dba (0.06 g, 0.05 mmol) was taken up in dry toluene (5 mL). The resulting purple solution was treated with PR_3 (**28a,b**: 0.1 mL, neat; **29a,b**: 1 mL of a 5% v/v toluene solution) and the mixture allowed to stir for 5 minutes, after which time it was brown/yellow in colour. $Se_2C_{12}H_8$ (0.03 g, 0.1 mmol) was then added. After stirring at room temperature overnight, concentration *in vacuo* followed by treatment with hexane resulted in the precipitation of brown/orange solids. Filtration followed by recrystallisation from toluene/hexane at -10 °C gave **28a** (red,

30 mg, 42% yield), **28b** (red, 20 mg, 14% yield), **29a** (red, 150 mg, 70% yield), **29b** (red, 30 mg, 18% yield).

Synthesis of 30a,b and 31a,b

Under argon $[PtCl_2(L)]$ (0.1 mmol; L = dppm, dppe) was taken up in 1,4-dioxane (5 mL) and the solution degassed. An ethene atmosphere was introduced, and the solution treated dropwise with $NaC_{10}H_8$ (~0.12 M solution in THF), complete conversion to $[Pt(C_2H_4)(L)]$ being evidenced by the green colour holding for approximately 2-3 minutes before clearing. The ethene atmosphere was replaced with argon, and a solution of $(FcSe)_2$ or $Se_2C_{12}H_8$ (0.1 mmol) in degassed toluene (2 mL) was added. After stirring at room temperature overnight, filtration gave a yellow or orange solid. **30a**: orange (37 mg, 33% yield), **30b**: yellow (24 mg, 21% yield), **31a**: yellow (13 mg, 15% yield), **31b:** orange (yield not recorded).

References

1 M. E. Weeks, *Discovery of the Elements, 7th Ed,* Journal of Chemical Education, Easton (1968).

2 D. McDonald, L. B. Hunt, *A History of Platinum and its Allied Elements,* Europa, London (1982).

3 N. N. Greenwood, A. Earnshaw, *Chemistry of the Elements, 2nd Ed,* Butterworth-Heinemann, Oxford (1995).

4 W. G. Proctor, F. C. Yu., *Phys. Rev.,* 76 (1949) 1729.

5 P. S. Pregosin, *Coord. Chem. Rev.,* 44 (1982) 247.

6 References include: Genesis *19*, 24; Deuteronomy *29,* 23; Job *18*, 15, Revelation *19,* 20. By no means however, should the bible be used as a reliable source of information.

7 H. L. Retcofsky, R. A. Friedel, *J. Am. Chem. Soc.,* 94 (1972) 6579.

8 J. Mason (Ed), *Multinuclear NMR*, Plenum Press, New York (1987).

9 R. K. Harris, B. E. Mann (Eds), *NMR and the Periodic Table*, Academic Press, London (1978).

10 K. Bindu, C. S. Kartha, K. P. Vijayakumar, T. Abe, Y. Kashiwaba, *Applied Surface Science*, 191 (2002) 138.

11 X. Zeng, X. Han, L. Chen, Q. Li, F. Xu, X. He, Z. Z. Zhang, *Tetrahedron Lett.*, 43 (2002) 131.

12 X. Nishiyama, M. Hirose, W. Kitagaito, N. Sonoda, *Tetrahedron Lett.,* 43 (2002) 1855.

13 J. Roberts, *PhD Thesis,* University of Wales, Swansea (2001).

14 E. G. Hope, W. Levason, *Coord. Chem. Rev.*, 122 (1993) 109.

15 S. E. Livingstone, *Q. Rev. Chem. Soc.,* 19 (1965) 387.

16 N. I. Sax, *Dangerous Properties of Industrial Materials,* Reinhold, New York (1960), p1095.

17 S. G. Luxon, *Hazards in the Chemical Laboratory, 5th Ed,* Royal Society of Chemistry, The Bath Press, Bath (1992).

18 A. Müller, E. Diemann in *Comprehensive Coordination Chemistry* (Ed: G. Wilkinson, R. D. Gillard, J. A. McCleverty), Pergamon, Oxford, 2 (1988) 551.

19 S. G. Murray, F. R. Hartley, *Chem. Rev.,* 81 (1981) 365.

20 C. G. Kuehn, S. S. Isied, *Prog. Inorg. Chem.,* 27 (1980) 153.

21 W. Levason, S. D. Orchard, G. Reid, *Coord. Chem. Rev.,* 225 (2002) 159.

22 J. Chatt, L. M. Venanzi, *J. Chem. Soc.,* (1955) 2787.

23 J. Chatt, L. M. Venanzi, *J. Chem. Soc.,* (1955) 3858.

24 J. Chatt, L. M. Venanzi, *J. Chem. Soc.,* (1957) 2351.

25 D. J. Gulliver, W.Levason, *J. Chem. Soc. Dalton Trans.,* (1982) 1895.

26 E. G. Hope, W. Levason, M. Webster, S. G. Murray, *J. Chem. Soc. Dalton Trans.,* (1986) 1003.

27 J. R. Allkins, P. J. Hendra, *J. Chem. Soc. A,* (1967) 1325.

28 P. L. Goggin, R. J. Goodfellow, S. R. Haddock, B. F. Taylor, *J. Chem. Soc. Dalton Trans.,* (1976) 459.

29 R. J. Cross, T. H. Green, R. Keat, J. F. Paterson, *J. Chem. Soc. Dalton Trans.,* (1976) 1486.

30 R. Oilunkaniemi, J. Komulainen, R. S. Laitinen, M. Ahlgren, J. Pursiainen, *J. Organomet. Chem.,* 571 (1998) 129.

31 J. C. Barnes, G. Hunter, M. W. Lown, *J. Chem. Soc. Dalton Trans.*, (1976) 1227.

[32] R. Oilunkaniemi, R. S. Laitinen, M. Ahlgren, *J. Chem. Soc. Chem. Commun.,* (1999) 585.

[33] R. Honeychuck, M. O. Okoroafor, L. H. Shen, C. H. Brubaker, *Organometallics,* 5 (1986) 482.

[34] M. O. Okoroafor, L. H. Shen, R. V. Honeychuck, C. H. Brubaker, *Organometallics,* 7 (1988) 1297.

[35] D. J. Gulliver, E. G. Hope, W. Levason, *J. Chem Soc. Perkin Trans. II,* (1984) 429.

[36] A. F. Chiffey, J. Evans, W. Levason, M. Webster, *J. Chem. Soc. Dalton Trans.,* (1994) 2835

[37] E. W. Abel, R. Khan, K. Kite, K. G. Orrell, V. Šik, *J. Chem. Soc. Dalton Trans.,* (1980) 1169.

[38] J. Plusec, A. D. Westland, *J. Chem. Soc.,* (1965) 5371.

[39] E. W. Abel, K. Kite, K. G. Orrell, V. Šik, B. L. Williams, *J. Chem. Soc. Dalton Trans.,* (1981) 2439.

[40] E. W. Abel, S. K. Bhargava, K. Kite, K. G. Orrell, B. L. Williams, *Polyhedron,* 1 (1982) 289.

[41] D. J. Gulliver, E. G. Hope, W. Levason, S. G. Murray, G. L. Marshall, *J. Chem. Soc. Dalton Trans.,* (1985) 1265.

[42] G. Hunter, R. C. Massey, *J. Chem. Soc. Dalton Trans.,* (1976) 2007.

[43] E. W. Abel, S. K. Bhargava, K. Kite, K. G. Orrell, V. Šik, B. L. Williams, *J. Chem. Soc. Dalton Trans.,* (1982) 583.

[44] E. W. Abel, K. G. Orrell, *Prog. Inorg. Chem.,* 32 (1984) 1.

[45] K. G. Orrell, *Coord. Chem. Rev.,* 96 (1989) 1.

[46] N. N. Greenwood, G. Hunter, *J. Chem. Soc. A,* (1967) 1520.

[47] H. J. Whitfield, *J. Chem. Soc. A,* (1970) 113.

[48] C. K. Lai, A. A. Naiini, C. H. Brubaker, *Inorg. Chim. Acta,* 164 (1989) 205.

[49] D. C. Goodall, *J. Chem. Soc. A,* (1969) 890.

[50] E. W. Abel, D. G. Evans, J. R. Koe, V. Sik, *J. Chem. Soc. Dalton Trans.,* (1989) 2315.

[51] E. W. Abel, D. G. Evans, J. R. Koe, M. B. Hursthouse, M. Mazid, *J. Chem. Soc. Dalton Trans.,* (1992) 663.

[52] E. W. Abel, K. Kite, P. S. Perkins, *Polyhedron,* 5 (1986) 1459.

[53] E. W. Abel, K. Kite, P. S. Perkins, *Polyhedron,* 6 (1987) 549.

[54] E. G. Hope, W. Levason, S. G. Murray, G. L. Marshall, *J. Chem. Soc. Dalton Trans.,* (1985) 2185.

[55] W. Levason, C. A. McAucliffe, S. G. Murray, *J. Chem. Soc. Dalton Trans.,* (1976) 269.

[56] K. Krylova, C. P. Kulatilleke, M. J. Heeg, C. A. Salhi, L. A. Ochrymowycz, D. B. Rorabacher, *Inorg. Chem.,* 38 (1999) 4322.

[57] R. J. Batchelor, F. W. B. Einstein, I. D. Gay, J. Gu, S. Mehta, B. M. Pinto, X, Zhou, *Inorg. Chem.,* 39 (2000) 2558.

[58] R. J. Batchelor, F. W. B. Einstein, I. D. Gay, J. Gu, B. D. Johnston, B. M. Pinto, *J. Am. Chem,. Soc.,* 111 (1989) 6583.

[59] T. Kumagai, S. Akabori, *Chem. Lett.,* (1989) 1667.

[60] N. R. Champness, P. F. Kelly, W. Levason, G. Reid, A. M. Z. Slawin, D. J. Williams, *Inorg. Chem.,* 34 (1995) 651.

[61] R. J. Batchelor, F. W. B. Einstein, I. D. Gay, J. Gu, B. M. Pinto, X. Zhou, *Inorg. Chem.,* 35 (1996) 3667.

[62] E. G. Hope, T. Kemmitt, W. Levason, *J. Chem. Soc. Perkin Trans. II,* (1987), 487.

[63] E. W. Abel, S. K. Bhargava, K. G. Orrell, A. W. G. Platt, V. Šik, T. S. Cameron, *J. Chem. Soc. Dalton Trans.*, (1985) 345.

[64] Ch. Elschenbroich, A. Salzer, *Organometallics, 2nd Ed.* VCH, Weinheim (1992).

[65] F. A. Cotton, G. Wilkinson, C. A. Murillo, M. Bochmann, *Advanced Inorganic Chemistry, 6th Ed,* Wiley, New York (1999).

[66] D. F. Shriver, P. W. Atkins, C. H. Langford, *Inorganic Chemistry,* Oxford University Press, Oxford (1990).

[67] S-X. Xiao, W. C. Trogler, D. E. Ellis, Z. Berkovitch-Yellin, *J. Am. Chem. Soc.,* 105 (1983) 7033.

[68] D. S. Marynick, *J. Am. Chem. Soc.,* 106 (1984) 4064.

[69] R. J. Morris, G. S. Girolami, *Inorg. Chem.,* 29 (1990) 4167.

[70] G. Pacchioni, P. S. Bagus, *Inorg. Chem.,* 31 (1992) 4391.

[71] C. A. Tolman, *J. Am. Chem. Soc.,* 92 (1970) 2956.

[72] C. A. Tolman, W. C. Seidel, L. W. Gosser, *J. Am. Chem. Soc.,* 96 (1974) 53.

[73] R. Mason, D. W. Meek, *Angew. Chem. Int. Ed. Engl.,* 17 (1978) 183.

[74] A. Musco, W. Kuran, A. Silvani, M. W. Anker, *Chem. Commun.*, (1973) 938.

[75] M. Matsumoto, H. Yoshioka, K. Nakatsu, T. Yoshida, S. Otsuka, *J. Am. Chem. Soc.,* 96 (1974) 3322.

[76] J. Iggo, *NMR Spectroscopy in Inorganic Chemistry,* Oxford University Press, Oxford (2000).

[77] C. A. Tolman, *Chem. Soc. Rev.,* 1 (1972) 337.

[78] J. K. Kochi, *J. Organomet. Chem.,* 300 (1986) 139.

[79] J. F. Young, J. A. Osborn, F. H. Jardine, G. Wilkinson, *Chem. Commun.,* (1965) 131.

[80] J. A. Osborn, F. H. Jardine, J. H. Young, G. Wilkinson, *J. Chem. Soc. A,* (1966) 1711.

[81] C. O'Connor, G. Wilkinson, *J. Chem. Soc. (A),* (1968) 2665.

[82] W. S. Knowles, *Acc. Chem. Res.,* 16 (1983) 106.

[83] H. B. Kagan, T-P. Dang, *J. Am. Chem. Soc.,* 94 (1972) 6429.

[84] M. D. Fryzuk, B. Bosnich, *J. Am. Chem. Soc.,* 99 (1977) 6262.

[85] G. W. Parshall, *Acc. Chem. Res.,* 8 (1975) 113.

[86] R. F. Heck, *Acc. Chem. Res.,* 12 (1979) 146.

[87] S. T. Nguyen, L. K. Johnson, R. H. Grubbs, *J. Am. Chem. Soc.,* 114 (1992) 3974.

[88] P. Schwab, R. H. Grubbs, J. W. Ziller, *J. Am. Chem. Soc.,* 118 (1996) 100.

[89] I. Lalezari, A. Shafiee, *Tetrahedron. Lett.,* 58 (1969) 5105.

[90] I. Lalezari, A. Shafiee, M. Yalpani, *J. Org. Chem.,* 36 (1971) 2836.

[91] A. Caplin, *J. Chem. Soc. Perkin Trans. I,* (1974) 30.

[92] H. Meier, E. Voigt, *Tetrahedron,* 28 (1972) 187.

[93] H. P. Braun, H. Meier, *Tetrahedron,* 31 (1975) 637.

[94] H. Meier, G. Trickes, E. Laping, U. Merkle, *Chem. Ber.*, 113 (1980) 183.

[95] R. N. Butler, D. A. O'Donoghue, *J. Chem. Soc. Perkin Trans. I,* (1982) 1223.

[96] K. H. Pannell, A. J. Mayr, R. Hoggard, J. S. McKennis, J. C. Dawson, *Chem. Ber.,* 116 (1983) 230.

[97] A. J. Mayr, B. Carrasco-Flores, F. Cervantes-Lee, K. H. Pannell, L. Párkányi, K. RaghuVeer, *J. Organomet. Chem.,* 405 (1991) 309.

[98] M. M. Muir, M. E. Cadiz, A. Baez, *Inorg. Chim. Acta,* 151 (1988) 209.

[99] T. L. Gilchrist, P. G. Mente, C. W. Rees, *J. Chem. Soc. Perkin Trans. I,* (1972) 2165.

[100] G. N. Schrauzer, H. Kisch, *J. Am. Chem. Soc.,* 95 (1973) 2501.
[101] A. J. Mayr, K. H. Pannell, B. Carrasco-Flores, F. Cervantes-Lee, *Organometallics,* 8 (1989) 2961.
[102] K. H. Pannell, A. J. Mayr, R. Hoggard, R. C. Peterson, *Angew. Chem. Int. Ed. Engl.,* 19 (1980) 632.
[103] K. H. Pannell, A. J. Mayr, D. VanDerveer, *Organometallics,* 2 (1983) 560.
[104] K. H. Pannell, A. J. Mayr, D. VanDerveer, *J. Am. Chem. Soc.,* 105 (1983) 6186.
[105] A. J. Mayr, B. Carrasco-Flores, L. Párkányi, K. H. Pannell, *J. Am. Chem. Soc.,*114 (1992) 5467.
[106] F. Cervantes-Lee, L. Párkányi, R. N. Kapoor, A. J. Mayr, K. H. Pannell, Y. Pang, T. J. Barton, *J. Organomet. Chem.,* 562 (1998) 29.
[107] J. Knebel, C. P. Morley, G. Wilke, C. Kruger, J. M. Wallis, *J. Organomet. Chem.,* 334 (1987) C39.
[108] R. Hoffmann, *Angew. Chem. Int. Ed. Engl.,* 21 (1982) 711.
[109] C. P. Morley, *Organometallics,* 8 (1989) 800.
[110] C. P. Morley, R. R. Vaughan, B. J. Wheatley, *J. Organomet. Chem.,* 353 (1988) C39.
[111] C. P. Morley, R. R. Vaughan, *J. Chem. Soc. Dalton Trans.,* (1993) 703.
[112] M. R. J. Dorrity, A. Lavery, J. F. Malone, C. P. Morley, R. R. Vaughan, *Heteroatom Chem.,* 3 (1992) 87.
[113] C. P. Morley, R. R. Vaughan, *J. Organomet. Chem.,* 444 (1993) 219.
[114] P. K. Khanna, C. P. Morley, *J. Chem. Res. (S),* (1995) 64.
[115] S. Ford, C. P. Morley, M. Di Vaira, *J. Chem. Soc. Chem. Commun.,* (1998) 1305.
[116] C. P. Morley, S. Ford, M. Di Vaira, *Polyhedron,* 23 (2004) 2967.
[117] S. Ford, P. K. Khanna, C. P. Morley, M. DiVaira, *J. Chem. Soc. Dalton Trans.,* (1999) 791.
[118] P. Arsenyan, K. Oberte, K. Rubina, S. Belyakov, *Tetrahedron Lett.,* 46 (2005) 1001.
[119] Y. Nishiyama, Y. Hada, K. Iwase, N. Soroda, *J. Organomet. Chem.,* 611 (2000) 488.
[120] S. Ford, *PhD Thesis,* University of Wales, Swansea (2000).
[121] A. J. Mayr, H. Shan-Lien, K. H. Pannell, L. Parkanyi, *Organometallics,* 4 (1985) 1580.
[122] C. W. Bird, E. M. Hollins, *J. Organomet. Chem.,* 4 (1965) 245.
[123] U. Behrens, P. Berges, R. Bieganowski, W. Hinrichs, C. Schiffling, G. Klar, *J. Chem. Res. (S),* (1986) 326.
[124] U. Behrens, P. Berges, R. Bieganowski, W. Hinrichs, C. Schiffling, G. Klar, *J. Chem. Res. (M),* (1986) 2801.
[125] C. M. Bates, P. K. Khanna, C. P. Morley, M. Di Vaira, *J. Chem. Soc. Chem. Commun.,* (1997) 913.
[126] S. Ford, C. P. Morley, M. Di Vaira, *New. J. Chem.,* 23 (1999) 811.
[127] S. Ford, C. P. Morley, M. Di Vaira, *Inorg. Chem.,* 43 (2004) 7101.
[128] L. Engman, *J. Heterocyclic Chem.,* 21 (1984) 413.
[129] S. Murata, T. Suzuki, *J. Heterocyclic Chem.,* 28 (1991) 433.
[130] M. R. Bryce, A. Chesney, A. K. Lay, A. S. Batsanov, J. A. K. Howard, *J. Chem. Soc. Perkin Trans. I,* (1996) 2451.
[131] E. Block, M. Birringer, C. He, *Angew. Chem. Int. Ed. Engl.,* 38 (1999) 1604.
[132] R. D. Adams, B. Captain, J. L. Smith Jr., *J. Organomet. Chem.,* 689 (2004) 65.
[133] E. W. Abel, P. K. Mittal, K. G. Orrell, V. Šik, T. S. Cameron, *J. Chem. Soc. Chem. Commun.,* (1984) 1312.

[134] E. W. Abel, P. K. Mittal, K. G. Orrell, V. Šik, *J. Chem. Soc. Dalton Trans.*, (1986) 961.
[135] E. W. Abel, P. K. Mittal, K. G. Orrell, *Polyhedron,* 6 (1987) 2073.
[136] E. W. Abel, P. K. Mittal, K. G. Orrell, V. Šik, *J. Chem. Soc. Dalton Trans.*, (1985) 1569.
[137] A. R. Siedle, R. A. Newmark, A. A. Kruger, H. Pignolet, *Inorg. Chem.,* 20 (1981) 3399.
[138] B-K. Teo, P. A. Snyder-Robinson, *Inorg. Chem.,* 20 (1981) 4235.
[139] T. Chivers, R. W. Hilts, *Coord. Chem. Rev.,* 137 (1994) 201.
[140] G. G. Briand, T. Chivers, M. Krahn, *Coord. Chem. Rev.,* 233-234 (2002) 237.
[141] V. W. Day, D. A. Lesch, T. B. Rauchfuss, *J. Am. Chem. Soc.,* 104 (1982) 1290.
[142] V. P. Ananikov, I. P. Beletskaya, G. C. Aleksandrov, I. L. Eremenko, *Organometallics,* 22 (2003) 1414.
[143] R. Oilunkaniemi, R. S. Laitinen, M. Ahlgrén, *J. Organomet. Chem.,* 587 (1999) 200.
[144] K-T. Aye, J. J. Vittal, R. J. Puddephatt, *J. Chem. Soc. Dalton Trans.,* (1993) 1835.
[145] A. J. Canty, H. Jin, B. W. Skelton, A. H. White, *Inorg. Chem.,* 37 (1998) 3975.
[146] V. G. Albano, M. Monari, I. Orabona, A. Panunzi, F. Ruffo, *J. Am. Chem. Soc.,* 123 (2001) 4352.
[147] V. G. Albano, M. Monari, I. Orabona, A. Panunzi, G. Roviello, F. Ruffo, *Organometallics,* 22 (2003) 1223.
[148] A. Panunzi, G. Roviello, F. Ruffo, *Organometallics,* 21 (2002) 3503.
[149] U. T. Mueller-Westerhoff, B. Vance, *Comprehensive Coordination Chemistry,* (Eds: G. Wilkinson, R. D. Gillard, J. A. McCleverty), Pergamon, Oxford, 2 (1987) 595.
[150] A. Davison, E. T. Shawl, *Inorg. Chem.,* 9 (1970) 1820.
[151] W. B. Heuer, A. E. True, P. N. Swepston, B. M. Hoffman, *Inorg. Chem.,* 27 (1988) 1474.
[152] W. B. Heuer, P. J. Squattrito, B. M. Hoffman, J. A. Ibers, *J. Am. Chem. Soc.,* 110 (1988) 792.
[153] C. M. Bolinger, T. B. Rauchfuss, *Inorg. Chem.,* 21 (1982) 3947.
[154] B. Gautheron, G. Tainturier, S. Pouly, F. Théobald, H. Vivier, A. Laarif, *Organometallics,* 3 (1984) 1495.
[155] F. Wudl, E. T. Zellers, S. D. Cox, *Inorg. Chem.,* 24 (1985) 2864.
[156] G. Matsubayashi, A. Yokozawa, *J. Chem. Soc. Dalton Trans.,* (1990) 3535.
[157] G. Matsubayashi, S. Tanaka, A. Yokozawa, *J. Chem. Soc. Dalton Trans.,* (1992) 1827.
[158] J. P. Cornelissen, C. Faulmann, J. P. Legros, P. Cassoux, J. G. Haasnoot, P. J. Nigey, J. Reedijk, *Inorg. Chim. Acta,* 202 (1992) 131.
[159] C. Faulmann, J. P. Legros, P. Cassoux, J. Cornelissen, L. Brossard, M. Inokuchi, H. Tajima, M. Tokomotu, *J. Chem. Soc. Dalton Trans.,* (1994) 249.
[160] G. Wolmershäuser, R. Johann, *Angew. Chem. Intl. Ed. Engl.,* 28 (1989) 920.
[161] I. Hawkins, A. E. Underhill, *J. Chem. Soc. Chem. Commun.,* (1990) 1593.
[162] O. A. Dyachenko, S. V. Konovalikhin, A. I. Kotov, G. V. Shilov, E. B. Yagubskii, C. Faulmann, P. Cassoux, *J. Chem. Soc. Chem. Commun.,* (1993) 508.
[163] S. Schenk, I. Hawkins, S. B. Wilkes, A. E. Underhill, A. Kobayashi, H. Kobayashi, *J. Chem. Soc. Chem. Commun.,* (1993) 1648.
[164] P. Deplano, L. Marchio, M. L. Mercuri, L. Pilia, A. Serpe, E. F. Trogu, *Polyhedron,* 22 (2003) 2175.

[165] M. Kajitani, M. Ito, N. Kobayashi, T. Akiyama, A. Sugimori, *Chem. Lett.,* (1986) 1537.

[166] M. Kajitani, R. Ochiai, N. Kobayashi, T. Akiyama, A. Sugimori, *Chem. Lett.,* (1987) 245.

[167] D. M. Giolando, T. B. Rauchfuss, A. L. Rheingold, *Inorg. Chem.,* 26 (1987) 1636.

[168] M. A. Ansari, C. H. Mahler, J. A. Ibers, *Inorg. Chem.,* 28 (1989) 2669.

[169] S. Ford, M. R. Lewtas, C. P. Morley, M. Di Vaira, *Eur. J. Inorg. Chem,* (2000) 933.

[170] M. R. Lewtas, *PhD Thesis,* University of Wales, Swansea (1999).

[171] S. Nagao, H. Seino, T. Okada, Y. Mizobe, M. Hidai, *J. Chem. Soc. Dalton Trans.,* (2000) 3546.

[172] C. P. Morley, C. D. Jones, C. A. Webster, M. Di Vaira, *Phosphorus, Sulfur and Silicon,* 180 (2005) 801.

[173] W. Paw, S. D. Cummings, M. A. Mansour, W. B. Connick, D. K. Geiger, R. Eisenberg, *Coord. Chem. Rev.,* 171 (1998) 125.

[174] G. Matsubayashi, Y. Hiroshige, *Inorg. Chim. Acta,* 183 (1991) 173.

[175] S. M. Dibrov, R. E. Bachman, *Inorg. Chim. Acta,* 357 (2003) 1198.

[176] M. J. Brown, J. F. Corrigan, *J. Organomet. Chem.,* 689 (2004) 2872.

[177] N. Robertson, L. Cronin, *Coord. Chem. Rev.,* 227 (2002) 93.

[178] T. Akutagawa, T. Nakamura, *Coord. Chem. Rev.,* 198 (2000), 297.

[179] P. Cassoux, *Coord. Chem. Rev.,* 185-186 (1999) 213.

[180] E. Canadell, *Coord. Chem. Rev.,* 185 (1999) 629.

[181] M. Fourmigué, *Coord. Chem. Rev.,* 178-180 (1998) 823.

[182] P. Cassoux, L. Valade, H. Kobayashi, A. Kobayashi, R. A. Clarke, A. E. Underhill, *Coord. Chem. Rev.,* 110 (1991) 115.

[183] M. Bousseau, L. Valade, J-P. Legros, P. Cassoux, M. Garbauskas, L. V. Interrante, *J. Am. Chem. Soc.,* 108 (1986) 1908.

[184] T. Nakamura, T. Akutagawa, K. Honda, A. E. Underhill, A. T. Coombers, R. H. Friend, *Nature,* 394 (1998) 159.

[185] W. E. Broderick, E. M. McGhee, M. R. Godfrey, B. M. Hoffmann, J. A. Ibers, *Inorg. Chem.,* 28 (1989) 2904.

[186] J. D. Martin, E. Canadell, *Inorg. Chem.,* 31 (1992) 3176.

[187] G. Matsubayashi, K. Douki, H. Tamura, M. Nakano, *Inorg. Chem.,* 32 (1993) 5990.

[188] S. Elliot, *The Physics and Chemistry of Solids,* Wiley, Chichester (1998).

[189] P. I. Clemenson, A. E. Underhill, M. B. Hursthouse, R. L. Short, *J. Chem. Soc. Dalton Trans.,* (1988) 1689.

[190] A. T. Coomber, D. Beljonne, R. H. Friend, J. L. Brédas, A. Charlton, N. Robertson, A. E. Underhill, M. Kurmoo, P. Day, *Nature,* 380 (1996) 144.

[191] R. Vicente, J. Ribas, S. Alvarez, A. Segui, X. Solans., *Inorg. Chem.,* 26 (1987) 4004.

[192] B. S. Kang, L. H. Wenig, D. X. Wu, F. Wang, Z. Guo, L. R. Huang, Z. Y. Huang, H. Q. Liu, *Inorg. Chem.,* 27 (1988) 1130.

[193] J. V. Rodrigues, I. C. Santos, V. Goma, R. T. Henriques, J. C. Waerenborgh, M. T. Duarte, M. Almeida, *J. Chem. Soc. Dalton Trans.,* (1994) 2655.

[194] U. T. Mueller-Westerhoff, B. Vance, D. I. Yoon, *Tetrahedron,* 47 (1991) 909.

[195] U. T. Mueller-Westerhoff, R. W. Sanders, *Organometallics,* 22 (2003) 4778.

[196] R. J. Angelici, *Polyhedron,* 16 (1997) 3073.

[197] M. J. Sanger, R. J. Angelici, *Organometallics,* 13 (1994) 1821.

[198] C. J. White, R. J. Angelici, M-G. Choi, *Organometallics,* 14 (1995) 332.
[199] W. D. Jones, R. M. Chin, T. W. Crane, D. M. Baruch, *Organometallics,* 13 (1994) 4448.
[200] M-G. Choi, R. J. Angelici, *J. Am. Chem. Soc.,* 112 (1990) 7811.
[201] M-G. Choi, R. J. Angelici, *J. Am. Chem. Soc.,* 113 (1991) 5651.
[202] C. J. White, R. J. Angelici, *Organometallics,* 13 (1994) 5132.
[203] A. J. Arce, A. J. Deeming, Y. De Sanctis, R. Machado, J. Manzur, C. Rivas, *J. Chem. Soc. Chem. Commun.,*(1990) 1568.
[204] A. J. Arce, R,Machado, C. Rivas, Y. De Sanctis, A. J. Deeming, *J. Organomet. Chem.,* 419 (1991) 63.
[205] D. S. Choi, I. S. Lee, S. U. Son, Y. K. Chung, *Organometallics,* 20 (2001) 3617.
[206] M. L. Spera, W. D. Harman, *Organometallics,* 18 (1999) 1559.
[207] W. D. Jones, R. M. Chin, *Organometallics,* 11 (1992) 2698.
[208] W. D. Jones, R. M. Chin, *J. Organomet. Chem.*, 472 (1994) 311.
[209] D. A. Vicic, A. W. Myers, W. D. Jones, *Organometallics,* 16 (1997) 2751.
[210] M. Hernández, G. Miralrio, A. Arévalo, S. Bernès, J. J. García, C. López, P. M. Maitlis, F. del Rio, *Organometallics,* 20 (2001) 4061.
[211] J. J. Garcia, B. E. Mann, H. Adams, N. A. Bailey, P. M. Maitlis, *J. Am. Chem. Soc.,* 117 (1995) 2179.
[212] J. J. Garcia, A. Arevalo, S. Capella, A. Chehata, M. Hernandez, V. Montiel, G. Picazo, F. Del Rio, R. A. Toscano, H. Adams, P. M. Maitlis, *Polyhedron,* 16 (1997) 3185.
[213] J. J. Garcia, A. Arevalo, V. Montiel, F. Del Rio, B. Quiroz, H. Adams, P. M. Maitlis, *Organometallics,* 16 (1997) 3216.
[214] A. Iretskii, J. J. Garcia, G. Picazo, P. M. Maitlis, *Catalysis Lett.,* 51 (1998) 129.
[215] A. Arévalo, S. Bernès, J. J. García, P. M. Maitlis, *Organometallics,* 18 (1999) 1680.
[216] J. Chantson, H. Görls, S. Lotz, *J. Organomet. Chem.,* 687 (2003) 39.
[217] K. Yu, H. Li, E. J. Watson, K. L. Virkaitis, G. B. Carpenter, D. A. Sweigart, *Organometallics,* 20 (2001) 3550.
[218] D. H. Williams, I. Fleming,, *Spectroscopic Methods in Organic Chemistry, 5th Ed.* McGraw-Hill, London (1995).
[219] F. E. Wood, M. M. Olmstead, J. P. Farr, A. L. Balch, *Inorg. Chim. Acta,* 97 (1985) 77.
[220] C. M. Lukehart, A. T. McPhail, D. R. McPhail, J. B. Myers Jr., H. K. Soni, *Organometallics,* 8 (1989) 1007.
[221] J. R. Berenguer, M. Bernechea, J. Forniés, A. Garcia, E. Lalinde, M. T. Moreno, *Inorg. Chem.,* 43 (2004) 8185.
[222] R. Usón, J. Forniés, M. Tomás, B. Menjón, R. Navarro, J. Carnicer, *Inorg. Chim. Acta,* 162 (1989) 33.
[223] G. M. Sheldrick, *University of Göttingen* (1997).
[224] J. Clayden, N. Greeves, S. Warren, P. Wothers, *Organic Chemistry,* OUP, Oxford (2001) 107.
[225] A. Altomare, M. C. Burla, G. Camalli, G. Cascarano, C. Giacovazzo, A. Guagliardi, A. G. G. Moliterni, G. Polidori, R. Rizzi, *J. Appl. Cryst.,* 32 (1999) 115.
[226] M. R. Lewtas, C. P. Morley, M. Di Vaira, *Polyhedron*, 19 (2000) 751.
[227] A. Bencini, M. Di Vaira, R. Morassi, P. Stoppioni, F. Mele, *Polyhedron,* 15 (1996) 2079.
[228] H. Buhl, B. Seitz, H. Meier, *Tetrahedron*, 33 (1977) 449.

229 T. Chivers, K. McGregor, M. Parvez, *J. Chem. Soc., Chem. Commun.,* (1993) 1021.

230 J. Harada, K. Ogawa, *J. Am. Chem. Soc.,* 123 (2001) 10884.

231 D. F. Shriver, P. W. Atkins, *Inorganic Chemistry, 3rd Ed.* OUP (1999).

232 T. M. Klapötke, M. Broschag, *Compilation of Reported ^{77}Se NMR Chemical Shifts – up to the year 1994,* Wiley. Chichester (1996).

233 J. D. Kennedy, W. McFarlane, R. J. Puddephatt, P. J. Thompson, *J. Chem. Soc., Dalton Trans.,* (1976) 874.

234 A. Iretskii, H. Adams, J. J. Garcia, G. Picazo, P. M. Maitlis, *Chem. Commun.,* (1998) 61.

235 A. G. Davies, C. H. Scheisser, *J. Organomet. Chem.,* 389 (1990) 301.

236 R. Oilunkaniemi, R. S. Laitinen, M. Ahlgrén, *J. Organomet. Chem.,* 623 (2001) 168.

237 S. Akabori, T. Kumagai, T. Shirahige, *Organometallics,* 6 (1987) 526.

238 H. Matsuzaka, J-P. Qö, T. Ogino, M. Nishio, Y. Nishibayashi, Y. Ishii, S. Uemura, M. Hidai, *J. Chem. Soc. Dalton Trans.*, (1996) 4307.

239 E. C. Alyea, G. Ferguson, S. Kannan, *Polyhedron*, 17 (1998) 2231.

240 V. K. Jain, S. Kannan, E. R. T. Tiekink, *J. Chem. Res. (S),* (1994) 85.

241 M. S. Hannu, R. Oilunkaniemi, R. S. Laitinen, M. Ahlgrén, *Inorg. Chem. Commun.,* 3 (2000) 397.

242 M. S. Hannu-Kuure, J. Komulainen, R. Oilunkaniemi, R. S. Laitinen, R. Suontamo, M. Ahlgrén, *J. Organomet. Chem.,* 666 (2003) 111.

243 S. Jing, C. P. Morley, C. A. Webster, M. Di Vaira, *Dalton Trans.,* accepted for publication.

244 A. Singhal, V. K. Jain, B. Varghese, E. R. T. Tiekink, *Inorg. Chim. Acta,* 285 (1999) 190.

245 W. Massa, *Crystal Structure Determination,* Springer, Berlin (1996).

246 W. Clegg, *Crystal Structure Determination,* Oxford University Press, Oxford (1998).

247 T. Hahn (Ed.), *Internatonal Tables for Crystallography,* Volume A, Kluwer, Dordrecht (1983).

248 L. J. Farrugia, *J. Appl. Cryst.,* 30 (1997) 565.

249 G. M. Sheldrick, *University of Göttingen* (1986).

250 P. Bhattacharyya, A. M. Z. Slawin, M. B. Smith, *J. Chem. Soc. Dalton Trans.,* (1998) 2467.

251 S. Jing, *PhD Thesis*, University of Wales, Swansea (2006).

252 E. W. Abel, N. J. Long, K. G. Orrell, A. G. Osborne, V. Šik, *J. Organomet. Chem.,* 367 (1989) 275.

253 A. J. Barton, W. Levason, G. Reid, *J. Organomet. Chem.,* 579 (1999) 235.

254 W. Levason, B. Patel, G. Reid, A. J. Ward, *J. Organomet. Chem.,* 619 (2001) 218.

255 C. E. Housecroft, *The Heavier d-Block Metals*, OUP, Oxford (1999).

256 R. J. Errington, *Advanced Practical Inorganic and Metalorganic Chemistry,* CRC Press Inc., U.S. (1997).

257 G. Mugesh, A. Panda, H. B. Singh, N. S. Punekar, R. J. Butcher, *J. Am. Chem. Soc.,*123 (2001) 839.

258 M. Herberhold, P. Leitner, *J. Organomet. Chem.,* 336 (1987) 153.

259 T. Yoshida, T. Matsuda, S. Otsuka, *Inorg. Synth.,* 28 (1990) 122.

260 G. W. Parshall, *Inorg. Synth.,* 12 (1970) 26.

261 G. B. Kaufmann, L. A. Teter, *Inorg. Synth.,* 7 (1963) 245.

262 M. F. Rettig, P. M. Maitlis, *Inorg. Synth.,* 28 (1990) 110